Mechanistic Insights Towards Understanding FRG1 Mediated Regulation of Breast Tumorigenesis and Angiogenesis in Different Molecular Subtypes

By

Bratati Mukherjee
LIFE 11201604013

National Institute of Science Education and Research (NISER)
Bhubaneswar

A thesis submitted to the
Board of Studies in Life Sciences

In partial fulfillment of requirements
for the Degree of
DOCTOR OF PHILOSOPHY
of
HOMI BHABHA NATIONAL INSTITUTE

April, 2023

STATEMENT BY AUTHOR

This dissertation has been submitted in partial fulfillment of requirements for an advanced degree at Homi Bhabha National Institute (HBNI) and is deposited in the Library to be made available to borrowers under rules of the HBNI.

Brief quotations from this dissertation are allowable without special permission, provided that accurate acknowledgement of source is made. Requests for permission for extended quotation from or reproduction of this manuscript in whole or in part may be granted by the Competent Authority of HBNI when in his or her judgment the proposed use of the material is in the interests of scholarship. In all other instances, however, permission must be obtained from the author.

Bratati Mukherjee

DECLARATION

I, hereby, declare that the investigation presented in the thesis has been carried out by me. The work is original and has not been submitted earlier as a whole or in part for a degree / diploma at this or any other Institution / University.

Bratati Mukherjee

List of publications arising from the thesis

1. *Reduced expression of FRG1 facilitates breast cancer progression via GM-CSF/MEK-ERK axis by abating FRG1 mediated transcriptional repression of GM-CSF*; **Mukherjee, B.,** Tiwari, A., Palo, A., Pattnaik, N., Samantara, S., Dixit, M. **Cell Death Discovery (Springer Nature)**, **2022**, 8(1):442, DOI: https://doi.org/10.1038/s41420-022-01240-w.

2. *Reduced FRG1 expression promotes angiogenesis via activation of the FGF2-mediated ERK/AKT pathway*; **Mukherjee, B.,** Brahma, P., Mohapatra, T., Chawla, S., Dixit, M, **FEBS Open Bio (FEBS Press), 2023**, DOI: https://doi.org/10.1002/2211-5463.13582.

Other Publications

1. *Reduced FRG1 expression promotes prostate cancer progression and affects prostate cancer cell migration and invasion*; Tiwari, A., **Mukherjee, B.,** Hassan, MK., Pattanaik, N., Jaiswal, AM., Dixit, M. **BMC Cancer (Springer Nature), 2019**, 19(1):346, DOI: 10.1186/s12885-019-5509-4.

2. *MicroRNA Key to Angiogenesis Regulation: miRNA Biology and Therapy*; Tiwari A[1], **Mukherjee B[1],** Dixit M. **(Joint first author), Current Cancer Drug Targets (Bentham Science), 2018**, 18(3):266-277, DOI: 10.2174/1568009617666170630142725.

Conference Proceedings

1. **Mukherjee. B.,** Dixit M. *Direct binding of FRGI on GM-CST promoter inhibits EMT via regulating the MEK-ERK signaling axis in breast cancer.* 15th International Symposium on Recent Trends in Cancer Prevention and Interception: Bench to Bedside. Jawaharlal Nehru University, School of Life Sciences, New Delhi, India, 22nd - 23rd February 2022.

2. **Mukherjee, B.,** Dixit M. *Transcriptional repression of GM-CSF by FRG1 inhibits breast cancer progression by abating the GM-CSF/MEK-ERK signaling cascade*. HBNI Theme Meeting on Life Sciences. Raja Ramanna Centre for Advanced Technology (RRCAT), Indore, India, 7th - 9th September 2022.

3. **Mukherjee, B.,** Tiwari A, Dixit M. *Novel tumor suppressor FRG1 reduces cancerous properties of breast cancer cell lines by regulating ERK pathway, irrespective of molecular*

subtypes. Cancer Research (2020), 80 (16_Supplement): 5969, AACR Annual Meeting, 27th - 28th April 2020.

4. **Mukherjee, B.,** Tiwari A, Dixit M. *Elucidate the Role and Mechanism of FRG1, The New Player in Cancer Development*. International Symposium on Tumor Microenvironment and Cancer Prevention & Therapeutics Conference. Jawaharlal Nehru University, School of Life Sciences, New Delhi, 8th - 9th February 2019.

Name and signature of the student

Dedicated to Ma, Baba, Tukai

&

Mr. Shyama Prasad Sain

Acknowledgment

The English Noble laureate T.S Eliot once said that the journey was more important than the destination – and at the end of my Ph.D. journey, I would like to thank all my companions who not only made this journey memorable but also helped me to land to my dream destination. Today, when I look back on the past, I remember so many people who helped to bring out the best in me. My heartfelt gratitude to all of them.

At this moment of accomplishment, I am greatly obligated to my parents, ***Mrs. Ratna Mukherjee*** *and* ***Mr. Nabankur Mukherjee****, for supporting me in pursuing my passion for research. Since my childhood, they always made sure to relieve me from any household responsibilities so that I could give my level best in academics. The only thing that my mother envisions for herself is her daughter's success. I consider myself privileged to have parents like them. It's all of their faith, support, and sacrifices that constantly motivate me to excel in life.*

When it comes to my scientific career, first and foremost, I am indebtedly grateful to my Ph.D. supervisor ***Dr. Manjusha Dixit****. Without her guidance, persistent push, and scientific input, this thesis would have never been completed. The effort and time she invests in every student are really unmatchable. She is a woman of perfection. Dr. Dixit's strict personality as a mentor, dedication to research, and perseverance have contributed profoundly to shaping my personality.*

I owe my deepest gratitude to my B.Sc. teacher ***Mr. Shyama Prasad Sain****. His fantastic brainstorming classes strived me to traverse deeply into the subject. He is the only reason behind choosing research as a career.*

I would like to thank my ex-lab mate, ***Dr. Ankit Tiwari****, for mentoring me during the initial years of my Ph.D. I will always remember our scientific discussions that led to the foundation of many successful experiments.*

My words will fall short to express how much I am indebted to ***Sumitava****. His exceptional support always held me high in any difficulties. The way he helped in my personal and professional life has allowed me to focus peacefully on accomplishing my professional goals. His tremendous commitment to research, excellent presentation skills, and hard work have always been the constant source of my motivation.*

It seems like yesterday I joined NISER. Now, six and half years down the lane, when I look back at my former self, I can clearly see the differences. Life takes us on so many unexpected paths. In NISER, I have met so many people who actually molded me and showed me the world outside the book pages. Therefore, my sincere thanks to my fellow NISERites, ***Aranya, Chandan,***

Tathagata, Ramani, Saptarshi, Prerna, Vinay, Arjama, Debashis, and Indrajit. *I would like to specifically mention the name of* ***Aranya, Ramani,*** *and* ***Arjama.*** *Their kind cooperation and insightful discussion helped me to troubleshoot many failed experiments.* ***Aranya*** *and* ***Chandan*** *showed me what friendship was. Our group study during the coursework, the campus round after the dinner, our never-ending talks, the pizza parties, sudden Bhubaneswar trips, and so many countless memories that will stay with me lifelong. I am extremely thankful to* ***Natasha, Somlata, Anwehsa, Sumela, Tusharadri, Shalini, Debashruti, Rashmi, and Sagarika*** *for making my hostel and campus life memorable. I will never forget how* ***Somlata*** *used to take care of me when I fell sick.*

I have been able to progress with my thesis with the assistance of all of my present and past lab mates. Hence, I would like to acknowledge ***Dr. Ankit, Dr. Dinesh, Dr. Khurshid, Saket, Talina, Vinay, Soham, Mohit****, and* ***Dr. Supriya****.* ***Saket*** *deserves special thanks for helping me unconditionally many times. I owe* ***Talina*** *for assisting me in many personal crises. Also, I love to cherish the times I spent with the Master's students of the MD lab-* ***Abhishek, Prasannajit, Tithi, Sanchita, Deeptima, Subhanjali, Rehan, Kirti, Biswahere, Neha****,* ***Pratush, Monali.*** *I am fortunate to get the opportunity to mentor the Master's students* ***Harini, Abhishek,*** *and* ***Sanchita*** *toward the completion of their thesis. I have learned a lot while working with them; without that my Ph.D. training would have never been fulfilled. The summer of 2018 has a very special place in my heart. Along with my then lab mates and visiting summer students* ***Charu*** *and* ***Harini****, we enjoyed those days to the fullest. I am grateful to* ***Dr. Himani*** *and* ***Nirmala Kushwaha*** *for their great companionship.*

Outside the NISER, I would like to thank my friend ***Bipasha,*** *who always lends her hands in any need.*

I got my first research exposure at IISER, Mohali. In this regard, I am grateful to ***Dr. Sudip Mondal*** *for giving me the opportunity to work in his lab. Those two months at the IISER enriched me with lifelong experiences and memories. I was lucky enough to work under the great mentorship of* ***Miss. Sakshi Gupta.*** *Apart from her, there I learned many new techniques and concepts from* ***Dr. Saikat Ghosh, Dr. Poonam Agarwal, Dr. Haleen Kaur,*** *and* ***Yogesh Bangal.*** *I owe them for introducing me to the world of research.*

My love for research became more intense because of some exceptional faculties at the Presidency University. I can recall how keen my former self was to gain more knowledge in the field of Cancer Biology. The entire credit should go specifically to ***Dr. Sutapa Saha, Dr. Atreyi Chatterjee, Dr. Amlan Ghosh,*** *and* ***Dr. Shantanu Chatterjee.*** *Later I joined the lab of* ***Dr. Sutapa Saha*** *for my M.Sc. dissertation. I am immensely thankful to Dr. Saha for her*

constructive criticism that really helped me to make my personality stronger. The lessons I learned from her were extremely beneficial for me to stride forward in the research world. I would like to thank my lab mate ***Dr. Sudipa Maity;*** *my friends* ***Malini Bhattacharya, Priyanka Choudhury, Priyanka Bose, Natasha Khan, Prerna Maheswari, Maitri Singh*** *and* ***Partha Sarathi*** *at Presidency University for providing me a wonderful environment of learning.*

I have been lucky to have some good friends at Burdwan Raj College. I am grateful to ***Jayashri Das, Sharmistha Medda, Souvick Mukherjee, Sulagna Mukherjee, Shanta Pramanik, Sayantani Sinha, Kushankur Bhattacharya****, and* ***Mou Biswas*** *for giving me a wonderful college life. I owe my deepest gratitude to all the faculties of the Zoology Department, Burdwan Raj College, for imbibing the excitement for Biology within me. In this regard, I wish to wholeheartedly thank* ***Dr. Apurba Chatterjee (then HOD), Dr. Arup Sadhu, Dr. Jagannath Santra, Dr. Buddhadev Mondal,*** *and* ***Dr. Soma Banerjee****. Wherever I go, a part of Burdwan Raj College always stays with me.*

I am forever thankful to all of the teachers from the school (Bharati Balika Vidyalaya), college (Burdwan Raj College), and university (Presidency University).

I consider myself fortunate to have a sibling, ***Tukai****, who always supports me in every aspect of life. Her encouragement uplifted me many times from downhill. I have a bunch of 'my people', my cousins, who are literally my strength. I can't imagine myself here without the support of* ***Mr. Sudipta Chakroborty (Deep Dada), Dr. Koushik Mukherjee (Bumba), and Ms. Urmi Padey****.* ***Sudipta*** *has always been the 'stressbuster' of our group and my constant source of encouragement. While* ***Bumba*** *gave me insightful suggestions in many decision-making phases of my life. Their company is my real comfort zone. I would like to thank my pisi* ***Dr. Swapna Bandopadhaya,*** *aunt* ***Dr. Smritikana Mukherjee,*** *and uncle* ***Dr. Premankur Mukherjee*** *for all their support throughout these years. I remember my grandfather* ***Late Narayan Mukherjee****. I am sure that he will be the happiest if he could be able to see this day.*

With a heavy heart, I like to acknowledge ***Fini,*** *who had been an integral part of my family and a source of my joy from the year 2011 to Nov 2022.*

My sincere gratitude to my doctoral committee members for their valuable suggestions. I am also obliged to the administrative and academic staff of NISER, the central instrumentation facility of the SBS, NISER, the animal care facility, and the excellent Central Library facility of NISER. This work would have never been possible without our collaborators ***Dr. Niharika Pattnaik (AMRI Hospital) and Dr. Subrat Samantara****. I also want to thank Mr.* ***Sashibhusan Dash*** *for his help with the tissue sample collection. I extend my thanks to* ***Dr. Saurabh Chawla, Mr. Kuna Meher, and Mr. Surya.*** *They helped me a lot in conducting the animal experiments.*

I also appreciate the contribution of the people who helped me in various ways, but their names have been unintentionally unmentioned.

Now, sometimes I really miss that 'old' me who used to find all her enjoyment amidst Albert, Lehninger, Gilbert, and Weinberg.

In the end, I wish to thank that stubborn, small-town girl who desperately wanted to see herself in this place since the year 2010 and never allowed anything to down her dreams.

Contents

Summary

FRG1 has gained most of the research interest owing to its role in FSHD pathophysiology and muscle development. Several other studies have documented its functional importance in F-actin bundling, pre-mRNA processing, and *Xenopus* vascular development. Reduced expression of FRG1 in oral, gastric, and colorectal carcinomas indicates its potential role in cancer development.

To understand FRG1's role and prognostic relevance in cancer, we have investigated the unexplored mechanism of FRG1 in breast cancer EMT and angiogenesis, the two crucial characteristics of cancer. Using breast cancer cell lines of different molecular subtypes, we have demonstrated that reduced FRG1 level leads to increased cell proliferation, migration, and invasion regardless of the breast cancer molecular subtypes. Depletion of FRG1 leads to activation of the ERK/MEK signaling axis. Enhanced levels of phospho-ERK, due to the depletion of FRG1, upregulate the expression of the EMT markers Snail, Slug, and Twist. Besides ERK, reduction in FRG1 levels also elevates expression of other oncogenic cytokines, including CXCL1, CXCL8, GM-CSF, PDGFα, and PDGFβ, which may facilitate the process of EMT. To provide detailed mechanistic insights underlying FRG1-mediated suppression of EMT, we have shown that FRG1 acts as a transcriptional repressor of GM-CSF which in turn suppresses the downstream ERK-mediated EMT in breast cancer.

As FRG1 level depletion affects the tumorigenic properties of breast cancer cells through the activation of ERK, next we have investigated if it possesses any role in the regulation of apoptosis, another major hallmark of cancer. Reduction of FRG1 levels in MCF7 cells significantly decreases phospho-p53. Depleted FRG1 in breast cancer cells stimulates the activation of ERK, which inhibits the apoptotic pathway by reducing AKT and p53 phosphorylation. We have further validated our *in vitro* findings in patient samples. In accordance with our cell line-based observation, we detected lesser FRG1 expression in breast

cancer tissues compared to the adjacent normal control. In breast cancer patient tissues, an inverse relationship between the levels of phospho-ERK and FRG1 further substantiates the *in vitro* results. Next, we *l*ooked at the prognostic relevance of FRG1. Analysis of RNA sequencing data from the publicly available GEPIA web server depicts that increased FRG1 transcripts in breast cancer patients correlate with a better probability of disease-free survival compared to the patients with lesser FRG1. Using the integrated TCGA dataset, Kaplan-Meir survival analysis also demonstrates that breast cancer patients with high levels of FRG1 and wild-type p53 have a greater likelihood of relapse-free survival than the patients with lower levels of FRG1. Thus, identifying FRG1 as an upstream regulator of GM-CSF and the interplay between ERK and AKT cascade may aid in establishing a more effective therapeutic approach.

Furthermore, the effect of FRG1 depletion on tumor growth has been assessed in the orthotopic mice model. Administration of mice mammary carcinoma-derived 4T1 cells with reduced FRG1, resulting in enlarged tumor growth and more tumor weight in female BALB/c mice compared to the control. Protein harvested from the same mice shows significant upregulation of phospho-ERK and EMT marker Snail levels. An opposite trend has been observed in the mice injected with 4T1 cells with elevated FRG1 levels. To check the metastatic potential of FRG1 *in vivo*, we have found that depleted FRG1 levels increase the metastatic nodules in the lungs. We have established a mice model to measure the therapeutic potential of anti-GM-CSF therapy in reduced FRG1 conditions. Intraperitoneal administration of GM-CSF neutralizing monoclonal antibody reduces tumor volume, phospho-ERK, and Snail levels in the mice, injected 4T1 cells with reduced FRG1 level. Henceforth our work provides the scope of developing an anti-GM-CSF-based therapeutic strategy, especially in breast cancer patients harboring low FRG1 levels.

As the process of angiogenesis is concurrent with metastatic spread, in addition to exploring the role of FRG1 in tumorigenesis, we have investigated if FRG1 expression perturbation

affects angiogenesis. We have examined the impact of pro-angiogenic substances present on the conditioned medium of FRG1 knockdown and FRG1 expressing breast cancer cells on the proliferative, migratory, and tubulogenic ability of Human Umbilical Vein Endothelial Cells (HUVECs). Co-culture of HUVECs with the conditioned medium harvested from MCF7 cells with FRG1 depletion and MDA-MB-231 cells with elevated FRG1 levels increases the aforementioned properties in HUVECs. Increased angiogenesis in matrigel plug and skin wound-healing assays in mice due to FRG1 reduction confirms the angiogenic potential of FRG1 in vivo. Mechanistically, FRG1 depletion in breast cancer cells elevates the expression of Fibroblastic Growth Factor 2 (FGF2) via ERK activation. Subsequently, this secreted FGF2 activates the FGF receptor in HUVECs that triggers the downstream ERK and AKT signaling cascades to facilitate angiogenesis.

In conclusion, FRG1 expression affects breast cancer tumorigenesis independent of its molecular subtype. Our study first time establishes the effect of FRG1 on both breast tumorigenesis and angiogenesis. Numerous findings of this thesis provide essential understandings of the FRG1-mediated direct transcriptional regulation of GM-CSF. Reduced expression of FRG1 in breast cancer facilitates GM-CSF-mediated activation of ERK. ERK activation promotes EMT and FGF2-mediated tumor angiogenesis. This work shows that GM-CSF can be targeted therapeutically in breast cancer patients having reduced FRG1 expression.

List of Figures

List of Tables

Chapter 1

Introduction

Breast cancer is a heterogeneous disease comprising diverse molecular subtypes representing distinct clinical consequences (1). Identifying several genetic mutations and the underlying signaling cascade in different molecular subgroups contributed to discovering various effective targeted medicines for breast cancer (2). However, despite substantial improvements in diagnosis and therapeutics, the prognosis for advanced-stage breast patients still remains dismal. Breast cancer is the second most prevalent cancer to be diagnosed and possesses the fifth highest fatality rate among all cancers (3). Most breast cancer-associated deaths are driven by epithelial-to-mesenchymal transition (EMT), which entails spreading malignant cells to new locations by intravasation and forming secondary metastatic nodules (4). Several key transcriptional factors are reported to promote EMT during breast tumorigenesis, including ZEB1/2, TWIST1/2, and SNAI2 (5). Apart from these transcriptional regulators, numerous cytokines, growth factors, and matrix-metalloproteases (MMPs) are reported to play a pivotal role in the development and progression of breast cancer. To name a few cytokines such as interleukin-6 (IL-6) (6), tumor necrosis factor α (TNF-α) (6), transforming growth factor β (TGF-β) (7), chemokines comprised of C-C motif chemokine ligand 2 (CCL2), CCL5, CXCL12 (8); MMPs including MMP-3, MMP7 (9), MMP-9 (10), MMP-2 (11) are reported to be the potential EMT inducers in breast cancer. To facilitate the metastatic spreading of breast cancer, angiogenesis occurs along with EMT to provide the constant requirement of oxygen and nutrients to the proliferating cancer cells (12). Angiogenesis is regulated via the secretion of various pro-angiogenic factors such as vascular endothelial growth factors (VEGF), basic fibroblast growth factors (FGF2), interleukin-8 (IL-8), and TGF-β by the cancer cells (13), (14), (15).

Several therapeutic approaches are implemented for treating breast carcinoma, depending on the stage of the disease. Generally, a combination of two or more treatment strategies, including surgery, chemotherapy, endocrine therapy, radiation therapy, and targeted therapy, are used

(16). While surgery is fruitful only for localized breast cancer treatment, radiation and chemotherapy are used both for treating localized and metastatic breast cancer (17). Precise medicines targeting the Estrogen receptor (ER), Human epidermal growth factor receptor (HER2), Epidermal growth factor receptor (EGFR), GATA-3, and Myc have been developed using the most recent advancements in molecular biology and immunotherapy to stop the growth and spread of breast cancer more effectively (18), (19). The invention of Trastuzumab, a humanized monoclonal antibody against HER-2/neu, offers the very first evidence of targeted therapy for breast cancer and is now largely recognized as standard targeted therapy (20). However, the development of resistance to the existing therapy that leads to metastasis recurrence still poses a problem in treating advanced-stage breast cancer (21). Targeting the VEGF receptors (VEGFR) using the chemotherapeutic agents Bevacizumab, Sorafenib, and Sunitinib for a long time led to chemoresistance by activating the major oncogenic pathways such as MAPK, AKT, and EGFR (22). Similarly, administering drugs that inhibit the FGF-mediated signaling cascade has fewer survival benefits because it triggers other signaling pathways, including MEK, ERK, and AKT (23), (24). Dual tyrosine kinase that simultaneously inhibits VEGFR and FGF receptor (FGFR) is clinically proven to delay the onset of resistance. Still, the underlying signaling crosstalk between both the pathways frequently fails to slow the angiogenesis process and thus promotes cancer progression (25). Therefore, further research into understanding the molecular mechanisms of additional genes that function upstream of these oncogenic signaling pathways is essential to develop a more effective therapeutic approach to overcome the acquired resistance.

The discovery of several inhibitors has reformed our understanding of chemotherapeutic-based treatment, and it largely depends on inhibiting the central oncogenic signaling or angiogenesis process. However, there hasn't been much work done to find a single molecule that controls both angiogenic and tumorigenic processes. Hence, identifying such a molecule can aid in

inhibiting the metastatic spread of cancerous cells more efficiently. Furthermore, if they are effective regardless of the molecular subtypes of breast cancer, all breast cancer patients can use the same treatment plan. In this thesis, we emphasized on exploring such novel protein that plays an indispensable role in regulating a number of tumorigenic processes, including EMT, apoptosis, and angiogenesis.

Our previous findings suggest that FSHD region gene 1 (FRG1) can be one such molecule. In earlier reports, our group found that gastric, colorectal, and oral carcinomas had lower levels of the FRG1 protein. (26). Previously, our group discovered the tumor-suppressive role of FRG1 in prostate cancer (27). Reduction in FRG1 levels promotes the oncogenic properties in androgen receptor-negative prostate cancer cell lines DU-145 and PC-3 through the activation of p38-MAPK signaling. Knockdown of FRG1 elevated the transcripts level of numerous tumorigenic cytokines, growth factors, and MMPs, including MMP1, Granulocyte-macrophage colony-stimulation factor (GM-CSF), Placental growth factor (PLGF), Platelet-derived growth factor α (PDGFα), and CXCL1, both in DU-145 and PC-3 cells. A multivariate-based optimal model study has recently shown that elevated levels of FRG1 have a protective role in multiple cancers, with a significant effect on gastric and cervical cancer (28). A report suggested that FRG1 might play a role in angiogenesis in the *Xenopus* model (29). The direct association of FRG1 in human tumor angiogenesis was first established by Tiwari *et al*. (26). They showed that elevated expression of FRG1 in HEK 293T cells decreased tubule formation and migration of Human Umbilical Vein Endothelial Cells (HUVECs) in a paracrine manner (26), yet the mechanistic explanations remained elusive.

Although the involvement of FRG1 in tumor progression is evident in the above-mentioned studies, a comprehensive evaluation of the available reports indicates several gaps in understanding the role of FRG1 as a tumor suppressor. Firstly, our group previously reported that FRG1 depletion led to increased levels of GM-CSF, PDGFA, and CXCL1 transcripts in

FRG1-depleted prostate cancer cells (27). However, it was not addressed whether these altered transcripts levels were directly regulated by FRG1 or by some other downstream signaling molecules. Secondly, although reduced FRG1 level correlated to enhanced oncogenic properties in prostate cancer cells and HEK 293T cells, the underlying fundamental mechanism of how exactly FRG1 inhibits tumor progression was unresolved. Thirdly, no study was done to reveal if FRG1 had any prognostic significance in breast cancer. Lastly, there was a complete lack of knowledge underpinning the molecular mechanism of FRG1-mediated tumor angiogenesis.

There has never been a thorough investigation into elucidating the role and molecular basis of the function of FRG1 in breast tumorigenesis and tumor angiogenesis. The presence of molecular subtypes imposes added difficulty in using a common treatment pattern.

Therefore, finding new targets that can act regardless of breast cancer molecular subtypes will aid in developing more potent and cost-effective therapeutic strategies. In breast cancer, our preliminary work suggests that the knockdown of FRG1 led to increased cell proliferation, migration, and invasion in hormone receptor-positive breast cancer cells MCF7. But no research was conducted to understand the impact of FRG1 on triple-negative breast cancer cells. Therefore, this study was undertaken to address the lacunae mentioned earlier, which will provide significant insights into understanding the underlying molecular mechanism of FRG1's contribution towards tumorigenesis and angiogenesis of both hormone receptor-positive and negative breast cancer cells. We also emphasized identifying and assessing the therapeutic potential of the oncogenic mediators that are the direct targets of FRG1.

In the first objective (Sub Chapter 4A) of the thesis, we have unravelled that reduced FRG1 level in breast cancer patients negatively regulates the GM-CSF expression, which triggers MEK/ERK-mediated EMT, irrespective of molecular subtypes. Prior to this study, no information was available on the detailed mechanism of how GM-CSF promotes EMT in any

cancer. GM-CSF, a potent hematopoietic growth factor mainly known for its immunomodulatory function in the tumor niche, has recently been reported to play a role in EMT in colon cancer (30). Elevated expression of GM-CSF is clinically correlated with advanced histological grade, metastasis, and poor prognosis in patients with prostate cancer, breast cancer (31), and pancreatic ductal carcinoma (32). Nevertheless, little is known about the upstream regulation and downstream signaling mechanism coordinating GM-CSF-mediated metastatic colonization. Here we have shown that FRG1 binds to the GM-CSF promoter and inhibits its transcription. The loss of FRG1 resulted in increased cell proliferation, migration, and invasion triggered by increased levels of GM-CSF and the activation of the MEK/ERK pathway in both the molecular subtypes. We have also demonstrated that GM-CSF-mediated upregulation of ERK in FRG1-depleted cells subsequently reduces AKT and p53 phosphorylation, that results in ERK-dependent suppression of the apoptotic process.

In the second objective (Sub Chapter 4B), we have validated our *in vitro* findings in the mouse model. Here we have shown that decreased FRG1 levels enhanced the tumor volume through the activation of ERK, and elevated FRG1 levels had the opposite trend. Our findings indicate that reduced FRG1 levels gave a higher metastatic potential to the breast cancer cells *in vivo*. We have also shown the therapeutic potential of anti-GM-CSF antibody in the mouse model. Overall, the first two chapters summarize the role and molecular mechanism of FRG1 in breast cancer, which has the potential to be explored as a therapeutic target irrespective of the molecular subtype.

In the third objective (Sub Chapter 4C), we perturbed the expression of FRG1 in breast cancer cell lines and used the conditioned medium to study its effect on human endothelial cell properties relevant to angiogenesis. *In vitro* findings were further proven by the Matrigel plug and skin wound-healing assays in mice. Mechanistically we showed that FRG1 is the upstream regulator of FGF2, which eventually activated the AKT/ERK signaling axis in the endothelial

cells leading to angiogenesis induction. Collectively, across the three chapters, using multiple *in vitro* and *in vivo* systems, we have demonstrated that reduced FRG1 level affects tumorigenesis, EMT, and tumor angiogenesis, and we have also identified the underlying molecular mechanism.

To summarize the significance of our findings, we believe that our work provides a detailed understanding on the role of FRG1 in breast tumorigenesis and tumor angiogenesis. As FRG1 affects multiple processes implicated in breast tumorigenesis and affects multiple pathways regardless of molecular subtypes, it may open up new therapeutic approaches which have a lesser possibility of resistance development.

Chapter 2

Review of Literature

2.1. Breast Cancer Overview

Breast cancer is the most frequently diagnosed cancer (24.5%) (Fig. 2.1.1.A) and the leading cause of cancer-related mortality (15.5%) among women globally (Fig. 2.1.1.B). It is listed as the fifth major cause of cancer-associated deaths (6.9%) in both sexes combined (Fig. 2.1.1.C) (3).

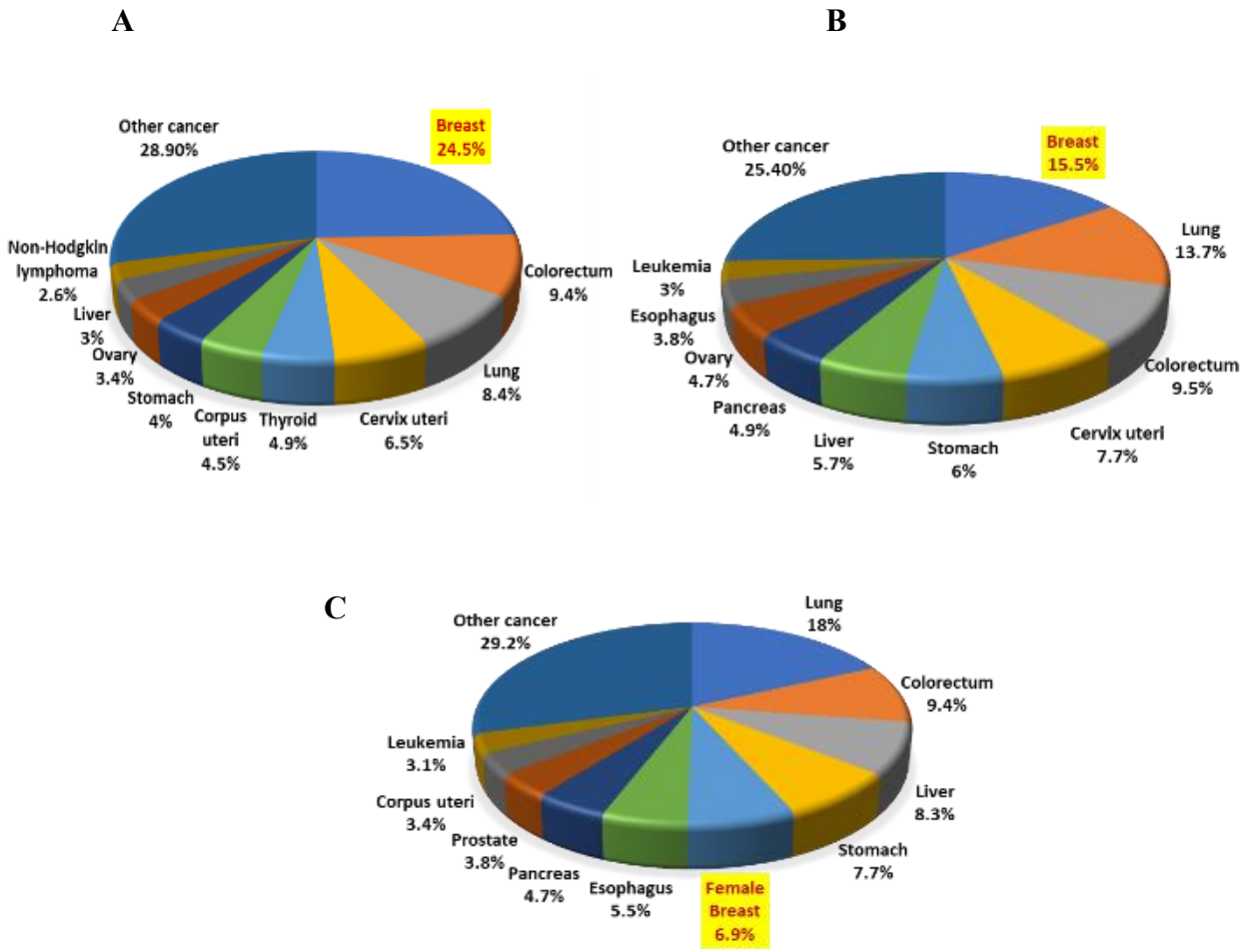

Figure 2.1.1. Distribution of cancer incidence and mortality for the top ten most common cancers in 2020. **(A),** *The pie chart depicts the percentage of cancer incidence (patients diagnosed with cancer) among the women, according to the GLOBOCAN 2020 data.* **(B),** *The pie chart illustrates the distribution of the mortality percentages in females due to cancer, as per the GLOBOCAN 2020 data.* **(C),** *The pie chart shows the percentage of women who died of cancer in both the sexes, based on the GLOBOCAN 2020 data.*

Overall, 2,261,419 (11.7% of all sites) new breast cancer cases were reported in 2020, with a total mortality of 684,996 (6.9% of all deaths) (3). The incidence rate of breast cancer is 88% higher in developed countries (55.9 per 100,000 women) compared to developing countries (29.7 per 100,000 women). In India, the age-adjusted occurrence of breast cancer is 25.8 per 100,000 women, with a mortality of 12.7 per 100,000 women (33). Overall, the statistics indicate the increasing global burden of cancer incidence and mortality.

Breast cancer is a heterogeneous disease that is categorized based on its histological traits or molecular characteristics. According to the presence of the hormone receptors, breast cancer is subdivided into five molecular subtypes such as luminal A (ER+PR+HER2-KI67-), luminal B (ER+PR+HER2-KI67+), HER2 overexpression (ER-PR-HER2+), basal (ER-PR-HER2-KI67), and normal like (ER+PR+HER2-KI67-) (34). Each group represents its own distinct morphology, different molecular characteristics, and discrete clinical outcome. Luminal breast carcinoma accounts for 64.3% of all breast cancers with a good prognosis (Fig. 2.1.2). HER2 overexpression group represents around 15% of all invasive breast cancer (Fig. 2.1.2). This type of breast cancer implies poor clinical outcome. Around 15% of breast cancers are comprised of the basal category, where the hormone receptors are absent (Fig. 2.1.2). Due to the lack of hormonal receptors, this group is the most therapeutically challenged and associated with more aggressiveness and poor prognosis.

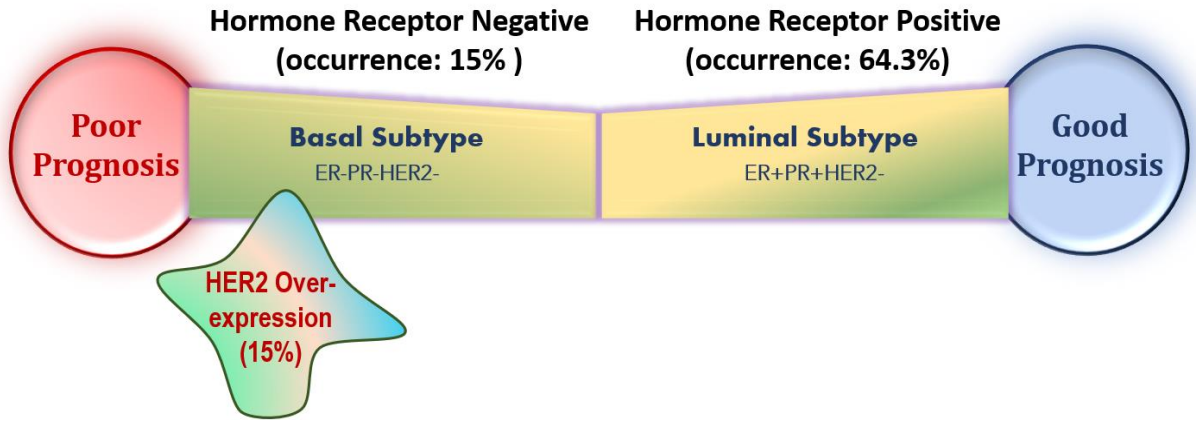

Figure 2.1.2. Classification of different subtypes of breast cancer. *The diagram demonstrates that breast cancer patients who are positive for hormone receptors (Luminal type: ER+PR+HER2-) have a better prognosis compared to the patients who lack hormone receptors (Basal type: ER-PR-HER2-).*

Normal like breast cancer have around 7.8% occurrence with intermediate clinical outcome (34). Histologically the cytoarchitectural features of breast cancer further classify it as ductal carcinoma or lobular carcinoma (35). Along with the conventional categorisation, some breast cancers are classified as extremely rare in occurrence. Invasive cribriform carcinoma (0.8%–3.5%), Mucinous carcinoma (2%) (35), Invasive papillary carcinoma 1%-2%), Invasive micropapillary carcinoma (2%), Apocrine carcinoma (1%-4%), Neuroendocrine carcinoma (2%), Metaplastic carcinoma (1%), Lipid-rich carcinoma (1%-1.6%), Secretory juvenile carcinoma (>0.15%), Adenoid cystic carcinoma (0.1%), fall in this group (35).

2.2. Breast Cancer Etiology

Breast cancer has an intricate etiology. Factors that contribute to the progression of breast cancer can be broadly classified as (a) genetic predisposition and (b) environmental factors (Fig. 2.2.1).

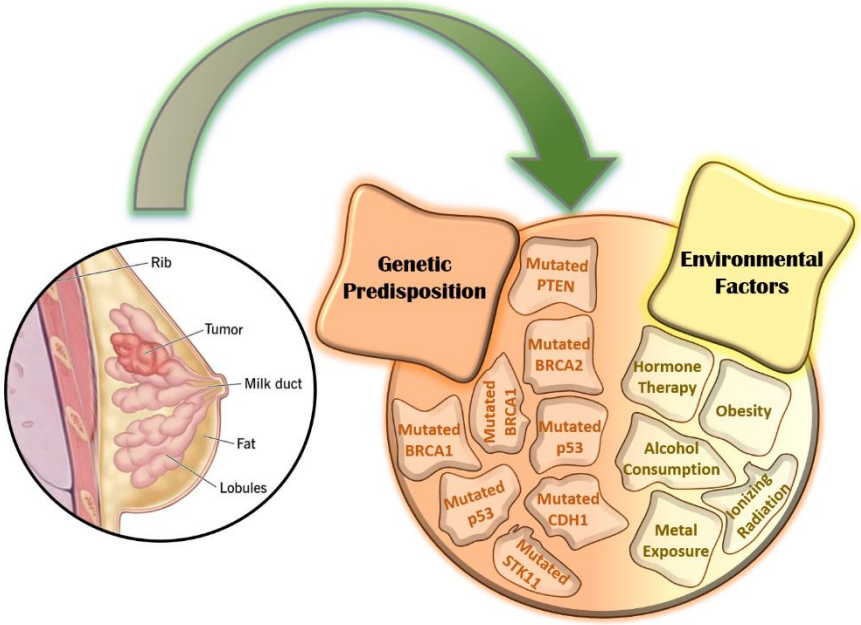

Figure 2.2.1. Factors associated with breast cancer. *The diagram illustrates several genetic and environmental mediators contributing to the development of breast cancer.*

(a) Genetic Predisposition: Several mutations have been linked with an increased risk of breast cancer. Genetic predisposition is involved in about 30% of breast cancer cases (36). Deletion or rearrangement in BRCA1 and BRCA2 genes are the most common causes of hereditary breast cancer (37). In normal cells, these genes aid in the production of proteins that repair DNA damage. Mutated forms of these proteins promote aberrant cell division leading to cancer. Mutation in BRCA1 or BRCA2 gene increases the risk of developing breast cancer 56%-87% by the age of 70 (38). Other major genes mutated in hereditary breast cancer are

PTEN, TP53, CDH1, and STK11 (36), (39). An additional 2%-3% of hereditary breast cancers are caused by the mutation in CHEK2, BRIP1, ATM, and PALB2 genes (36).

(b) Environmental Factors: Around 90% of breast cancer cases are associated with environmental exposures. Multiple environmental factors are responsible for the development and progression of breast cancer. Being a hormonally dependent malignancy, evidence suggests an association between consuming oral contraceptives and breast cancer (40). A combination of estrogen–progesterone hormone therapy at menopause also makes an individual susceptible to developing breast cancer (41). High body mass index and obesity accelerate the risk of post-menopausal breast cancer (42). More than 100 studies from different nations throughout the world, using case-control and cohort designs, have established alcohol intake as a causative factor in breast cancer (43).

Alcohol intake does seem to have a greater impact on ER+/PR+ cancers than ER-/PR- malignancies (44). *In vivo* studies using rodent model further corroborated the observation (45). However, there is little epidemiologic evidences linking metal exposure to breast cancer risks. Very few reports have documented that lead and cadmium exposure can raise the risk of developing breast cancer (46), (47), since these two metals harbour estrogenic effects (48). Other contributing components that may have an impact on breast cancer but not fully established are exposure from ionizing radiation (49), including computed tomography, radiographs, and fluoroscopy (50); Bisphenol A, Parabens, Phthalates, Polybrominated Diphenyl Ethers, Benzene, pesticides and polycyclic aromatic hydrocarbons (40).

2.3. Breast Cancer Pathogenesis

2.3.1. Epithelial to mesenchymal (EMT) transition: The major hallmark of cancer

Epithelial-mesenchymal transition (EMT) is a complex and dynamic process that enables polarised epithelial cells to adopt a mesenchymal phenotype, which involves enhanced migratory properties, invasiveness, augmented resistance to apoptosis, and significantly

increased production of extracellular matrix (ECM) components (51), (52) (Fig. 2.3.1.1). Most of the cancer-associated deaths are caused by EMT, which entails the detachment of cancerous cells from their primary origin, intravasation, and formation of metastatic nodules at distant sites (53). Multiple molecular pathways are involved in facilitating the event of EMT. These consist of the synthesis of the ECM degrading enzymes, activation of transcription factors, expression of particular microRNAs, alterations in the expression of specific cell-surface proteins, reorganization, and expression of cytoskeletal proteins (54).

A number of EMT-inducing transcription factors, including Snail, Slug, HGF, EGF, PDGF, TGFβ, ZEB1, Twist, Goosecoid, and FOXC2, appear to be induced or functionally activated in cancer cells as a result of signals coming from the tumor-associated stroma (55), (56), (57), (58), (59). Activation of these transcriptional factors can act pleiotropically to coordinate the intricate EMT program.

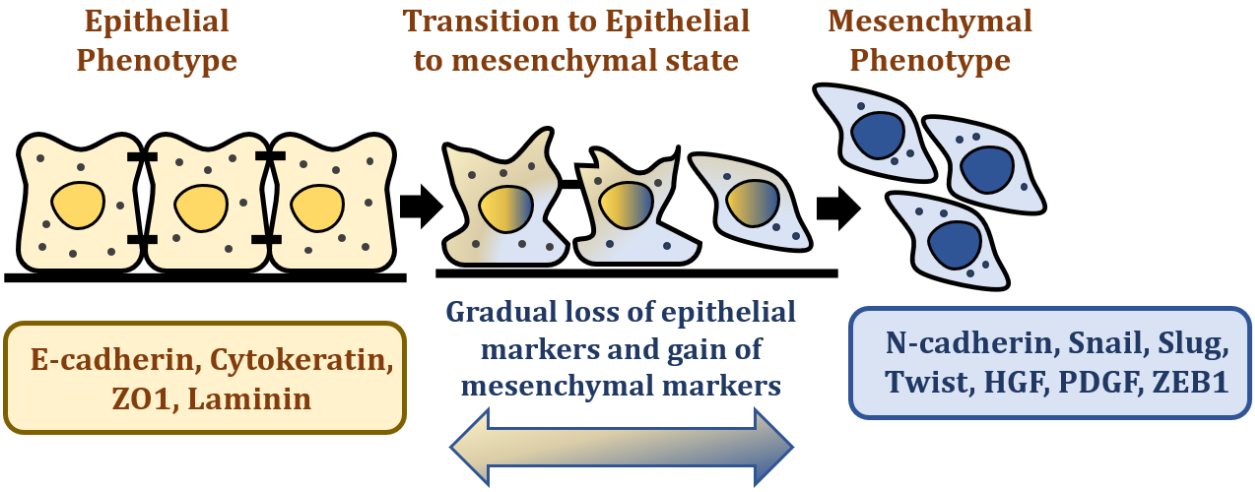

Figure 2.3.1.1. Steps of epithelial to mesenchymal transition. *Pictorial representation of the cells undergoing epithelial to mesenchymal transition. The image shows that several epithelial markers such as E-cadherin, Cytokeratin, ZO1, and Laminin are expressed by the epithelial cells. The process of EMT is characterized by the gradual loss of epithelial markers and*

acquisition of mesenchymal markers. In the mesenchymal state, cells express numerous mesenchymal markers: N-cadherin, Snail, Slug, Twist, HGF, PDGF, and ZEB1.

2.3.1.1. EMT in breast cancer

EMT underlies 90% of deaths related to breast cancer (60). The complex process of EMT enables breast cancer cells to acquire stem cell-like characteristics, chemoresistance, enhanced migration, and invasion abilities (Fig. 2.3.1.1.1) (61). The development and clinical outcome of mesenchymal traits vary among different subtypes of breast cancer. Compared to the more differentiated luminal phenotype, patients with triple-negative breast cancer, which mimics the undifferentiated phenotype similar to the normal mammary stem cells, had a worse prognosis and a higher prevalence of EMT within three years after diagnosis (62) (63). Among the several transcriptional factors that promote EMT, Snail, and Twist can trigger the EMT cascade in human immortalized human mammary epithelial cells (64) (65). Moreover, $CD44^{high}/CD24^{low}$ cells isolated from normal and neoplastic human tissue samples exhibit elevated expression of EMT markers CDH2 (N-cadherin), FN1 (Fibronectin), ZEB2 (SIP1), FOXC2, SNAIL1 (Snail), SNAIL2 (Slug), Twist 1/2, as well as low level of CDH1 (E-cadherin) transcripts (64). TGF-β, Notch, Wnt, Hedgehog, and receptor tyrosine kinases are the major endogenous signaling pathways that orchestrate the EMT event. Exogenous signals from various sources, including the extracellular matrix, directly affect endogenous pathways and tumor microenvironment, which promote EMT in a paracrine manner.

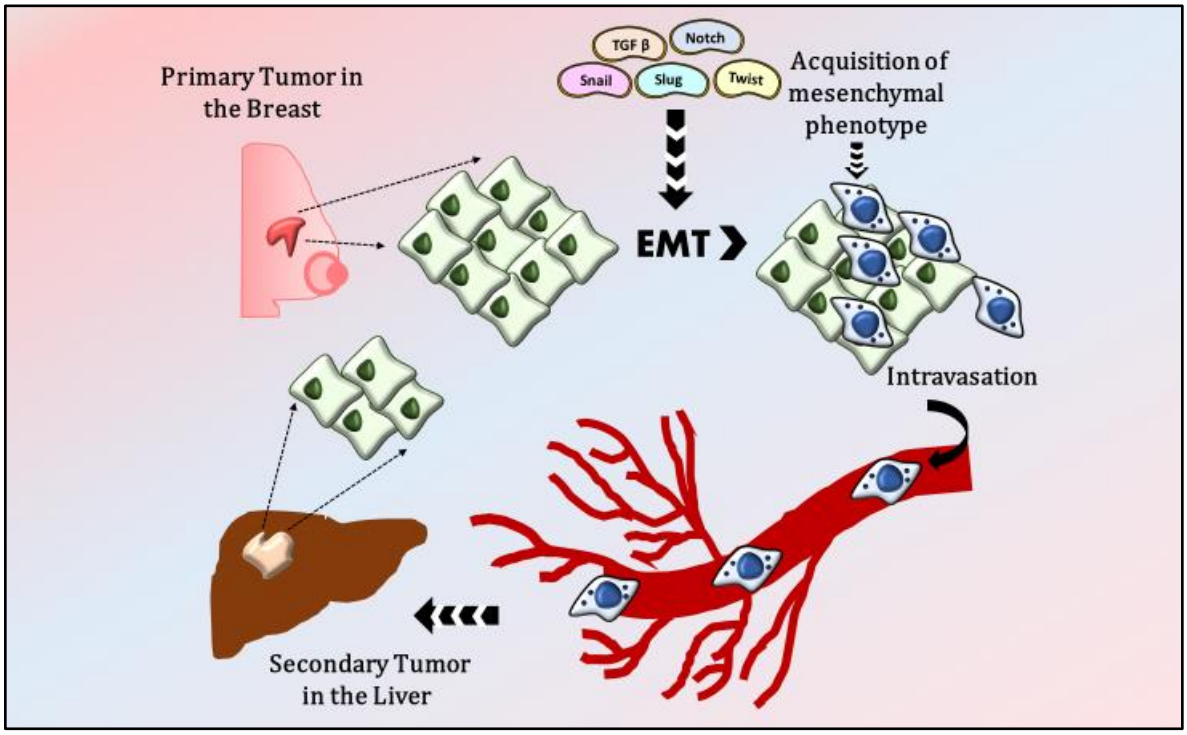

Figure. 2.3.1.1.1. EMT enables the metastatic dissemination of breast cancer cells. *Pictorial representation shows that breast cancer cells acquire mesenchymal characteristics due to the activation of the genes Snail, Slug, Twist, TGF β, and Notch. These mesenchymal cells invade the endothelial cell barriers and come to the blood circulation. Through the blood circulation, these cells invade other fresh tissues and form secondary tumors.*

2.3.1.2. Therapeutic strategy targeting breast cancer EMT

Inventing therapeutic strategies targeting breast cancer EMT has occupied the scientists for decades. Since the relationship between the EMT program and the cancer stem cell (CSC) state offers an alluring prospect for therapeutic development, EMT inhibitors may be used to treat CSC-enriched breast cancer subtypes like the claudin-low group, which are highly aggressive and clinically resistant to chemotherapy. Differentiation therapy involving activation of adenosine 3',5'-monophosphate, and protein kinase A (PKA) might induce tumor-initiating

cells (TICs) via histone demethylase PHF2 to undergo epigenetic reprogramming leading to mesenchymal-to-epithelial transition (MET) in mesenchymal human mammary epithelial cells (66). Furthermore, *in vitro* and *in vivo* findings in the triple-negative breast cancer (TNBC) model suggest the potential role of Mangiferin, a naturally occurring glucosylxanthone, in reversing the EMT process by lowering the level of matrix metalloproteinase (MMP)-7 and -9 and inhibiting β-catenin pathway (67).

Another possible treatment approach for EMT involves using monoclonal antibodies or oligonucleotide aptamers that can bind to the proteins on the surface of cancer cells and prevent them from adhering to the extracellular matrix via integrins. Anti-EGFR CL4 aptamer treatment in the TNBC cell line impairs the integrin αvβ3-mediated cell adherence on matrigel by preventing the interaction between matrix-induced integrin αvβ3 and EGFR (68).

Trastuzumab, a monoclonal antibody against HER2, is reported to possess a comparable impact by promoting the loss of integrin αvβ6 and HER2 in breast cancer xenografts (69). The targeted delivery of therapeutic siRNAs or medications to breast cancers utilizing aptamers as delivery vehicles is an additional intriguing aptamer-based strategy. The combination of aptamers that target EpCAM, and siRNAs that target PLK kinase, necessary for mitosis, has been demonstrated to block CSCs and promote tumor regression in the TNBC xerograph model (70). Targeted delivery of tumor-promoting exo-miRNAs or replenishing the tumor-suppressive miRNAs are also reported as potential metastatic suppressors of breast cancer. Studies show miR520c can repress the STAT3-mediated EMT progression in luminal cell line MCF7 (71). Ectopic expression of miR-200c in the p53 null-claudin low breast tumor model exhibits a disruption in EMT, accompanied by decreased cell proliferation and enhanced sensitivity to chemotherapy (72). Reduction of miR-10b in mice model corresponds with decreased EMT by targeting twist (73). Hence, blocking the EMT cascade is a potential approach to treat breast

carcinoma. Targeting EMT can be useful, particularly in the case of basal breast carcinoma, where targeted therapy is not an option.

2.3.2. Angiogenesis: An inevitable process in normal physiology and cancer

Angiogenesis is the process that gives rise to new blood vessels from pre-existing venules. In normal physiology, angiogenesis is an indispensable phenomenon since it provides adequate nutrients to the healing or developing tissue during wound healing, reproduction, or embryonic development. In healthy cells, a dynamic equilibrium between several pro-angiogenic and anti-angiogenic factors allows the dormant endothelial cells to divide in a monolayer and unfurl the circulatory network as far as it is necessary to meet the needs of growing tissues. During early embryogenesis, endothelial cell precursors or angioblasts differentiate to form the primitive vascular plexus from the mesoderm (74). Once the primary capillaries are formed, various soluble angiogenic factors such as VEGF, FGF, PDGF, and ANG stimulate the newly generated endothelial cells to form new capillaries by sprouting or splitting in the process of angiogenesis (75). However, in normal tissue, the endothelial cell proliferation rate is minimal and occurs only if the body needs it during the menstruation cycle or physiological repairing (76). The coordination among several angiogenic factors that lead to the maturation and modification of the newly formed microvessels are outlined in Table 2.3.2.1 (77).

Table 2.3.2.1: Overview of different angiogenic modulators #

Category	Names	Major functions
Proteolytic enzymes	(i) Matrix metalloproteinases (MMPs): matrilysin (MMP-7), interstitial collagenase (MMP-1), neutrophil collagenase (MMP-8), collagenase-3 (MMP-13), stromelysin-1 (MMP-3), stromelysin-2 (MMP-10), stromelysin-3 (MMP-11), metalloelastase (MMP-12), MMP-19, enamelysin (MMP-20), gelatinase A (MMP-2), gelatinase B (MMP-9), MT1-MMP (MMP-14), MT2-MMP (MMP-15), MT3-MMP (MMP-16), MT4-MMP (MMP-17) (ii) Plasminogen activators (PAs)	MMPs; taking different substrates according to MMPs; substrates can be collagen, gelatin, laminin, fibronectin, proteoglycans, and proMMPs
Angiogenesis inducers	Vascular endothelial growth factor family (VEGF-A or VEGF, PlGF, VGGF-B, VEGF-C, VEGF-D, orf virus VEGF or VEGF-E), fibroblast growth factor family (aFGF, bFGF, etc.), angiopoietin 1 (Ang-1), transforming growth factor-alpha/beta (TGF α/β), platelet-derived growth factor (PDGF), hepatocyte growth factor/scatter factor (HGF/SF), tumor necrosis factor-alpha (TNFα), interleukin-1/8, angiogenin, ephrins, integrins $\alpha_v\beta_3$, $\alpha_v\beta_5$, $\alpha_5\beta_1$, cyclooxygenase-2 (COX-2)	(i) Induction of EC proliferation, migration, and differentiation (ii) TGF-β shows opposite effect in some contexts
Angiogenesis inhibitors	Thrombospondin-1/2 (TSP-1/2), angiostatin (plasminogen fragment), endostatin (collagen XVIII fragment), vasostatin (calreticulin fragment), tumstatin, platelet factor-4 (PF4), antiangiogenic antithrombin III, kringle 5 (plasminogen fragment), prolactin 16-kD fragment, fragment of SPARC, 2-methoxyestradiol, metalloproteinase inhibitors (TIMPs), interferon-alpha/beta/gamma (IFN $\alpha/\beta/\gamma$), interleukin-12 (IL-12), IP-10, Ang-2	(i) Inhibit EC proliferation/migration (ii) Induce EC apoptosis (iii) TIMPs: inhibit MMP or uPA activity (iv) Ang-2: inhibit blood vessels maturation, antagonist of Ang-1

Table is adapted from the reference 77

The multistep process of angiogenesis comprises the following events (Fig. 2.3.2.1). At first, numerous angiogenic stimuli boost the proliferation and permeability of endothelial cells to support the lengthening of the new capillary sprout. In the second step, matrix metalloproteases, in association with plasminogen activators, start proteolytic degradation of the basement membrane and extracellular matrix (78). Lastly, the endothelial cells proliferate and migrate to form the tubular structure. Smooth muscle cells in the bigger arteries and pericytes in the microvessels are drawn to the abluminal surface of the endothelium cells.

Adherent junctions and basement membranes are built to support the blood flow through the capillaries.

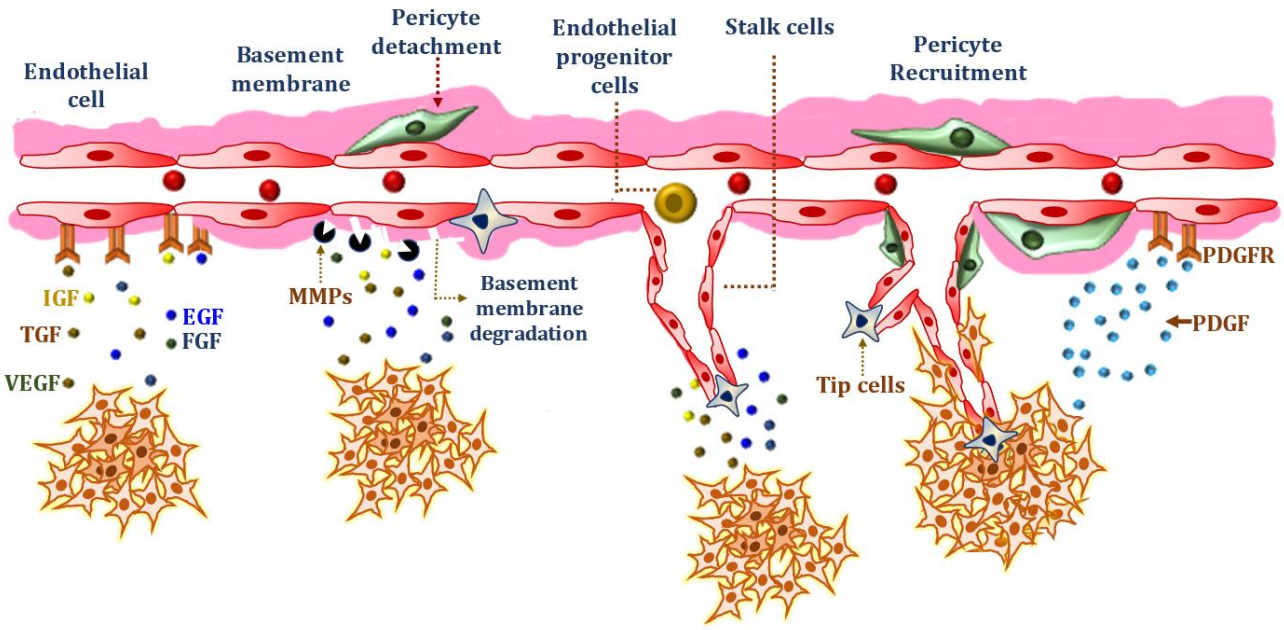

Figure 2.3.2.1. Multiple events during angiogenesis. *Firstly, several angiogenic stimuli enhance the permeability and proliferation of endothelial cells. Secondly, MMPs and plasminogen activators promote the proteolytic degradation of the basement membrane. Thirdly, endothelial cells move away from the existing capillaries and proliferate. In the fourth step, the migrating endothelial cells form the tubular structure of new blood vessels. In the last step, Angiopoietin, and TGF β recruit pericytes and stabilize the newly form vessels through the construction of adherent junctions, endothelial cells, and the basement membrane.*

Unbalanced angiogenesis can cause numerous pathogenesis ranging from cancer, macular degeneration, ischaemic heart disease, diabetic retinopathy, myocardial infarction, coronary artery disorders, rheumatoid arthritis, and chronic wounds (79). To meet the requirement of

aberrant growth and proliferation, tumor cells largely depend on angiogenesis for an adequate supply of oxygen and nutrients (80). Without angiogenesis tumor, cells undergo remission after a certain size (2-3 mm^3) (77). Although tumor induced neovascularization is somewhat similar to normal angiogenesis, they harbour numerous structural abnormalities. Unlike the well-differentiated normal vessels, the luminal surface of the tumor vasculature represents a 'mosaic' vessel made up of endothelial cells and tumor cells (81). They often branch irregularly, evasive, convoluted, and hyperpermeable (82). The tumor vasculature has aberrant bulges, blind ends with a broken endothelial cell lining, and a dysfunctional basement membrane in addition to the absence of functional pericytes (82) (75). To facilitate the blood vessels formation, tumor cells recruit bone marrow-derived endothelial cell progenitors that resemble the angioblasts of normal vasculature (83).

2.3.2.1. Key regulators of angiogenesis

Disruption in the equilibrium between the positive and negative angiogenic regulators during tumor angiogenesis causes a switch to the angiogenic state and expands the microvessels. Amongst the various angiogenic mediators, the synergistic effect of VEGF and bFGF are the most well-established (84), (77).

2.3.2.1.1. Role of VEGF superfamily members in angiogenesis

The elevated level of VEGF has been reported in breast cancer (85), renal cancer (86), ovarian cancer (87), and lung cancer (88). Disruption of the VEGF gene results in embryonic lethality in mice model, accompanied by severe developmental abnormalities and impaired angiogenesis (89). Five members of the VEGF superfamily (VEGFA, B, C, D, Placental growth factor or PlGF) are found to exert their effect on endothelial cells survival, proliferation, migration, and invasion by binding to the VEGF receptors (90). VEGFA, a 45 KD heparin-binding homodimeric mitogenic glycoprotein, is the most characterized member of the VEGF family. VEGFA is reported as one of the most potent angiogenic stimulators. (91). Alternative

splicing of VEGFA mRNA generates four isoforms having 121, 165, 189, and 206 amino acids, respectively ($VEGF_{121}$, $VEGF_{165}$, $VEGF_{189}$, $VEGF_{206}$). (92). VEGFA associates with its receptor VEGFR1 or VEGFR2 (mostly VEGFR2) and promotes angiogenesis by enhancing endothelial cell proliferation, proteolytic activity, migration, and microvascular leakage (93). Compelling pieces of evidence suggest an inconsistent role of VEGFB in angiogenesis. Some studies report that VEGFB promotes angiogenesis (94), (95), whereas some others propose the dispensable role of VEGFB in angiogenesis (96), (97). VEGFB controls vascular survival under pathological conditions (98). VEGFB-deficient homozygous mice ($VEGFB^{-/-}$) show a mild cardiac effect with no overall implication in angiogenesis (99). On the other side, VEGFC, D, and their receptor VEGFR3 are mostly reported to be a critical regulator of lymphangiogenesis, and also possess a role in angiogenesis at early embryogenesis (100). VEGFC (101) and D (102) are well reported to induce vascular permeability.

2.3.2.1.2. Signal transduction through VEGF and their receptors

VEGF signaling cascade initiates after the binding of soluble VEGF ligands to the receptor tyrosine kinase (RTK) superfamily of proteins known as VEGFR1, VEGFR2, and VEGFR3 present on the endothelial cells (90). VEGFA, VEGFB, and PlGF bind to the N-terminal domain of VEGFR1 in response to the angiogenic stimuli (103), (104). Hypoxic condition promotes VEGFA production by the binding of hypoxia-inducible factor (HIF) to the hypoxia response element (HRE) of the VEGF promoter (105). Low-oxygenated tumor core utilizes this mechanism and ensures uninterrupted vascular supply. The binding of VEGFA/PIGF heterodimer to VEGFR1 stimulates the PI3K/AKT signaling axis (106). VEGFR2-VEGFA signaling axis facilitates endothelial cell migration through focal adhesion kinase (FAK) (107), endothelial cell survival via the PI3K/AKT pathway (108), proliferation of endothelial cells by PLCγ (109), and division of endothelial cells by the Raf-MEK-MAP kinase cascade (110). VEGFA-mediated activation of VEGFR2 also regulates vascular permeabilization (111)

through the recruitment of FAK. Activated VEGFR2 promotes the reorganization of the actin cytoskeleton via the p38-MAPK pathway (112).

Interestingly VEGFR3 is the only member of the VEGFR family for which naturally occurring mutations have been found, and its implications have been described in lymphatic dysfunction causing primary lymphoedema (113). The effect of elevated VEGFR3 and its ligand VEGFC is associated with upregulated lymphangiogenesis and metastatic spread in mice model (114). The binding of VEGF /VEGF to VEGFR3 corresponds with the activation of VEGFR3 mediated downstream signaling event by phosphorylating at Tyr^{1063},Tyr^{1068}, Tyr1230, Tyr^{1231}, Tyr^{1265}, Tyr^{1337}, and Tyr^{1363} sites (90). Phosphorylation at Tyr^{1063} causes recruitment of CRKI/II to the activated VEGFR3 receptor that finally stimulates the c-Jun N-terminal kinase-1/2 (JNK1/2) pathway via the mitogen-activated protein kinase kinase-4 (MKK4) (115). This process contributes to the pro-survival signaling of human umbilical vein endothelial cells via VEGFR3. Activation at $Tyr^{1230/1231}$ sites along with Tyr^{1337} directly employs growth factor receptor–bonus protein (GRB2) to the VEGFR3 and arbitrates the survival, proliferation, and migration of primary endothelial cells cell by activating both the AKT and ERK pathway (115). In human primary microvascular endothelium derived lymphatic endothelial cells, VEGFC/D associates with their receptor VEGFR3 to direct their survival, growth, and migration via protein kinase C-mediated activation of the p42/p44 MAPK pathway (116).

2.3.2.1.3. Role of FGF superfamily members in angiogenesis

The members of the FGF superfamily comprise 22 proteins, 18 of which are involved in triggering several biological processes, including angiogenesis, cell proliferation, metabolism, tissue regeneration, cell survival, and differentiation by binding to 4 receptor tyrosine kinases (FGFR 1-4) (117). In the 1970s, the first two fibroblast growth factor (FGF) family members, FGF1 and FGF2, were identified and known as acidic and basic FGF, respectively (118). Elevated expression of FGF1/2 transcripts is associated with hepatocellular carcinoma (HCC)

(119), prostate cancer (120), (121), and oral squamous cell carcinomas (122). Upregulation of FGF2 is correlated with poor clinical outcomes in small cell lung carcinoma (SCLC) (123) and bladder cancer (124).

Compelling evidence suggests the involvement of FGF1 and FGF2 in angiogenesis (125). Inhibition of FGF2 by anti-FGF2 neutralizing antibody prevents neovascularization in CAM assay, which supports the crucial role of FGF2 in the vascular development of chick (126). Similarly, the pro-angiogenic effect of FGF2 has been elucidated in a dose-dependent manner in rabbit cornea (127) and mice (125). Besides inducing the expression of VEGF, FGF2 may elicit angiogenesis independent of VEGF (128). However, the lack of significantly impaired angiogenesis in genetically knockout FGF2 mice shows that FGF2 alone is insufficient to elucidate the angiogenesis process (129). Conversely, transgenic mice with ectopic expression of FGF2 show vascularized cysts with significantly increased angiogenesis (130).

Available literature reports FGF2 as the most potent pro-angiogenic mediator among the FGF superfamily (125). Among the other members of the FGF family, FGF4 has been reported to induce therapeutic angiogenesis, vascular permeability, and arteriogenesis when administrated into rabbit hind limb ischemia using the adenoviral gene transfer method (102). In situ hybridization and immunohistochemistry detect the expression of FGF4 in neural cells near the proliferating vascular cells, further supporting the angiogenic properties of FGF4 *in vivo* (131). FGF7, or keratinocyte growth factor (KGF), induces endothelial cell proliferation and migration and stimulates angiogenesis in avascular rat cornea (132). The effect of FGF8b in eliciting the angiogenic response has been proved using *in vivo* CAM and in *vitro* immortomouse brain capillary endothelial cells (IBEC) assay (133). The same report also suggests that the potential of FGF8b to promote tumor growth in murine breast cancer cells S115 is likely significantly influenced by its angiogenic capacity. Besides harboring a role in fastening wound healing, FGF10, the structurally similar resemblant of KGF7, has pro-

migratory effects in bovine capillary endothelial cells (132). Human breast cancer cells MCF10A with ectopic expression of FGF3 has been found to promote neovascularization in CAM assay (134). Administration of conditioned medium harvested from the same cells leads to the formation of capillaries from the pre-existing mesenteric blood vessels in the rat mesentery (134). Endothelial cell proliferation, migration, and degradation of the extracellular matrix represent some imperative events during angiogenesis. FGF1, FGF2, and FGF4 mediated activation of FGFR1 or FGFR2 promotes endothelial cell proliferation (135), (136). FGF1, FGF2, and FGF4 enhance extracellular matrix degradation by uplifting the expression of MMPs and urokinase-type plasminogen activator (uPA) (125). FGFs modulate endothelial cell migration by promoting uPA cell surface receptors on endothelial cells that permit proteolytic activity at the leading edge of the cells (137).

2.3.2.1.4. Signal transduction through FGFs and their receptors

The binding of FGFs to FGF receptors (FGFR) result in their dimerization followed by autophosphorylation that leads to the activation of various signaling cascades such as RAS-MAPK, PI3K-AKT and phospholipase Cγ (PLCγ) (138). Compared to 22 types of FGFs, only four types of FGFRs have been discovered so far. However, alternative splicing and exon skipping in FGFR1, FGFR2, and FGFR3 contribute to receptor diversity by generating multiple receptor isoforms with altered specificity for FGF binding (139). FGFRs are the tyrosine kinases expressed on the cell surface. They are composed of an N-terminal extracellular domain consisting of three IgG-like domains: IgI, IgII, and IgIII; a transmembrane domain containing a single α-helix and an intracellular tyrosine kinase domain (140). The IgIII domain is one of the most crucial determining factors for alternative splicing. The invariant IgIIIa exon of the FGFR1, FGFR2, and FGFR3 IgIII domain is alternatively spliced to generate either IgIIIb or IgIIIc. This process also determines the receptor specificity of FGFs during signal transduction (124).

FGFs are small polypeptides primarily found in the extracellular matrix, where they interact with heparin and heparan sulphate proteoglycans and endure in an inactivated form (141). Bound FGF1/2 get activated and presented to their receptors by Fibroblast growth factor-binding protein (FGF-BP) (141). Lack of FGF availability keeps the FGFR in a nascent monomeric form on the cell membrane (142). Upon binding to their ligands, FGFRs undergo a conformational change that dimerizes two FGFRs. This dimerization places the tyrosine kinase domains of the two receptor molecules so close together that their kinase domains get auto-phosphorylated, and receptor activation takes place (142). This activation subsequently phosphorylates FGFR substrate a (FRS2a) and FGFR substrate b (FRS2b) and facilitates the binding of FRS2b to growth factor receptor-bound protein 2 (GRB2). In the next step, when this GRB2 interacts with SOS, GRB2-associated-binding protein 1 (GAB1) and Casitas B-cell lymphoma (CBL) protein, as a consequence, FGFR mediated signal transduction through Ras, Raf, ERK, P38, JNK, PI3K occurs (143). Numerous genetic alterations ranging from mutation, amplification, and translocation of the FGFR gene cause aberrant FGFR activation (144). So far, seven tyrosine residues in FGFR1 (Y577, Y760, Y770, Y724, Y463, and Y730) have been discovered that show autophosphorylation (145). Many of these sites are conserved in other FGFRs, too (146). The specific signal transduction initiated by the FGF-FGFR determines whether the biological outcome will be proliferative, apoptotic, or migratory. Generally, the FGF/FGFR-mediated MAPK signaling is responsible for cellular growth and differentiation; The PI3K/AKT cascade is implicated in cell survival and fate determination; and the PI3K-PKC controls the cellular polarity (124). Studies indicate that Y724 of FGFR3 is the most potent residue to activate the p44/42 MAPK (ERK), PI3K, STAT1, STAT3, and Shp2-mediated cellular transformation in HEK 293T cell line (146). FGFR1 is the primary receptor expressed on endothelial cells, followed by FGFR2 (147), (148). FGF2 stimulates the activation of p38-MAPK and Notch ligand Jagged 1 (147). Although the p38 signaling plays a role in blood

vessel maturation, alternatively, negative regulation of p38-MAPK pathway in FGF2-mediated angiogenesis and endothelial cell proliferation, and survival is also reported (149). Vascular endothelial cells experience a coordinated set of changes in their interactions among themselves and also with the extracellular matrix elements during angiogenesis. FGF2 can alter the expression of several integrins, including αvβ3, by modulating the synthesis of alpha or beta subunits in microvascular endothelial cells (150). FGF2 reduces the adhesion between the endothelial cells to facilitate migration during angiogenesis (151), (152).

2.3.2.2. Therapeutic strategy targeting breast cancer angiogenesis

In preclinical models, hyperplastic breast papillomas and normal breast lobules adjacent to cancerous breast tissue in mice exhibit neovascularization, demonstrating the indispensable role of angiogenesis in transforming hyperplasia into malignancy in breast carcinoma. Tumor cells undertake necrosis or even apoptosis due to inadequate vascular circulation (153), (154). Hence, developing anti-angiogenic inhibitors has always been of much research interest (155).

There are numerous therapeutic strategies for reducing angiogenesis, most of which target the VEGF, VEGFR, FGF, or FGFR employing monoclonal antibodies or small-molecule tyrosine kinase inhibitors (156). Despite VEGF targeting chemotherapy treatments greatly enhancing patient survival, they frequently lose their efficacy due to evasive resistance of the patient, cross-talks with another signaling that leads to the initiation of EMT, or innate VEGF inhibitor resistance (157). To compensate this problem, multiple FDA-approved regimens targeting FGF or FGFR are available (158), (159). FGF inhibition therapy also frequently triggers additional membrane signaling cascades, such as ERBB3, EGFR, and MET, which do not benefit patient survival (159).

Bevacizumab (Avastin, Roche Genetech) has emerged as the first humanized recombinant anti-VEGF monoclonal antibody that specifically binds to all the circulating isoforms of VEGF and

inhibits the VEGF-mediated angiogenic signaling (160). In 2005, Miller *et al.* showed the efficacy of Bevacizumab in metastatic breast cancer treatment (161). In the treatment of metastatic breast cancer, only Bevacizumab has demonstrated statistically significant therapeutic advantages (162). Ramucirumab (Cyramza, ImClone) has been developed targeting VEGFR2 (163). Although treating gastric, colon, and non-small cell lung carcinoma patients with Ramucirumab and the conventional chemotherapeutic drugs were approved by US FDA in 2014, in the case of metastatic breast cancer, its efficacy is yet to be studied thoroughly (164), (156). Few clinical trials suggest no difference in the overall survival of breast cancer patients after treatment with Ramucirumab (165), (166), (162).

Small molecule tyrosine kinase inhibitors (TKIs), which act on these receptors' intracellular domain and restrict the catalytic activity of these receptors, are frequently being used in clinical studies to treat breast cancer by inhibiting angiogenesis (156), (167). Early clinical trials on breast cancer patients revealed a limited efficacy for Sorafenib (Nexavar, Bayer), the multikinase inhibitor of VEGFR, PDGFR, and Raf (168). In renal carcinoma, hepatocellular cancer, and thyroid cancer, Sorafenib has been proven to show considerable clinical benefits (169), (170). Sunitinib (Sutent), another multi-targeted oral anti-angiogenic agent against VEGFR1/2 and PDGFR α/β, has been found effective in renal cell cancer, gastrointestinal stromal tumors, and pancreatic neuroendocrine tumors (171), (172). However, in breast cancer, Sunitinib is associated with adverse side effects and no improved survival benefits (173), (174). Patients with recurrent or metastatic breast cancer demonstrated acceptable toxicities and favorable results when given the oral form of Pazopanib (Votrient), which targets the VEGFR, PDGFRs, FGFR, and c-KIT (175). Preclinical and clinical studies involving anti-angiogenic therapeutic regimens targeting FGF or FGFR include Levatinib, Anlotinib, and combinational administration of Infigratinib + Bevacizumab, Lenvatinib and Gefitinib (176). However, their efficacy in breast cancer remains limited and has to be explored further.

2.4. Breast cancer and apoptosis

In addition to unrestricted cellular proliferation, reduced apoptosis significantly contributes to breast cancer progression (177). Apoptosis is a process of programmed cell death wherein cells are designed to perish once they are detected to be cellularly damaged (178). Numerous conventional morphologies include cell shrinkage due to cleavage of lamins and actin filaments in the cytoskeleton, the disintegration into membrane-bound apoptotic particles, and subsequent phagocytosis by surrounding phagocytic cells, distinguish the apoptotic cells (Fig. 2.4.1) (179).

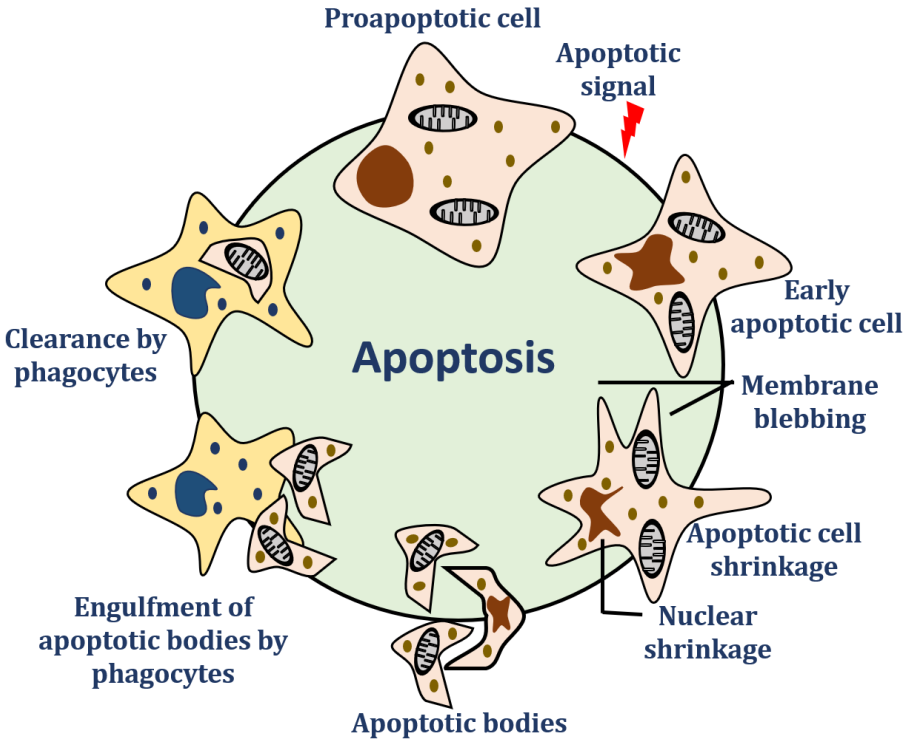

Figure 2.4.1. Overview of the apoptotic cell death. *Graphical representation summarizes the morphological changes during different stages of apoptosis. Following the apoptotic signals, pro-apoptotic cells start to shrink. The disintegration of the chromatin leads to nuclear condensation, and blebbing is found in the cell membrane. The process of cell shrinkage*

continues until the cells break into multiple fragments, called the apoptotic bodies. Subsequently, these apoptotic bodies are engulfed by the phagocytic macrophages.

The two primary mechanisms that make up apoptosis are the death receptor pathway (extrinsic pathway) and the mitochondrial pathway (intrinsic pathway), both perpetuated by a caspase cascade that ultimately induces apoptosis (180).

Apoptosis is crucial to each stage of ductal morphogenesis, involution, and lactation in the normal breast's development (181). Aberrant regulation of several proapoptotic and anti-apoptotic proteins leads to their disrupted balance and play a significant role in breast tumorigenesis (182). The significance of different factors those are essential to apoptosis, are discussed below.

2.4.1. Key regulators of apoptosis in breast cancer

The crucial mediators of the apoptosis process encompass the Bcl-2 protein family (178), transcriptional factors that include p53 (183), NF-κβ (184), the ubiquitin-proteasome system (182), PI3K, IAPs, and so on. Bcl-2 protein members are one of the most important regulators of apoptosis (185). Pro-apoptotic proteins of the Bcl-2 family comprise of Bax, Bak, Bad, Bcl-Xs, Bid, Bik, Bim, and Hrk, whereas anti-apoptotic participants include Bcl-2, Bcl-XL, Bcl-W, Bfl-1, and Mcl-1 (186). Anti-apoptotic members of the Bcl-2 protein family suppress apoptosis by preventing the release of cytochrome c (187). Bcl-2 protein is expressed in about 70% of breast cancer patients (188), and is associated with better survival (189).

Expression of mutant p53 in MCF7 cells reduced the expression of Bcl-2 protein (190) and associated with poor prognosis (191). The tumor suppressive activity of p53 is significantly regulated by the MEK/ERK pathway (192). Anti-apoptotic nature of ERK is widely reported (193), (194). Inhibition of the ERK signaling induces the activation of p53 and upregulates its

downstream pro-apoptotic members p21 and Bax in MCF7 cells (192). Activation of the ERK pathway acts as a transcriptional activator of Mdm-2, which is a negative regulator of p53 (195). Thus, ERK inhibits apoptosis by facilitating the Mdm-2-mediated degradation of p53. The important connection between apoptosis and its aforementioned regulators has gained more research interest in developing inhibitory drugs that target the anti-apoptotic machinery during tumorigenesis.

2.4.2. Targeting apoptosis in patients with breast carcinoma

Selecting adjuvant therapy that assures the most benefits and least side effects is the major concern in treating breast cancer (177). The equilibrium between apoptosis and proliferation is crucial in deciding the progression or remission of tumor in the course of chemotherapy, radiotherapy, and hormonal treatments (196), (197). In breast carcinoma, targeting the caspase cascade, Bcl-2 family proteins, and other apoptosis-related factors has evolved as the major therapeutic strategy (198). More than 50% of human malignancies, including breast cancer, are reported to be eradicated with the use of therapeutic drugs intended to restore the normal activity of the apoptotic signalling pathways (199). Bcl-2 inhibitors including Flavipirodol, Gossypol, Depsipeptide, ABT-737, ABT-264, Fenretinide, HA 14-1, and GX15-070 are some of the small molecules that inhibit BCl-2 by reducing their expression (200), (201), (202). Among the other small molecule-based therapeutics that restore the p53 function, CP-31398 (203) and Phikan083 (198) has attracted considerable clinical interest. CP-31398 interacts with the p53-bound DNA, leading to destabilisation of the p53-DNA interaction, which ultimately restores the p53 function (203). Phikan083 is a carbazole derivative that has the ability to restore mutant p53 (198). Nutlins, Tenovins, and MI-219 are examples of small molecules that disrupt the interaction between p53 and MDM2 and protect p53 from MDM2-mediated degradation (204), (205), (206). Finding out novel upstream regulators of ERK can aid more in the development of chemotherapeutic drugs targeting apoptosis.

2.5. FSHD Region Gene 1 (FRG1)

The human FSHD region gene1 (FRG1) was discovered in 1996 during exploring the genes in the distant region of human chromosome 4q35, which houses the locus for facioscapulohumeral muscular dystrophy (FSHD) (207). The mature FRG1 transcript is 1042 bp long and holds nine exons corresponding to the protein having 258 amino acid residues (207). FRG1 is surrounded by a group of genes called ANT1, FRG2, and DUX4, potentially related to FSHD (208). Putative structural analysis revealed the possible presence of a lipocalin domain, a fascin-like motif, and an N-terminal nuclear localisation sequence (NLS) followed by a C- terminal bipartite (BP) nuclear transportation signal within the FRG1 protein (209) (Fig. 2.5.1). The predicted NLS signal of FRG1 was further validated in U2OS cells with ectopic expression of EGFP tagged FRG1, which showed the localization of FRG1 in the nucleolus, Cajal bodies, and in the nuclear speckles of the 60% to 70% of the cells (209). Fascins are small, globular actin-binding proteins that help in cellular adhesion, motility, and invasion. Elevated fascin expression is associated with non-small cell lung carcinoma, gastric cancer, and high-grade astrocytoma (210), (211).

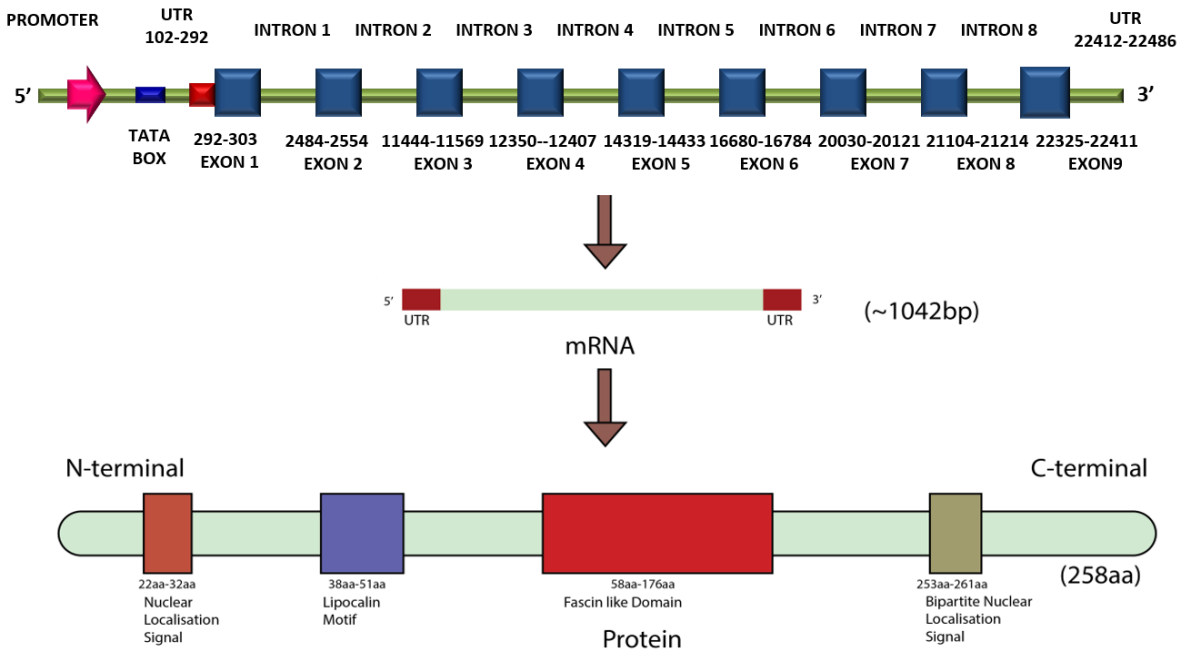

Figure 2.5.1. Structural overview of FRG1. *The image shows that the gene FRG1 consists of nine exons that transcribe to the mRNA of 1042 bp long. The mature FRG1 mRNA consists of an N-terminal nuclear localization sequence (NLS), a lipocalin motif, a fascin-like motif, and a C-terminal bipartite (BP) nuclear transportation signal. The figure is adapted from the reference* 212.

Although FRG1 was discovered as a candidate gene for FSHD, the primary function of FRG1 in normal physiology is yet to be established (213). FRG1 protein possesses 97% similarity with mouse homolog, 81% similarity to *Xenopus*, and 42% identity with *C. elegans* (213). The highly conserved sequence of FRG1 from invertebrates to vertebrates indicates its critical importance in normal physiology (Fig. 2.5.2) (214).

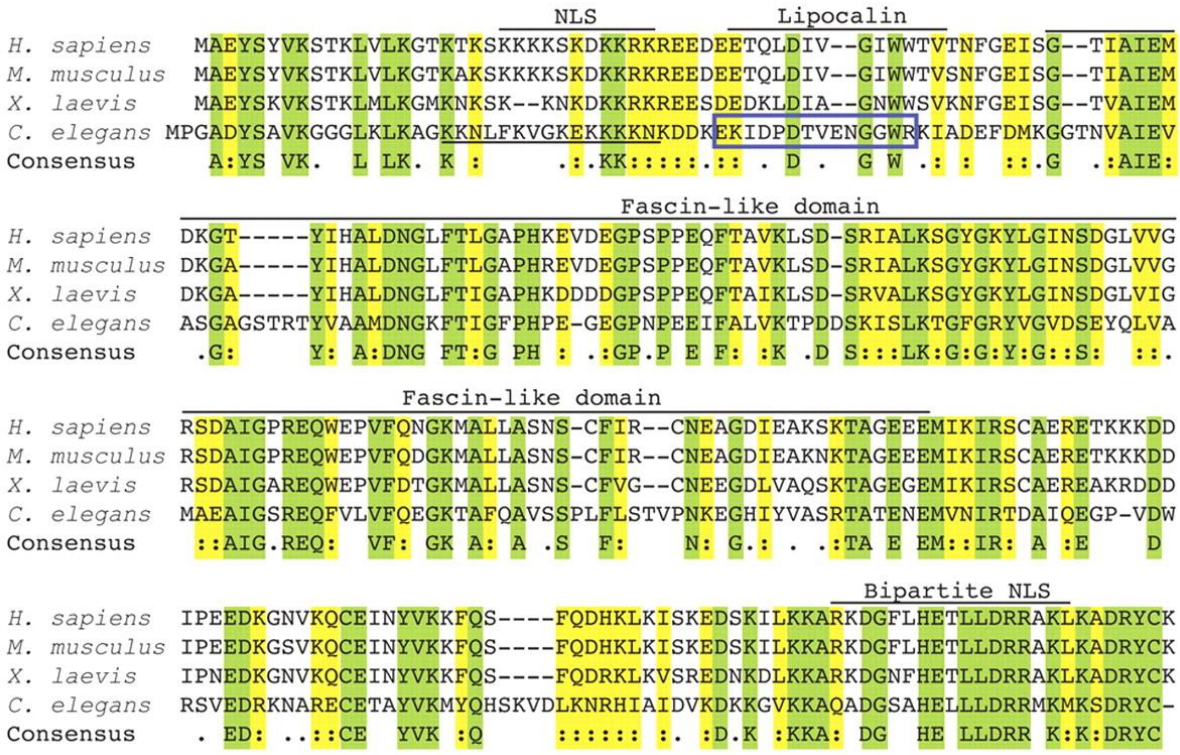

Figure 2.5.2. Evolutionary conservation of FRG1 protein across the species. *Pictorial illustration of different domains of FRG1 protein shows the sequence similarity of FRG1 among different species. Here, the amino acids, highlighted in green, are conserved in human, mice, Xenopus and C.elegans. Yellow highlighted amino acids are conserved among the three species. The figure is adapted from the reference* 185.

The possible function of FRG1 includes muscle development, actin binding, RNA processing, mRNA splicing, and angiogenesis. In 2006, Gabellini *et al.* showed that transgenic mice overexpressing the FRG1 gene developed an FSHD-like phenotype (208). Furthermore, elevated expression of FRG1 was associated with disrupted skeletal muscle and formation of abnormal epaxial and hypaxial muscle in *C.elegans,* suggesting its role in muscle development (215). The involvement of FRG1 in muscle development might be implicated by the presence of the fascin-like actin-binding domain with muscle attachment sites (213). All these evidences

points to the significance of preserving an adequate level of FRG1 to ensure normal muscle function.

The presence of FRG1 in the spliceosome complex (216) supports its role in pre-mRNA processing and RNA biogenesis (217). This study involving the yeast-two-hybrid system demonstrates the interaction of FRG1 with SMN, PABPN1, and FAM71B, the possible mediator of RNA biogenesis. Further evidence for the function of FRG1 in pre-mRNA splicing comes from the study that reports aberrant splicing patterns of the fast skeletal muscle troponin T (Tnnt3) and myotubularin-related protein 1 (Mtmr1) transcripts in transgenic mice expressing FRG1 (218).

Based on the literatures described above, we can speculate that FRG1 is a multifunctional protein, but further study is required to substantiate this assertion.

2.6. Indirect association of FRG1 in EMT and cellular proliferation

A few reports suggest the possible role of FRG1 in EMT or MET during development. Dental epithelial and mesenchymal cells have been reported to express FRG1 at the early event of mice odontogenesis (219). The same study has revealed that Bone morphogenetic protein 4 (BMP4), a known tumor suppressor, affects the localization of FRG1 in mouse dental epithelial cells mDE6. mDE6 cells treated with BMP4 translocate FRG1 from the nucleus to the cytoplasm, suggesting its role in the morphogenesis of tooth germ cells. Vimentin is a known mesenchymal marker. Malignant cells, which participate in EMT, are typically associated with increased Vimentin levels. In *Xenopus*, FRG1 knockdown affected the dermomyotome's formation, contributing to the formation of connective tissues from the mesenchymal cells (220)*;* this decreased Vimentin level, indicating the necessity of FRG1 in EMT during the early developmental phase. Administration of the FRG1 morpholino in *Xenopus* embryos reduces Vimentin from the mesenchymal cells on the lateral sides of the embryos; this suggests the functional importance of FRG1 in regulating the formation of mesenchymal cells

during *Xenopus* development (221). The same study also suggests that depletion of FRG1 reduces the cell migration from the *Xenopus* myotome.

In contrast, another study involving transgenic mice that overexpressed FRG1 showed reduced proliferation of the myoblast cells and decreased activation of retinoblastoma (Rb) protein, coupled with prolonged cell division time and an increased number of cells in the G1 phase (222). Reduced proliferation of myoblast cells can be explained by the decreased activation of phospho-Rb in the FRG1-expressing myoblasts because phospho-Rb is an essential driver of the cell cycle. Reduced activation of pRb causes E2F-mediated transcriptional repression of the genes involved in G1/S progression (223). Even though these findings indicate the possible connection between FRG1 and several EMT-inducing factors during the developmental process of various organisms, the fundamental question remains whether FRG1 plays any role in modulating tumorigenic properties.

2.7. Association of FRG1 with angiogenesis

The observation that 50%-75% of FSHD patients exhibit anomalies in their retinal vasculature led to the hypothesis that FRG1 expression and angiogenesis might be related (224). Out of 34 characterized or partially characterized genes associated with FSHD, 17 genes, including CCN2, CCN3, CD44, ICAM-1, melanoma cell adhesion molecule, MAGP-2, phosphodiesterase 4B, syndecan 2, are also involved in the growth of endothelial cells (225). In *Xenopus*, a decrease in FRG1 levels reduced vascular marker dab2 and vice versa (29). The same study has also detected enhanced angiogenesis and the association of edemas and vascular abnormalities in *Xenopus* due to elevated FRG1 expression. Despite FRG1's participation in vascular development, studies on its contribution to tumor angiogenesis have been mostly disregarded. The first evidence of FRG1's potential involvement in human tumor angiogenesis came from a study by Tiwari *et al*. in 2017. The group has shown that increased FRG1 levels decreased the tubule formation and migration of HUVECs in a paracrine manner (26). Even

though this result has contradicted the earlier *Xenopus* observation, these findings have certainly laid the foundation for future angiogenesis research on delineating the function of FRG1 in higher organisms. Therefore, we took the opportunity to take our work a step forward to advance our understanding of the role and mechanism of FRG1 in tumor angiogenesis, which can be investigated to determine its therapeutic potential in the future.

2.8. Association of FRG1 with cancer

As angiogenesis is concurrent with metastatic dissemination, the association of FRG1 with angiogenesis led us to investigate if FRG1 is linked to cancer. Some studies indicate the role of FRG1 in cancer indirectly. Transcriptome analysis of normal individuals and FSHD patients showed significant upregulation of the genes in FSHD patients that are associated with Ewing's sarcoma (226). Intriguingly, this study suggests that, out of 12 differentially expressed genes in FSHD myoblasts, five are linked to Ewing's sarcoma, two are linked to rhabdomyosarcoma, two are linked to neuroblastoma, three are linked to Burkitt's lymphoma. FSHD myotubes' biopsies showed a number of 11, 7, 6, and 1 genes specific to Ewing's sarcoma, rhabdomyosarcoma, neuroblastoma, and Burkitt's lymphoma, respectively. It is interesting to note that DUX4, a potent transcription factor expressed in 4q35, mediates the pathogenesis of both FSHD and Ewing's sarcoma (227), (228).

Few studies report mutations in FRG1 in cancer or cancer cell lines which also indirectly indicates the possible association of FRG1 with cancer. Expression profiling of MDA-MB-231 cells identified FRG1 among the substantially downregulated genes associated with the migratory property in triple-negative breast cancer (TNBC) (229). In calcifying fibrous malignancies of the pleura and in thyroid cancer cell lines, whole-exome sequencing revealed mutations in the FRG1 gene (178), (179). Whole exome sequencing using the cell-free DNA from prostate cancer patients has shown that mutation frequency in the FRG1 gene is higher in the patients resistant to the Dicycloplatin treatment (230). Chinese cohort of colorectal cancer

patients (n = 57) has shown FRG1 as one of the most frequently mutated genes (231). However, the functional importance of these mutations was not explored.

The earliest evidence of FRG1's direct role in carcinogenesis comes from Tiwari *et. al*. (27). They reported that a reduced level of FRG1 promotes prostate carcinogenesis by activating the p38-MAPK pathway. The same study also identified the upregulation of several oncogenic cytokines and growth factors such as MMP1, PDGFA, CXCL1, and GM-CSF due to FRG1 depletion (27). This group has previously documented a reduction of FRG1 in gastric, colon, and oral cancer patients (26). Increased cell migration and invasion due to FRG1 knockdown in HEK 293T cells further substantiated this observation (26). A multivariate-based optimal model study has recently shown that elevated levels of the FRG1 protein have a protective role in multiple cancers, with a significant effect on gastric and cervical cancer (28). These studies clearly suggest that FRG1 expression levels might be crucial for tumor progression, but the detailed molecular mechanism underpinning this role remained unknown. The current investigation aims to determine how FRG1 expression precisely regulates tumor progression.

Chapter 3

Materials and Methods

3.1. Cell Culture

3.1.1. Materials for cell culture

3.1.1.1. Cell lines

Human embryonic kidney 293T cell lines (HEK 293T), human breast cancer cells MCF7, and MDA-MB-231 were procured from the cell repository of the National Centre for Cell Science, Pune, India. Mice mammary carcinoma cell line 4T1 was purchased from American Type Culture Collection (ATCC, MNZ, USA). Human Umbilical Vein Endothelial Cells (HUVECs) were procured from Lonza (MD, USA). The origin and detailed information of the aforementioned cell lines are summarised in Table 3.1.1.1.1.

Table 3.1.1.1.1: List of human and mice cell lines used

Sr. No.	Cell Lines	Type	Origin
1.	MCF7	Luminal Cells; ER+ PR+ HER2-	Breast adenocarcinoma cells of human
2.	MDA-MB-231	Basal Cells; ER-PR-HER2-	Breast adenocarcinoma cells of human
3.	HEK 293T	Transformed cell lines	Human embryonic kidney cells
4.	4T1	Basal cells; ER-PR-HER2-	Mice mammary cancer cells
5.	HUVEC	Primary cells	Primary endothelial cells derived from human

3.1.1.2. Cell culture reagents

Dulbecco's Modified Eagle Media (DMEM; HiMedia, Maharashtra, India), Roswell Park Memorial Institute Media (RPMI; HiMedia, Maharashtra, India), Endothelial Cell Basal Medium-2 (EBM-2; Lonza, MD, USA), EGM-2^{TM} SingleQuotes® (Lonza, MD, USA), Dulbecco's phosphate-buffered saline pH 7.4 (DPBS; HiMedia, Maharashtra, India), Fetal Bovine Serum-US origin (FBS; HiMedia), Antibiotic-antimycotic solution (MP Biomedicals,

OH, USA), Trypsin EDTA 0.25% (HiMedia, Maharashtra, India), Dimethyl Sulfoxide (DMSO; MP Biomedicals, OH, USA).

3.1.1.3. Plasticwares for cell culture

T25 tissue culture flask (JET BIOFIL), T75 tissue culture flask (JET BIOFIL), serological pipette (Nunc™, NY, USA), 35 mm tissue culture dish (Eppendorf, Hamburg, Germany), 60 mm tissue culture dish (Eppendorf, Hamburg, Germany), 100 mm tissue culture dish (Eppendorf, Hamburg, Germany), 6 well plates for cell culture (Eppendorf, Hamburg, Germany), 12 well plates for cell culture (Eppendorf, Hamburg, Germany), 24 well plate for tissue culture (Eppendorf, Hamburg, Germany), 96 well plate for tissue culture (Eppendorf, Hamburg, Germany), Sartolab® RF Vacuum Filtration Units of 0.22 µm pore size (Sartorius, Goettingen, Germany), 1 mL filter tips (P'fact Gujrat, India), 200 µL filter tips (P'fact, Gujrat, India), 20 µL filter tips (P'fact, Gujrat, India), Cryo Chill vial (Tarsons, Kolkata, India)

3.1.1.4. Instruments for cell culture

Cell culture biosafety cabinet (Thermo Scientific, China), cell culture incubator (New Brunswick, Hamburg, Germany), upright microscope (Nikon, Japan), -80ºC refrigerator (Eppendorf, Hamburg, Germany), refrigerated centrifuge machine (Thermo Scientific, Germany), liquid nitrogen tank (Chart Inc, GA, USA), Countess® II FL hemacytometer (Invitrogen, USA), Countess 3 FL cell counter (Invitrogen, USA).

3.1.2. Methods for cell culture

3.1.2.1. Preparation of cell culture medium

To prepare the complete cell culture medium, DMEM, and RPMI were supplemented with 0.025 µg/mL Amphotericin B, 100 units/mL of Penicillin, and 50 µg/mL Streptomycin (1X PSA). 10% FBS (v/v) was added to the DMEM (10% DMEM). Both 10% and 15% FBS (v/v) was added to the RPMI (10% and 15% RPMI, respectively) media. To prepare the complete endothelial cell growth medium for HUVECs, EBM-2 Basal Medium, along with the EGM-2

SingleQuots supplements, were combined according to the manufacturer's instructions. All the complete media were filtered through a 0.22 μm vacuum-driven filter unit and stored at 4ºC.

3.1.2.2. Culture of human breast cancer cells, mice mammary carcinoma cells, HEK 293T and HUVECs

Human breast cancer cells MCF7 and MDA-MB-231 were maintained in the 10% DMEM and 15% RPMI respectively. Mice mammary carcinoma-derived 4T1 cells were maintained in the 10% RPMI. To culture the HEK 293T cells, 10% DMEM was used. Primary cells HUVECs were grown in the complete EBM2 medium. All the cells were maintained in a sterile T25 or T75 flask and kept inside the humidified chamber at 37ºC temperature and 5% CO_2.

3.1.2.3. Trypsinization, splitting, and subculture of cells

Once cancer or primary endothelial cells acquired 80%-90% confluency, splitting, and subculture were done. Before splitting the cells, the old medium was decanted, and the adherent cells were washed with DPBS (1 mL for the T25 flask and 2 mL for the T75 flask) once. Then DPBS was discarded, and depending on the adherence properties of the cells, 1 mL to 4 mL of 0.25% trypsin-EDTA was added to detach the cells from the flask. Cells were incubated for 1 to 3 minutes in the incubator (at 37ºC and 5% CO_2), and the trypsin was neutralized by adding 1-2 mL of the respective complete medium. The cell suspension was aspired by a 10 mL serological pipette and transferred to a 15 mL centrifuge tube along with the medium. After that, cells were centrifuged at 1000 RPM (243.7 RCF) for 5 minutes. Following the centrifugation, the supernatant was discarded, and the cell pellet was resuspended into the complete medium. Using a hemacytometer, the trypan-blue method was used to count the total number of viable cells in a digital cell counter (Countess 3 FL, instrument). In order to conduct further experiments, the required number of viable cells was plated in the cell culture dishes.

3.1.2.4. Cryopreservation and revival of the cells

Cryopreservation was carried out once the cells attained 70% confluency and were in healthy condition. Trypsinization and cell pellet were obtained as described previously (Section. 3.1.B.3). The pellet was then resuspended in the DMSO and complete fresh medium (1:9 ratio v/v). The cell suspension containing around 1×10^6 cells was stored in a sterile cryovial and kept at -80ºC in a cryo 1ºC cooler. After 12 hours, the vials were transferred to liquid nitrogen till further use.

To revive the cryopreserved cells, a 25 mL glass beaker was half filled with distilled water and warmed till it reached 37ºC. A few drops of tincture iodine solution were added to the water. Afterward, the cryovials were taken out from the liquid nitrogen tank and immediately kept in the pre-warmed water. When the cells were thawed properly, they were transferred to a T25 flask containing the respective complete medium and kept inside the incubator (37ºC and 5% CO_2) until the cells got adhered to the flask (for up to 4 hours). Once the cells were attached to the flask, the old medium was discarded to eliminate the DMSO, and fresh medium was added.

3.2. Generation of Stable Cell Lines

3.2.1. Materials for the generation of stable cell lines

3.2.1.1. Transfection reagents for the generation of stable cell lines

Opti-MEM-Reduced Serum Medium (Gibco, NY, USA), Lipofectamine 3000 (Invitrogen, MA, USA), Puromycin (Sigma Aldrich, MO, USA), and Blasticidin (10µg/mL) (Sigma Aldrich, MO, USA).

3.2.2. Methods

3.2.2.1. Generation of stable cell lines by shRNA-based transfection

To generate the stable cells, FRG1 knockdown (pLKO.1_FRG1sh, TRCN0000075012) and expression (PLX304_FRG1, HsCD004 21091) vectors were purchased from the Sigma (MO, USA) and Harvard PlasMID Database (MA, USA), respectively. Approximately 2×10^6 cells

were seeded into a 24-well plate to perform the transfection. First, the old medium was discarded from the wells, and cells were kept in 800 µL (per well in a 24-well plate) of Opti-MEM-Reduced Serum Medium for an hour. Meanwhile, a cocktail of 200 µL of Opti-MEM-Reduced Serum Medium, 1.5 µL of transfection reagent Lipofectamine 3000, 1 µL of P3000 reagent, and 1.5 µg of DNA was prepared and incubated for 30 minutes (the amount of the reagents is for each well of a 24-well plate). Subsequently, 200 µL of this transfection cocktail was dropwise administrated into each well, followed by mild spinning to ensure equal distribution of the complex. After 12 hours, each well received 1 mL of complete medium, and the entire medium was replaced by 1 mL of complete media after 24 hours. The plate was kept inside the incubator containing 37ºC temperature and 5% CO_2 for 48 hours. After 48 hours, antibiotics treatment was started in accordance with the table (Table: 3.2.2.1.1). Antibiotics were given at two-day intervals. Single cell-derived colonies were verified by Western blot.

Table. 3.2.2.1.1: List of the antibiotics used to prepare the stable cells

Sr. No.	Cell Lines	Antibiotic dosage
1.	MCF7 (FRG1 Knockdown)	Puromycin, 1 µg/mL
2.	MCF7 (FRG1 Overexpression)	Blasticidin, 10 µg/mL
3.	MDA-MB-231 (FRG1 Overexpression)	Blasticidin, 10 µg/mL
4.	HEK 293T (FRG1 Knockdown)	Puromycin, 1 µg/mL
5.	HEK 293T (FRG1 Overexpression)	Blasticidin, 10 µg/mL
6.	4T1 (FRG1 Knockdown)	Puromycin, 1 µg/mL
7.	4T1 (FRG1 Overexpression)	Blasticidin,10 µg/mL

3.2.2.2. Generation of knockout cells

To develop the knockout cells, the single-guided RNA cloning vector (Cas9 sgRNA vector) pSpCas9 (BB)-2A-Puro (PX459) V2.0 was purchased from Addgene. The cloning vector contained two BbsI sites at the end of the human U6 promoter. Single-guide RNA (sgRNA) was designed in the CHOP-CHOP version 3 web tool (https://chopchop.cbu.uib.no/). sgRNA primers used to knockout the FRG1 gene contained the sequence 5'-

TTCTGGACGAGTATGTGAGT-3' and 5'-AAGACCTGCTCATACACTCA-3'. sgRNA cloning was confirmed by direct DNA sequencing. The plasmids were extracted from the constructs following the protocol given in (Appendix IV.2). Transfection was done with the vector constructs following the protocol mentioned above (Section 3.2.2.1). Single cell-derived colonies were selected using puromycin (5µg/mL). Knockout was confirmed by Western blot.

3.3. Cell-Based Assays

3.3.1. Materials for MTS-based cell proliferation assay

CellTiter 96® AQueous One Solution Reagent (Promega, WI, USA), Varioskan Flash multimode reader (Thermo Fisher Scientific, MA, USA).

3.3.2. Method for the MTS-based cell proliferation assay

To perform the MTS-based cell proliferation assay in MCF7 and MDA-MB-231 cell lines, 5000 cells were seeded in a 96-well plate containing 100 µL of 10% DMEM and 15% RPMI, respectively. Cells were allowed to grow for 24 hours inside the incubator at 37ºC temperature and 5% CO_2. The next day, 20 µL of CellTiter 96® AQueous One Solution Reagent was added to each well, followed by incubation of the cells in a humidified incubator at 37ºC temperature and 5% CO_2 for an hour. Afterward, absorbance was recorded in a Varioskan Flash multimode reader at 490 nm.

To measure the proliferation rate in HUVECs, 5000 cells were seeded in a 96-well plate in 100 µL of EBM2 medium. Once the cells adhered to the plate, the old medium was replaced by a 100 µL mixture of EGM2 and conditioned medium in a 1:1 ratio and incubated for 24 hours inside the incubator. After 24 hours, 20 µL of CellTiter 96® AQueous One Solution Reagent was added to each well and kept for an hour inside the incubator. Finally, the absorbance was measured at 490 nm using a Varioskan Flash multimode reader.

3.3.3. Materials for the Colony Formation Assay

Methanol (Himedia, Maharashtra, India), Giemsa's stain, practical grade (Himedia, Maharashtra, India).

3.3.4. Method for the Colony Formation Assay

To carry out the colony formation assay, 700 cells were plated in a 6-well plate in the complete cell culture medium. Cells were grown for 15 days in the humidified incubator at 37ºC and 5% CO_2. After 15 days, when cell colonies were visible, the plate was taken out from the incubator, and the colonies were gently cleaned with DPBS. To fix the colonies, 1 mL of methanol was added to each well and kept for 15 minutes. After that, 1 mL of Giemsa's stain was added to each well and kept for 15 minutes. The colonies were carefully cleaned with DPBS until the residual stains were washed off. The plates were inverted and kept on tissue paper to remove the excess water. Once the plates dried, images were captured by a digital camera (Nikon). Colony numbers were counted by using ImageJ software.

3.3.5. Materials for the Insert Migration and Invasion Assay

Millicell® Cell Culture Inserts (8 µm pore size; Merck, Hesse, Germany), Matrigel® Matrix Basement Membrane - Growth Factor Reduced (Corning, NY, USA), Methanol (Himedia, Maharashtra, India), Giemsa's stain, practical grade (Himedia, Maharashtra, India), paraformaldehyde (HiMedia, Maharashtra, India), Upright brightfield microscope (Olympus, Tokyo, Japan).

3.3.6. Methods for the Insert Migration Assay

To perform the Insert migration assay, 0.5×10^6 HUVECs were resuspended into the cocktail of 500 µL EBM2-growth medium and 500 µL conditioned medium obtained from MCF7 and MDA-MB-231 cells with FRG1 level perturbation. The cell suspension was administrated into the cell culture inserts of 8 µm pore size. The inserts were placed in a 24-well plate. To induce cellular migration, the bottom chamber of each well was filled with 1 mL of complete EBM2-media. After 24 hours of incubation in a humidified chamber (37ºC and 5% CO_2), plates were

taken out, and the inserts were taken out with the help of forceps. The inserts were carefully washed with DPBS. To fix the cells, 1 mL of methanol was applied to each well for 15 minutes. Following the fixation, cells were incubated with 500 µL of Giemsa's stain for 30 minutes. After 30 minutes, the dye was discarded, and the cells were carefully washed with DPBS to eliminate any cellular debris and residual stains. The remaining non-migrated cells on the upper side of the chamber were gently removed by a cotton bud soaked in DPBS. Multiple images of the migrated cells on the outer surface of the chamber of different fields were captured in an upright brightfield microscope at 10X magnification. Lastly, the total number of cells was counted.

3.3.7. Methods for the Matrigel Invasion Assay

In the Matrigel invasion assay, first, the cell culture inserts were coated with growth factor-reduced matrigel. To coat the inserts, the growth factor-reduced matrigel (concentration 8.8 mg/mL) was diluted into the serum-free medium to attain the final concentration of 0.8 mg/mL. Each insert was filled with 100 µL of this diluted matrigel and kept inside the incubator at 37 °C for two hours. When the matrigel solidified, the inserts were placed in a 24-well plate, and the remaining steps of the procedure were carried out as described in section 3.3.6.

3.3.8. Materials for the Scratch Wound Healing Migration Assay

6 well plates for cell culture (Eppendorf, Hamburg, Germany), Inverted microscope (Nikon, Japan).

3.3.9. Method for the Scratch Wound Healing Migration Assay

For the Wound healing migration assay, 1×10^6 cells were plated into the 6-well plate. Once the cells reached 90% confluency, the complete cell culture medium was carefully aspirated with a 10 mL serological pipette. After that, a fine scratch was carefully created in the middle of the plate with a 200 µL pipette tip. The plate was gently washed with 1 mL of DPBS to remove the detached cells. At this stage, the first image of the wounds at '0' hour was captured using an

inverted microscope. Then 1 mL of growth factor-reduced medium containing 2% FBS was added to each of the wells, and the plate was kept inside the incubator (37ºC and 5% CO_2). Plates were taken out to capture the images at 24 and 36 hours. Finally, the percentage of wound healing was analyzed by ImageJ (NIH, MD, USA) software.

3.3.10. Materials for the Enzyme-linked Immunoassay (ELISA)

Quantikine ELISA Kit (R&D Systems, MN, USA), Varioskan Flash multimode reader (Thermo Fisher Scientific, MA, USA).

3.3.11. Method for preparation of conditioned medium

To prepare the conditioned medium, 2×10^6 cells were plated in a 100 mm dish in the cell culture medium containing 2% FBS. The plates were maintained in the incubator at 37ºC and 5% CO_2 for three days. After three days, the supernatant was collected in a 15 mL tube and centrifuged at 4000 RPM (3899.6 RCF) for 5 minutes at 4ºC. The supernatant was then aliquoted in 1 mL tubes and stored at -80ºC until further use.

3.3.12. Method for quantification of GM-CSF and VEGFA

Detailed methodology is given in Appendix IV.4.

3.3.13. Materials for Caspase Activity Assay

Caspase-Glo® 3/7 Assay System (Promega, WI, USA), Nunclon™ Delta Surface plate (Thermo Fisher Scientific, Kamstrupvej, Denmark), Varioskan Flash multimode reader (Thermo Fisher Scientific, MA, USA).

3.3.14. Method for the Caspase 3/7 Assay

To measure the caspase 3 and 7 activities in the cells, Caspase 3/7 assay was done using the Caspase-Glo® 3/7 Assay kit. First, the provided Caspase-Glo® 3/7 Buffer and lyophilized Caspase-Glo® 3/7 Substrates were equilibrated to room temperature. The entire ingredients of Caspase-Glo® 3/7 Buffer were transferred to the amber-colored bottle containing Caspase-Glo® 3/7 Substrate and mixed thoroughly before use. Next, 100 µL of this Caspase-Glo® 3/7

Reagent was added to the suspension of previously plated 1×10^3 cells in a white-walled Nunclon™ Delta Surface plate. To ensure uniform mixing, the plate was gently swirled for 5 minutes, followed by incubation at room temperature for 20 minutes. The luminescence of each sample was recorded using a Varioskan Flash multimode reader.

3.3.15. Materials for the inhibition and activation assays with pharmacological compounds

ERK inhibitor II (FR 180204; Merck, MA, USA), ERK activator (Ceramide C6; Santa-Cruz, CA, USA), CXCR2 antagonist Cpd 19 (Merck, MA, USA), anti-human GM-CSF antibody (BioLegend, CA, USA), human recombinant GM-CSF (Sigma Aldrich, MO, USA), anti-mouse GM-CSF neutralizing antibody (Bio-Xcell, NH, USA), FGF receptor (FGFR) inhibitor (Infigratinib; MedChemExpress, NJ, USA).

3.3.16. Method for the inhibition and activation assays with pharmacological compounds

Methods are described in the respective result section.

3.3.17. Materials for the Annexin V-FITC-based Apoptosis Assay

BD Pharmingen ™ Annexin V: FITC Apoptosis Detection Kit (BD Biosciences, USA), FACS Caliber (BD Biosciences, USA).

3.3.18. Method for the Annexin V-FITC-based Apoptosis Assay

We determined the effect of FRG1 depletion on the percentage of cells undergoing apoptosis using the FITC Annexin V apoptosis detection kit. To perform the Apoptosis assay, we used 1×10^6 MCF7 cells with reduced FRG1 level and Control. We harvested cells from the culture plate and centrifuged them at 3000 RPM (2193.5 RCF) for 5 minutes at 4ºC, followed by washing the cell pellet with ice-cold DPBS twice. We transferred the cells into a 1.5 mL microcentrifuge tube and resuspended the pellet into the 1X binding buffer provided with the kit. The microcentrifuge tubes were labeled as 1, 2, 3, 4, and 5, depending on the staining type. Tube 2 and 3 were used as positive control for Annexin V FITC, and PI, respectively. For the

positive controls, we exposed the cells to UV light inside the cell culture hood for 30 minutes before harvesting. Next, we added 5 µL of FITC-Annexin V and 5 µL PI into the cell suspension. The cells were gently vortexed and incubated for 15 minutes at room temperature in the dark. Lastly, we added 400 µL 1X binding buffer to each tube and transferred each sample to the FACS tube. After the incubation, the acquisition was carried out in a FACS Caliber instrument, and analysis was done using the CellQuest Pro software (BD Biosciences). Table. 3.3.18.1 depicts the setup for the FACS.

Table 3.3.18.1: Reaction setup for the analysis of cellular apoptosis

Staining Type	Name of the Cells	
Unstained (Tube 1)	Control_Sc	
Annexin V FITC (Tube 2: Positive control for Annexin V FITC)	Control_Sc	
Propidium Iodide (PI) (Tube 3: Positive control for Propidium Iodide)	Control_Sc	
Annexin V FITC + PI (Tube 4: Cells positive for both Annexin V FITC + PI)	Control_Sc	
Annexin V FITC + PI (Tube 5: Cells positive for both Annexin V FITC + PI)		FRG1_KD

3.3.19. Material for the Tubule Formation Assay

µ-slide angiogenesis plate (Ibidi, Munich, Germany), Matrigel Matrix® (Corning, NY, USA).

3.3.20. Method for the Tubule Formation Assay

The Tubule formation assay of HUVECs was performed in a µ-slide angiogenesis plate. First, the wells of the µ-slide were coated with 10 µL Matrigel Matrix, avoiding bubbles. The µ-slide was kept inside the incubator for an hour to solidify the matrix. Meanwhile, 7000 HUVECs

were suspended in the EBM2-Growth media and conditioned medium in a 1:1 ratio. 50 µL of this cocktail was added to each of the wells, coated with the Matrigel Matrix. The µ-slide was kept inside the incubator. Images of the tubules were captured at '0' and '6' hours. Further, the Angiogenesis Analyzer tool of ImageJ software was used to analyze various tubulogenic parameters.

3.4. Assay to Check the Transcriptional Activation

3.4.1. Materials for Luciferase Assay

pGL4.23 vector (luc2/minP) (Promega, WI, USA), pGL4.74 (hRluc/TK) (Promega, WI, USA), Dual-Luciferase® Reporter Assay System (Promega, WI, USA), LightShift™ Poly (dI-dC) (Thermo Scientific, IL, USA), NunclonTM Delta Surface plate (Thermo Fisher Scientific, Kamstrupvej, Denmark), Varioskan Flash multimode reader (Thermo Fisher Scientific, MA, USA).

3.4.2. Method for the Luciferase Assay

We procured the luciferase cloning vector pGL4.23 [luc2/minP] and control pGL4.74 [hRluc/TK] from Promega. 976 bp of GM-CSF promoter was cloned into the pGL4.23 vector. Detailed procedure for cloning has been described in section 3.7 (Cloning of the GM-CSF promoter). After confirming the colonies by colony PCR and restriction-digestion method, we transfected the cells with the vector constructs using Lipofectamine 3000 (detailed steps of transfection are given in section 3.2.2.1). Following illustration depicts the transfection setup (Fig. 3.4.2.1) After two days, we harvested the cells and measured the signal of Firefly and renilla luminescence using the Dual-Luciferase® Reporter Assay System Kit. The detailed procedure is described in Appendix IV.6. The firefly luciferase activity and renilla luciferase activity were measured in a Varioskan Flash multimode reader. For each sample, firefly luciferase activity was normalized to renilla luciferase activity.

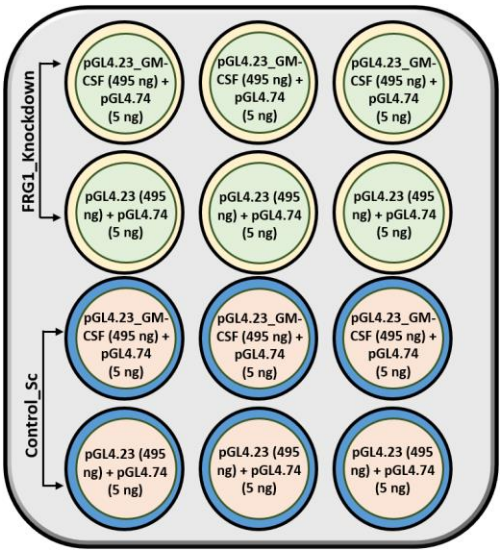

Figure 3.4.2.1. Overview of the transfection setup. *The picture depicts that the wells of the first and second lanes contained the FRG1 knockdown cells. The first three lanes were transfected with 495 ng of pGL4.23 vector cloned with GM-CSF promoter (pGL4.23_GM-CSF) and 5 ng of control renilla pGL4.74 vector. The three wells of the second lane were transfected with 495 ng of empty vector control pGL4.23 and 5 ng of renilla pGL4.74 vector. The well of the third and fourth lanes contained the Control_Sc cells. The first three wells were transfected with 495 ng of pGL4.23 vector cloned with GM-CSF promoter (pGL4.23_GM-CSF) and 5 ng of internal control renilla pGL4.74 vector. The wells in the fourth lane were transfected with 495 ng of empty vector control pGL4.23 and 5 ng of renilla pGL4.74 vector.*

3.5. Assays to Check the DNA-protein Binding

3.5.1. Materials for Electrophoretic Mobility Shift Assay (EMSA)

NE-PER^{TM} Nuclear and Cytoplasmic Extraction Reagents (Thermo Scientific, IL, USA), Chemiluminescent Nucleic Acid Detection Module Kit (Thermo Scientific, IL, USA), nylon membrane (Thermo Scientific, IL, USA), 0.5X TBE, nuclease-free water (NFW; GeNeI, Bangalore, India), ChemiDoc^{TM} XRS+ Imaging System (Bio-Rad, CA, USA).

3.5.2. Method for EMSA

We perform the EMSA to detect whether FRG1 binds to the GM-CSF promoter. Biotinylated and unbiotinylated probes were designed against the first CTGGG site, present on the 363 bp upstream of the first exon of the GM-CSF promoter. The probes were commercially procured from Integrated DNA Technologies (IDT; IA, USA), and the sequence is listed in Appendix III.

3.5.2.1. Extraction of Nuclear Protein from the Cells

Nuclear protein was extracted from the HEK 293T cells with ectopic FRG1 expression using the NE-PER Nuclear and Cytoplasmic Extraction Reagent. To isolate the nuclear protein extract, first, we took 5×10^6 cells in a 1.5 mL microcentrifuge tube by centrifuging the cell suspension at 500 g for 5 minutes. After that, the pellet was dried, and 200 µL of CER I reagent was added to the pellet. To suspend the entire pellet into the CER I reagent, the microcentrifuge tube was vigorously vortexed at the highest speed for 15 seconds, followed by incubation on ice for 10 minutes. Next, as per the manufacturer's protocol, we added 11 µL of pre-chilled CER II reagent to the cells. Again, the tube was vortexed for 5 seconds at the highest settings. After centrifuging the cell suspension, we centrifuged the microcentrifuge tube for 5 minutes at 16000 g. The supernatant containing the cytoplasmic protein extract was transferred to another tube. We suspended the pellet containing the nuclear protein extract into 100 µL of NER reagent provided with the kit. The cell suspension was vortexed at the highest settings for 15 seconds to get a homogeneous mixture. The sample containing the tube was kept on ice for 40 minutes, and we continued vertexing for 20 seconds at an interval of 10 minutes. Next, the microcentrifuge tube was centrifuged at 16000 g for 10 minutes, and the supernatant, containing the nuclear protein extract, was collected in a pre-chilled tube. This nuclear protein extract was stored at -80ºC till further use.

3.5.2.1.2. Detection the binding of FRG1-GM-CSF promoter complex

During the EMSA experiment, we prepared five types of reaction mixtures. In the first set, we took only the biotinylated probes (30 fmol). We incubated the biotinylated probe for 35 minutes at room temperature along with 10X binding buffer (1 µL) and NFW (8 µL).

In the second set, we took the nuclear protein extract (4 µL) and 30 fmol of biotinylated probes. We incubated the mixture at room temperature along with 10X binding buffer (1 µL), Poly (dI-dC) (1 µL), and 3 µL NFW. In the third set, to attain competitive binding, we added 30 pico-mole of unbiotinylated probes and 30 fmol of biotinylated probes in the nuclear protein extract (4 µL). We incubated the complex for 30 minutes at room temperature along with 10X binding buffer (1 µL), Poly (dI-dC) (1 µL), and 2 µL NFW. In the fourth set, the reaction mixture contained the same components as the third set, except for the unlabelled probes. To visualize if there was any supershift, we incubated the mixture at room temperature for 40 minutes along with the 1.5 µg FRG1 antibody. In the fifth set, we incubated the nuclear protein extract (4µL) for 30 minutes at room temperature with 30 fmol of biotinylated probes, 30 pico-mole of mutated unbiotinylated probes, 10X binding buffer (1 µL), Poly (dI-dC) (1 µL), and 2 µL NFW. Once the incubation was over, we loaded the samples into 10% native polyacrylamide gels, followed by the separation of the DNA-protein complex in 0.5X TBE buffer at 100V for an hour. After an hour, the complex was transferred for 45 minutes at 100V to a nylon membrane at 4ºC. The complex in the membrane was crosslinked upon UV exposure for 5 minutes. Signal development was done using Chemiluminescent Nucleic Acid Detection Module Kit and detected in the ChemiDoc™ XRS+ Imaging System.

3.5.3. Materials for the Chromatin Immunoprecipitation Assay (ChIP)

ChIP Kit (Abcam, USA), Sonicator (Cole-Parmer, IL, USA), 360º Moving Rocker (Tarsons, West Bengal, India), Ultrasonic Processor Sonicator (Cole-Parmer, IL, USA), QuantStudio 7 Flex Real-Time PCR Systems (Thermo Fisher Scientific, CA, USA).

3.5.4. Method for the ChIP Assay

We performed the ChIP assay using the kit procured from Abcam. We took the pellet of 1×10^6 HEK 293T cells and resuspended the pellet into 15 µL Buffer A, 6.3 µL formaldehyde, and 0.2 µL PBS. The cell suspension mixture was incubated at room temperature for 10 minutes to promote the crosslinking of the DNA-protein complex. After 10 minutes, we added 1.5M glycine to quench the process of cross-linking. The mixture was centrifuged at 500 g for 5 minutes at 4ºC, and the cell pellet was washed with PBS. Again, the cells were centrifuged at 500 g for 5 minutes at 4ºC, and we processed the pellet for cell lysis. The pellet was resuspended into lysis buffer (Buffer B), provided with the kit, and incubated at room temperature for 10 minutes. We centrifuged the cell suspension at 500 g for 5 minutes at 4ºC to get the pellet. Next, the pellet was suspended into 32 µL Buffer D and 1.3 µL 25X PI, provided with the kit. The lysed cell pellet was sonicated into 200-600 bp chromatin fragments in a sonicator for 35 seconds, 30 times at maximum speed. The chromatin suspension was centrifuged at 14000 g for 5 minutes at 4ºC, and fragmented chromatin containing supernatant was kept in the ice. Afterward, we immunoprecipitated the DNA-protein complex by incubating it with FRG1 antibody or IgG (negative control) overnight at 4ºC in a 360º moving rocker. The complex of antibody and protein was incubated with protein A beads, followed by washing and purifying the DNA using the DNA purifying slurry included in the ChIP kit. The DNA (2 µL) was then used for q-RT PCR analysis using FRG1-specific primers.

3.6. RNA Extraction and Quantitative Real-Time PCR (q-RT PCR)

3.6.1. Materials for RNA extraction and q-RT PCR

3.6.1.1. Materials for RNA Extraction

RNeasy Mini Kit (Qiagen, Hilden, Germany), RNase-Free water (Qiagen, Hilden, Germany), NanoDrop one^c (Thermo Scientific, WI, USA).

3.6.1.2. Materials for cDNA Synthesis

Verso cDNA Synthesis Kit (Thermo Scientific, Vilnius, Lithuania), NFW (GeNei, Bangalore, India).

3.6.1.3. Materials for q-RT PCR

Power Up™ SYBR™ Green Master Mix (Applied Biosystem, Vilnius, Lithuania), NFW (GeNei, Bangalore, India), Primers (Integrated DNA Technologies, USA), MicroAmp® Fast Reaction Tubes (8 Tubes/Strip) (Applied Biosystem, China), MicroAmp® Optical 8-Cap Strip (Applied Biosystem, China), Spinwin MC-00 (Tarsons, Kolkata, India), QuantStudio 7 Flex Real-Time PCR Systems (Thermo Fisher Scientific, CA, USA). The sequences of primers have been listed in Appendix II.

3.6.2. Methods for RNA extraction and q-RT PCR

3.6.2.1. Methods for Extraction of RNA and cDNA Synthesis

Cells were plated in a 35 mm dish. At around 70% confluency, RNA was extracted from the cells using the RNeasy mini kit (Qiagen, Hilden, Germany). The detailed procedure for RNA extraction has been described in Appendix IV.1. The concentration of the RNA was measured in the spectrophotometer (NanoDrop), and the quality was assessed by running the RNA in 1.5% agarose gel at 85V for 15 minutes. Subsequently, 1 µg RNA was taken to synthesize the cDNA using the Verso cDNA Synthesis Kit. Table 3.6.2.1.1 enlists the reaction mixture utilized for the cDNA synthesis. The cDNAs were synthesized in one cycle at 42ºC for 30 minutes, followed by 2 minutes of inactivation at 95 °C.

Table 3.6.2.1.1: Preparation of reaction mixture (20 µL) for a single reaction of cDNA synthesis

Sr. No.	Components	Volume
1.	5X cDNA synthesis buffer	4 µL
2.	dNTP Mix	2 µL (500 µM each)
3.	RNA Primer (random hexamer: anchored oligo dT: 3:1)	1 µL
4.	RT Enhancer	1 µL
5.	Verso Enzyme Mix	1 µL
6.	RNA Template	2 µL (1 µg)
7.	NFW	Upto 20 µL

3.6.2.2. Methods for Real-time PCR

For the real-time PCR, first, we designed the transcript-specific primers using the Primer-BLAST tool (NCBI, MD, USA). We diluted the cDNA into NFW to attain the final concentration of 10 ng/µL. The reaction was set up in an 8-well strip and covered with a clear optical cap, followed by centrifugation at the highest speed for 1 minute in a mini spinner. The components and the volume of the reaction mixture have been listed in Table 3.6.2.2.1. The q-RT PCR reaction was performed in the QuantStudio 7 Flex Real-Time PCR Systems, using cycling conditions as mentioned in Table 3.6.2.2.2. Relative expression of the transcripts was calculated using the ΔΔCT method.

Table 3.6.2.2.1: Components and volume of the reaction mixture for qRT-PCR (single reaction)

Sr. No.	Component	Volume
1.	Power Up™ SYBR™ Green Master Mix (2X)	5 µL
2.	Forward Primer (2.5 µM)	1 µL
3.	Reverse Primer (2.5 µM)	1 µL
4.	Template cDNA (20 ng)	2 µL
5.	NFW	1 µL
Total		10 µL

Table 3.6.2.2.2: Cycling conditions for QuantStudio 7 Flex Real-Time PCR System

Sr. No.	Stage	Temperature	Time
1.	Holding	50ºC	2 minutes
2.	Holding	95 ºC	10 minutes
3.	Melting (40 cycles)	95 ºC	15 seconds
4.	Annealing and extension (40 cycles)	60 ºC	1 minute

3.7. Protein Extraction, SDS-PAGE Electrophoresis, and Western blotting

3.7.1. Materials

3.7.1.1. Materials for cell lysis

RIPA lysis buffer (Thermo Scientific, IL, USA), Halt™ Protease and Phosphatase Inhibitor Single-Use Cocktail (100X) (Thermo Scientific, IL, USA), Vortex (Select Bio Products, USA).

3.7.1.2. Materials for protein estimation

Pierce™ BCA Protein Assay Kit (Thermo Fisher Scientific, IL, USA), Varioskan Flash multimode reader (Thermo Fisher Scientific, MA, USA).

3.7.1.3. Materials for sample loading dye for Western blot

4X Laemmli buffer. The composition of the buffer is provided in Appendix V.1.

3.7.1.4. Materials for SDS-PAGE Electrophoresis

30% Acrylamide solution [Acrylamide (MP Biomedicals, OH, USA) + N, N'-Methylene-bis-Acrylamide (MP Biomedicals)], Tris 1M (pH: 6.8) for stacking gel, Tris 1.5M (pH:8.8) for resolving gel, 10% Sodium Dodecyl Sulfate (SDS: MP Biomedicals, OH, USA), 10% Ammonium Persulfate (APS; MP Biomedicals; France, OH, USA), N,N,N′,N′-Tetramethyl ethylenediamine (TEMED; Thermo Scientific, IL, USA), 10X electrophoresis running buffer, Mini PROTEAN® Tetra Cell (BIO-RAD, China), PowerPac™ Basic (BIO-RAD, Singapore), Mini PROTEAN® Tetra Cell hand casting accessory kit (BIO-RAD, USA).

Detailed procedure for buffer preparation has been provided in Appendix V.1

3.7.1.5. Materials for Western blot

Immobilon PVDF membrane 0.45µm (Merck Life Sciences, Bangalore, India), Restore™ PLUS Western Blot Stripping Buffer (Thermo Scientific, IL, USA), Tween 20 (Sigma-Aldrich, Saint-Quentin-Fallavier, France), Bovine Serum Albumin Lyophilized Powder (MP Biomedicals, OH, USA), Skim Milk (Himedia, Maharashtra, India), PageRuler™ Plus Prestained Protein Ladder (Thermo Fisher Scientific, Vilnius, Lithuania), SuperSignal™ West Femto Maximum Sensitivity Substrate (Thermo Scientific, IL, USA), 10X Wet Transfer Buffer, Mini Trans-Blot® Electrophoretic Transfer Cell (BIO-RAD, USA), Mini Trans-Blot Cell Accessories (BIO-RAD, USA), Rocker (Labnet, NJ, USA).

Detailed procedure for buffer preparation has been listed in Appendix V.1.

3.7.2. Methods

3.7.2.1. Method for the preparation of whole cell lysate

Western blotting was carried out to detect the expression level of a specific protein present on the whole cell lysate. To achieve this, first, we prepared whole-cell protein extract. Cell culture flasks or dishes were maintained in the incubator at 37ºC temperature and 5% CO_2 with their respective complete medium. The media was decanted, and the cells were washed with DPBS.

We added an appropriate volume of RIPA buffer to lyse the cells and detached the cells with a scrapper. The cell suspension was collected in a 1.5 mL microcentrifuge tube. The tube was kept on the ice for 20 minutes. We vortexed the tube for 30 seconds at an interval of 10 minutes for maximum lysis. Next, we centrifuged the tube at the highest speed (15000 RPM or 21000 RCF) for 30 minutes at 4ºC to remove the cellular debris. We collected the supernatant and added a suitable volume of 4X Laemmli buffer. Prepared protein lysate was kept at -80ºC till further use.

3.7.2.2 Method for quantification of protein concentration by BCA method

We estimated the protein concentration by BCA method, using the Pierce™ BCA Protein Assay Kit. To prepare the protein samples, Bovine Serum Albumin (BSA) of 2 mg/mL concentration was serially diluted to make standard protein samples of 25 µg/mL, 125 µg/mL, 250 µg/mL, 500 µg/mL, 750 µg/mL, 1000 µg/mL, 1500 µg/mL. We prepared the BCA working reagent by mixing the BCA Reagent A and B in a 50:1 ratio. Then 10 µL of protein sample was added to each well of a transparent 96-well plate. After that, we dispensed 200 µL of BCA working agent to the protein sample into each well. The 96-well plate was covered with aluminum foil and incubated at 37ºC for 30 minutes. After 30 minutes, absorbance was measured at 562 nm using a Varioskan Flash multimode reader.

3.7.2.3. Method for separation of proteins in Sodium Dodecyl Sulfate-Polyacrylamide Gel Electrophoresis (SDS-PAGE)

Proteins were separated according to their molecular mass in the SDS-PAGE method. The buffers used for this procedure have been listed in Appendix V.1. We prepared 5% of stacking gel and 10% or 12% resolving gel, depending on the molecular size of the proteins. Table 3.7.2.3.1 provides the volume of various components needed to cast the gels.

Once the gel got solidified, we transferred the gel from the gel casting tray to the gel-running electrophoresis apparatus. The buffer tank was filled with 1X TGS electrophoresis buffer.

Meanwhile, the protein samples were taken out from -80ºC and thawed on the ice. The protein samples were boiled at 100ºC in a dry block heater for 5 minutes. Next, 20-25 µg of protein was loaded into each well of the gel. A pre-stained protein ladder was loaded in a well of the same gel. The power pack was connected to the gel running unit, and the proteins were separated at 90V until the bromophenol blue dye reached the bottom of the gel.

Table. 3.7.2.3.1: The volume of the components used to cast the SDS-PAGE gels of the indicated concentrations and volume

Sr. No.	Components for 5% Stacking gel (3 mL)	Required volume (mL)	Components of Resolving gel	Required volume (mL)	
				10% (10 mL)	12% (10 mL)
1.	Milli-Q water	2.1	Milli-Q water	4	3.3
2.	Acrylamide (30%)	0.5	Acrylamide (30%)	3.3	4
3.	Tris-Cl (1.0M, pH 6.8)	0.38	Tris-Cl (1.0M, pH 6.8)	2.5	2.5
4.	10% SDS	0.03	10% SDS	0.1	0.1
5.	10% APS	0.03	10% APS	0.1	0.1
6.	TEMED	0.003	TEMED	0.004	0.008

3.7.2.4. Methods for the Immunoblotting

Once the proteins were resolved in the SDS-PAGE, we transferred the proteins from the gel to the PVDF membrane. For this, we removed the gel from the gel casting glasses (1.5 mm) and kept it in the wet transfer buffer for 5 minutes. Also, we soaked the PVDF membrane in the methanol for 5 minutes to reduce the hydrophobicity. Next, the gel and PVDF membrane was placed within the transfer cassette and placed inside the Mini Trans-Blot® Electrophoretic Transfer Cell transfer module filled with pre-chilled transfer buffer. The module was connected to a powerpack, and the protein transfer was carried out for 6 hours at 50V inside a 4ºC room. Once, the transfer was done, the PVDF membrane was removed from the transfer cassette and dipped into the blocking solution (5% BSA to check protein phosphorylation or 5% skimmed milk to check the endogenous protein) for an hour at room temperature in a rocker. Then we

washed the blot thrice for five minutes each time, with 0.1% TBST wash buffer to remove the excess blocking reagent. The PVDF membrane was then probed with the respective antibodies (listed in Appendix I) and kept at room temperature. After an hour, the blot was transferred to a 4ºC refrigerator and incubated overnight. The next day, the blot was again washed thrice with 0.1% TBST and incubated with the HRP-conjugated secondary antibody solution, with constant shaking for 1 hour at room temperature in a rocking shaker. After that, the blot was washed thrice in 0.1% TBST. Imaging was done in the ChemiDoc XRS system.

3.7.2.5. Methods for stripping and reprobing of the blot

To strip the pre-existing antibodies from the blot, we kept the blot in a prewarmed (55ºC for 10 minutes) stripping buffer and vigorously rocked at the highest speed for 15 minutes in a rocking shaker. The blot was then washed three times for ten minutes each for a total of 30 minutes in 1X TBS. Subsequently, blocking and probing with antibodies were done as described in section 3.7.2.4.

3.8. Immunohistochemistry (IHC)

3.8.1. Materials for IHC

3.8.1.1. Human tissue samples

Formalin-fixed paraffin-embedded (FFPE) breast cancer tissue samples with adjacent normal counterpart, Tissue microarray (Biomax, MD, USA).

3.8.1.2. Poly-L-Lysine coating of slides

Microscope Slides (Borosil, Maharashtra, India), Poly-L-Lysine solution (Sigma-Aldrich, MO, USA), EMPLURA® Acetic acid glacial 99-100% (Merck Life Sciences Privet Limited, Maharashtra, India), EMSURE® Ethanol ACS grade (Sigma-Aldrich, Hesse, Germany).

3.8.1.3. Immunohistochemistry reagents

Xylene (Merck Life Sciences Privet Limited, Maharashtra, India), EMSURE® Ethanol ACS grade (Sigma-Aldrich, Hesse, Germany), EnVision™ Flex Target Retrieval Solution, high pH

(Dako, Denmark), EnVision™ Flex Wash Buffer (Dako, Denmark), EnVision™ Flex Peroxidase Blocking Reagent (Dako, Denmark), EnVision™ Flex Substrate Buffer (Dako, Denmark), EnVision™ Flex DAB+ Chromogen (Dako, Denmark), EnVision™ Flex HRP secondary antibody (Dako, Denmark), Haematoxylin-Harris (HiMedia, Maharashtra, India), D.P.X mountant (Fisher Scientific, Maharashtra, India), Liquid Blocker Super Pap Pen-2 mm (Daido Sangyo Co. Ltd., Tokyo, Japan), Slide Staining box (Tarsons, Kolkata, India), Coplin jar (Tarsons, Kolkata, India), StableTemp Ceramic Top Stirring Hot Plate (Cole-Parmer, IL, USA).

3.8.2. Methods for IHC

3.8.2.1. Collection of human FFPE samples

The Institutional Ethics Committee of the National Institute of Science Education and Research (NISER) (Approval No. NISER/IEC/2021-02) approved the study related to human samples. The Department of Pathology at Apollo Hospital, Bhubaneswar; SRL Diagnostic Lab, Bhubaneswar; and AHRCC provided the archival Formalin-fixed paraffin-embedded (FFPE) blocks of 104 breast cancer cases and 46 adjacent normal counterparts. The clinicopathological features of the patients were noted, including histological type, tumor size, tumor-node-metastasis (TNM) stage, and lymphovascular invasion.

In addition, a tissue microarray containing 90 tumors and ten samples of normal tissue was purchased.

3.8.2.2. Poly-L-Lysine coating of the slides

First, we cleaned the slides with soap water and washed them thoroughly with tap water. Next, the slides were dispensed into a glass beaker containing the solution of 1% acetic acid (acetic acid and ethanol in a 1:9 ratio) for 20 minutes. Then the slides were cleaned with tap water and then washed twice with distilled water. Thereafter the slides were kept horizontally and dried inside the incubator at 55ºC overnight. Finally, the slides were dispensed into the 0.1% poly-

L-Lysine solution twice for five minutes each time. The coated slides were then left to air dry at 37°C overnight.

3.8.2.3. Staining for IHC

Tumors of 5 μm thin section were cut from the FFPE biopsy samples and taken onto the poly-L-Lysine coated slides. The samples were first deparaffinized on the hot plate by heating at 80ºC for an hour, followed by dipping the slides twice into the coupling jar containing prewarmed xylene (55ºC) for 2 minutes. Samples were rehydrated by submerging the slides into a gradient of 100% ethanol (3 minutes), 90% ethanol (3 minutes), 70% ethanol (3 minutes), 50% ethanol (3 minutes), and distilled water. Heat-induced antigen retrieval was carried out by dispensing the slides into EnVision™ FLEX Target Retrieval High pH Citrate Buffer (pH: 9) thrice (twice at 720 W and once at 540 W in the micro oven) for 5 minutes each. When the slides were cooled down, they were thoroughly washed with distilled water, followed by an additional wash into EnVision™ FLEX Wash Buffer. The tissue section on the slide was marked with a pap pen. 500 μL of EnVision™ FLEX Peroxidase Blocking Buffer was added to each section and kept for 10 minutes. Slides were washed with wash buffer and incubated with the primary antibody (1:100 dilution) overnight at 4ºC. Slides were washed with the wash buffer thrice to eliminate the excess antibodies and then incubated with EnVision™ FLEX HRP secondary antibody for 30 minutes. Subsequently, the slides were washed with the wash buffer thrice. One drop of EnVision™ FLEX DAB+ Chromogen was added to 1 mL of EnVision™ Flex Substrate Buffer and incubated for 5 minutes. For counterstaining, 500 μL of Haematoxylin was added to each section and incubated for 2 minutes. Next, the slides were washed under running tap water. Dehydration of the samples was done by keeping them in the gradient of 90% ethanol (2 minutes), 100% ethanol (2 minutes), and xylene (2 minutes). The slides were air-dried overnight. Finally, the sections were mounted with D.P.X mountant and covered with a cover slip.

3.8.2.4. Immunohistological scoring

The expression level of FRG1 in cancer samples and the adjoining normal counterpart was measured by the Allred score method (26). The stained slides were analyzed by a pathologist. The Allred score was calculated by the following formula: FRG1's staining intensity in the cytoplasm + percentage of FRG1 positive cells. Based on the staining percentage, FRG1 positive tumor and normal tissues were scored as follows: the score was given '0' if the staining intensity was 0%. Similarly, '1' for the staining intensity of 1%, '2' for the staining intensity of 2-10%, '3' for the staining intensity of 11%-33%, '4' for the staining intensity of 34%-66%, and '5' for the staining intensity more than 67%. The intensity of staining was considered as 'weak' if it was within the range of '0-2', 'moderate' if the intensity range was '3 to 6', and 'strong' if the intensity range was '7 to 8'. Each sample was compared to the adjacent uninvolved tissue (if present) as a control.

3.9. Cloning of the GM-CSF Promoter

3.9.1. Materials for cloning

3.9.1.1. Bacterial culture

Luria Bertani (LB) Broth, Miller (Himedia, Maharashtra, India), Luria Bertani (LB) Agar, Miller (Himedia, Maharashtra, India), Ampicillin sodium salt (Sigma-Aldrich, China) in 100 mg/mL concentration, New Brunswick Innova® 42 Incubator shaker (Eppendorf, Hamburg, Germany).

3.9.1.2. Preparation of DH5α competent cells

Inoue Buffer (55mM $MnCl_2.4H_2O$, 15 mM $CaCl_2.2\ H_2O$, 250 mM KCl, 10 mM PIPES in autoclaved milli-Q water); $MnCl_2.4H_2O$ (HiMedia), $CaCl_2.2\ H_2O$ (HiMedia), KCl (Sigma-Aldrich, MO, USA), PIPES (Sigma-Aldrich, MO, USA).

3.9.1.3. Extraction of plasmids

QIAprep® Spin Miniprep Kit (Qiagen, Hilden, Germany), NFW (GeNei, Bangalore, India).

3.9.1.4. Restriction-digestion and cloning

Template DNA (for insert and vector), restriction enzymes: KpnI-HF® (NEB, MA, USA), XhoI (NEB, MA, USA), 10X CutSmart® Buffer (NEB, MA, USA).

3.9.1.5. Polymerase Chain Reaction (PCR)

10X Standard *Taq* Reaction buffer (NEB, MA, USA), 10 µM dNTPs (NEB, MA, USA), 10 µM of forward and reverse primer (IDT, IL, USA), template DNA (100 ng), Taq DNA Polymerase (1 unit/25 µL PCR reaction) (NEB, MA USA), NFW (GeNei, Bangalore, India), C1000 Touch™ Thermal Cycler (Bio-Rad, USA).

3.9.1.6. Colony PCR

Required materials are the same as PCR (described in 2.7.A.5) except for the template DNA. Here a colony was used as the template.

3.9.1.7. Agarose gel electrophoresis

SeaKem® LE Agarose (Lonza, ME, USA), 50X TAE (50 mM EDTA sodium salt, 2M Tris, Glacial acetic acid 1M), Ethidium bromide (Sigma-Aldrich, MO, USA), 1 Kb DNA ladder (NEB, MA, USA), 50 bp DNA ladder (NEB, MA, USA), Gel Loading Dye Purple (6X) (NEB, MA, USA), Mini-Sub® Cell GT electrophoresis unit (Bio-Rad, China).

3.9.2. Methods for cloning

3.9.2.1. Preparation of ultra-competent DH5α cells

The Inoue method was used to prepare the ultra-competent DH5α cells (232). From the glycerol stock of DH5α, cells were streaked in an LB agar plate. The plate was incubated at 37ºC in the incubator for 16 hours. After completion of 16 hours, a single colony of DH5α was picked up and subsequently transferred to a test tube containing 5 mL of LB broth and 5 µL of ampicillin (1 µg/mL). The broth was further incubated for 16 hours inside an incubator shaker at 220 RPM and 37ºC. 500 µL of this primary culture was transferred to a conical flask containing 250 mL LB broth and incubated at 18ºC for 16 hours. The bacteria were allowed to grow until the O.D.

reached 0.55. At 0.55 O.D., the culture flask was transferred to ice and incubated for 10 minutes. Then the cells were harvested in a 50 mL centrifuge tube by centrifuging the culture at 2500 g for 10 minutes at 4ºC. The supernatant was discarded, and the bacterial cells were resuspended into 80 mL of Inoue buffer. Next, the cells were again centrifuged at 2,500 g for 10 minutes at 4ºC. The culture broth was entirely removed, and the cells were resuspended into 20 mL Inoue buffer. Then we added 1.5 mL DMSO to the bacterial cell suspension and incubated it for 10 minutes on ice. 50 µL of this cell suspension was aliquoted to a pre-chilled 1.5 mL microcentrifuge tube. Finally, the tubes were snap chilled into liquid nitrogen and stored at -80ºC for long-term use.

3.9.2.2. Cloning of GM-CSF promoter

The GM-CSF promoter (907 bp ahead of transcription start site) region was amplified and cloned into the pGL4.23 vector using the following steps.

3.9.2.2.1. Primer design

Primers were designed in the Primer-BLAST tool (NCBI, MD, USA) against the 907 bp region of GM-CSF promoter, KpnI-HF, and XhoI restriction sites were added to the 5' and 3' end of the primer. Several properties of the primers, including GC content, melting temperature (Tm), secondary structure, self-dimer, and hetero-dimer tendencies, were checked using the OligoAnalyzer™ Tool of IDT (IL, USA)

3.9.2.2.2. Amplification of insert

Genomic DNA was isolated from MCF7 cells following the method described in Appendix IV.5. 907 bp of GM-CSF (hCSF2) promoter was amplified in the C1000 Touch^{TM} Thermal Cycler using the following primer set:

hCSF2 forward primer 5'-CGGGGTACCCTCTACCAGGCACCTGTATGTAC-3'

hCSF2 reverse primer 5'- CCGCTCGAGCTGTGAGAGACTTGAGTGTGAGG-3'

The PCR reaction was set up following the reaction mixture given in Table 3.9.2.2.2.1 and the cycling condition given in Table 3.9.2.2.2.

Table. 3.9.2.2.2.1: Components of PCR reaction mixture for amplifying the GM-CSF promoter region

Sr. No.	Components	Volume
1.	NFW	17.5 µL
2.	10X Standard *Taq* Reaction buffer	2.5 µL
3.	dNTP (10 µM)	2.5 µL
4.	Forward Primer (10 µM)	0.5 µL
5.	Reverse Primer (10 µM)	0.5 µL
6.	*Taq* DNA Polymerase (1 unit/reaction)	0.5 µL
7.	Template DNA (100 ng)	1 µL
Total		25 µL

Table. 3.9.2.2.2.2: PCR conditions for amplifying the GM-CSF promoter region

Sr. No.	Stages	Temperature	Time	Cycles
1.	Initial Denaturation	95ºC	5 minutes	1
2.	Denaturation Annealing Extension	95ºC 57ºC 72ºC	30 seconds 35 seconds 1 minute	34
3.	Final Extension	72ºC 4ºC	10 minutes Hold	1

3.9.2.2.3. Agarose gel electrophoresis of the PCR product

To isolate the desired GM-CSF promoter region, first, the PCR product (25 µL) was mixed with 4 µL of 6X gel loading dye. To run the sample, 1% agarose gel was prepared in 1X TAE buffer and 0.5 µg/mL ethidium bromide. The gel was subsequently placed into a horizontal electrophoresis unit and connected to the power pack. The PCR product was loaded into the gel and ran for 30 minutes at 85V. The anticipated band of the GM-CSF promoter region, which matched the corresponding DNA molecular marker, was visualized using a UV transilluminator. Under the UV transilluminator, the band was excised with a sterile scalpel. The PCR product was purified using the Qiagen gel extraction kit following the manufacturer's

protocol described in Appendix IV.3. Once the PCR product was purified, the concentration was measured using a spectrophotometer (NanoDrop).

3.9.2.2.4. Restriction digestion of the PCR product

Both the cloning vector (pGL 4.23) and insert (976 bp of GM-CSF promoter) were digested with the enzyme KpnI-HF® and XhoI for 3 hours at room temperature. The reaction mixture was set up according to Table 3.9.2.2.4.1 (for insert digestion) and Table 3.9.2.2.4.2 (for vector digestion).

Table 3.9.2.2.4.1: Reaction mixture for insert digestion

Sr. No.	Ingredients	Volume
1.	Insert (500 ng)	16 µL
2.	KpnI-HF® (1 unit/reaction)	1 µL
3.	XhoI (1 unit/reaction)	1 µL
4.	10X cut smart buffer	2 µL
Total		20 µL

Table 3.9.2.2.4.2: Reaction mixture for vector digestion

Sr. No.	Ingredients	Volume
1.	Vector (1 µg)	1 µL
2.	KpnI-HF® (1 unit/reaction)	1 µL
3.	XhoI (1 unit/reaction)	1 µL
4.	10X Cut Smart buffer	2 µL
5.	NFW	15 µL
Total		20 µL

3.9.2.2.5. Ligation of the vector and insert

The digested insert and the vector were ligated using the T4 DNA ligase. Prior to the ligation, the concentration of both the digested insert and vector was measured using a spectrophotometer (NanoDrop). The amount of the insert and vector needed for the ligation was determined using the ligation calculator tool, NEBioCalculator® (NEB, MA, USA). Here we used the insert and the vector in a 1:3 molar ratio for the ligation. The ingredients of the

ligation mixture have been described in Table 3.9.2.2.5.1. The ligation mixture was incubated for 10 hours at 16ºC in a thermal cycler.

Table 3.9.2.2.5.1: Components of the reaction mixture for ligation

Sr. No.	Ingredients	Volume
1.	Insert	70 ng (4 µL)
2.	Vector	100 ng (3 µL)
3.	T4 DNA Ligase	2 µL
4.	10X DNA ligase buffer	1 µL
Total		10 µL

3.9.2.2.6. Transformation of the Ligated Product into the ultra-competent DH5α Cells

We used the heat-shock method To transform the inserts into ultra-competent cells (233). First, the previously prepared ultra-competent DH5α cells (mentioned in 3.7.B.1) were taken out from -80ºC and incubated for 20 minutes on the ice to thaw the cells. Once the cells were thawed, 10 µL of the ligation mixture was directly added to the vial of competent cells (5 ng) and incubated on the ice for 30 minutes. Meanwhile, the water bath was set to the temperature of 42ºC. After 30 minutes, the vial containing the mixture of competent cells and plasmid inserts was removed from the ice and directly transferred to the 42ºC water bath and incubated for exactly 45 seconds. After 45 seconds, the vial was immediately transferred to the ice and incubated for 2 minutes. Subsequently, 1 mL of LB broth was added to the cells and incubated in the incubator at 37ºC for an hour at 240 RPM. After that, 500 µL of the cell suspension was spread in an LB agar plate (contained 100 µg/mL ampicillin added) with an L-shaped spreader and incubated at 37ºC. After 8 hours, colonies started appearing. Once the colonies were fully grown at 12 hours, we patched the single colonies into an LB agar plate (100 µg/mL ampicillin added) and grown for 12 hours at 37ºC to make the glycerol stock (for positive clones only).

3.9.2.2.7. Confirmation of the positive clones

We verified the positive colonies, carrying the GM-CSF promoter region, by colony PCR and double digestion with the restriction enzymes. For the colony PCR, one colony was picked up

with a 20 µL pipette tip. The pipette tip was dispensed into a test tube containing 5 mL of LB broth and 5 µL ampicillin (100 µg/mL). The tube was incubated at 37ºC for 16 hours at 220 RPM in an incubator shaker. Plasmid DNA was extracted from the culture using the QIAprep Spin Miniprep Kit, following the manufacturer's protocol, described in Appendix IV.2. We gently touched a colony with an autoclaved toothpick and inoculated it into the PCR reaction mixture. The component for each PCR reaction mixture and cycling conditions are given in Table 3.9.2.2.2.1. and 3.9.2.2.2.2. Once the PCR amplification was over, agarose gel electrophoresis in 0.8% agarose gel was carried out with the amplified PCR product. Thereafter, the gel was run at 85V for 30 minutes in a horizontal electrophoresis unit. The expected band position of the amplified GM-CSF promoter was visualized by comparing it with corresponding molecular weight markers in the gel, using a UV transilluminator.

We additionally validated the positive clones by double digesting the purified plasmid (500 ng) with the restriction enzymes KpnI and XhoI. The reaction mixture that we used for the digestion, is given in Table 3.9.2.2.7.1. The reaction mixture was incubated for three hours in a heat block at 37ºC. Next, we ran the double-digested plasmid in 0.8% agarose gel at 85V for 30 minutes using a horizontal electrophoresis unit. The undigested plasmid was simultaneously loaded as a negative control. The band positions were visualized by comparing them with corresponding molecular weight markers in the gel, using a UV transilluminator.

Table 3.9.2.2.7.1: Reaction mixture for the restriction double digestion of the plasmid

Sr. No.	Ingredients	Volume
1.	NFW	20.5 µL
2.	Insert (500 ng)	0.5 µL
3.	KpnI-HF® (1 unit/reaction)	1 µL
4.	XhoI (1 unit/reaction)	1 µL
5.	10X cut smart buffer	2 µL
Total		25 µL

3.10. Animal-Based Experiments

3.10.1. Materials for *in vivo* experiments

3.10.1.1. Materials for Tumor Development Assay

6-8 weeks old female BALB/c mice, Growth factor reduced matrigel (Corning, NY, USA).

3.10.1.2. Materials for *in vivo* GM-CSF Experiment

6-8 weeks old female BALB/c mice, anti-mouse GM-CSF neutralizing antibody (Bio-Xcell, NH, USA).

3.10.1.3. Materials for Matrigel Plug Assay

6-8 weeks old female C57/BL6 mice, Growth factor reduced matrigel (Corning, NY, USA).

3.10.1.4. Materials for Skin Wound Healing Assay

6-8 weeks old female BALB/c mice, 4-6 mm biopsy puncture, Silicon splint, 3-0 non-absorbable sterile surgical suture (Johnson and Johnson PVT. LTD, Maharastra, India), dressing film (3M Tegaderm India Limited, Maharastra, India), Tramadol (Bestochem Formulations Ltd, India).

3.10.2. Methods for animal-based experiments

All animal experiments were conducted in accordance with the Institutional Animal Ethics Committee (IAEC) guidelines (Protocol no. NISER/SBS/IAEC/AH-109). Two strains of 6-8 weeks-old female mice, BALB/c and C57/BL6 were used in the study. The animals were housed in autoclaved polysulfone cages with corncob bedding in a controlled environment with temperature and humidity ranging between 22±3°C and 40-70%, respectively. Animals were maintained in a room with artificial lighting set to 12 hours cycle of light and 12 hours of darkness. Purified UV-treated drinking water was provided to the animals. Animals were fed with a commercially available pellet diet.

3.10.2.1. Tumor Development Assay in Mice

The experiment was approved by the institutional animal ethics committee of NISER (approval no. NISER/SBS/IAEC/AH 109). To develop an orthotopic mice model, we used female BALB/c mice, 6-8 weeks old. Mice mammary carcinoma-derived cells 4T1 with FRG1 level perturbation were used to perform the tumor development experiment. 2×10^6 cells were suspended into 200 µL of DPBS, and the growth factor reduced matrigel in a 1:1 ratio. We injected the cocktail into the 4^{th} mammary fat pads of mice after shaving the fur from their abdomen region. Tumor size was measured at three days intervals using a digital vernier caliper. The volume of the tumors was calculated using the formula $(L \times W^2)/2$, (L = length, W = width). On the 21^{st} day, the mice were euthanized by exposing them to a gradually increased concentration of CO_2. The tumors were excised and cleaned with DPBS. Images of the tumors were taken using a digital camera. Fig. 3.10.2.1.1 shows the methodology used to develop the orthotopic mice model. Lastly, proteins were harvested from the tumors to measure the expression of phospho-ERK and EMT marker Snail.

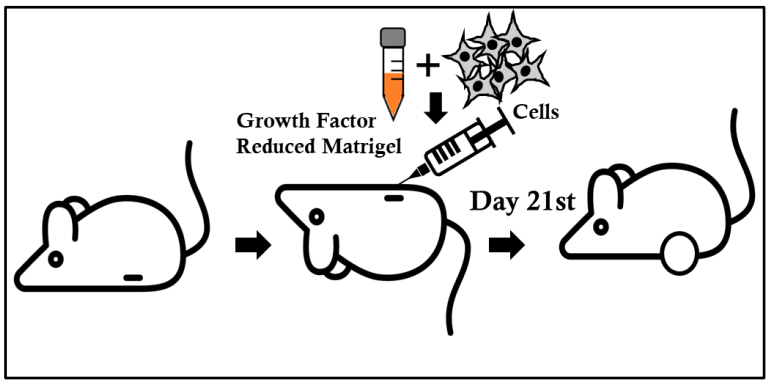

Figure 3.10.2.1.1 Overview of tumor generation in mice. *The schematic diagram describes the steps followed to generate the orthotopic mice model. The detailed protocol is written in the Method section above (3.10.2.1).*

3.10.2.2. Generation of metastatic mice model

We examined the metastatic potential of FRG1 *in vivo.* To perform this, we generated stable 4T1 cells with FRG1-level perturbation, following the procedure described in section 3.2.2.1. 6-8 weeks-old female BALB/c mice were anesthetized by the isoflurane-oxygen inhalation method. A glass beaker was filled ¾ with water and warmed at 37ºC. The tail of the mouse was dipped into that pre-warmed water for 5 minutes to increase vasodilation. A cotton pad was dipped into xylene and gently rubbed on the tail of the mouse for easy visualization of the vein. We suspended 1×10^6 cells into 100 µL of DPBS and filled it into a 1 mL insulin syringe with no air bubble. The needle was placed at a 45º angle, and the cells were slowly injected into the veins of the mice. The injected area was cleaned with 70% alcohol. The animals were transferred to their cages and monitored for 14 days. On day $14^{th,}$ animals were euthanized by CO_2 inhalation method. We removed their lungs and carefully cleaned them with DPBS. Lungs were photographed using a digital camera, and the number of lung nodules was counted. The overall process is depicted in Fig. 3.10.2.2.1.

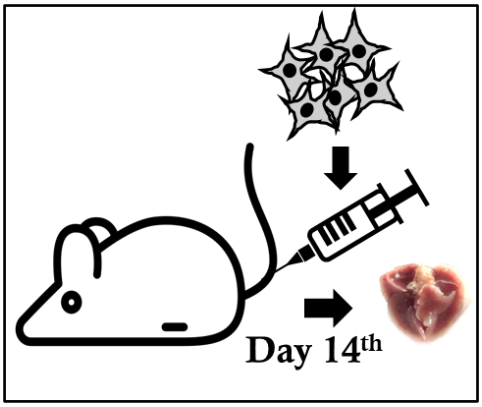

Figure 3.10.2.2.1. Overview of metastatic mice model. *The schematic diagram describes the steps followed to generate the metastatic mice model. The detailed protocol is written in the Method section above (3.10.2.2).*

3.10.2.3. Effect of GM-CSF Inhibition *in vivo*

We investigated the effect of GM-CSF inhibition in mice. Female BALB/c mice aged 6 to 8 weeks were divided into three groups (n = 4). Two groups of mice were administrated with 4T1 cells with depleted FRG1 levels, following the steps outlined in section 3.10.2.1. The other group of mice was injected with control 4T1 cells. On day 7th, we observed palpable tumors on the injected sites of the mice. On alternate days, a group of mice that had previously received 4T1 cells with decreased FRG1 levels were intraperitoneally injected with GM-CSF neutralizing anti-mouse monoclonal antibody (10 mg/kg body weight) until day 20. Tumor size and the weight of the animals were monitored every third day. Finally, the mice were euthanized by CO_2 inhalation method on day 21st. The tumors were removed and stored in DPBS at 4ºC. The overall process is summarised in Fig. 3.10.2.3.1. Tumors were minced, and the protein was extracted. Later the protein was used for Western blotting to assess the expression of phospho-ERK and EMT marker Snail.

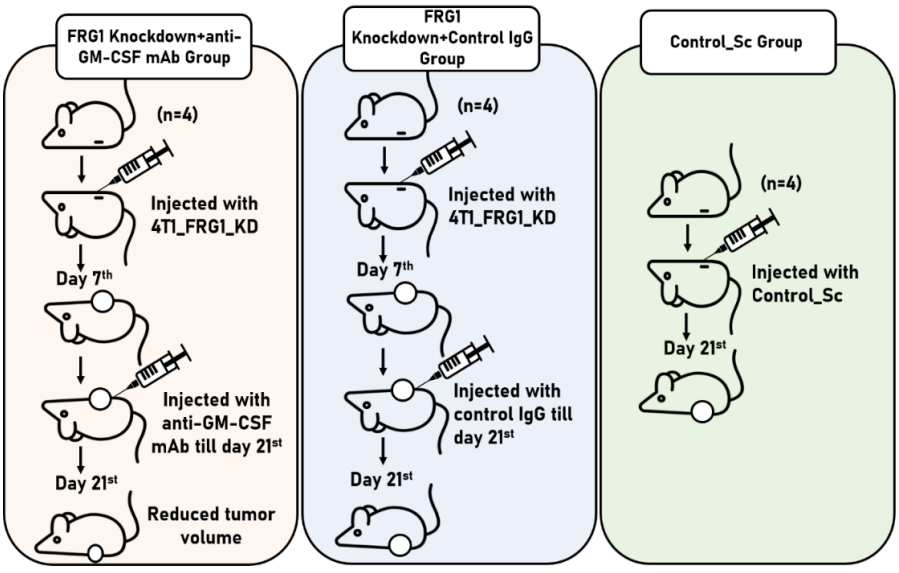

Figure 3.10.2.3.1. Overview of investigating the potential of anti-GM-CSF therapy in vivo. *The schematic diagram describes the steps followed to investigate the effect of anti-GM-CSF therapy in mice model. The detailed protocol is written in the Method section above (3.10.2.3).*

3.10.2.4. Matrigel Plug Assay in Mice

We performed the Matrigel Plug assay in 6-8 week old female C57BL/6 mice. A cocktail of growth factor-reduced matrigel and conditioned medium harvested from the 4T1 cells with reduced FRG1 levels were mixed in a 1:1 ratio. We shaved the fur from the right flank of the mice. Next, 200 µL of the freshly prepared cocktail was injected into the right side of the mice using a pre-chilled syringe with a 24G needle. Once the mixture turned into a solid gel plug inside the animals, they were transferred to their cages with a proper supply of food and water. After 7 days, the mice were euthanized by CO_2 inhalation method, and the plugs were carefully removed. Photographs of the plugs were captured using a digital camera. The overall method to develop the Matrigel plugs in mice is described in Fig. 3.10.2.4.1.

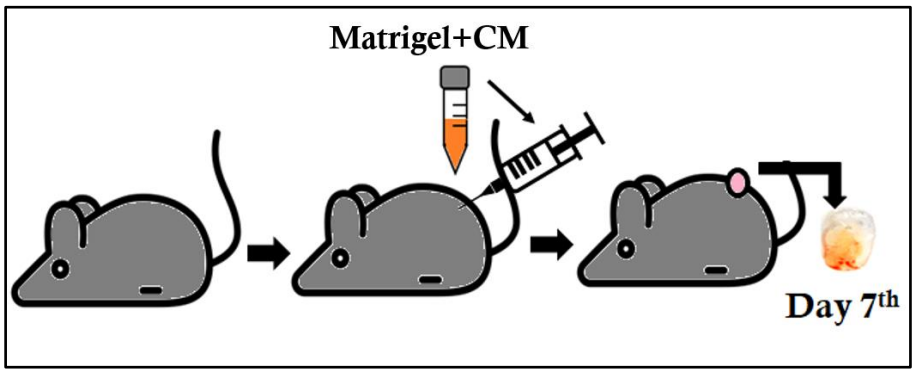

Figure 3.10.2.4.1. ***Overview of Matrigel plug assay in animal.*** *The schematic diagram describes the steps followed to generate the Matrigel plugs in mice. The detailed protocol is written in the Method section above (3.10.2.4).*

3.10.2.5. Wound Healing Assay in Mice

To assess the angiogenic potential of FRG1 *in vivo*, we carried out the wound healing assay in female BALB/c mice of 6-8 weeks old. Healthy mice without any skin injury or infection were selected for the experiment. First, we gently shaved all the furs from the dorsal side of the mice,

followed by anesthetizing them using the isoflurane-oxygen inhalation method. A wound was created on the dorsal side of the mice with the help of a puncture machine which was 4 to 6 mm in diameter. Using adhesive and 3-0 surgical suture (sterile and non-absorbable), a silicon splint (inner diameter: 8 mm, thickness: 0.5 mm) was placed around the incision. Finally, the wound was covered with a 3M Tagaderm dressing film. To reduce the suffering of the animals, intraperitoneal injection of the analgesic Tramadol (50mg/kg body weight) was given for two days at intervals of 12 hours. A cocktail of conditioned medium from the FRG1-depleted 4T1 cells and growth factor reduced matrigel was prepared in a 1:1 ratio. Each group's mice received 100 µL of this cocktail on the wounds every 12 hours for nine days, starting from the day of wound creation. Every third day the images of the wounds and the animals were taken with a digital camera till day 9. The area of the wound was measured with the help of ImageJ software. The wound healing rate was calculated using the following equation (Wound area on the day '0'-Wound area on a respective day) × 100/ Wound area on the day '0'.

3.11. Differential Expression and Survival Analysis

GEPIA webserver (http://gepia.cancer-pku.cn/about.html) was used to ascertain differential FRG1 transcript level (cancer patients vs. TCGA normal and GTEx, rest of the default parameters; p value cut-off 0.01, log_2FC value cut-off 1, log scale, and jitter size 0.4) and disease free survival (DFS) (group cut-off quartile) in BRCA dataset (accessed on 24th December 2021).

We did relapse free survival (RFS) analysis in Kaplan-Meier plotter (https://kmplot.com/analysis/, accessed on 16th Feb 2022) using mRNA gene chip data and auto select best cut-off in breast cancer patients with wild type p53. Hazard ratio (HR) with 95% of confidence interval (CI), and statistical significance were determined using log rank test.

3.12. Statistical Analysis

Statistical analysis was performed using GraphPad Prism 6.0 version (GraphPad Software Inc., CA, USA) and Microsoft Excel (Microsoft, WA, USA). To determine the statistical significance of difference in mean values, two-tailed unpaired Student's t-test was applied. Mann-Whitney U test was used to measure the correlation between Allred scores for FRG1 expression in cancer and normal samples. Data are presented as mean ± SD. p-value ≤ 0.05 was considered to be significant for all the tests.

Chapter 4

Result

Sub Chapter 4A
Result: Objective 1

Determination of the molecular subtype-specific mechanism of FRG1 in breast cancer progression and its implication in survival

This work has been published in part with the sub-chapter 4B as the following research article:

Mukherjee, B., Tiwari, A., Palo, A., Pattnaik, N., Samantara, S., Dixit, M. *Reduced expression of FRG1 facilitates breast cancer progression via GM-CSF/MEK-ERK axis by abating FRG1 mediated transcriptional repression of GM-CSF*. **Cell Death Discovery, 2022,** 8(1):442, DOI: https://doi.org/10.1038/s41420-022-01240-w

We have discussed the so far-reported function of FRG1 in cancer in the Introduction (Chapter 1) and Review of Literature section (Chapter 2). Based on the available literatures, we hypothesized that FRG1 might be involved in cancer progression and tumor angiogenesis. But before our study, no thorough investigation was carried out to explore the underlying molecular mechanism. Despite the fact that many cancer types have been associated with increased levels of GM-CSF, little is known about the regulatory processes that coordinate GM-CSF-mediated metastatic colonization. In the first objective (Sub Chapter 4A), we have conducted the first in-depth investigation to elucidate FRG1's thus far unexplored role and the underlying molecular mechanism in breast tumorigenesis *in vitro.* Here we have shown that FRG1 acts as a transcriptional repressor of GM-CSF. Increased GM-CSF levels, due to reduced FRG1, trigger the MEK/ERK pathway, leading to an increase in oncogenic properties regardless of breast cancer molecular subtypes. We have also discovered that GM-CSF-mediated ERK upregulation in FRG1-depleted cells lowered the AKT and p53 phosphorylation, leading to an ERK-dependent suppression of the apoptotic process. To summarize the significance of our findings in Objective 1, we have identified a molecule that can aid in inhibiting the metastatic spread of cancerous cells irrespective of breast cancer molecular subtypes. Using the *in vitro* system, we have found that FRG1 affects multiple tumorigenic events in breast cancer, comprising EMT and apoptosis, regardless of molecular subtypes.

The key findings pertaining to the first objective are described below.

4A.1. FRG1 level modulation affects the tumorigenic properties of breast cancer cell lines regardless of their molecular subtypes

To investigate the role of FRG1 in breast cancer, we started by examining its endogenous expression in the luminal cell line (positive for Estrogen and Progesterone receptors) MCF7 and basal cells (triple-negative breast cancer or TNBC) MDA-MB-231 (Fig. 4A.1.1.A). We generated shRNA-based stable MCF7 cells with depleted FRG1 levels (Fig. 4A.1.1.B). As

FRG1 is expressed in MCF7 at a moderate level, we also developed stable cells with elevated FRG1 expression (Fig. 4A.1.1.C). Since the endogenous FRG1 levels in MDA-MB-231 cell was lesser, we developed stable cells with elevated FRG1 expression only (Fig. 4A.1.1.D).

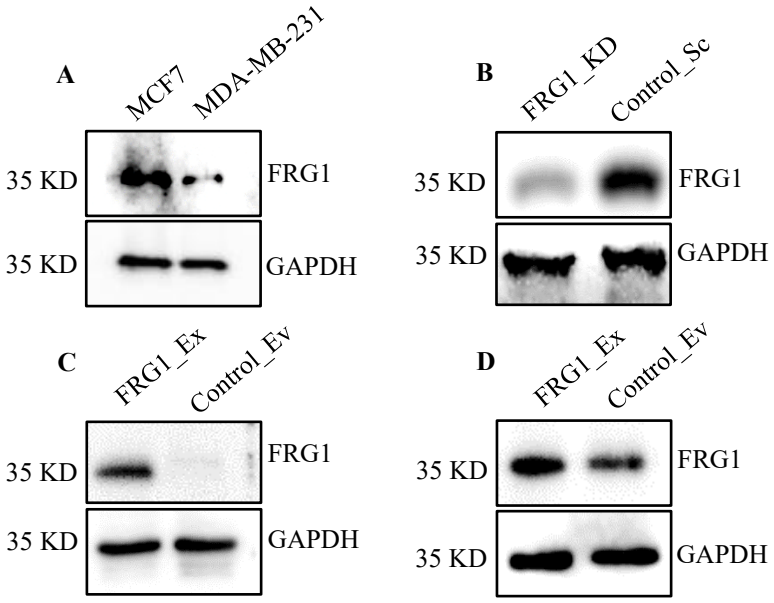

Figure 4A.1.1. Endogenous levels of FRG1 in breast cancer cells of different molecular subtypes and generation of stable cell lines. **(A),** *Western blot shows endogenous FRG1 levels in luminal cells MCF7 and basal cells MDA-MB-231.* **(B)**, The left *band of the Western blot (upper blot) depicts the stable knockdown of FRG1 protein in MCF7 cells (FRG1_KD) compared to the control (Control_Sc).* **(C),** *The left band of the upper blot represents the stable expression of FRG1 in MCF7 cells (FRG1_Ex) compared to the control (Control_Ev).* **(D),** *The left band of the upper blot detects the stable expression of FRG1 in MDA-MB-231 cells (FRG1_Ex) compared to the control (Control_Ev). GAPDH has been used as the loading control in all the blots.*

4A.1.2. *Elevated levels of FRG1 reduce tumorigenic phenotypes in MCF7 cells*

A preliminary study by our group detected that a reduction of FRG1 levels led to enhanced proliferation, migration, and invasion in MCF7 cells compared to the control. We further substantiated this observation in MCF7 cells with elevated FRG1 expression and the corresponding control. To inspect the effect of increased FRG1 levels on the proliferative property of breast cancer cells, we performed colony formation and MTS-based cell proliferation assays in MCF7 cells. There we found that ectopic expression of FRG1 reduced the proliferation in both assays (Fig. 4A.1.2.A and Fig. 4A.1.2.B). To investigate the effect of FRG1 overexpression on the regulation of the metastatic potential of breast cancer cells, we performed cell migration and invasion assays. Scratch wound healing assay revealed that elevated FRG1 expression reduced migration in MCF7 cells (Fig. 4A.1.2.C). This observation was corroborated by the matrigel invasion assay, where FRG1 overexpression was found to reduce cell invasion (Fig. 4A.1.2.D).

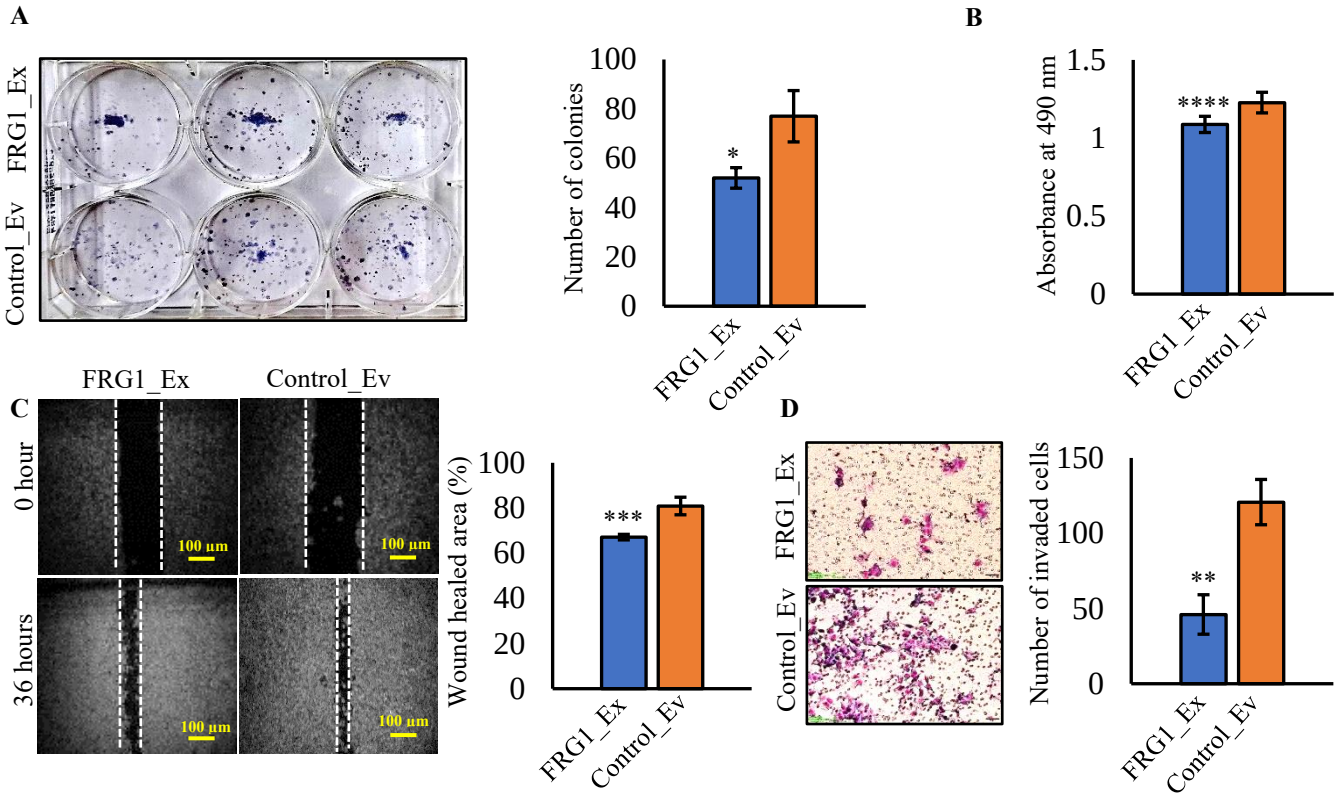

Figure 4A.1.2. Effect of ectopic FRG1 expression on tumorigenic properties of MCF7 cells. **(A),** *Representative image and bar graph of the colony formation assay shows the number of colonies in MCF7 cells with FRG1 overexpression (FRG1_Ex) and its corresponding control (Control_Ev).* **(B),** *The bar graph of the MTS-based cell proliferation assay shows the OD values measured at 96 hours at 490 nm in FRG1_Ex vs. Control_Ev.* **(C),** *Representative images of the scratch wound healing assay in FRG1_Ex and Control_Ev group at 0 and 24 hours. The bar graph shows the wound closure percentage in both groups. Scale bar: 100 µm.* **(D),** *Representative matrigel invasion assay of MCF7 cells with FRG1_Ex and Control_Ev. The bar graph shows the number of invaded cells in the two groups. Scale bar: 50 µm. All the experiments were replicated thrice. To derive the statistical significance of the difference between the two groups, two-tailed unpaired student's t-test was applied. Results are*

*represented as mean ± standard deviation (SD). *, $p \leq 0.05$; **, $p \leq 0.01$; ***, $p \leq 0.001$; ****, $p \leq 0.0001$.*

4A.1.3. *Elevated levels of FRG1 reduce tumorigenic phenotypes in MDA-MB-231 cells*

Furthermore, to ascertain if the impact of FRG1 was subtype-specific, we elevated the level of FRG1 in TNBC cell line MDA-MB-231, which possesses a basal level of FRG1 (Fig. 4A.1.1.A). In accordance with our findings in the FRG1 overexpression group in MCF7 cells, here also we noticed a reduction in cell proliferation (Fig. 4A.1.3.A, Fig. 4A.1.3.B), migration (Fig. 4A.1.3.C), and invasion (Fig. 4A.1.3.D) in the respective assays.

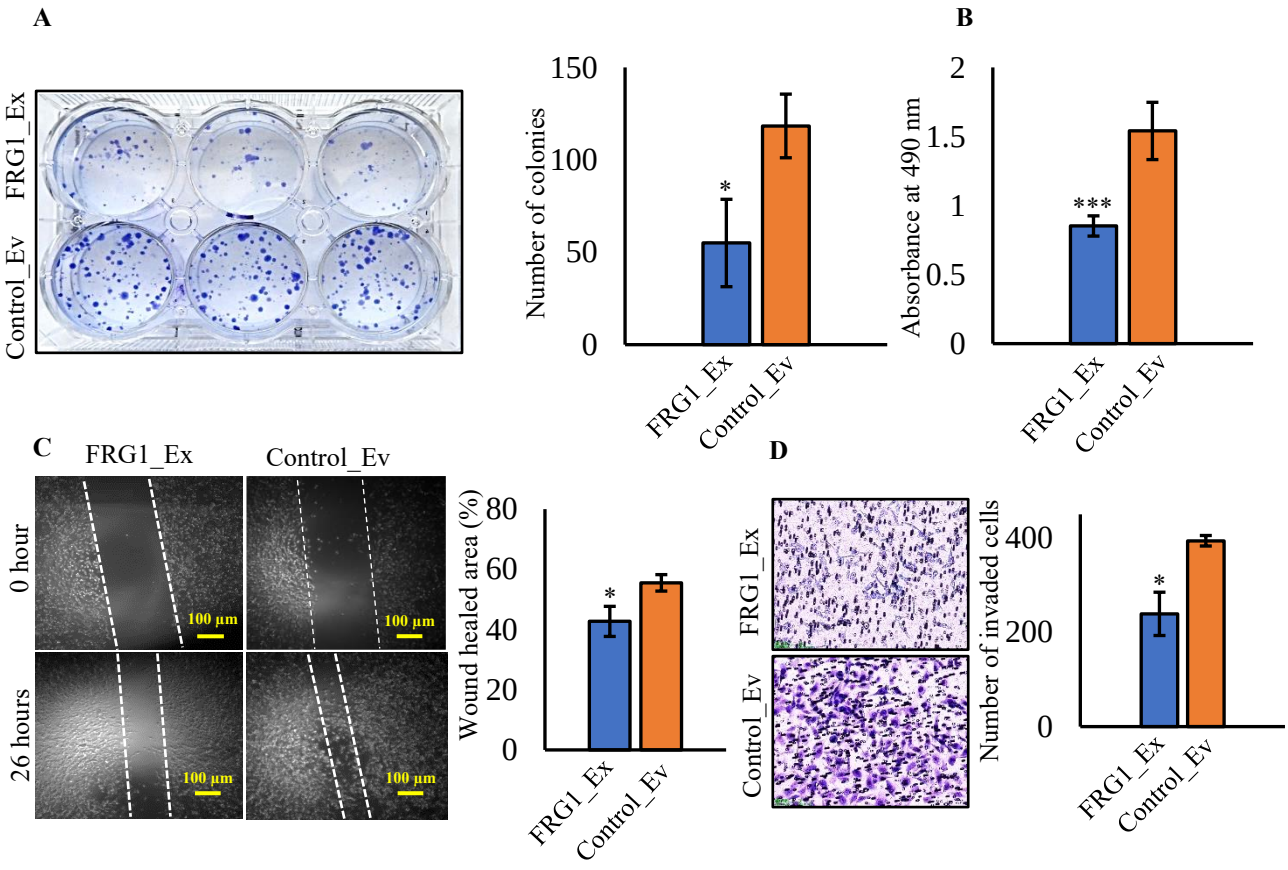

***Figure 4A.1.3. Effect of ectopic expression of FRG1 on tumorigenic properties of MDA-MB-231 cells.* (A),** *Representative image and bar graph of the colony formation assay shows the number of colonies in MDA-MB-231 cells with FRG1 overexpression (FRG1_Ex) and its*

corresponding control (Control_Ev). **(B),** *The bar graph of the MTS-based cell proliferation assay shows the OD values measured at 96 hours at 490 nm in FRG1_Ex vs. Control_Ev***. (C),** *Representative images of the scratch wound healing assay in FRG1_Ex and Control_Ev group at 0 and 24 hours. The bar graph shows the wound closure percentage in both groups. Scale bar: 100 µm.* **(D),** *Representative images of the matrigel invasion assay of FRG1_Ex and Control_Ev cells in MDA-MB-231 cells. The bar graph shows the number of invaded cells in the two groups. Scale bar: 50 µm. All the experiments were independently replicated thrice. To derive the statistical significance of the difference between the two groups, two-tailed unpaired student's t-test was applied. Results are represented as mean ± standard deviation (SD). *, $p \leq 0.05$; ***, $p \leq 0.001$.*

4A.1.4. *Effect of FRG1 knockout on the tumorigenic phenotypes of MCF7 cells*

Additionally, we generated CRISPR-Cas9-mediated stable FRG1 knockout in MCF7 cells (Fig. 4A.1.4.A) and investigated its effect on the oncogenic characteristics. In parallel to our previous findings, where reduction in FRG1 augmented the tumorigenic properties of MCF7 cells, we observed increased cell proliferation in the MTS-based cell proliferation assay (Fig. 4A.1.4.B) and enhanced migration in the insert migration assay (Fig. 4A.1.4.C).

So far, our results suggest that the overexpression of FRG1 reduces the tumorigenic properties of luminal cells MCF7 (Fig. 4A.1.2). Expectedly, we found enhanced tumorigenic characteristics due to the knockout of FRG1 (Fig. 4A.1.4). Similar to MCF7 cells, we observed reduced tumorigenic attributes in TNBC cells MDA-MB-231 with ectopic FRG1 expression (Fig. 4A.1.3).

Collectively, our findings imply that the effect of FRG1 level modulation is irrespective of breast cancer molecular subtypes.

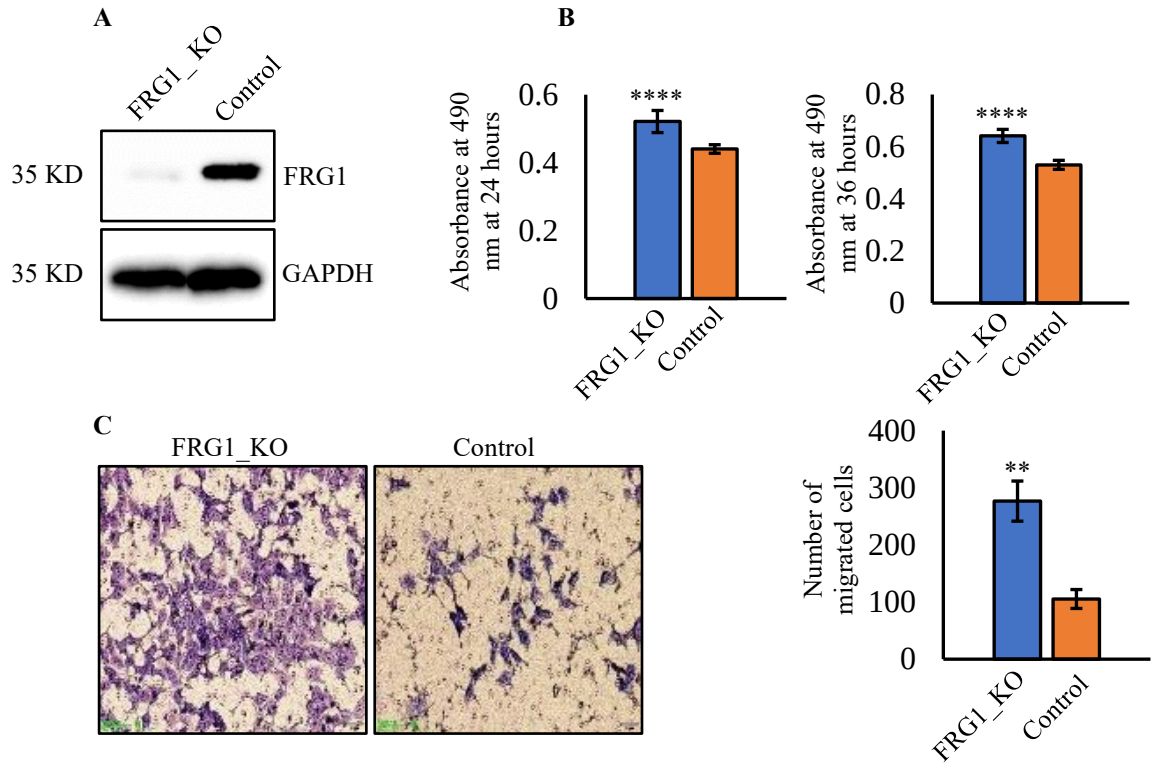

Figure 4A.1.4. Knockout of FRG1 in MCF7 cells affects cellular migration and proliferation. **(A)**, Representative Western blot shows the abolished expression of FRG1 due to its knockout in MCF7 cells (FRG1_KO), compared to the unmodified control. **(B),** *Bar graphs of the MTS-based cell proliferation assay show the OD values measured at 490 nm at 24 and 36 hours in FRG1_KO vs. Control.* **(C),** *Representative images of the insert migration assay illustrate the migration of FRG1_KO and Control cells. The bar graph represents the number of migratory cells in FRG1_KO vs. Control groups. Scale bar: 50 µm. All the experiments were independently performed thrice. To derive the statistical significance of the difference between the two groups, two-tailed unpaired student's t-test was applied. Results are represented as mean ± standard deviation (SD). **, $p \leq 0.01$; ****, $p \leq 0.0001$.*

4A.2. Reduced FRG1 expression activates the tumorigenic signaling cascade

Next, we analysed the molecular signaling underlying the increased tumorigenic properties due to the depletion of FRG1. We investigated its effect on ERK and AKT signaling, which are reported as the two most frequently altered pathways during tumorigenesis (234).

4A.2.1. *Depleted FRG1 levels in MCF7 cells promote the MEK-ERK signaling pathway*

In MCF7 cells, we found that a decrease in FRG1 level elevated the activation of ERK ($Thr^{202/204}$ position) and its upstream molecule MEK (Ser^{217} position) without affecting the level of total ERK and total MEK (Fig. 4A.2.1.A). The same pattern was noticed in FRG1 knockout MCF7 cells, where the absence of FRG1 upregulated the level of phospho-ERK (Fig. 4A.2.1.B). To further confirm our hypothesis that activation of ERK signaling in MCF7 cells was caused by FRG1 depletion, the FRG1 expression vector was transiently transfected into the stable MCF7 cells with FRG1 knockdown (Fig. 4A.2.1.C). The result suggested that FRG1 expression in MCF7 cells with depleted FRG1 levels nullified the alteration in phospho-ERK expression and matched with the control (Fig. 4A.2.1.C).

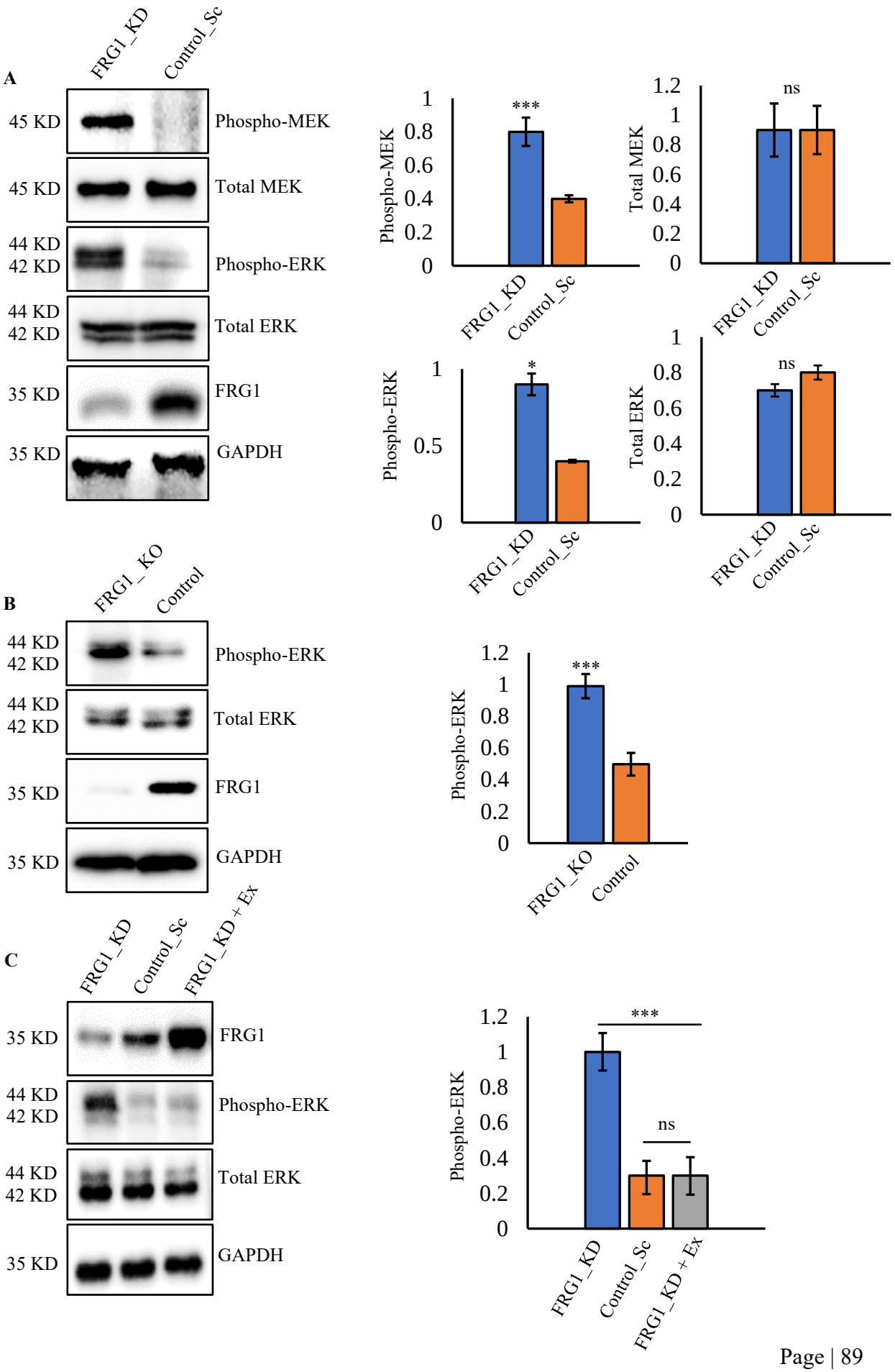
A
FRG1_KD
Control_Sc
45 KD
Phospho-MEK
45 KD
Total MEK
44 KD
42 KD
Phospho-ERK
44 KD
42 KD
Total ERK
35 KD
FRG1
35 KD
GAPDH
Phospho-MEK
***
Total MEK
ns
Phospho-ERK
*
Total ERK
ns
B
FRG1_KO
Control
44 KD
42 KD
Phospho-ERK
44 KD
42 KD
Total ERK
35 KD
FRG1
35 KD
GAPDH
Phospho-ERK
***
C
FRG1_KD
Control_Sc
FRG1_KD + Ex
35 KD
FRG1
44 KD
42 KD
Phospho-ERK
44 KD
42 KD
Total ERK
35 KD
GAPDH
Phospho-ERK
***
ns

Figure 4A.2.1. Effect of FRG1 reduction in the activation of ERK signaling in MCF7 cells. **(A),** *Western blots and the corresponding densitometry-based bar graphs show the activation of MEK and ERK in FRG1 depleted (FRG1_KD) MCF7 cells and also in its respective control (Control_Sc).* **(B),** *Western blots and the corresponding bar graphs show the levels of phospho-ERK between MCF7 cells with FRG1 knockout (FRG1_KO) and Control.* **(C),** *Representative Western blots are showing the rescue in ERK activation due to transient transfection of the FRG1 expression vector into the stable MCF7 cells with reduced FRG1 level (FRG1_KD+Ex). GAPDH has been used as internal control. The results presented here are the average of three separate tests. The statistical significance of the differential protein expression between the two groups was evaluated by using two-tailed unpaired student's t-test. The findings are shown as mean ± standard deviation (SD). ns, $p > 0.05$; *, $p \leq 0.05$; ***, $p \leq 0.001$.*

4A.2.2. *Elevated FRG1 levels reduce the activation of the MEK-ERK signaling pathway regardless of breast cancer molecular subtypes*

Next, we investigated if FRG1 overexpression had the opposite effect on the activation of MEK and ERK levels. We found declined levels of phospho-MEK (Ser^{217}) and phospho-ERK ($Thr^{202/204}$) when FRG1 was expressed ectopically in MCF7 cells (Fig. 4A.2.2.A). To further ascertain whether FRG1 affects regardless of breast cancer molecular subtypes, we measured the phospho-MEK and phospho-ERK levels in TNBC cells MDA-MB-231 with elevated FRG1 expression. Similar to the luminal cells, here also results showed reduced activation of MEK (Ser^{217}) and ERK ($Thr^{202/204}$) (Fig. 4A.2.2.B). No difference was observed in total MEK and total ERK expressions in both the subtypes.

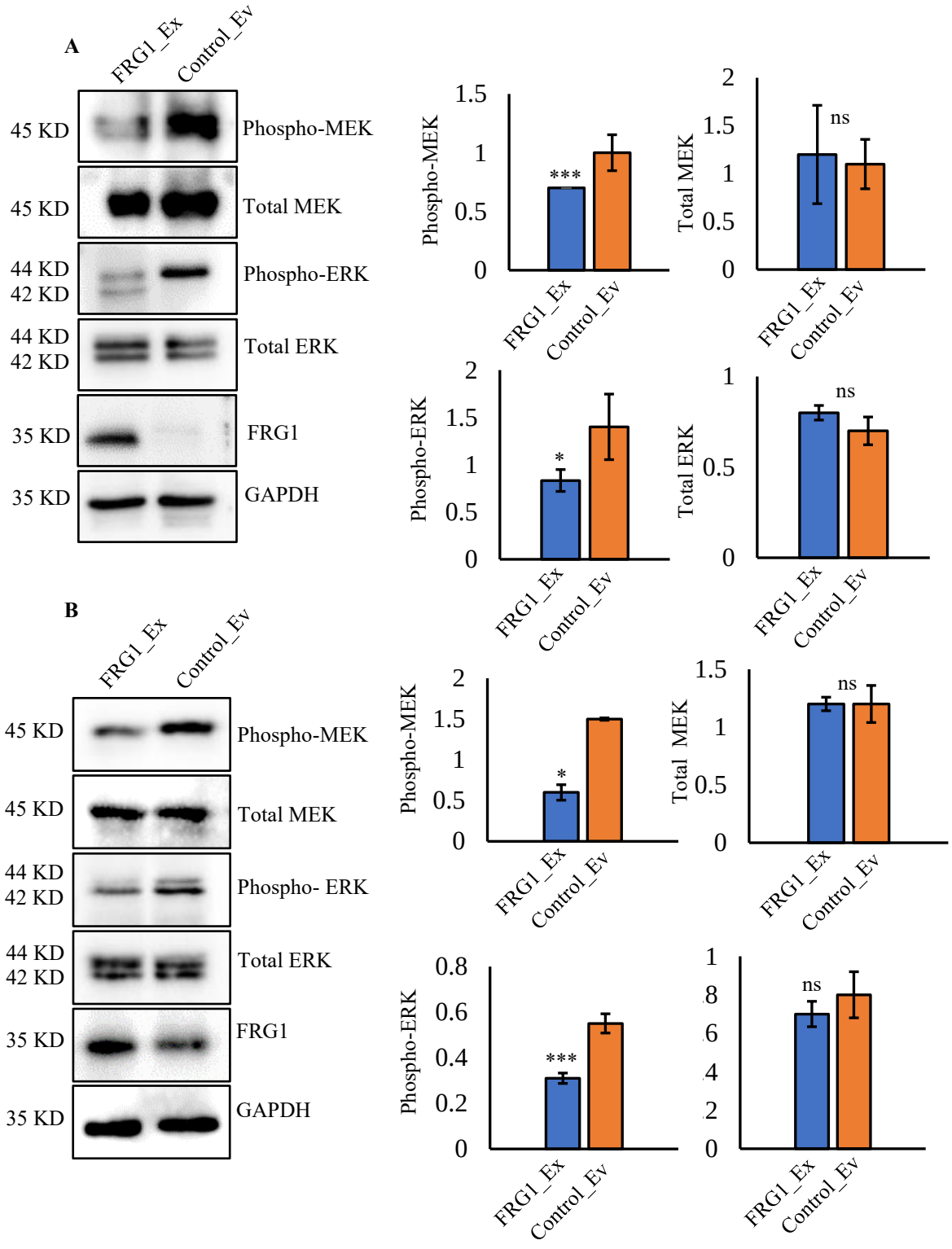

Figure 4A.2.2. Ectopic expression of FRG1 reduces the MEK/ERK activation. (A-B), *Western blots and the corresponding densitometry-based bar graphs showing the activated levels of MEK and ERK due to ectopic expression of FRG1 in MCF7 cells (FRG1_Ex)* **(A);**

and MDA-MB-231 (FRG1_Ex) cells, compared to their corresponding control **(B)**. *GAPDH has been used as internal control in all the blots. All the experiments were independently performed thrice. The statistical significance of the difference in protein expression between the two groups was evaluated by using two-tailed unpaired student's t-test. The findings are shown as mean ± standard deviation (SD). ns, $p > 0.05$; *, $p \leq 0.05$; ***, $p \leq 0.001$.*

4A.2.3. *Depleted FRG1 levels in MCF7 cells reduce AKT activation*

The interaction of the ERK and AKT pathways is crucial in determining whether a cell will undergo apoptosis or survival (235). Alteration of phospho-AKT levels is reported to be associated with several cancer types. While some of the AKT's downstream targets can be activated by phosphorylating it at the Thr^{308} site, activation of Ser^{473} in the C-terminal end is required to completely activate the AKT (236).

Hence, we checked the effect of FRG1 level perturbation on the phosphorylation of AKT on both the sites. Interestingly, reduced FRG1 levels in MCF7 cells decreased the activation of AKT only at the Thr^{308} position (Fig. 4A.2.3.A). As expected, increased FRG1 expression in MCF7 cells led to increased activation of AKT at the Thr^{308} location (Fig. 4A.2.3.B). Phosphorylation at the Ser^{473} position remained unchanged due to FRG1 reduction (Right side panel of Fig. 4A.2.3.A) or increase (Left side panel of Fig. 4A.2.3.B). Earlier reports stated that the AKT pathway could be suppressed by the activation of ERK (237). To test this, we repressed the ERK activation by administrating ERK inhibitor FR 180204 (10 μM) into FRG1-depleted MCF7 cells for two hours and found the rescue in phospho-AKT^{308} levels (Fig. 4A.2.3.C). Thus, our data provide evidence of ERK-mediated inhibition of AKT in FRG1-depleted MCF7 cells. Expectedly, ERK inhibition did not possess any impact on the phospho-AKT^{473} level.

Taken together, these findings indicate that reduced FRG1 levels may contribute to the development of breast cancer by stimulating the ERK signaling.

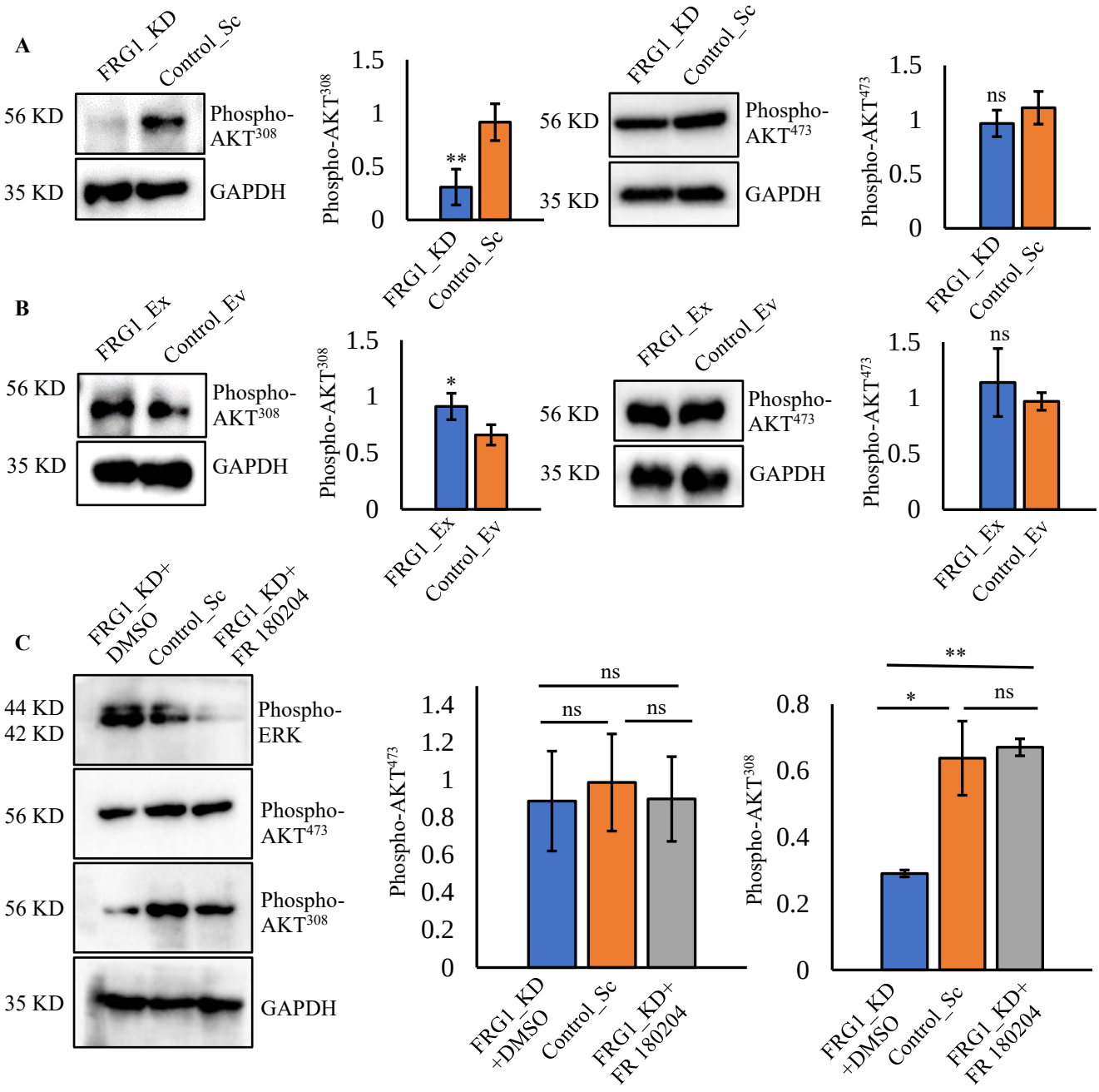

Figure 4A.2.3. Validation of the impact of FRG1 level perturbation on the AKT activation. **(A),** *Representative Western blots and densitometry-based bar graphs showing the levels of phospho-AKT^{308} (left panel) and AKT^{473} (right panel) in MCF7 cells with depleted FRG1 level (FRG1_KD) and control (Control_Sc).* **(B),** *Western blots and densitometry-based*

corresponding bar graphs denote the phospho-AKT^{308} (left panel) and phospho-AKT^{473} (right panel) expression in MCF7 cells with ectopic FRG1 expression (FRG1_Ex) and its control (Control_Ev). **(C),** *ERK inhibitor FR 180204 (10 μM) or its solvent DMSO was given to the FRG1_KD cells (FRG1_KD + FR 180204 and FRG1_KD + DMSO, respectively) for two hours. Thereafter, levels of phospho-AKT^{308} and phospho-AKT^{473} was measured by the Western blots. Corresponding bar graphs show the level of phospho-AKT^{308} and phospho-AKT^{473} in the three groups (FRG1_KD + DMSO, Control_Sc, and FRG1_KD + FR 180204). GAPDH has been used as internal control. Given results were derived from three independent experiments. The statistical significance of differential protein expression among the sets was measured by using two-tailed unpaired student's t-test. The findings are shown as mean ± standard deviation (SD). ns, $p > 0.05$; *, $p \leq 0.05$; **, $p \leq 0.01$.*

4A.3. Reduced FRG1 levels inhibit apoptosis via suppression of the p53 activation

A major hallmark of cancer is the loss of the apoptotic process (238). Decreased apoptosis prolongs the survivability of the cancer cells and provides more time for accumulating mutations (239). Decreased FRG1 expression in MCF7 cells considerably reduced the downstream caspase 3/7 levels compared to the control (Fig. 4A.3.A). In the flow-cytometry-based analysis of Annexin V/propidium-iodide, we found a lesser number of cells in the late apoptotic phase in MCF7 cells with FRG1 knockdown than in the control. It further confirms that reduced FRG1 levels decrease apoptosis and help in cell survival (Fig. 4A.3.B).

To understand the underpinning molecular signaling, we inspected the expression of reported apoptotic regulators in MCF7 cells with FRG1 knockdown and control. We found that the activation of p53 at the Ser^{46} position was decreased when FRG1 was reduced (Fig. 4A.3.C). Decreased apoptosis in FRG1-depleted cells may not be dependent on phospho-p38 level, as

our data shows no change in the activation of p38 at Thr^{180}/Tyr^{182} positions. (Fig. 4A.3.D). ERK-mediated induction of apoptosis by activation of p53 has been cited by several investigations (240), (192). To validate whether our finding was parallel to this, we inhibited the ERK activation in FRG1 knockdown MCF7 cells by treating the cells with ERK inhibitor FR 180204 or its solvent DMSO for two hours, followed by measuring of phospho-p53 levels (Fig. 4A.3.D). We observed a rescue in phospho-p53 level in MCF7 cells having reduced FRG1 expression, when treated with the ERK inhibitor (Fig. 4A.3.D).

Collectively our data suggest ERK-mediated suppression of phospho-p53 in FRG1-depleted MCF7 cells, which in turn reduces apoptosis.

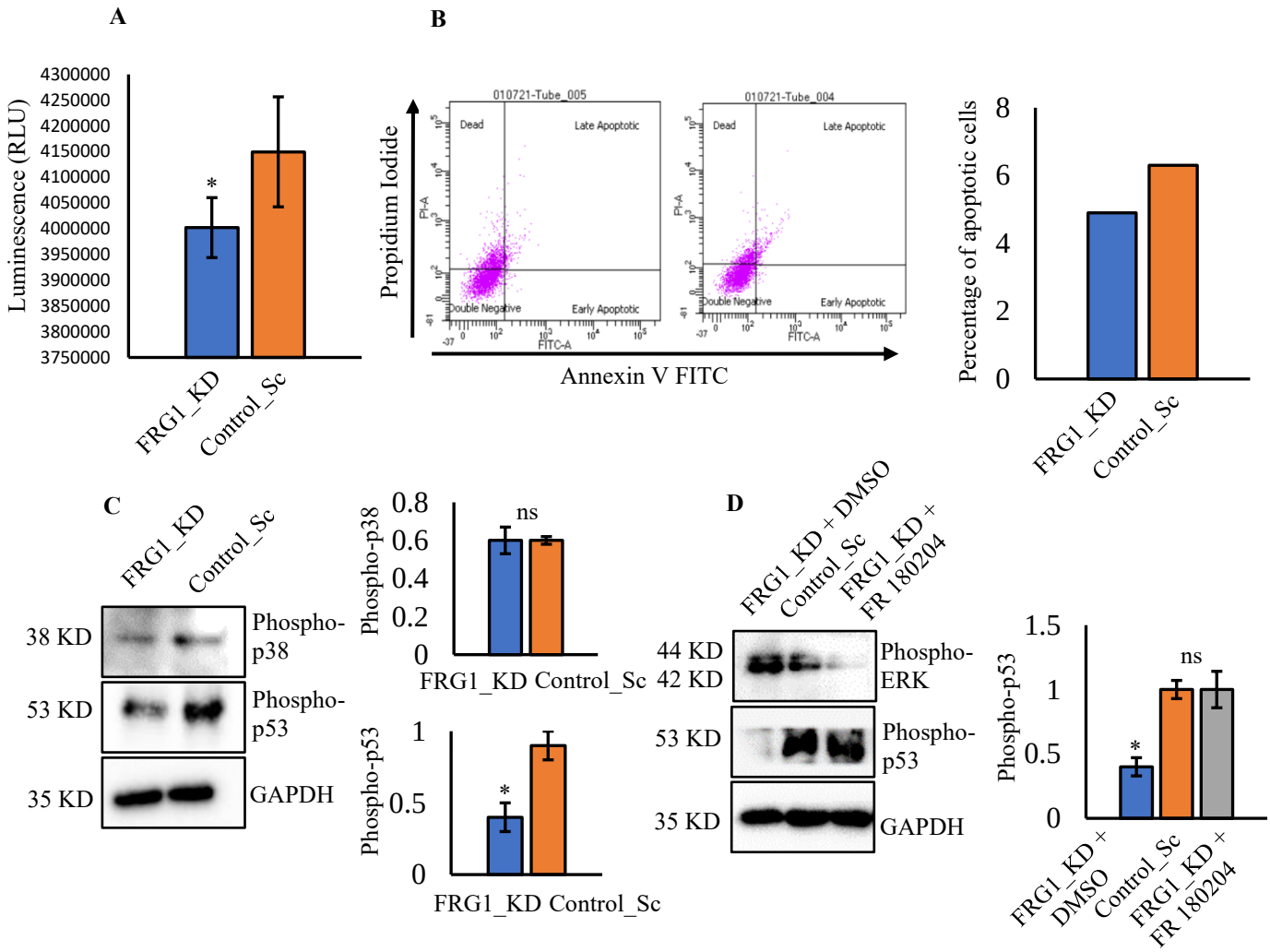

Figure 4A.3. FRG1 reduction suppresses cell death by ERK-p53 dependent mechanism. **(A),** *The bar graph of the Caspase 3/7 assay displays luminescence (RLU) in FRG1 knockdown (FRG1_KD) and the control (Control_Sc) MCF7 cells (n = 3).* **(B),** *The pictorial illustration of flow cytometry, showing Annexin V-FITC/Propidium iodide (PI)-based analysis of apoptosis in FRG1 knockdown (FRG1_KD) and control (Control_Sc) cells. Data was obtained using the 488 nm of excitation and 647 nm emission filters in the flow cytometry. The bar graph on the right side shows the percentage of cell deaths in the two groups (n = 1).* **(C),** *Representative Western blots and the densitometry-based bar graphs show the effect of FRG1 knockdown in the activation of p38 and p53 compared to the control (n = 3).* **(D),** *ERK inhibitor FR 180204 (10 μM) or its solvent DMSO was applied to the MCF7 cells with reduced FRG1 expression (FRG1_KD + FR 180204 and FRG1_KD + DMSO, respectively) for two hours. Western blot analysis was performed to determine the rescue of phospho-p53 level due to ERK inhibition (n = 3). The upper panel shows the abrogated ERK activation in FRG1_KD + FR 180204 group. The middle panel denotes the rescue of the phospho-p53 level due to the ERK inhibition. GAPDH has been used as the internal control. The statistical significance of the difference in protein expression was calculated by two-tailed unpaired student's t-test. Results are shown as mean ± standard deviation (SD). ns, $p > 0.05$; *, $p \leq 0.05$.*

4A.4. Loss of FRG1 triggers the EMT by activating the ERK signaling

EMT promotes cell motility, which further causes cancer cells to metastasize (241). As decreased FRG1 expression enhanced the cell migration and invasion, we further examined the effect of FRG1 level perturbation on the level of key EMT markers Snail, Slug, and Twist. These molecules are reported to play a significant part in EMT through ERK signaling (242), (243), (244). As anticipated, we found that FRG1-depleted MCF7 cells significantly elevated the expression of Snail, Slug, and Twist compared to the control (Fig. 4A.4.1.A). To further

confirm the participation of FRG1 in the metastatic program through ERK signaling, we inhibited the ERK activation in FRG1-depleted cells by treating the cells with ERK inhibitor FR 180204 (10 μM) or its solvent DMSO for two hours. Thereafter, we detected that ERK-mediated elevation of EMT marker Snail was no longer present (Fig. 4A.4.1.B). Scratch wound healing assay also revealed that ERK inhibition attenuated the migratory potential of FRG1-depleted cells and led the cells to return to the control level (Fig. 4A.4.1.C).

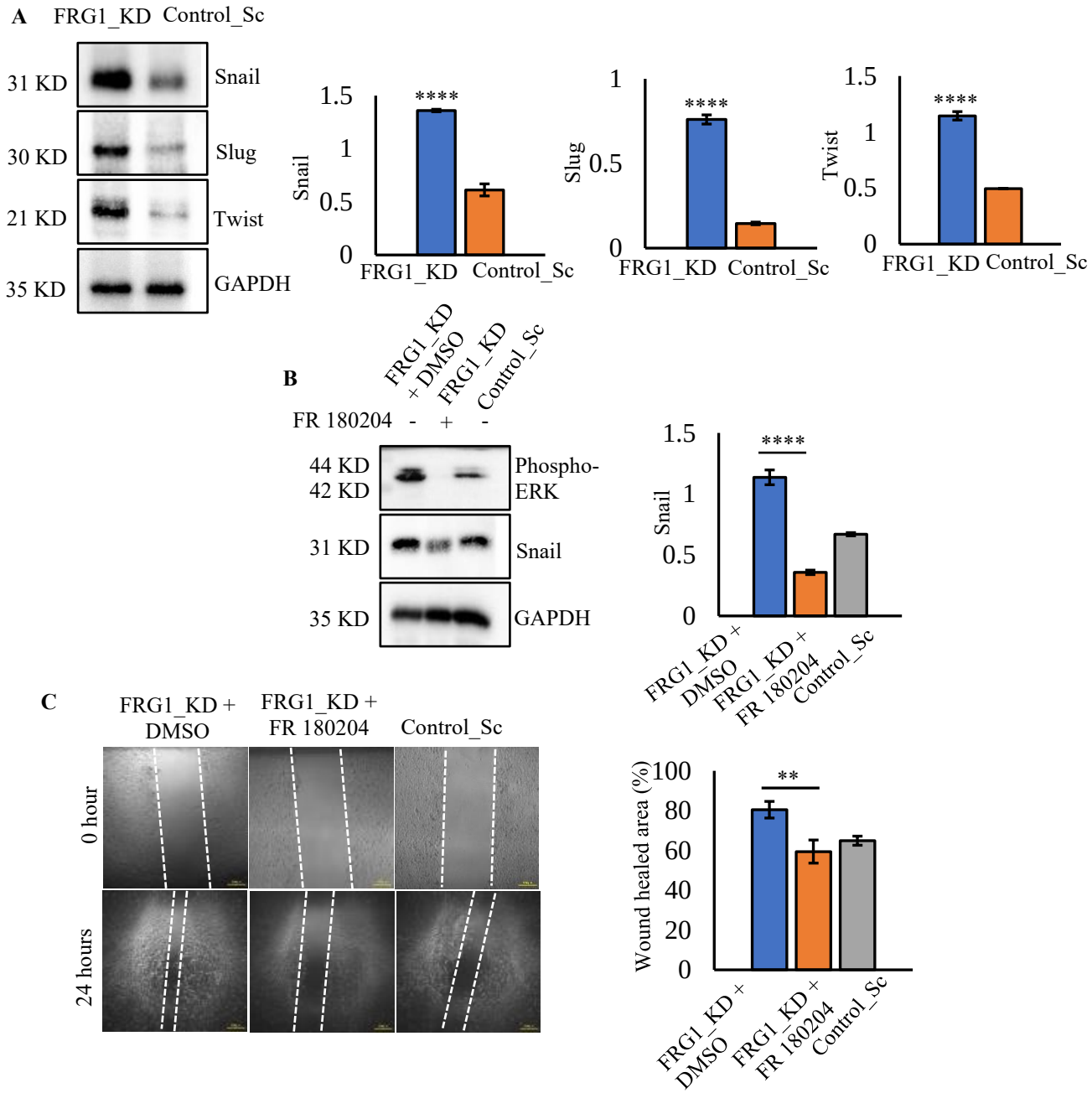

Figure 4A.4.1. Depleted FRG1 level enhanced EMT in MCF7 cells. **(A),** *Immunoblots and the corresponding bar graphs show the expression of EMT markers Snail, Slug, and Twist in MCF7 cells with reduced FRG1 level (FRG1_KD) and control (Control_Sc).* **(B),** *ERK inhibitor FR 180204 (10 μM) or its solvent DMSO were used for two hours to inhibit the ERK activation in FRG1_KD cells (FRG1_KD + FR 180204 or FRG1_KD + DMSO respectively) and subsequently subjected to immunoblotting. The uppermost blot confirms the ERK inhibition in FRG1_KD cells. The middle blot shows the effect of ERK inhibition on the Snail level in FRG1_KD cells. Corresponding bar graphs indicate the difference in the levels of Snail among FRG1_KD + DMSO, FRG1_KD + FR 180204, and Control_Sc groups.* **(C),** *Representative images and the corresponding bar graphs show the wound closure percentage in scratch wound healing assay in the same set as in* **B.** *GAPDH is used as internal control. The statistical significance of the difference was calculated by two-tailed unpaired student's t-test. Results were obtained from three independent experiments. Data are shown as mean ± standard deviation (SD). **, $p \leq 0.01$; ****, $p \leq 0.0001$.*

Parallelly, overexpression of FRG1 in MDA-MB-231 cells led to decreased expression of Snail, Slug, and Twist, indicating the effect of FRG1 on EMT was independent of breast cancer molecular subtypes (Fig. 4A.4.2.A). To corroborate our findings, we administrated ERK activator Ceramide (C6) (5 μM) or its solvent DMSO in MDA-MB-231 cells with ectopic FRG1 expression for two hours. Ceramide (C6) treatment recovered the phospho-ERK level in the Western blot (Fig. 4A.4.2.B). The same experimental setup restored the Snail levels and cell migration (Fig. 4A.4.2.C).

Together, this finding suggests that FRG1 level perturbation affects EMT independent of breast cancer molecular subtypes.

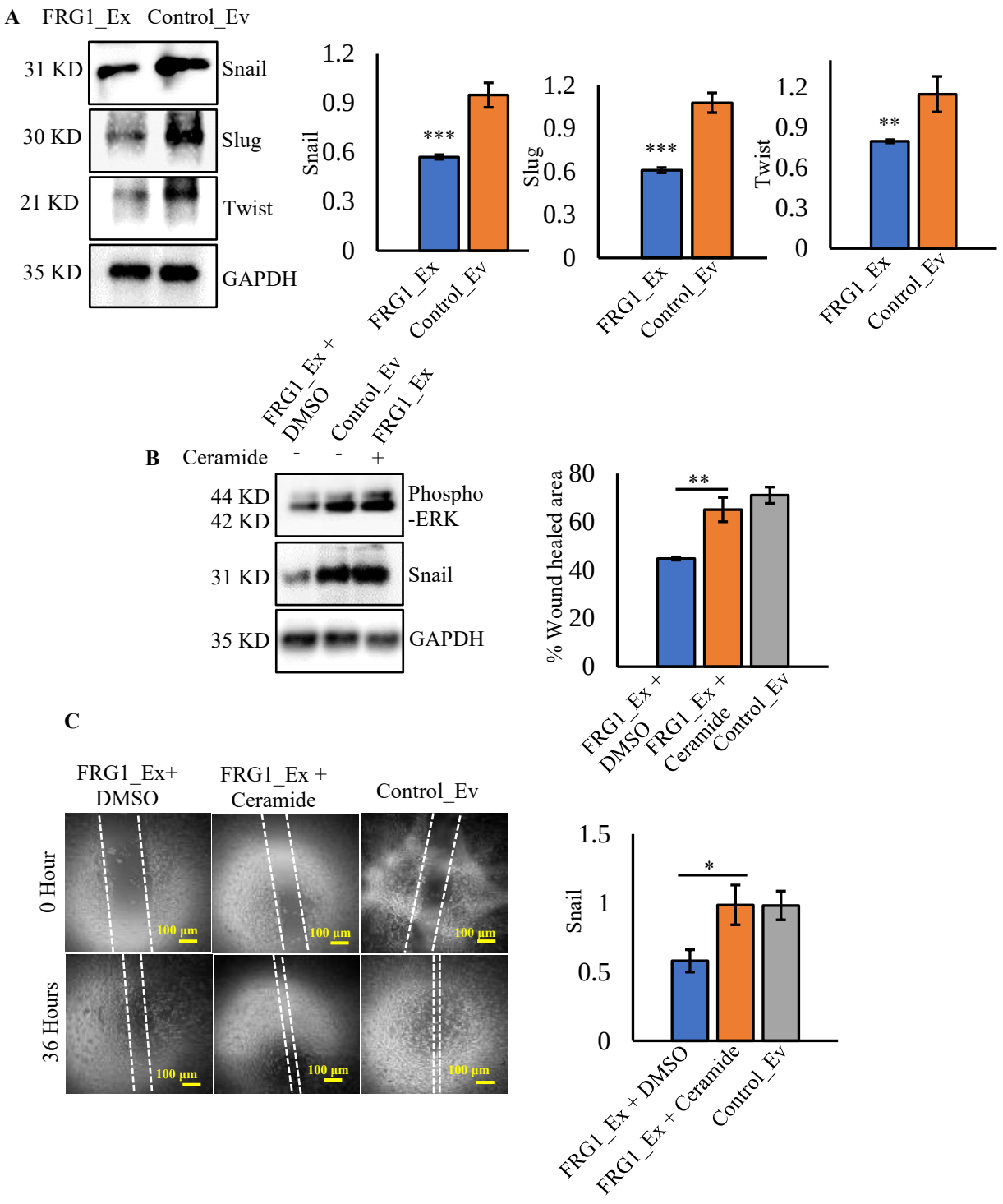

Figure 4A.4.2. Ectopic FRG1 level reduced EMT in MDA-MB-231 cells. **(A),** *Representative Western blots and the corresponding bar graphs show the level of EMT markers Snail, Slug, and Twist in MDA-MB-231 cells with elevated FRG1 levels (FRG1_Ex) and empty vector control (Control_Ev).* **(B),** *FRG1_Ex cells were treated with 5 µM of ERK activator ceramide*

(C6) or its solvent DMSO (FRG1_Ex + Ceramide or FRG1_Ex+DMSO respectively) for two hours, and Western blots were performed. The uppermost blot confirms the activation of ERK due to the Ceramide (C6) treatment in FRG1_Ex cells, followed by the rescue of EMT marker Snail level (middle blot). Bar graphs present the difference in the Snail levels in FRG1_Ex + DMSO, FRG1_Ex + Ceramide (C6), and Control_Ev group. **(C),** *Representative images and the corresponding bar graphs show the wound closure percentage in the same set as in* **B.** *GAPDH is used as internal control. The statistical significance of the difference was calculated by two-tailed unpaired student's t-test. Results were obtained from three independent experiments. Data are shown as mean ± standard deviation (SD). *, $p \leq 0.05$; **, $p \leq 0.01$.*

4A.5. Decreased FRG1 expression increases pro-tumorigenic cytokines and growth factors in breast cancer cells

Intrigued by the observations of ERK activation due to FRG1 knockdown, we sought the possible mechanisms. Numerous inflammatory cytokines and growth factors are indispensable in tumor development, progression, and metastasis (245). Our earlier research suggested that FRG1 level modulation altered the level of GM-CSF, PLGF, PDGFA, and CXCL1 in prostate cancer cells, which are reported to regulate EMT (27). We found that decreased FRG1 expression significantly raised the transcript levels of CXCL1/8, GM-CSF, and PDGFα/β in MCF7 cells (Fig. 4A.5.A). Elevated expression of FRG1 in MDA-MB-231 cells had the opposite impact (Fig. 4A.5.B). According to the literature, CXCL1 and CXCL8 act in part to stimulate the ERK pathway via binding to the CXCR2 receptors (246). To determine whether CXCL1/8 mediated activation of CXCR2 was responsible for the elevated phospho-ERK level and subsequent alteration in the EMT markers, we blocked the CXCL1/8 receptor CXCR2 in FRG1 knockdown MCF7 cells by treating with CXCR2 agonist Cpd19 for two hours (247). We observed that phospho-ERK and Snail levels did not change in the Western blot due to

Cpd19 treatment which means that the activation of ERK was independent of the CXCR2-CXCL1/8 (Fig. 4A.5.C). After that, to find out the other possible mechanism of ERK activation in FRG1-depleted MCF7 cells, we inhibited ERK signaling and checked the transcript levels of the cytokines mentioned above. We observed that ERK inhibition abrogated the CXCL1, CXCL8, PDGFα, and PDGFβ transcripts levels. It suggests that the effect of these cytokines is downstream of the ERK pathway (Fig. 4A.5.D). Interestingly, we noticed that the rise in GM-CSF in FRG1-depleted cells did not get reversed by the inhibition of the ERK pathway (Fig. 4A.5.D).

Further, we carried out ELISA to check the secreted GM-CSF protein level in the conditioned medium obtained from MCF7 with reduced FRG1 levels and MDA-MB-231 cells with elevated FRG1 levels. Corresponding to our qRT-PCR result, we observed enhanced and reduced levels of secreted GM-CSF protein in the conditioned medium harvested from FRG1 knockdown MCF7 cells (Fig. 4A.5.E) and MDA-MB-231 cells with ectopic FRG1 expression, respectively (Fig. 4A.5.F). It implies that GM-CSF acted upstream of the ERK.

Overall, we hypothesized that reduced FRG1 level caused ERK-mediated elevation of all the cytokines other than GM-CSF, and FRG1 might function upstream of GM-CSF.

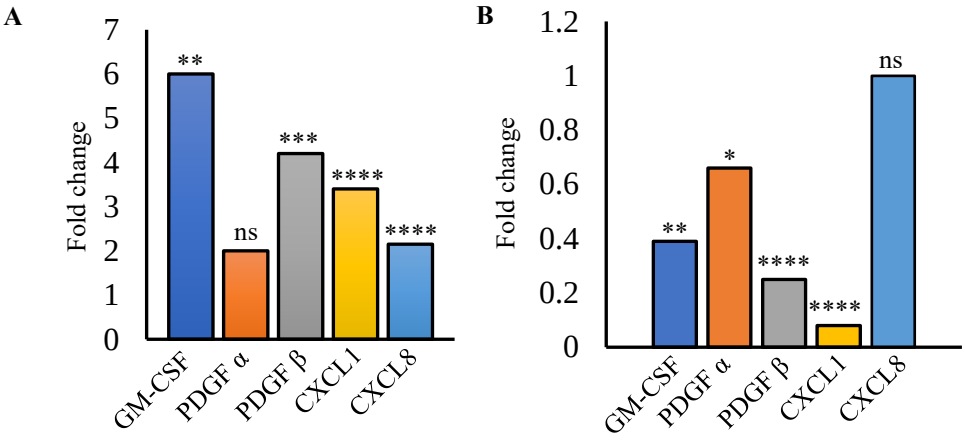

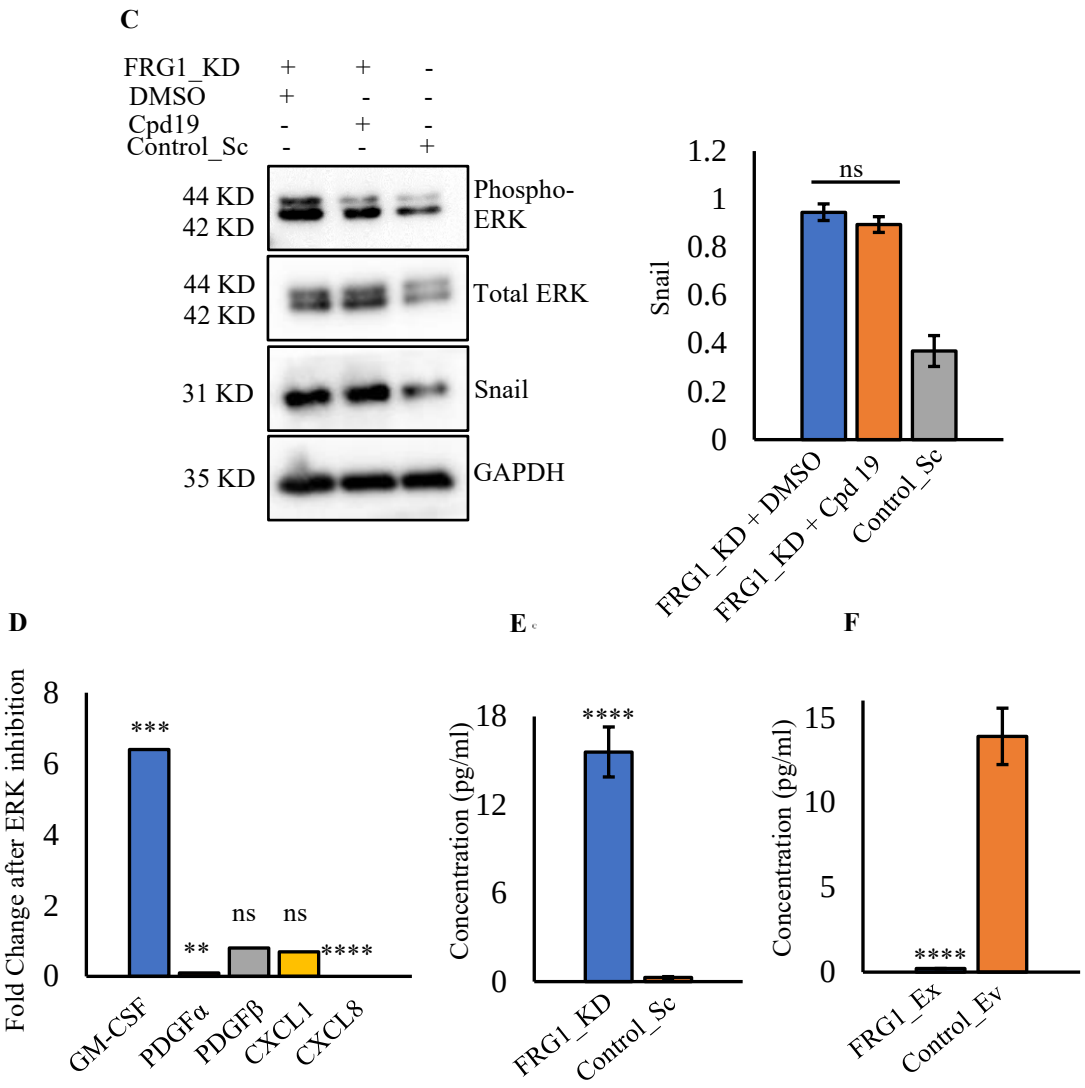

Figure 4A.5. Decreased FRG1 level increases the expression of the cytokines and growth factors. **(A-B),** *Representative bar graphs of the qRT-PCR showing the relative fold change in the mRNA level of* GM-*CSF, PDGFα, PDGFβ, CXCL1, and CXCL8 in MCF7 cells with depleted FRG1 level (FRG1_KD)* **(A);** *and MDA-MB-231 cells with increased FRG1 level (FRG1_Ex)* **(B)**. **(C),** *The CXCR2 receptor axis was inhibited in FRG1_KD cells (FRG1_KD+Cpd 19) by treating the cells with CXCR2 antagonist Cpd 19 (5 μM) for two hours. Representative Western blots show the effect of CXCR2 inhibition on the expression of phospho-ERK (first blot), total ERK (second blot), Snail (third blot) in FRG1_KD + DMSO, FRG1_KD + Cpd 19, Control_Sc respectively. Densitometry-based bar graph showing the level of Snail*

in the three groups as in **B. (D),** *Representative bar graphs of the q-RT PCR showing the relative fold change in the mRNA level of GM-CSF, PDGFα, PDGFβ, CXCL1, and CXCL8 in FRG1 knockdown cells treated with ERK inhibitor FR 180204 (10 μM) (FRG1_KD + FR 180204) for two hours.* **(E-F),** *Representative bar graphs of the ELISA show the amount of secreted GM-CSF in the supernatant of MCF7 cells with FRG1_KD* **(E)**; *and MDA-MB-231 cells with FRG1_Ex* **(F)**. *The statistical significance of the difference was calculated by two-tailed unpaired student's t-test. The given data is the representation of three independent experiments. Results are shown as mean ± standard deviation (SD). ns, $p > 0.05$; *, $p \leq 0.05$; **, $p \leq 0.01$; ***, $p \leq 0.001$; ****, $p \leq 0.0001$.*

4A.6. Direct binding of FRG1 on GM-CSF promoter regulates its expression

Based on the above-mentioned observations, we speculated that FRG1 might regulate the GM-CSF expression directly. The role of GM-CSF in breast cancer has not been thoroughly investigated. Before investigating if FRG1 acted as a transcriptional repressor of GM-CSF, we checked the effect of GM-CSF on breast cancer EMT.

4A.6.1. *Effect of exogenous GM-CSF on MCF7 cells*

To investigate the role of GM-CSF, we treated MCF7 cells with 100 nM of human recombinant GM-CSF (hGM-CSF) or its solvent PBS for an hour. We observed that the administration of hGM-CSF significantly elevated cell proliferation in the MTS-based cell proliferation assay (Fig. 4A.6.1.A). Matrigel invasion assay also revealed a similar trend (Fig. 4A.6.1.B). In parallel to investigating the tumorigenic properties, we studied the underlying molecular mechanism. In colorectal cancer, a report suggests that GM-CSF activated the ERK-mediated EMT by upregulating the expression of Snail (248). In support of the previous reports, we also found that the hGM-CSF activated ERK and led to increased levels of the EMT marker Snail in breast cancer (Fig. 4A.6.1.C).

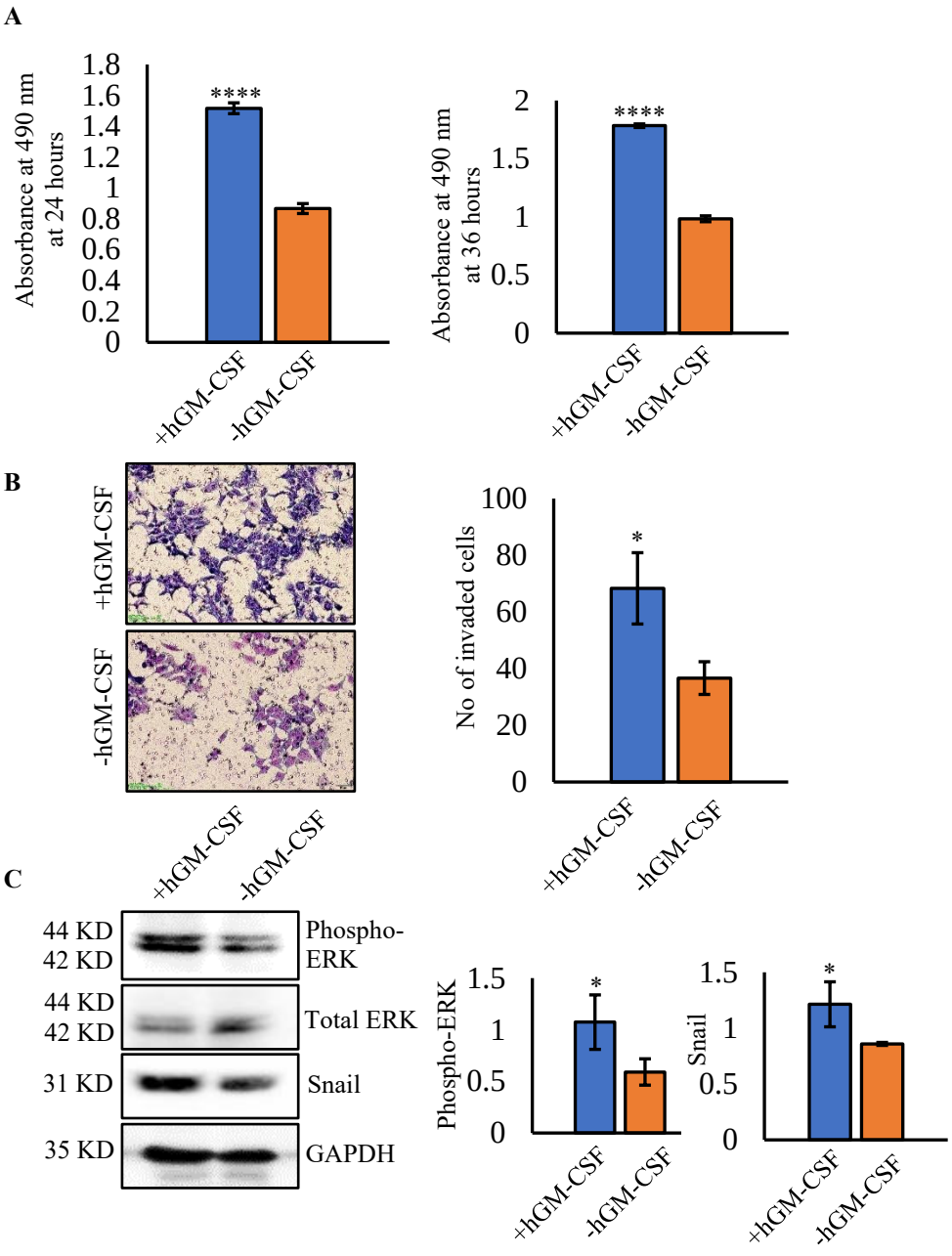

Figure 4A.6.1. Exogenous GM-CSF increases the tumorigenic properties of MCF7 cells. *MCF7 cells were treated with 100 nM of human recombinant GM-CSF (+hGM-CSF) or its solvent PBS (-hGM-CSF) for an hour.* ***(A),*** *Bar graphs of MTS-based proliferation assay shows the proliferation of MCF7 cells with or without exogenous GM-CSF treatment (+hGM-CSF and -hGM-CSF, respectively) in MCF7 cells at 24 hours and 36 hours. OD values were measured at 490 nm.* **(B),** *Representative images and bar graph show the number of invaded*

cells with (+hGM-CSF) or without GM-CSF (-hGM-CSF) treatment. Images were taken at 10X magnification. Sale bar: 50 μm. **(C),** *Western blots and the corresponding bar graphs show* the impact of exogenous GM-CSF in MCF7 cells *(+hGM-CSF and -hGM-CSF) in the level of phospho-ERK and EMT marker Snail. All the experiments were independently performed thrice. GAPDH has been used as internal control. The statistical significance of the difference is calculated by two-tailed unpaired student's t-test. Results are shown as mean ± standard deviation (SD). *, $p \leq 0.05$; ****, $p \leq 0.0001$.*

4A.6.2. *FRG1 negatively affects the GM-CSF expression*

Next, we checked the direct binding of FRG1 on the GM-CSF promoter. Earlier, our group identified that FRG1 binds to the 'CTGGG' sequence of the DNA (249). Within 907 bp of the transcription start point, we identified six "CTGGG" sequences in the GM-CSF promoter (Fig. 4A.6.2.A). To ascertain if FRG1 binds to this site, we cloned the 907 bp (upstream of the transcription start site) of the GM-CSF promoter into the pGL4.23 vector. We transfected this construct into the MDA-MB-231 cells with FRG1 overexpression along with the pGL4.73 renilla vector construct as an internal control. Administration of the GM-CSF promoter construct led to decreased luciferase activity in MDA-MB-231 cells with elevated FRG1 levels, compared to the empty vector control (Fig. 4A.6.2.B). No difference was found between the GM-CSF promoter construct and control groups in the relative luciferase activity of the MDA-MB-231 (Control_Ev) cells with basal FRG1 level (Fig. 4A.6.2.B). When the same constructs were transfected into the HEK 293T cells with decreased FRG1 levels, no difference in the relative luciferase activity was found between the GM-CSF promoter construct group and the empty vector control (Fig. 4A.6.2.C).

An enhanced luciferase activity was found in the control group than the GM-CSF promoter construct in HEK 293T cells (Control_Ev) cells with basal FRG1 level (Fig. 4A.6.2.C).

These findings indicate that FRG1 most likely had an inhibitory effect on GM-CSF expression, which is consistent with our earlier observations.

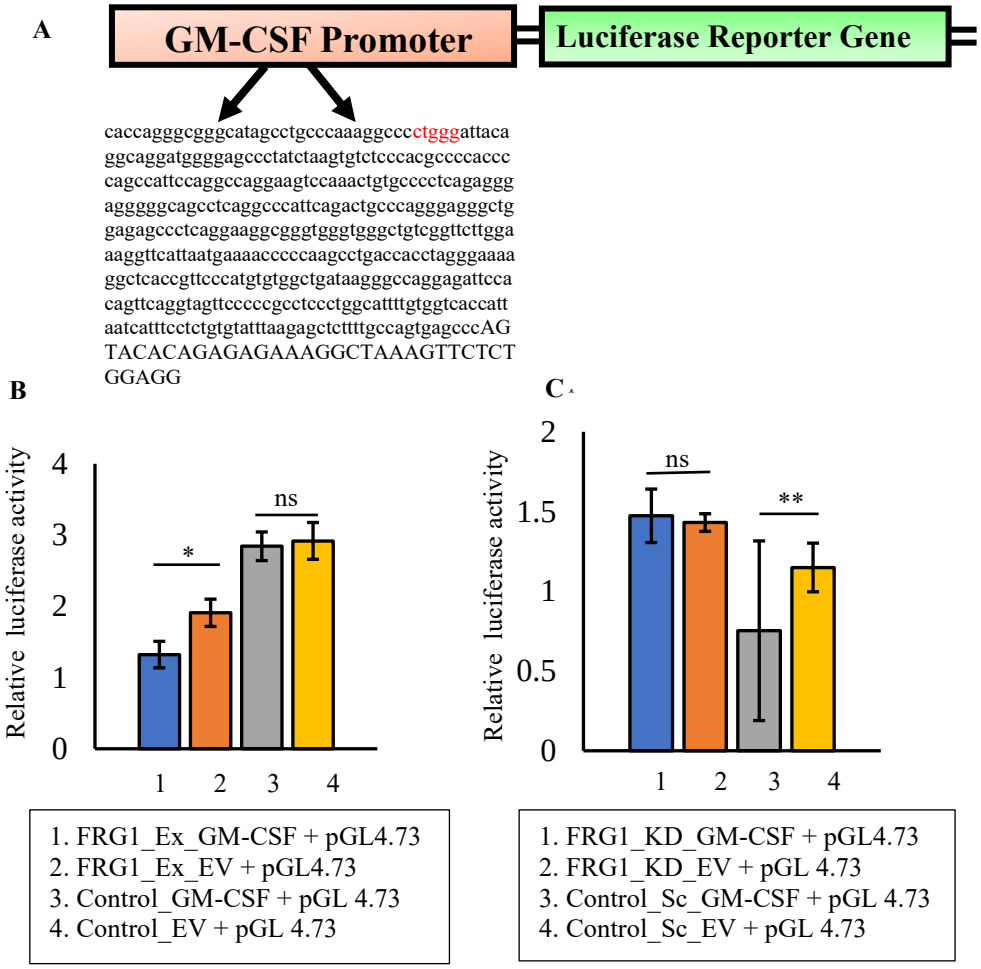

Figure 4A.6.2. Elevated FRG1 levels reduce the GM-CSF expression. **(A),** *The graphical representation shows the presence of the first CTGGG sequence (FRG1 binding site) on the GM-CSF promoter, 376 bp upstream of the transcription start point.* **(B),** *In one set of MDA-MB-231 cells with high FRG1 level (FRG1_Ex), the bar diagrams depict the variation in relative luciferase activity (firefly/renilla) utilizing the pGL 4.23 vector with the GM-CSF promoter (FRG1_Ex GM-CSF + pGL4.73) and empty vector (FRG1_Ex EV + pGL4.73. The second set of bars depict the variation in relative luciferase activity (firefly/renilla) in a different set of MDA-MB-231 cells with the control empty vectors (Control_Ev), where the same*

transfections were carried out (Control_Ev GM-CSF + pGL4.73 vs. Control_Ev + pGL4.73). **(C),** *In HEK 293T cells with decreased FRG1 level (FRG1_KD), the relative luciferase activity (firefly/renilla) was measured after transfecting with the pGL 4.23 vector with the GM-CSF promoter and the empty vector (FRG1_KD GM-CSF + pGL4.73 vs. FRG1_KD EV + pGL4.73). The relative luciferase intensity was also measured in another set of HEK 293T cells with endogenous FRG1 level (Control_Sc), using the same transfection (Control_Sc GM-CSF + pGL4.73 vs. Control_Sc EV + pGL4.73). The statistical significance of the difference was calculated by two-tailed unpaired student's t-test. Results are shown as mean ± standard deviation (SD). ns, $p > 0.05$; *, $p \leq 0.05$; **, $p \leq 0.01$.*

4A.6.3. *FRG1 directly binds to the GM-CSF promoter*

To confirm the direct binding of FRG1 on the GM-CSF promoter, EMSA was performed. We incubated the nuclear extract (from HEK 293T cell line with elevated FRG1 levels) with the labeled oligos (designed against the CTGGG sequence) and observed that the probe was bound to the nuclear extract. When we incubated the nuclear extract with an increased amount of unlabeled oligos along with the minimal amount of labelled oligos, the unlabeled oligos competed for the binding. Thereby a drastic reduction in the intensity of the shift was observed (Fig. 4A.6.3.A). Moreover, a supershift was seen in the fourth lane, once the binding complex was exposed to the FRG1-specific antibody, showing the specificity of FRG1 selectively binding to the oligos (Fig. 4A.6.3.A). This supports our hypothesis that FRG1 binds to the promoter of GM-CSF.

To validate it further, ChIP assay was carried out in HEK 293T cells with ectopic FRG1 levels. We incubated the chromatin fragments with the FRG1 antibody or IgG (negative control). Fig. 4A.6.3.B depicts that the FRG1 bound GM-CSF promoter fragment was enriched in qRT-PCR upon immunoprecipitation with the anti-FRG1 antibody but not by the IgG.

Overall our data provides compelling evidence that FRG1 directly binds to the GM-CSF promoter.

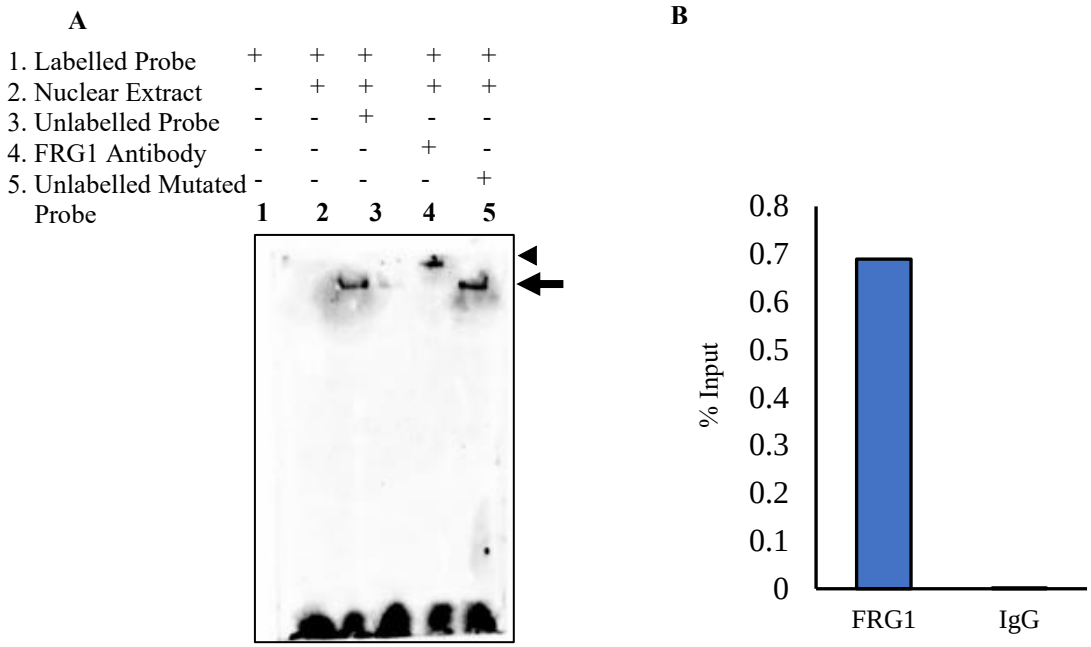

Figure 4A.6.3. Binding of FRG1 on the GM-CSF promoter. **(A),** *EMSA blot showing biotinylated probe in the first lane. The second lane shows the binding of the biotinylated probe with the nuclear protein extracts, obtained from the HEK 293T cells with increased FRG1 levels. The excess unlabeled probe and biotinylated probe are competitively bound to the nuclear protein extract is shown in the third lane. The super shift (arrowhead) in the probe mobility due to binding with the FRG1 antibody is visible in the fourth lane. The arrowhead in the fifth lane indicates the competitive binding between an excess of the mutant unbiotinylated probe and biotinylated probe and the nuclear protein extract; (n = 1).* **(B),** *Antibodies against the FRG1 protein and negative control IgG were used to immunoprecipitate the DNA fragments from HEK 293T cell line with elevated FRG1 expression. The percent input (% input) approach was used to quantify FRG1 binding site on the GM-CSF promoter; (n = 1).*

4A.7. FRG1's effect on ERK is GM-CSF mediated

Next, we assessed the effect of FRG1 binding on the downstream tumorigenic events. Moreover, we wanted to ascertain if GM-CSF operated upstream of the ERK and downstream of FRG1. To achieve this, we modulated the GM-CSF levels in MCF7 cells along with FRG1. Administration of anti-GM-CSF monoclonal antibody (mAb) to FRG1 knockdown MCF7 cells decreased the phospho-ERK and Snail levels (Fig. 4A.7.A). Phenotypically it showed reduced cellular migration in scratch wound healing assay (Fig. 4A.7.B). In correspondence to this, human recombinant GM-CSF treatment restored the levels of phospho-ERK and Snail in MCF7 cells with elevated FRG1 expression (Fig. 4A.7.C), which eventually increased the cell migration (Fig. 4A.7.D).

These findings indicate that FRG1 negatively regulates the GM-CSF-mediated EMT by reducing the activation of ERK.

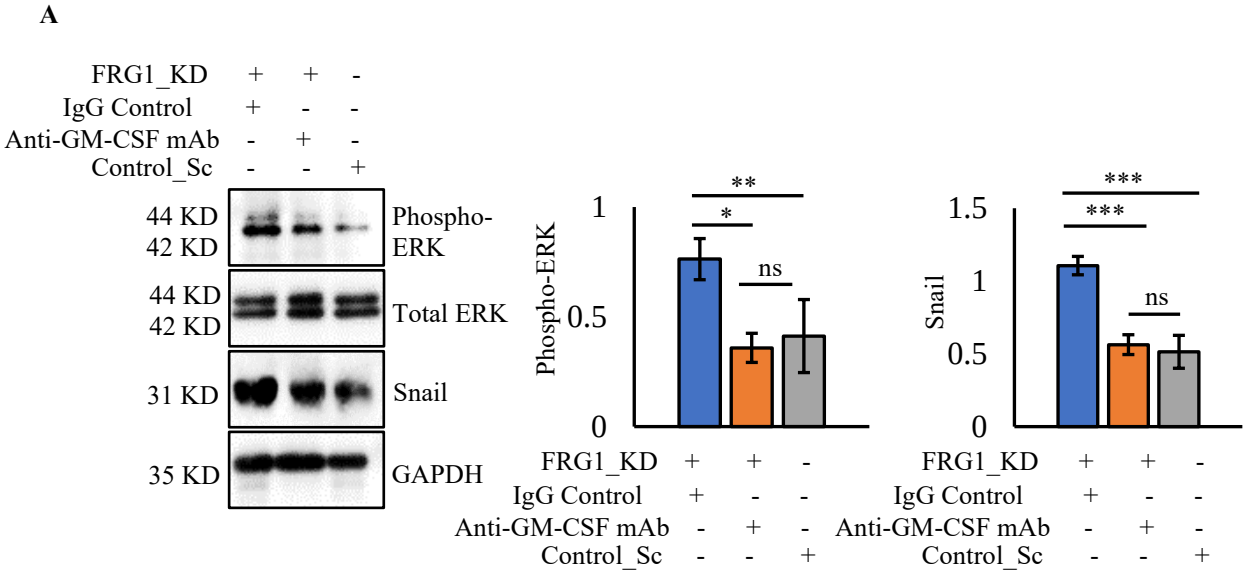

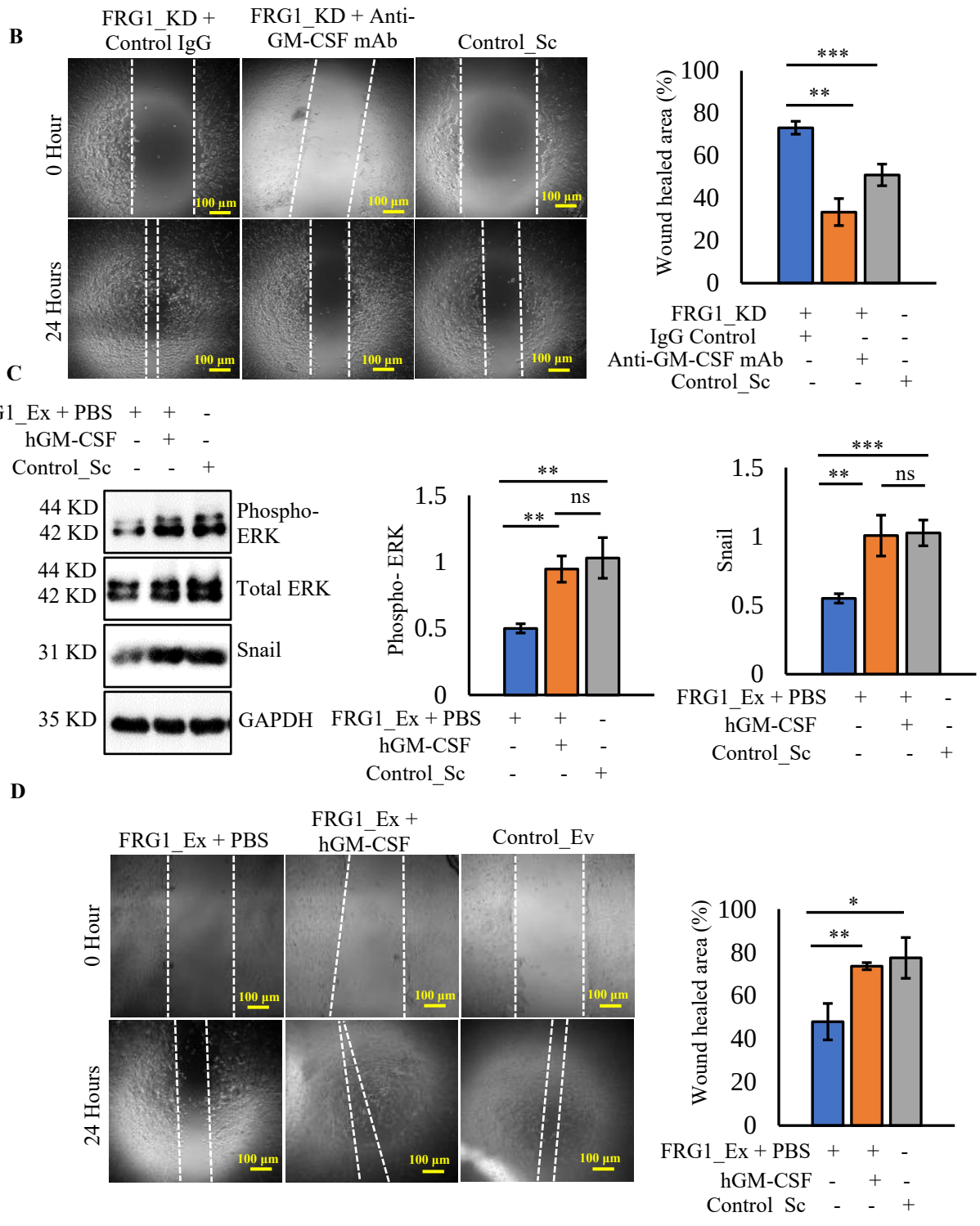

Figure 4A.7. Negative regulation of GM-CSF by FRG1 decreased the ERK-mediated EMT. **(A-B),** *MCF7 cells with decreased FRG1 level (FRG1_KD) were treated with 10 µg/ml of human anti-GM-CSF mAb (FRG1_KD + anti-GM-CSF mAb), and respective control IgG*

(FRG1_KD + IgG) for 30 minutes. The effect of GM-CSF inhibition on the level of EMT marker Snail and ERK **(A),** *and cell migration* **(B)** *is shown in the Western blots and scratch wound healing assay. Scale bar: 100 µm.* **(C-D),** *MCF7 cells with elevated FRG1 expression (FRG1_Ex) were treated with 100 ng/ml of exogenous human recombinant GM-CSF (MCF7_Ex + hGM-CSF) or its solvent PBS (FRG1_Ex + PBS) for an hour. Western blot* **(C)** *and scratch wound healing assay* **(D)** *show the effect of GM-CSF on the EMT marker Snail and ERK and in the migratory properties of the cells. Scale bar: 100 µm***.** *All the experiments were independently performed thrice***.** *GAPDH is used as internal control. The statistical significance of the difference was calculated by two-tailed unpaired student's t-test. Data are represented as mean ± standard deviation (SD). ns, $p > 0.05$; *, $p \leq 0.05$; **, $p \leq 0.01$; ***, $p \leq 0.001$.*

4A.8. FRG1 expression is reduced in breast cancer patients of different molecular subtypes

We examined the level of FRG1 in breast cancer and normal tissues using the publicly available database. Analysis of combined RNA sequencing data from the TCGA and GTEx datasets using the GEPIA web server showed reduced FRG1 transcript level in breast cancer patients (n = 1085) than normal tissues (n = 291) (Fig. 4A.8.A). To further authenticate the negative association of FRG1 expression in breast cancer, we performed immunohistochemistry (IHC) in 194 cancer samples and 56 adjacent normal tissue samples. We found significant downregulation of FRG1 levels in breast cancer tissues (Fig. 4A.8.B). Among the 56 normal counterparts, 71% (40 samples) tissues revealed high FRG1 levels (Allred Score: 7-8); 29% (16 samples) tissues revealed moderate levels of FRG1 (Fig. 4A.8.C). Low FRG1 expression was absent in normal tissues (Allred Score: 1-2). In contrast, analysis of FRG1 expression in 194 breast cancer patients suggests that 29% (57 samples) tissues exhibited high FRG1 levels

(Allred Score 7-8); 55% (106 samples) tissues exhibited moderate FRG1 levels (Allred Score 3-6), and 16% (31 samples) tissues exhibited low FRG1 levels (Fig. 4A.8.C).

To check if the expression of FRG1 was regardless of breast cancer molecular subtypes, we segregated the breast cancer samples according to their ER status. We analyzed if FRG1 showed any differential expression pattern in ER+ *vs.* TNBC patients. We did not observe any significant variation in the FRG1 levels between the ER+ (n = 78) and TNBC patient (n = 40) groups (Fig. 4A.8.D). It further supports our cell-based data that FRG1 acts regardless of breast cancer subtypes.

Next, we performed IHC in breast cancer samples to decipher the correlation of FRG1 levels with phospho-ERK expression. In accordance with the *in vitro* result, we found an inverse expression trend between phospho-ERK and FRG1 in patients (n = 10) (Fig. 4A.8.E). Collectively our patient sample-based observation supports the *in vitro*-based findings.

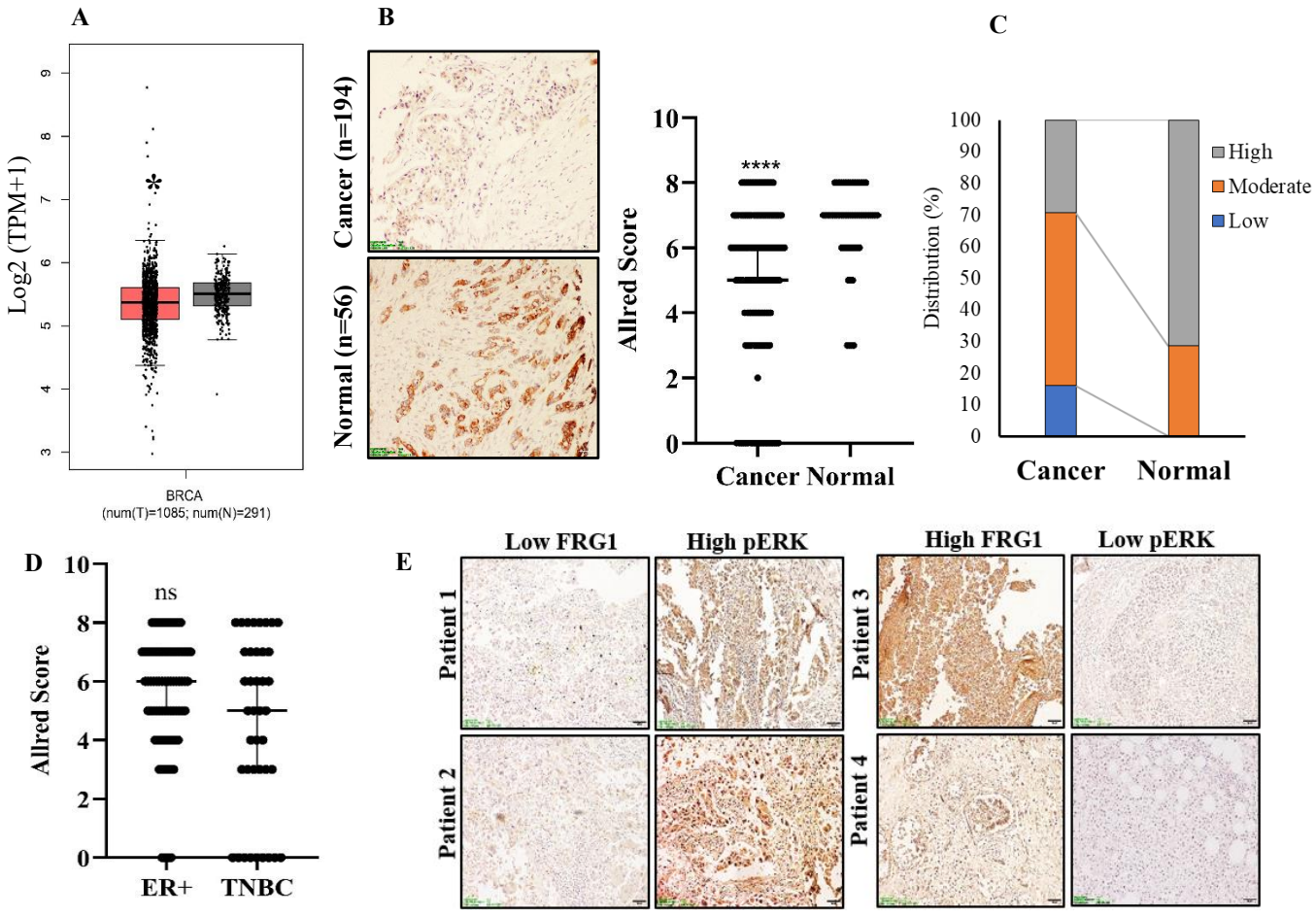

Figure 4A.8. FRG1 level is inversely correlated with breast carcinoma and phospho-ERK expression in patients. **(A),** *RNA sequencing data obtained from TCGA and GTEx datasets were analyzed by the GEPIA web server. Corresponding bar graphs suggest a lesser FRG1 transcripts in breast cancer patients (n = 1085) compared to normal individuals (n = 291).* **(B),** *The left panel represents the IHC image of breast cancer tissue and the surrounding normal counterpart, stained with FRG1 antibody. The scatter plot on the right side compares the median Allred score of expression of FRG1 between cancer tissues (n = 194) and adjoining normal regions (n = 56). The statistical significance of the difference in FRG1 expression was measured by the Mann-Whitney U* test. **(C),** *The frequency distribution of FRG1 protein in cancer (n = 194) vs. normal (n = 56) tissues were derived from the Allred score. Two groups, cancer and normal, are denoted by the X-axis. The proportion of people with high, moderate, and low FRG1 levels is shown on the Y-axis.* **(D),** *Distribution of FRG1 protein among the estrogen receptor-positive patients (n = 78) and TNBC patients (n = 40) according to their respective Allred scores.* **(E),** *IHC images showing the association of FRG1 and Phospho-ERK levels in breast cancer patients (n = 10). Scale bar: 50 μm. All the experiments were independently performed thrice. The statistical significance of the difference was calculated by a two-tailed unpaired student's t-test. Data are represented as mean ± standard deviation (SD). ns, $p > 0.05$; *, $p \leq 0.05$;****, $p \leq 0.0001$.*

4A.9. Elevated FRG1 level is associated with higher patient survival

So far, our *in vitro* and patient sample-based findings suggest that the expression of FRG1 suppresses tumor progression. This led us to hypothesize that FRG1 most likely possesses a protective role in patient survival. To answer this, we analyzed the FRG1 transcripts level from publicly available databases. GEPIA web server-based analysis depicted that breast cancer patients with a higher level of FRG1 had a greater likelihood of disease-free survival (DFS)

(Fig. 4A.9.A). The Kaplan-Meier survival analysis using the combined TCGA datasets also showed a similar trend. It revealed that breast cancer patients harboring wild-type p53 had a higher chance of recurrence-free survival (RFS) (Fig. 4A.9.B).

Together these observations suggest the possible prognostic value of FRG1 in breast cancer.

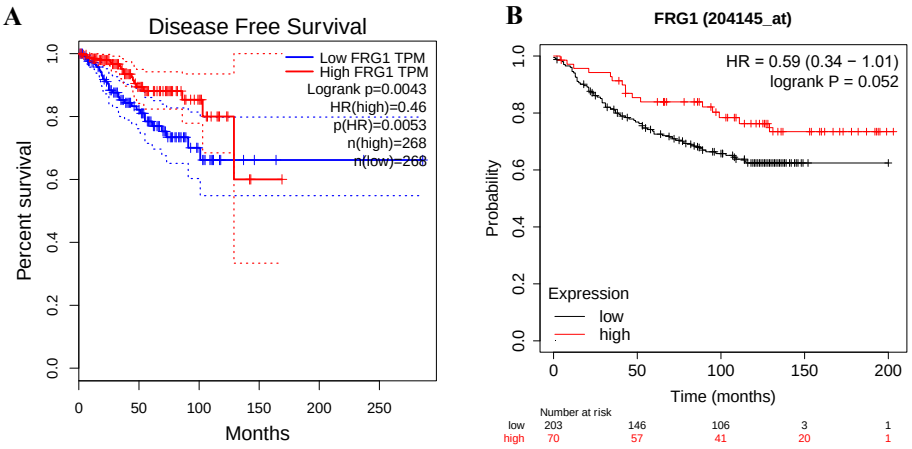

Figure 4A.9. Effect of FRG1 on breast cancer patient survival. **(A),** *The TCGA and GTEx dataset's RNA sequencing results were analyzed through the GEPIA web server. The findings indicate that patients with a higher FRG1 expression (n = 268) had a better chance of surviving without developing the disease (DFS; disease-free survival) than individuals with a lower level of FRG1 expression (n = 268).* **(B),** *The likelihood of recurrence-free survival (RFS) in the patients with higher FRG1 (n = 70) level, harboring wild-type p53 and low FRG1 (n = 203) groups were found to be higher through analysis of combined datasets using the Kaplan-Meier plotter.*

4A.10. Reduction in FRG1 level activates the estrogen receptor (ER) in MCF7 cells

The ER-mediated signaling is principally responsible for the progression of the luminal subtype of breast cancer (250). Around 70% of luminal breast cancer patients are ERα positive (251).

Constitutive activation of ERα is reported to have significant implications in the development of breast tumors and metastasis (252).

Therefore, we checked if FRG1 level perturbation had any effect on the activation of ERα. FRG1 depletion in MCF7 cells increased the activation in ERα level at the Ser^{118} position (Fig. 4A.10.A). The opposite trend was observed when FRG1 was overexpressed in MCF7 cells (Fig. 4A.10.B).

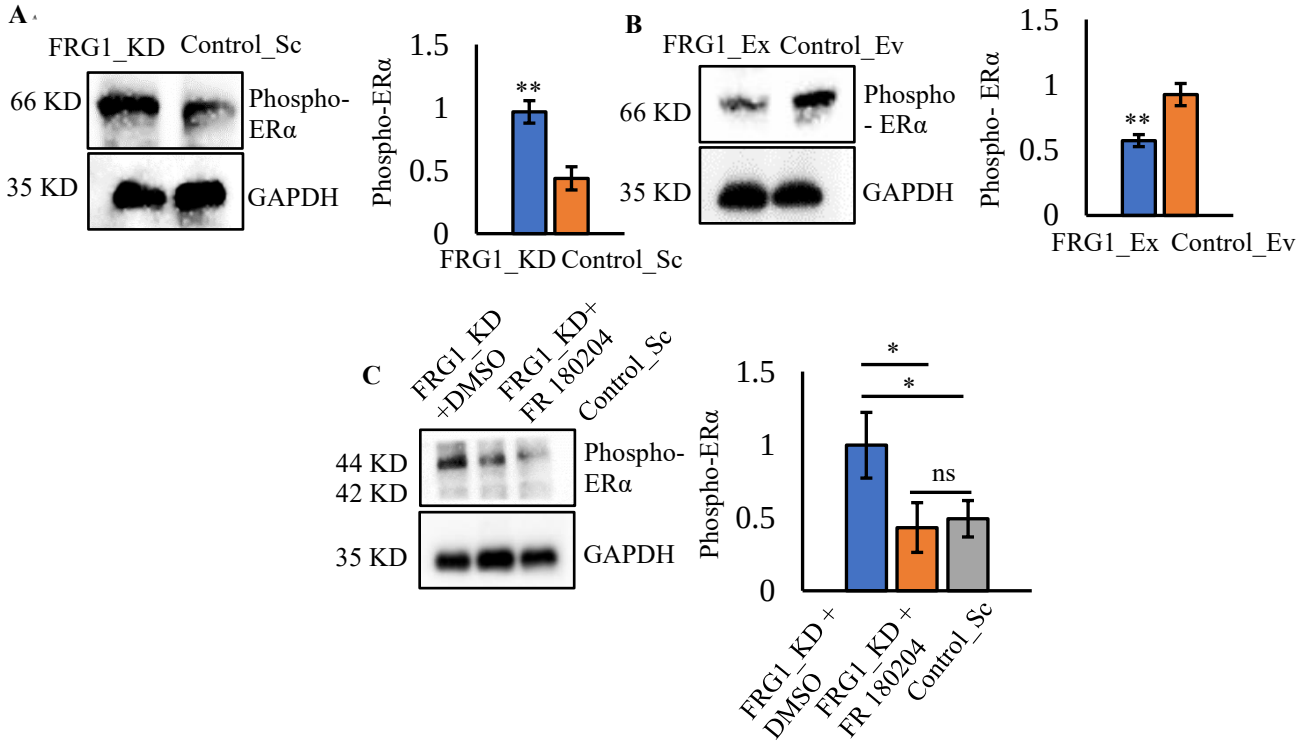

Figure 4A.10. Reduced FRG1 expression activates the ER through ERK. **(A-B),** *Immunoblot and the corresponding bar graph showing the activation of ERα in serine^{118} positions in MCF7 cells with depleted FRG1 levels (FRG1_KD) compared to the control (Control_Sc).* **(B),** *Western blot detected phospho-ERα (serine^{118}) levels in MCF7 cells due to the ectopic expression of FRG1 (FRG1_Ex vs. Control_Ev).* **(C),** *FRG1_KD cells were treated with the ERK inhibitor FR 180204 (10 μM), or its solvent DMSO for two hours.* Western blot shows the effect of ERK inhibition on the activation of ERα in MCF7 cells with FRG1 knockdown (FRG1_KD + FR 180204). *All the experiments are independently performed thrice. The*

*statistical significance of the difference was calculated by a two-tailed unpaired student's t-test. Data are represented as mean ± standard deviation (SD). ns, $p > 0.05$; *, $p \leq 0.05$; **, $p \leq 0.01$.*

As we found increased levels of phospho-ERK due to FRG1 reduction, next, we explored if the upregulation of phospho-ERK resulted in the activation of downstream ERα or vice versa. Multiple reports suggest that ERK regulates the activation of ERα (Ser^{118}) (253), (254). To see whether ERα activation was directly via FRG1 or due to ERK activation, we repressed the ERK activation in FRG1-depleted MCF7 cells by treating the cells with the ERK inhibitor. Inhibition of ERK diminished the earlier observed increased phospho-ERα levels in Western blot (Fig. 4A.10.C).

This observation implies that the increased level of phospho-ERK in FRG1-depleted cells activates the ERα in MCF7 cells, eventually contributing to the growth of breast cancer cells.

Sub-Chapter 4B

Result: Objective 2

To decipher the effect of FRG1 level perturbation *in vivo*

This work has been published in part with the sub-chapter 4A as the following research article:

Mukherjee, B., Tiwari, A., Palo, A., Pattnaik, N., Samantara, S., Dixit, M. *Reduced expression of FRG1 facilitates breast cancer progression via GM-CSF/MEK-ERK axis by abating FRG1 mediated transcriptional repression of GM-CSF*. **Cell Death Discovery, 2022,** 8(1):442, DOI: https://doi.org/10.1038/s41420-022-01240-w

In objective 1 (Sub Chapter 4A), we have delineated the molecular basis of FRG1-mediated regulation of GM-CSF in breast cancer *in vitro*. An elevated level of GM-CSF activates the downstream ERK that eventually triggers the EMT process. Using breast cancer cell lines of different molecular subtypes, we have demonstrated that depleted FRG1 levels contribute to the acquisition of enhanced oncogenic properties. In objective 2 (Sub Chapter 4B), we have mostly validated our cell line-based observation in the mice model. We sought to ascertain whether the modulation of FRG1 level had an impact on tumor growth and metastasis in mice. A major drawback of the current breast cancer treatment is disease recurrence driven by acquired chemoresistance. As the activation of ERK signaling is associated with drug resistance (1), finding out the upstream regulators of ERK can be the target of therapeutic intervention to overcome the resistance. Hence, the major aim of this objective was to assess the scope for the development of GM-CSF-based treatment in breast cancer patients with reduced FRG1 expression.

4B.1. Altered FRG1 level modulates tumor growth *in vivo*

We developed an orthotopic mice model to demonstrate the impact of FRG1 level perturbation *in vivo.* For this purpose, we generated shRNA-mediated stable 4T1 (mice mammary carcinoma derived) cells with depleted FRG1 levels. Along with this, we generated stable 4T1 cells with elevated FRG1 levels. We used these stable cells in the tumor development assay.

4B.1.1. *Reduced FRG1 levels promote tumor growth in mice*

We implanted 2×10^6 4T1 cells with reduced expression of FRG1 and scrambled control into the mammary fat pads of 4-6 weeks old female BALB/c mice (n = 4). Tumor growth was monitored every third day, consecutively for 21 days until euthanization. A markedly visible difference in tumor volume between the two groups can be seen in (Fig. 4B.1.1.A). Further, we measured the tumor weight and tumor volume. Analysis suggested that FRG1 knockdown significantly augmented the tumor volume (Fig. 4B.1.1.B) and weight compared to the control

group (Fig. 4B.1.1.C). Additionally, we measured the weight of the mice every third day for a total of 21 days. We did not detect any difference in the body weight of the mice (Fig. 4B.1.1.D).

In accordance with our *in vitro* observation, this finding suggest that a depleted FRG1 level promotes tumorigenesis.

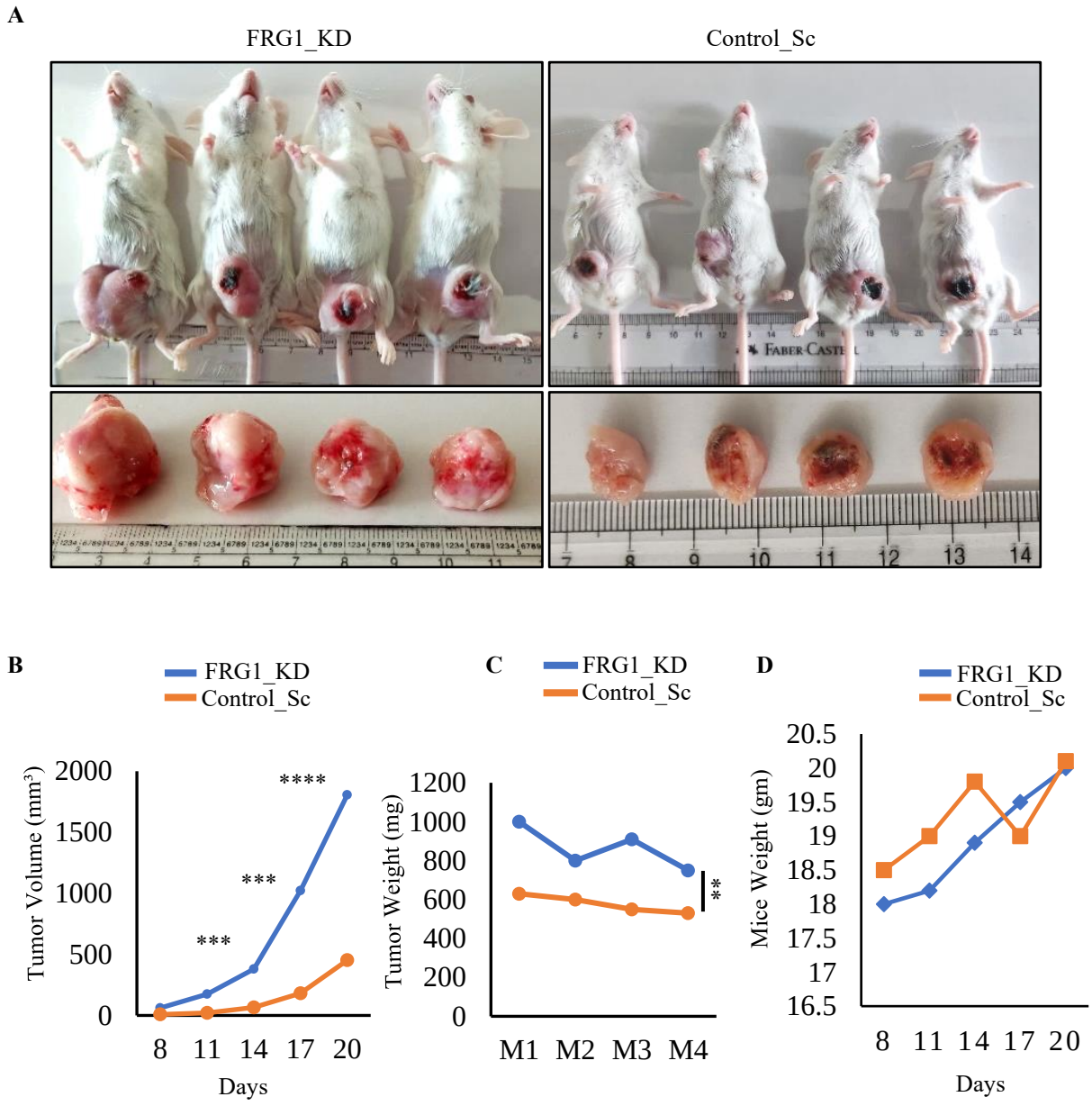

Figure 4B.1.1. Depleted FRG1 level enhances tumor development in BALB/c mice. **(A),** *Images showing the orthotopic tumors developed in BALB/c mice (n = 4) after being injected*

with 4T1 cells with reduced FRG1 level (FRG1_KD) and control (Control_Sc). **(B),** *The bar graph shows the tumor volume in the mice injected with FRG1_KD and Control_Sc cells. The tumor volume was recorded at the interval of three days.* **(C),** *The weight of the tumors in the same group was measured after the removal of the tumors (on day 21st).* **(D),** *The bar graph represents the body weight of the mice of both groups. M1:mouse 1, M2: mouse 2, M3: mouse 3, and M4: mouse 4. The statistical significance of the difference was compared using the two-tailed unpaired student's t-test. **, $p \leq 0.01$; ***, $p \leq 0.001$; ****, $p \leq 0.0001$.*

4B.1.2. *Elevated FRG1 levels abrogate tumor growth in mice*

Since we observed that FRG1 knockdown increased the volume and weight of the tumor, we were interested to find out if FRG1 overexpression had the tumor suppressive effect. Hence, we injected 2×10^6 4T1 cells with elevated FRG1 levels and empty vector control into the mammary fat pads of 4-6 weeks-old female BALB/c mice (n = 4). For 21 days, tumor development was continuously recorded every third day. Tumor volume between the two groups exhibited a quite distinct difference (Fig. 4B.1.2.A). Once the mice were sacrificed on the day 21st, we measured the tumor weight and volume. Analysis suggests that the over-expression of FRG1 in 4T1 cells substantially reduced the tumor volume (Fig. 4B.1.2.B) and weight (Fig. 4B.1.2.C) in mice than the control group. Furthermore, for 21 days, we weighed the mice every third day, but we did not find any difference in the body weight between the two groups (Fig. 4B.1.2.D).

Together, these findings point to the tumor-suppressing effect of FRG1 *in vivo*.

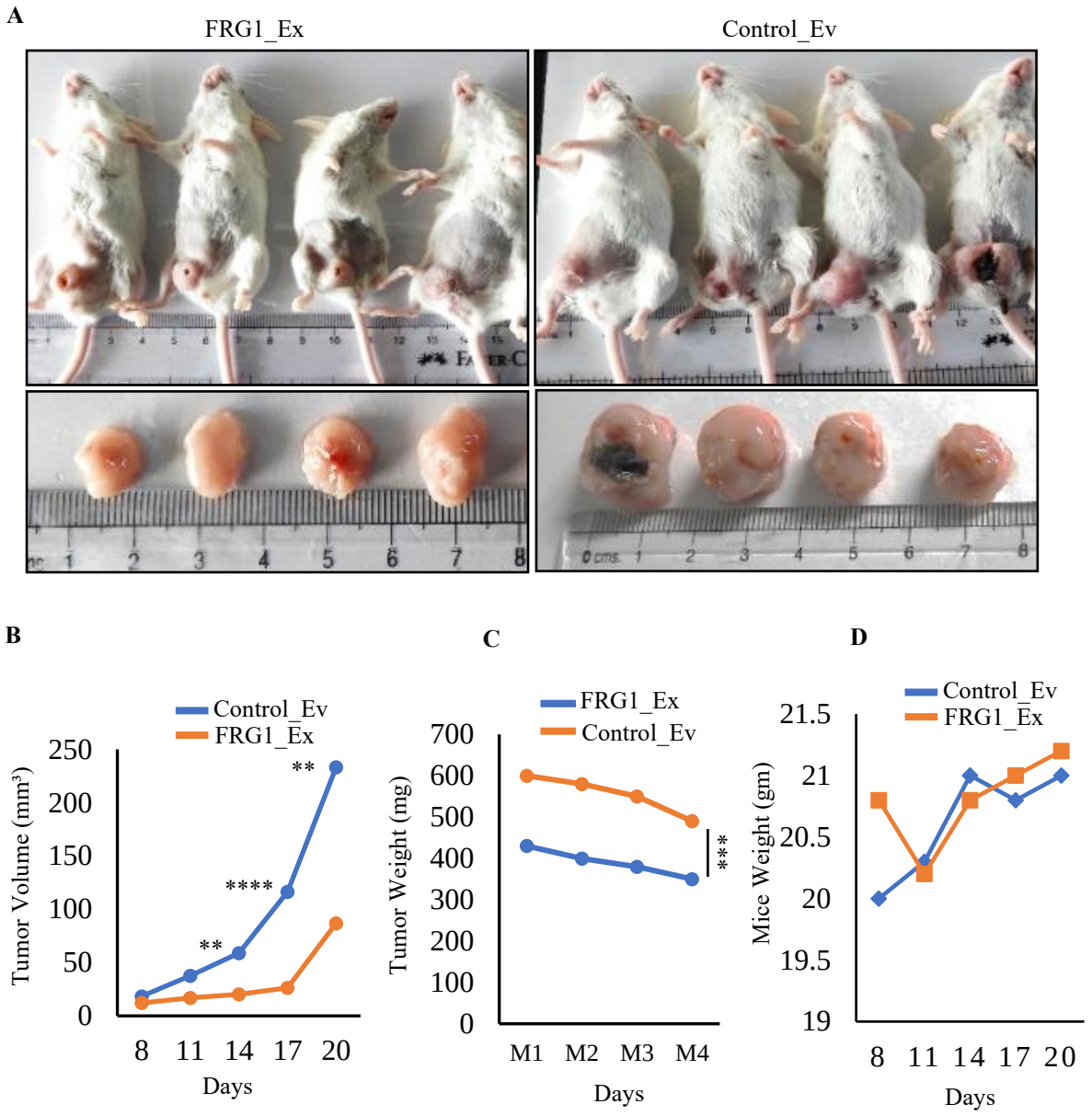

Figure 4B.1.2 Ectopic level of FRG1 reduces tumor development in BALB/c mice. **(A),** *Images show the tumors grown in the mammary fat pads of the BALB/c mice (n = 4), injected with 4T1 cells with elevated FRG1 level (FRG1_Ex) and empty vector control (Control_Ev).* **(B),** *The progression of tumor volume in FRG1_Ex and Control_Ev set is depicted in the bar graph at the intervals of every third day.* **(C),** *Following the tumor excision on day 21st, the weights of the tumors in the same group were measured and displayed in the bar graphs.* **(D),** *The bar graph represents the body weight of the mice of both groups. M1:mouse 1, M2: mouse*

*2, M3: mouse 3, and M4: mouse 4. The statistical significance of the difference was compared using the two-tailed unpaired student's t-test. **, $p \leq 0.01$; ***, $p \leq 0.001$; ****, $p \leq 0.0001$.*

4B.2. FRG1 inhibits tumor growth by suppressing the ERK activation

In objective 1, we found that the elevated expression of phospho-ERK resulted in increased oncogenic properties in breast cancer cell lines. Therefore, we checked the underlying signaling pathway responsible for increased tumor volume in FRG1-depleted mice and vice versa. We harvested protein from the tumors grown in the mice described above (section 4B.1). In parallel with our *in vitro*-based findings, we observed that over-expression of FRG1 led to a lesser activation of ERK (Fig. 4B.2). Ectopic expression of FRG1 also reduced the level of EMT marker Snail in mice (Fig. 4B.2). Similarly, the protein was harvested from the tumors grown in the mice injected with 4T1 cells with reduced FRG1 levels. We found an elevated level of phospho-ERK and Snail in the FRG1 knockdown group compared to the control (Fig. 4B.4.2). This data further substantiate our cell line-based findings showing the ERK-mediated induction of EMT in FRG1-depleted cells.

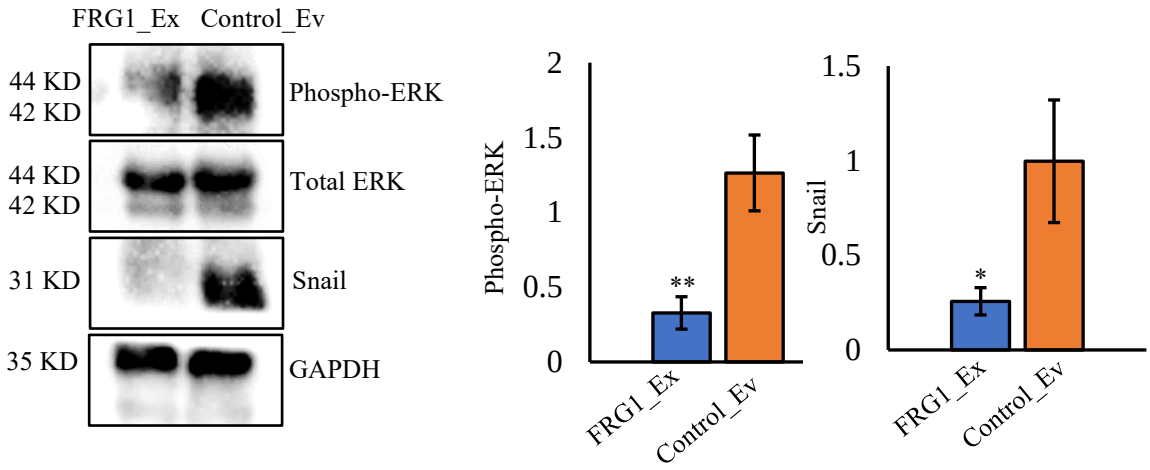

Figure. 4.B.2 Depleted FRG1 levels activated the ERK in vivo. *Western blot and the densitometry-based bar graphs represent the expression of phospho-ERK and EMT marker Snail in the tumors of the respective groups. The statistical significance of the differential*

*protein expression between the two groups was compared using the two-tailed unpaired student's t-test. The result was derived from the three independent experiments. Results are represented as mean ± standard deviation (SD). *, $p \leq 0.05$; **, $p \leq 0.01$.*

4B.3. Reduced FRG1 level increased the metastatic nodules in mice

ERK-mediated upregulation of Snail is reported to promote EMT in breast cancer (255). Our cell-based findings in objective 1 (Sub chapter 4A) also supported the same. As we found increased expression of phospho-ERK and Snail in mice tumors, we investigated if FRG1 level modulation possessed any effect on the metastatic potential of mice. Therefore, we injected 2×10^5 4T1 cells with reduced FRG1 level into the tail vein of 6-8 weeks-old female BALB/c mice (n = 3). After 14 days, mice were sacrificed, and lungs were excised to count the metastatic nodules. FRG1 reduction resulted in increased nodules in the lungs compared to the control group (Fig. 4B.3.A). Correspondingly, we injected 2×10^5 4T1 cells with elevated FRG1 levels into the tail vein of mice. In parallel to the knockdown group, ectopic FRG1 level reduced the number of metastatic lung nodules (Fig. 4B.3.B).

This data confirms that loss of FRG1 contributes to metastasis *in vivo.*

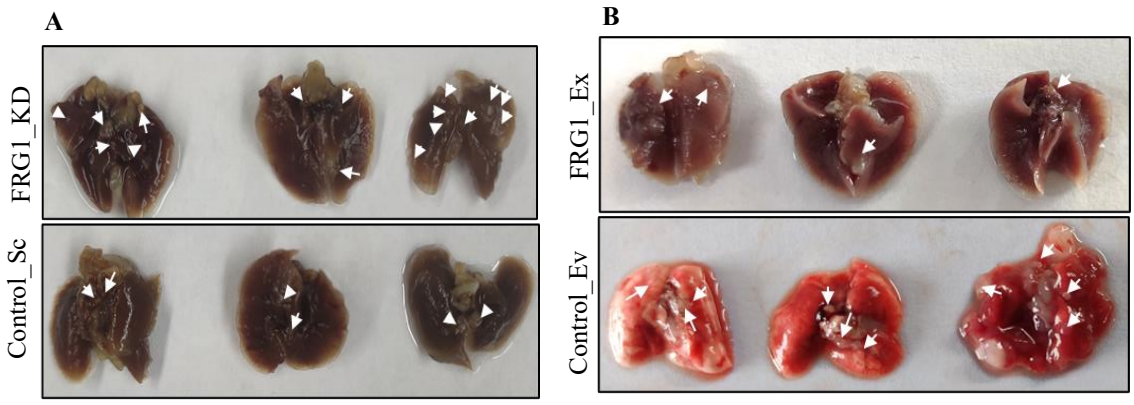

Figure 4B.3. FRG1 level perturbation affects the metastasis in vivo. **(A-B),** *BALB/c mice's tail-vein was administrated with 4T1 cells with FRG1 level modulations. Subsequently, the*

lungs were removed after seven days, and the number of lung nodules was calculated. **(A),** *Images of the lung nodules developed in BALB/c mice after being injected with FRG1-depleted 4T1 (FRG1_KD) and control (Control_Sc) cells.* **(B),** *Images of the lung nodules grown in the BALB/c mice following injection with 4T1 cells with elevated FRG1 levels (FRG1_Ex) and empty vector control (Control_Ev).*

4B.4. Anti-GM-CSF therapy reduces FRG1-mediated tumor burden *in vivo*

Our findings in objective 1 (Sub Chapter 4A) suggest that inhibition of GM-CSF reduced the tumorigenic properties and the level of EMT marker Snail in MCF7 cells with reduced FRG1 level. Therefore, herein, we evaluated the clinical implication of anti-GM-CSF therapy *in vivo*. We performed a mouse model-based study to assess the therapeutic benefits of anti-GM-CSF treatment.

4B.4.1. *Anti-GM-CSF treatment reduces the tumor volume in mice*

We first checked the effect of GM-CSF inhibition in the mice model. Female BALB/c mice of 6-8 weeks-old were subcutaneously administrated with 4T1 cells with depleted FRG1 levels along with their control in the mammary fat pads. After seven days, when the tumors reached a palpable size, one group of mice (n = 4), previously injected with 4T1 cells with reduced FRG1 level, were intraperitoneally injected with GM-CSF neutralizing monoclonal antibody (10 mg/kg body wt.) on each alternate day till day 21 (Fig. 4B.4.1.A). The other FRG1 knockdown cells bearing mice (n = 4) were administrated with the control IgG antibody of the same dose and duration. The mice injected with the control cells were left untreated. Tumor growths were monitored among the three groups till the day of sacrifice. We detected a substantial reduction in tumor volume in the group treated with GM-CSF neutralizing monoclonal antibody compared to IgG (Fig. 4B.4.1.B).

Hence, our result demonstrates that the anti-GM-CSF therapy has the potential to reduce the tumor growth in FRG1-depleted mice.

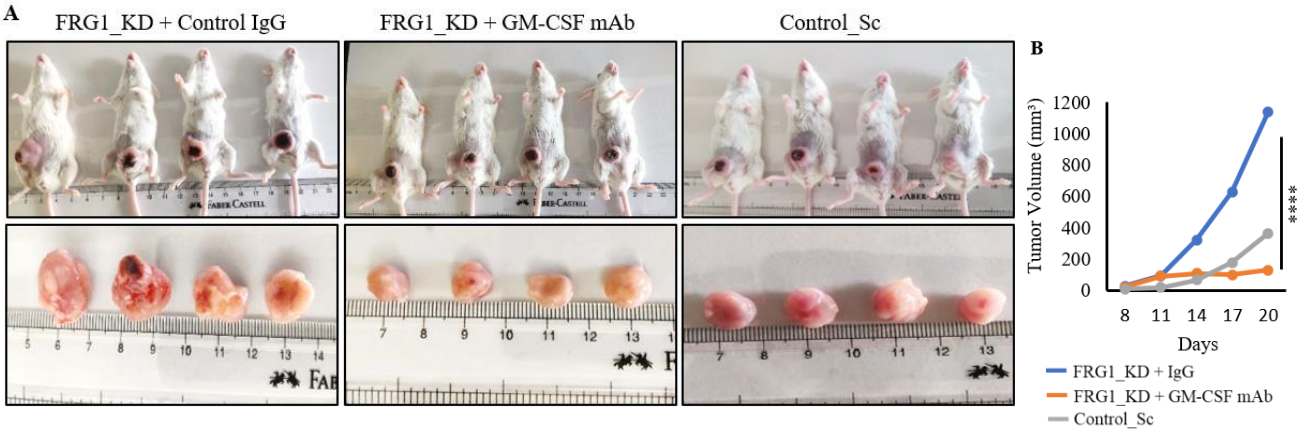

Figure 4B.4.1. Effect of anti-GM-CSF therapy in the tumor volume of the mice with FRG1 depletion. **(A-B),** *FRG1 knockdown (FRG1_KD) and control (Control_Sc) in 4T1 cells were subcutaneously implanted into the mammary fat pads of BALB/c mice to develop the tumors. After seven days, mice in the FRG1_KD group received either 10mg/kg anti-GM-CSF monoclonal antibody (FRG1_KD + GM-CSF mAb) or control IgG (FRG1_KD + Control IgG) treatments until the day 21st. Mice with the Control_Sc cells were left untreated. n = 4 for each group.* **(A)**, *Images showing the tumors grown on the BALB/c mice in the three groups: FRG1_KD, FRG1_KD + GM-CSF mAb, and Control_Sc.* **(B),** *The bar graph represents the progression of tumor volume among the three groups of mice as in* **A**. *Tumor volume was measured at three days intervals till day 21st. ****, $p \leq 0.0001$.*

4B.4.2 . *Anti-GM-CSF therapy decreases the activation of ERK and its downstream molecule Snail*

We checked the level of phospho-ERK and EMT marker Snail in the tumors of the three groups of mice as described in the above section (4B.4.1). Protein was extracted from all the tumors and subjected to Western blot. In consistence with our cell line-based observation, here also we

noticed a decreased expression of phospho-ERK and Snail in the mice treated with GM-CSF neutralizing antibody (Fig. 4B.4.2).

Hence, our results demonstrate that the GM-CSF-mediated activation of ERK, which induces EMT in FRG1-depleted cells, can be rescued by suppressing the GM-CSF. To recap the study's importance, we suggest that our findings open up the possibility of developing anti-GM-CSF-based therapies, particularly for breast cancer patients who have low FRG1 levels.

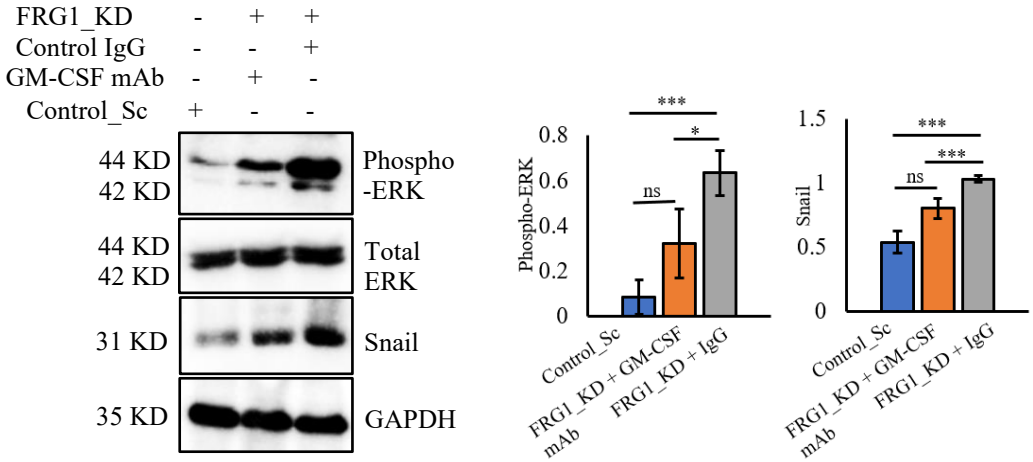

Figure 4B.2. Effect of anti-GM-CSF therapy in the mice with FRG1 level depletion. *FRG1 knockdown (FRG1_KD) and control (Control_Sc) in 4T1 cells were subcutaneously implanted into the mammary fat pads of BALB/c mice to develop the tumors. After seven days, mice in the FRG1_KD group received either 10mg/kg anti-GM-CSF monoclonal antibody (FRG1_KD + GM-CSF mAb) or control IgG (FRG1_KD + Control IgG) treatments until the day 21st. Mice with the Control_Sc cells were left untreated. n = 4 for each group. The representative Western blot depicts the effect of GM-CSF inhibition in the expression of phospho-ERK and Snail in mice models. GAPDH has been used as loading control. The statistical significance of the difference was calculated by a two-tailed unpaired student's t-test. Data are presented as mean ± standard deviation (SD). ns, $p > 0.05$; *, $p \leq 0.05$; ***, $p \leq 0.001$.*

Sub Chapter 4C
Result: Objective 3

To understand FRG1's function and the underlying molecular signaling cascade in tumor angiogenesis

This work has been published as the following research article:

Mukherjee, B., Brahma, P., Mohapatra, T., Chawla, S., Dixit, M. *Reduced FRG1 expression promotes angiogenesis via activation of the FGF2-mediated ERK/AKT pathway*. **FEBS Open Bio**, **2023**, DOI: https://doi.org/10.1002/2211-5463.13582

In the first two objectives of the thesis, using *in vitro* (Sub Chapter 4A) and *in vivo* systems (Sub Chapter 4B), we have established the role of FRG1 in breast tumorigenesis. There we have revealed how FRG1 negatively regulates the transcription of GM-CSF, which leads to the ERK-mediated progression of EMT. Tumor growth and metastasis are reported to be largely associated with angiogenesis. Like other solid tumors, breast cancer cells need a consistent supply of nutrients and oxygen that is facilitated by angiogenesis (12). The first evidence of FRG1's involvement in angiogenesis came from a study on *Xenopus*, where low FRG1 levels were accompanied by decreased levels of the angiogenic marker dab2 and vice versa. The direct association of FRG1 in tumor angiogenesis was first established by Tiwari *et al*., who suggested elevated expression of FRG1 is concurrent with decreased tubule formation and migration property of HUVECs in a paracrine manner, but the mechanistic insights were not explored. Finding the molecules that can control both tumorigenesis and angiogenesis may open up the possibility of a new therapeutic approach. Moreover, if they act regardless of breast cancer molecular subtypes, it will help in determining a common treatment strategy for all breast cancer patients. As no report was available on the detailed mechanism of FRG1-mediated tumor angiogenesis, in the third objective of the thesis (Sub Chapter 4C), we have explored the molecular mechanism underlying FRG1-mediated regulation of angiogenesis during the process of breast cancer. Using the conditioned media from FRG1-depleted breast cancer cells of different molecular subtypes, we have shown its effect on the angiogenic properties of HUVECs.

We further validated our cell-based observations with the Matrigel plug and skin wound-healing assay in mice. Mechanistically we showed that FRG1 is the upstream regulator of FGF2, which eventually activated the AKT/ERK signalling axis in endothelial cells leading to angiogenesis induction. The findings from this objective are described below.

4C.1. Reduction in FRG1 level in breast cancer cells promotes angiogenesis *in vitro*

The process of angiogenesis is concurrent with tumor development (80). Without angiogenesis, tumor cells cannot grow beyond a specific size (77). Hence, we checked the angiogenic potential of FRG1 in breast cancer cells of different molecular subtypes (MCF7, positive for Estrogen and Progesterone receptor; MDA-MB-231, triple-negative breast cancer cell). To ascertain the paracrine effect of FRG1 on breast cancer angiogenesis, first, we harvested the conditioned medium from MCF7 cells with reduced FRG1 levels and MDA-MB-231 cells with elevated FRG1 levels. The method for preparing the conditioned medium is described in the Materials and Methods (section: 3.3.11).

The key characteristic of tumor angiogenesis comprises endothelial cells' ability to proliferate, migrate, and form tubules in response to the angiogenic substances secreted by tumor cells. Therefore, we investigated the impact of angiogenic factors present on the conditioned medium of FRG1 knockdown and FRG1 over-expressing cells on the proliferation, migration, and tubule formation of HUVECs.

4C.1.1. *Depleted FRG1 expression induces the proliferation of endothelial cells in a paracrine manner*

Increased proliferative property enables the endothelial cells to form new sprouts from the existing vasculature (256). Therefore, we established a co-culture setup where HUVECs were incubated for 24 hours with the conditioned medium, collected from MCF7 cells with reduced FRG1 levels, and the control. Colorimetric-based MTS assay showed significantly increased proliferation of HUVECs due to the angiogenic factors present on the conditioned medium of FRG1-depleted MCF7 cells (Fig. 4C.1.1.A).

An opposite trend was observed in HUVECs, treated with the conditioned medium from MDA-MB-231 cells with elevated FRG1 expression compared to the control. MTS assay suggested

significantly reduced proliferative properties of HUVECs due to the expression of FRG1 (Fig. 4C.1.1.B).

Thus, the result suggests that altered FRG1 levels in breast cancer cells can modulate the proliferation of endothelial cells regardless of their molecular subtype.

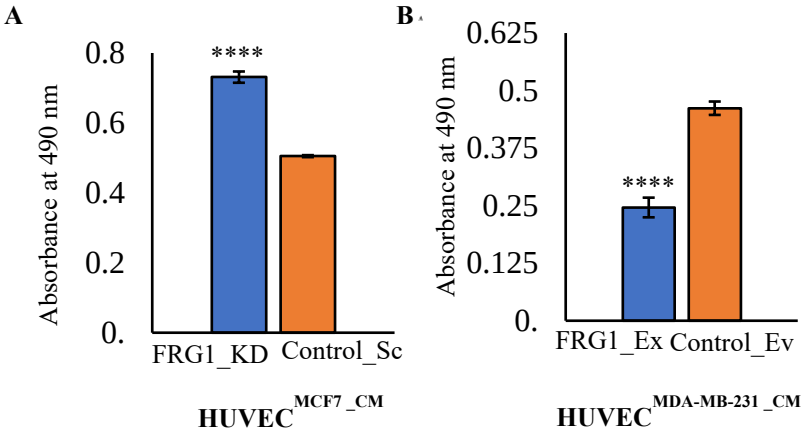

Figure 4C.1.1. Effect of FRG1 level perturbation on endothelial cell proliferation. **(A),** *Bar graphs showing the comparative cell proliferation of HUVECs supplemented with the conditioned medium (CM) obtained from MCF7 cells with depleted FRG1 (FRG1_KD) level vs. the corresponding control (Control_Sc).* **(B),** *Cell proliferation was measured in HUVECs incubated with the CM, harvested from MDA-MB-231 cells with ectopic FRG1 expression (FRG1_Ex), and control (Control_Ev). OD values were measured at 490 nm. All the experiments were replicated thrice. Statistical significance of difference was calculated by two-tailed unpaired student's t-test. Results are shown as mean ± standard deviation (SD). ****, $p \leq 0.0001$.*

4C.1.2. *Depleted FRG1 expression induces migration of endothelial cells in a paracrine manner*

Acquisition of enhanced migratory property is essential for angiogenic sprout formation. It enables the growth of the capillaries. Insert migration assay was carried out to assess the potential of FRG1 on the migration of endothelial cells. HUVECs were co-cultured in the cell inserts with EBM2 culture medium and the conditioned medium from MCF7 cells with reduced FRG1 level for 24 hours in a 1:1 ratio. Decrease in FRG1 level caused a significant increase in HUVECs migration (Fig. 4C.1.2.A). On the other hand, HUVECs cultured in the medium, conditioned with elevated FRG1 levels in MDA-MB-231 cells, showed reduced migration properties (Fig. 4C.1.2.B).

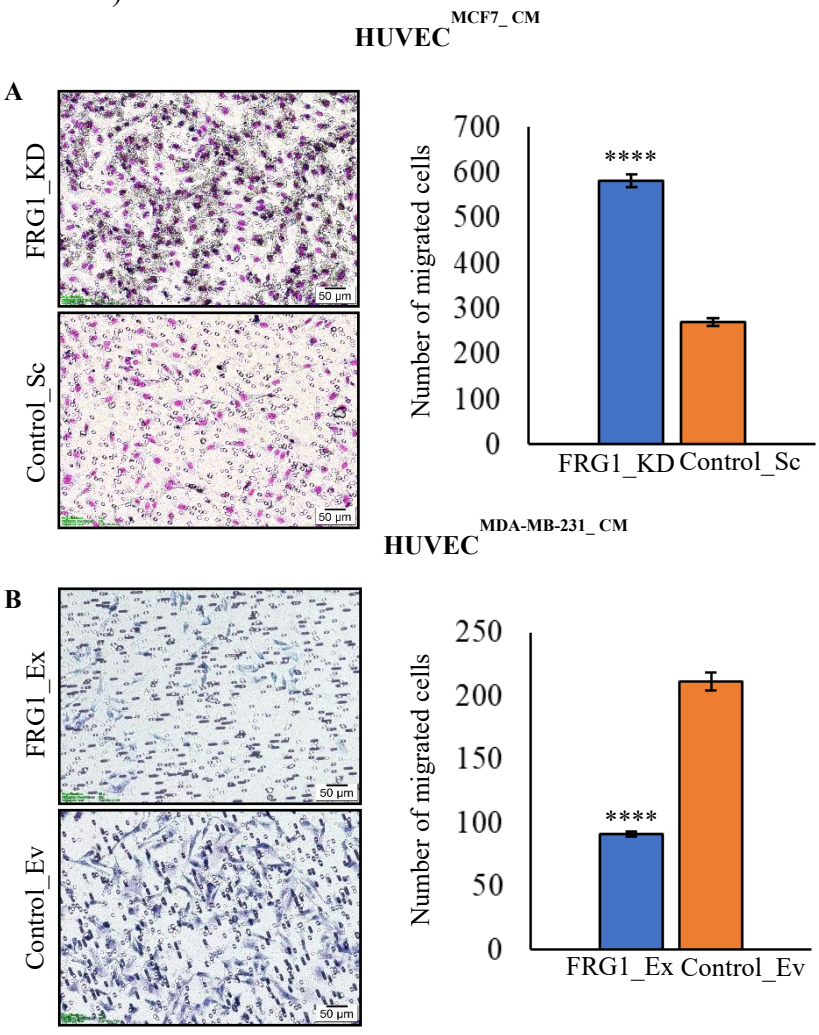

***Figure 4C.1.2. FRG1 affects endothelial cell migration*. (A),** *HUVECs were co-cultured with the conditioned medium (CM) from FRG1-depleted MCF7 cells (FRG1_KD). Representative images and the corresponding bar graphs showing the number of HUVECs, migrated to the outer side of the cell inserts in 24 hours. Scale bar: 50 μm. Images were captured at 10X magnification.* **(B),** *HUVECs were incubated with the CM from MDA-MB-231 cells with ectopic FRG1 expression (FRG1_Ex). The number of HUVECs that migrated to the outer side of the cell inserts in 24 hours is depicted in representative images and the related bar graphs. Scale bar: 50 μm. Images were captured at 10X magnification. All the experiments were independently performed thrice. The statistical significance of the differences in the number of migratory cells was calculated by two-tailed unpaired student's t-test. Results are shown as mean ± standard deviation (SD). ****, $p \leq 0.0001$.*

4C.1.3. *The effect of FRG1 level perturbation on tubule formation property of endothelial cells is irrespective of molecular subtypes*

As a part of the angiogenesis process, endothelial cells first proliferate and migrate towards an angiogenic stimulation, then subsequently differentiates into tubular structures to enable blood flow. This phenomenon is termed tubulogenesis and takes place at the later stage of angiogenesis (257). To detect the effect of FRG1 level alteration on the differentiation of endothelial cells, tubule formation assay was performed.

4C.1.3.1. *Depleted FRG1 expression induces tubule formation property of endothelial cells in a paracrine manner*

We grew the HUVECs in the conditioned medium from MCF7 cells with depleted FRG1 levels. Fig. 4C.1.3.1.A shows that reduced FRG1 levels led to a higher number of tubules compared to the control. We further analyzed several tubulogenic parameters using the Angiogenesis Analyzer tool of ImageJ software. Analysis shows that when HUVECs were co-cultured with

the FRG1-depleted conditioned medium, six out of twenty angiogenic parameters were dramatically enhanced (Fig. 4C.1.3.1.B). The result showed a statistically substantial elevation in the number of segments, nodes, meshes, junctions, master segments, and peaces (Fig. 4C.1.3.1.B). Due to the absence of basal FRG1 level, other tubulogenic features such as master junction numbers, total mesh area, interval of branching, length of total master segments, as well as, total segments, and length of the total branches also increased, but the difference was not statistically significant (Fig. 4C.1.3.1.C).

This result strongly indicates that FRG1 reduction in breast cancer cells promotes the tubule formation capacity of endothelial cells that, in turn, facilitates angiogenesis.

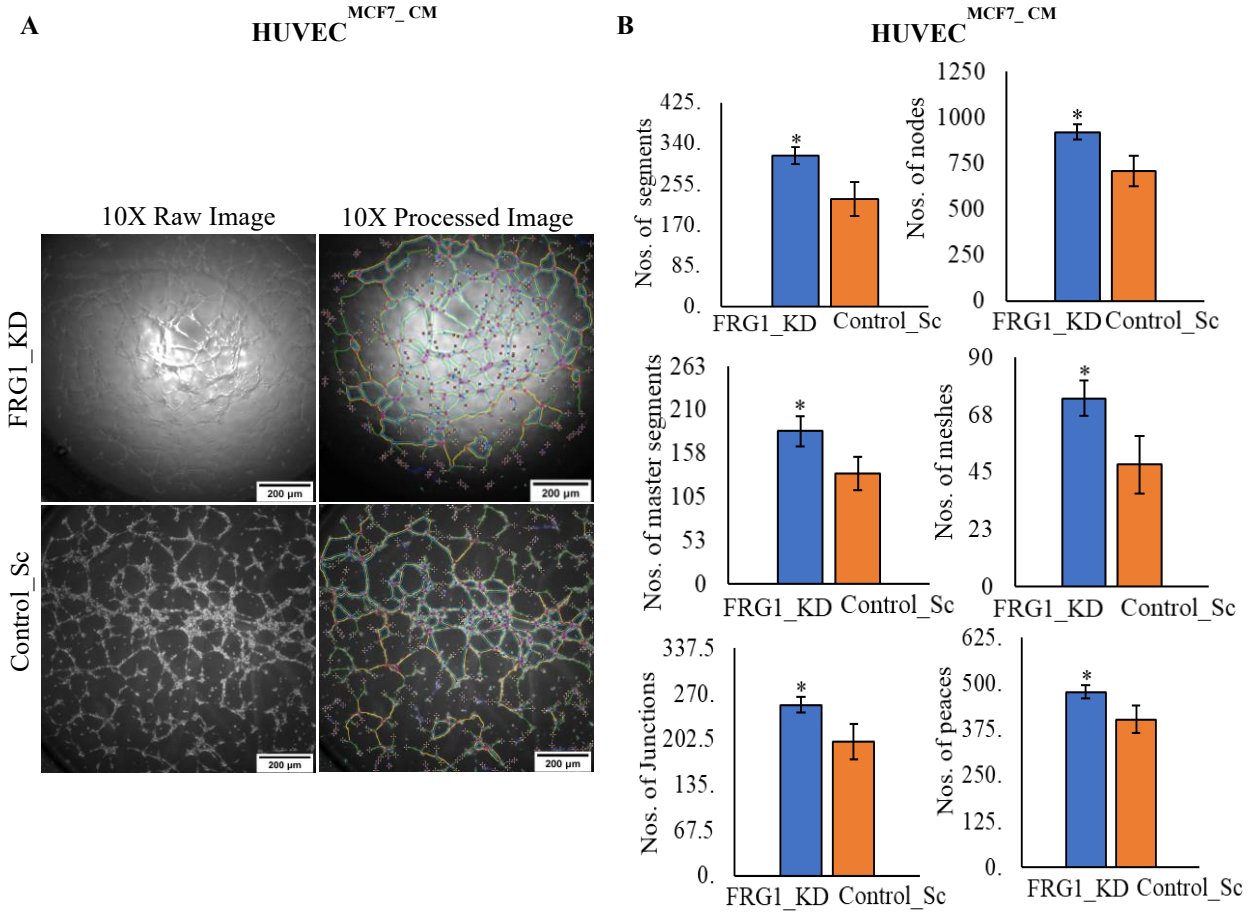

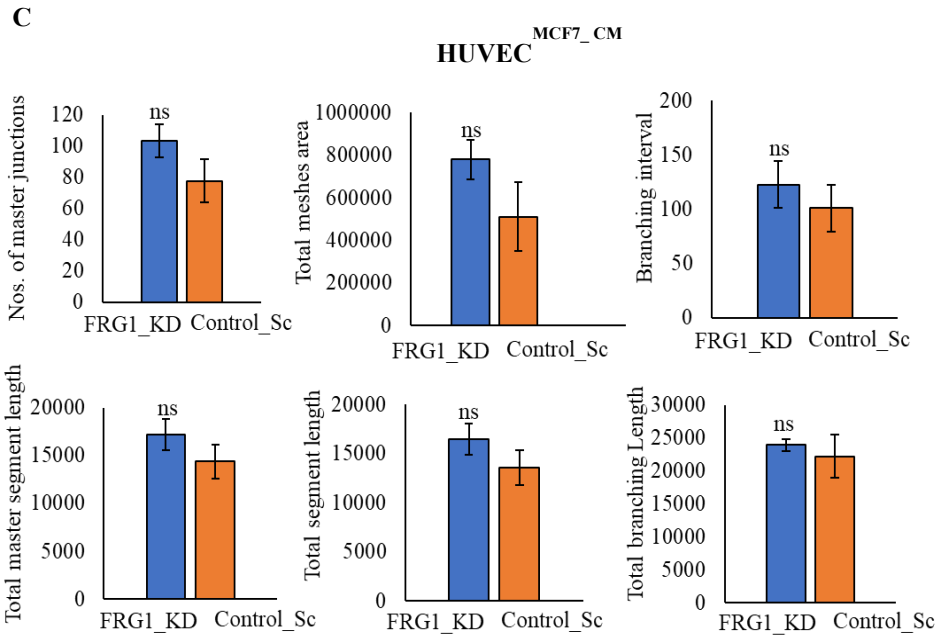

Figure 4C.1.3.1. **Reduced FRG1 levels enhanced tubulogenesis.** *Conditioned medium (CM) was harvested from MCF7 cells with reduced FRG1 level (FRG1_KD) and control (Control_Sc). HUVECs were incubated with the CM for six hours. Images were taken at 10X magnification. Scale bar: 200 µm. Various tubulogenic parameters were further analyzed by the Angiogenesis Analyzer tool of ImageJ software.* **(A),** *The left panel shows the representative raw images of HUVECs, generating the tubules after being treated with the FRG1_KD and Control_Sc CM.* **.** *The right panel illustrates the same image in a processed format in the Angiogenesis Analyzer tool.* **(B),** *Bar graphs, derived from the ImageJ software, suggest the statistical significance of the difference in various tubulogenic parameters in the same set.* **(C),** *shows the different tubulogenic parameters, increased in HUVECs due to the FRG1_KD CM than the control but not statistically significant. The statistical significance of the difference was calculated by two-tailed unpaired student's t-test. All the experiments were independently performed thrice. Results are shown as mean ± standard deviation (SD). ns, $p > 0.05$; *, $p \leq 0.05$.*

4C.1.3.2. *Ectopic expression of FRG1 reduces the tubule formation property of HUVECs in a paracrine manner*

Next, we wanted to explore if the effect of FRG1 level modulation on tubulogenesis was regardless of breast cancer molecular subtypes. We harvested the conditioned medium from TNBC cell line MDA-MB-231 with elevated FRG1 levels and empty vector control. Subsequently, we incubated the HUVECs in the conditioned medium. We observed that HUVECs exhibited a decreased capacity for tubule formation when cultured in the conditioned medium taken from MDA-MB-231 cells with increased FRG1 expression than the control (Fig. 4C.1.3.2.A). ImageJ analysis revealed that among the twenty tubulogenesis measuring parameters, six parameters including, the number of segments, nodes, meshes, junctions, master segments and, peaces were significantly reduced due to elevated FRG1 levels. In the same set (Fig. 4C.1.3.2.B), other parameters such as master junction numbers, interval of branching, total length, total area of mesh, length of total master segments, as well as segments and branching, also displayed a declining trend. However, they were not statistically significant (Fig. 4C.1.3.2.C).

This result suggests that FRG1 level perturbation affects the tubule formation capacity of endothelial cells regardless of the breast cancer molecular subtypes.

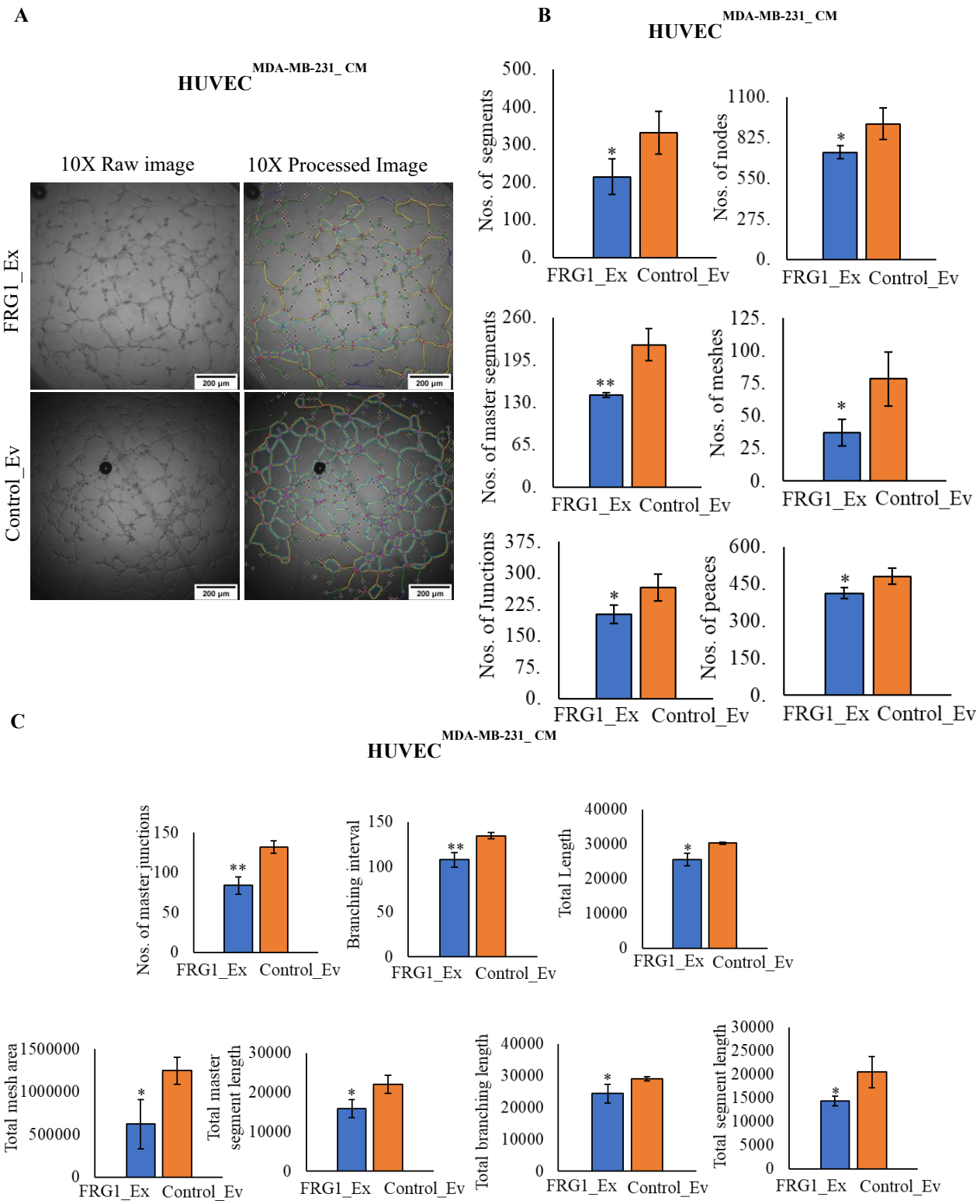

Figure 4C.1.3.2. Perturbation of FRG1 level affects HUVEC's tubule-forming potential.

Conditioned medium (CM) was harvested from the MDA-MB-231 cells with elevated FRG1

level (FRG1_Ex) and empty vector control (Control_Ev). HUVECs were incubated with the CM for six hours. Images were taken at 10X magnification. Scale bar: 200 μm. Various tubulogenic parameters were further analyzed by the Angiogenesis Analyzer tool of ImageJ software. **(A),** *The left panel displays the raw images of HUVECs producing vascular tubules following treatment with the CM from FRG1_Ex and Control_Ev cells. The same image is shown in a processed format in the right panel.* **(B),** *Bar graphs produced by the ImageJ software show the statistical significance of differences in the major tubulogenic characteristics within the same set that are significant statistically.* **(C),** *Bar graphs demonstrate the several tubulogenic parameters that are decreased in HUVECs owing to FRG1_Ex CM compared to the control but are not statistically significant. All the experiments were performed thrice. The statistical significance of the difference in tubulogenic properties was calculated by two-tailed unpaired student's t-test. Results are shown as mean ± standard deviation (SD). ns, $p > 0.05$; *, $p \leq 0.05$; **, $p \leq 0.01$.*

4C.2. Low FRG1 level in breast cancer cells promotes angiogenesis *in vivo*

We further validated our *in vitro* findings in the mice model. We performed Matrigel plug assay in C57/BL6 mice and wound healing assay in BALB/c mice with the conditioned medium, obtained from 4T1 cells with depleted FRG1 level and the corresponding control.

4C.2.1. *Reduced FRG1 is associated with the increased number of vascular plugs*

Matrigel plug assay is carried out to ascertain the angiogenesis potential of a molecule or protein *in vivo* (258). Newly formed blood vessels that are sprouted into the plugs in response to certain angiogenic factors, can be evaluated by this technique (259). To perform the Matrigel plug assay, first, we mixed the growth factor reduced matrigel, with the conditioned medium from 4T1 cells with FRG1 knockdown or control, in a 1:1 ratio. Next, the mixture was subcutaneously injected into the right flank of 6-8 weeks old female C57/BL6 mice. After seven

days, the plugs were excised, and further analysis was done by H&E staining and IHC using angiogenic marker CD31. Fig. 4C.2.1.A clearly suggests more blood vessels in the transplanted gel plugs in FRG1 knockdown group compared to the control. Both the H&E and IHC staining with CD31 antibody detected more blood vessels in the plugs containing the conditioned medium, obtained from 4T1 cells with reduced FRG1 levels compared to the control. (Fig. 4C.2.1.B).

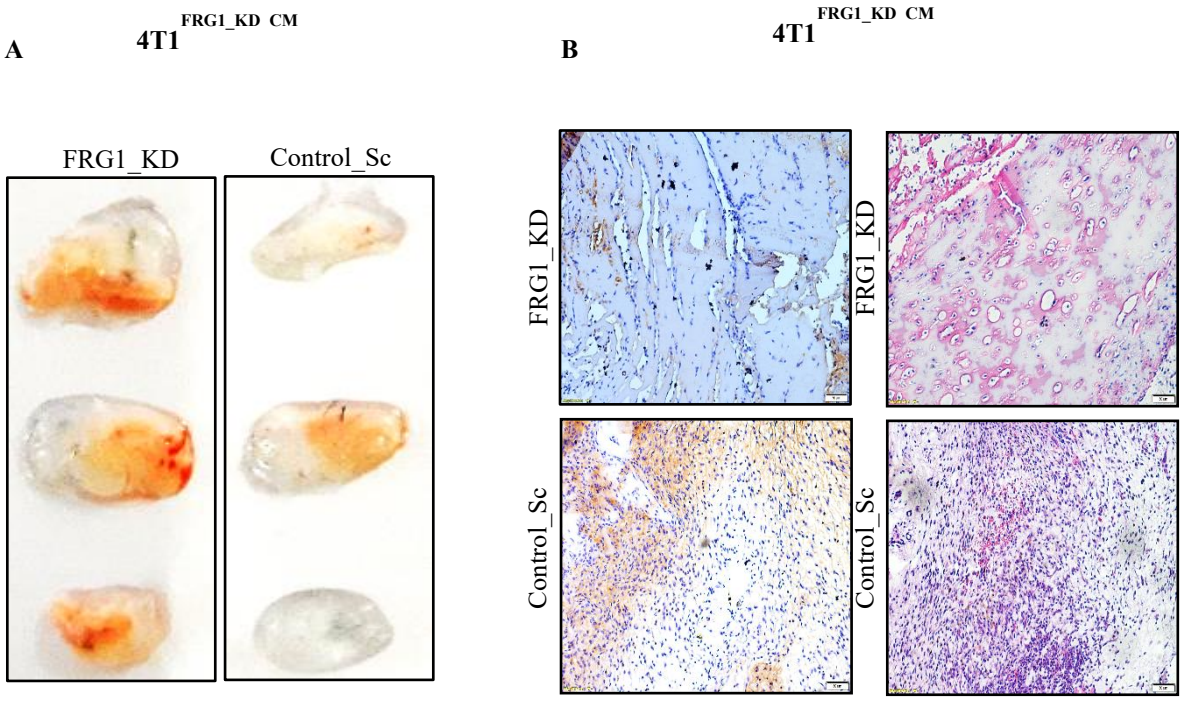

Figure 4C.2.1. Depleted FRG1 levels enhance the generation of plugs in mice model. (A), *Pictorial overview of the matrigel plugs, supplemented with the conditioned medium (CM) derived from FRG1-depleted 4T1 cells, and grown in the C57/BL6 mice (n=3). Plugs were removed on the seventh day from the administration of the cocktail of matrigel and CM.* ***(B),*** *The left panel shows the immunohistochemistry images of the plugs, stained with CD31 antibody. The right panel shows the plugs in the same set with H&E staining. Images were captured at 4X magnification. Scale bar: 50 µm.*

4C.2.2. Quick wound recovery due to loss of FRG1 supports its angiogenic potential

Three separate but overlapping phases make up the complex, multi-step process of adult skin healing; (a) inflammation, (b) proliferation, and (c) remodelling and maturation (260).

The inflammatory phase involves augmented vascular permeability followed by chemotaxis of cells, including neutrophils and macrophages from the circulation to the wound site, and the release of numerous growth factors and cytokines that trigger the activation of migratory cells (261). During the proliferative phase, fibroblasts and endothelial cells proliferate. This stage is also characterised by the migration of fibroblasts towards the wound site (261), deposition of extracellular matrix (ECM), and granulation of tissue (wound connective tissue) formation (262). FGF2 and VEGF which are released at the wound site by macrophages and damaged endothelial cells, promote angiogenesis at this step (263). Report suggest that stimulation of angiogenesis speeds up the healing process (262). Collagen-rich matrix is deposited surrounding the wound during the last or maturation and remodelling stage of the wound-healing cascade (264).

As the angiogenesis process is crucial for wound healing, we next checked the effect of FRG1 depletion in the wound healing process of BALB/c mice and compared it with the control. A wound was created on the back side of the mice that were surrounded by a silicon splint and covered with a dressing film. Mice were treated with the cocktail of growth factor reduced matrigel and the conditioned medium harvested from FRG1-depleted 4T1 cells or control, twice a day. Wound size was measured on days 3^{rd}, 6^{th}, and 9^{th} in both groups (Fig. 4C.2.2.A). Analysis of the wound area using the ImageJ software revealed a quicker wound healing that almost reached to a complete closure of the wound on day 9^{th} in the mice treated with the FRG1-depleted conditioned medium, compared to the control (Fig. 4C.2.2.B).

Hence, the observation from the animal wound healing-based assay corroborates our hypothesis that reduced FRG1 levels promote angiogenesis.

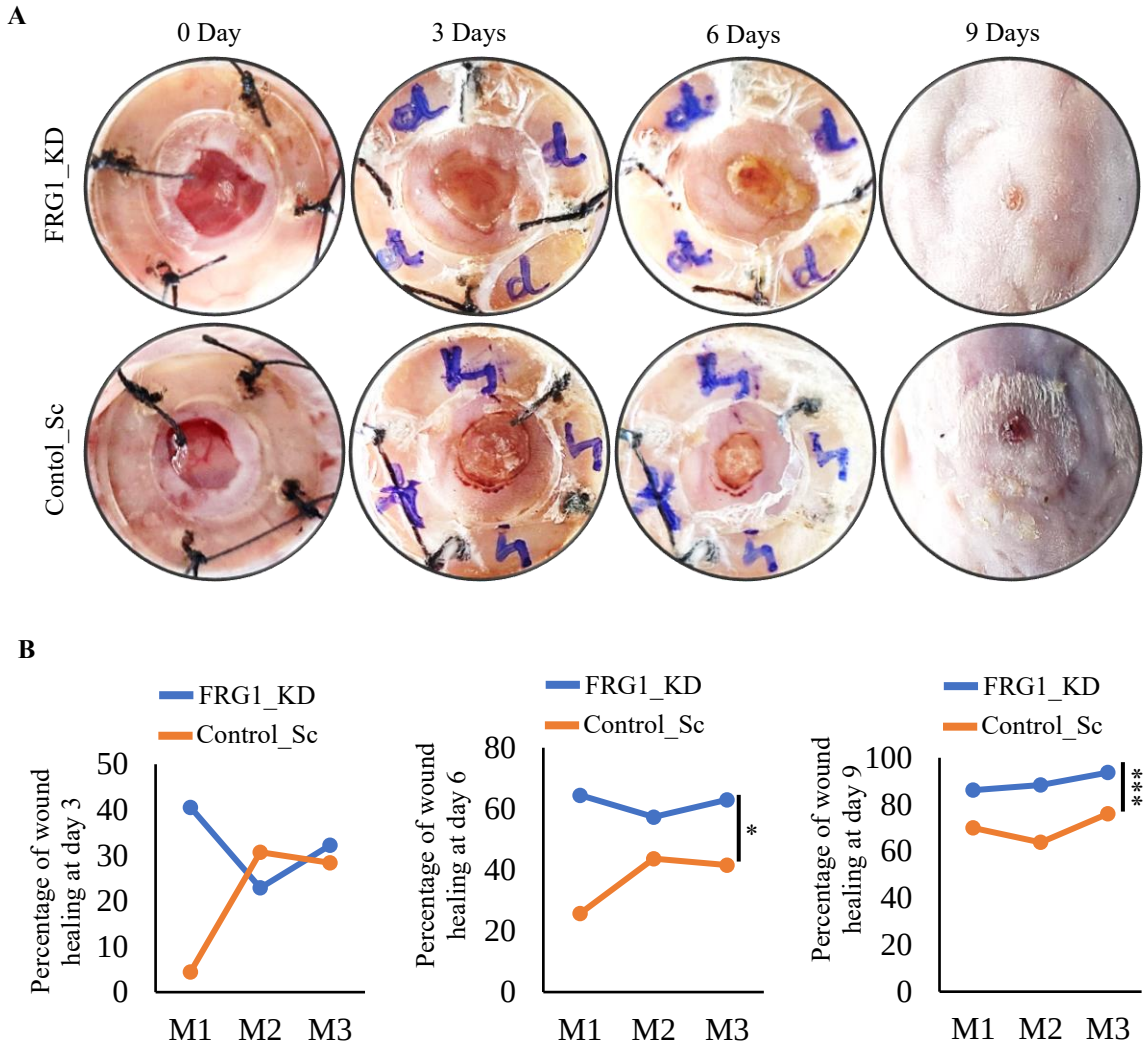

Figure 4C.2.2. Effect of FRG1 depletion on the wound recovery of BALB/c mice. **(A),** *Images illustrate the progression in the wound recovery process in mice that received the conditioned medium (CM) from FRG1 depleted (FRG1_KD) or control (Control_Sc) 4T1 cells over the wounds twice a day. Images were captured on every third days.* **(B),** *Graphical representation compares the difference in wound healing percentage in mice given the FRG1_KD or Control_Sc CM. Two-tailed unpaired student's t-test are used to compare the statistical significance of the difference between the two groups. ns, $p > 0.05$, *, $p \leq 0.05$; ***, $p \leq 0.001$. M1: mouse 1, M2: mouse 2, and M3: mouse 3.*

4C.3. *Depleted FRG1 expression elevates the level of proangiogenic factors in breast cancer cells*

To check the differential expression of major angiogenic modulators due to FRG1 level perturbation, we performed qRT-PCR. Proteins belong to the VEGF and FGF superfamily are reported as the most potent regulators of angiogenesis (84), (128). ELISA did not detect any change in the secreted VEGFA level in the supernatant of MCF7 cells with FRG1 knockdown (Fig. 4C.3.A) and MDA-MB-231 cells with FRG1 overexpression. (Fig. 4C.3.B). The mRNA level of other isoforms of VEGFs i.e. VEGFB and VEGFD showed a slightly increasing trend due to the knockdown of FRG1 (Fig. 4C.3.C). In contrast, ectopic expression of FRG1 in MCF7 cells shows almost no change in the level of VEGFB and VEGFD in terms of fold change (Fig. 4C.3.D). MDA-MB-231 cells with elevated FRG1 levels show an decreased expression of VEGFB and VEGFD transcripts (Fig. 4C.3.E).

Next, we inspected the level of FGF, another crucial regulator of angiogenesis (136). Among the four isoforms of FGF, FGF2 plays a major significant role in tumor angiogenesis (25). Our qRT-PCR data suggested a significant upregulation in FGF2 mRNA level due to FRG1 depletion in MCF7 cells (Fig. 4C.3.F). Correspondingly, downregulation in FGF2 mRNA in MCF7 cells with increased FRG1 expression further corroborated our observation (Fig. 4C.3.G).

Collectively this data suggests that a decrease in FRG1 level stimulates angiogenesis via upregulating the expression of FGF2.

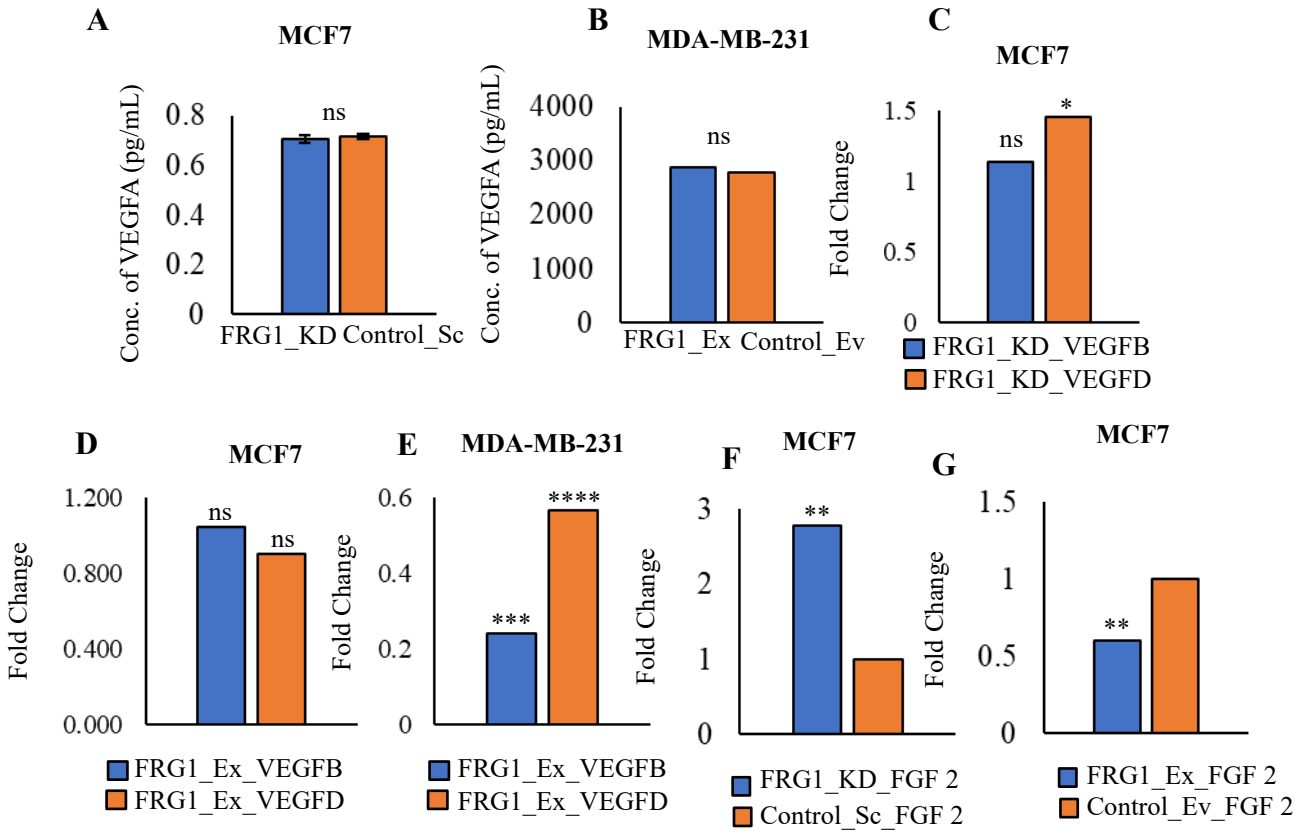

Figure 4C.3. Effect of FRG1 level modulation on the expression level of pro-angiogenic cytokines. **(A),** *Corresponding bar graphs of ELISA quantify the level of VEGFA, present in the supernatant of FRG1-depleted (FRG1_KD) and control (Control_Sc) MCF7 cells. OD was recorded at 490 nm.* **(B),** *Bar graphs of ELISA showing the amount of VEGFA, present in the supernatant of MDA-MB-231 cells with FRG1 overexpression (FRG1_Ex) and control (Control_Ev). OD was recorded at 490 nm.* **(C-D),** *Corresponding bar graphs of q-RT PCR show the difference in the fold change of VEGFB and VEGFD transcripts levels due to FRG1 knockdown (FRG1_KD)* **(C);** *and elevated condition (FRG1_Ex)* **(D),** *compared to their respective controls in MCF7 cells.* **(E),** *Bar graph showing the difference in the fold change of VEGFB and VEGFD transcript levels in MDA-MB-231 cells with elevated FRG1 level (FRG1_Ex), compared to the control.* **(F-G),** *Bar graphs demonstrating the difference in the fold change of FGF2 transcripts present on the MCF7 cells with reduced FRG1 (FRG1_KD)*

(F); *and elevated condition (FRG1_Ex)* **(G),** *compared to their respective control. The statistical significance of the difference was calculated by two-tailed unpaired student's t-test. All the experiments were independently performed thrice. Data are represented as mean ± standard deviation (SD). ns, $p > 0.05$; *, $p \leq 0.05$; **, $p \leq 0.01$; ***, $p \leq 0.001$; ****, $p \leq 0.0001$.*

4C.4. *Reduced FRG1 level promotes the activation of the ERK-AKT signaling cascade in HUVECs*

Intrigued by the effect of FRG1 level perturbation on FGF2 level alteration in breast cancer cells, we investigated the downstream molecules of FGF2 to ascertain the signaling mechanism underlying FRG1-mediated tumor angiogenesis.

FGF2 is widely reported to promote angiogenesis through activating the AKT and ERK signaling axis in endothelial cells (265), (266). Therefore, we measured the paracrine effect of FRG1 on the activation of AKT and ERK in HUVECs. HUVECs were co-cultured for 24 hours with the conditioned medium harvested from MCF7 cells with depleted FRG1 expression and MDA-MB-231 cells with elevated levels of FRG1. Western blot demonstrates that increased FGF2 levels present in the conditioned medium from FRG1-depleted MCF7 cell led to the activation of ERK and AKT signaling in HUVECs (Fig. 4C.4.A). To check if the effect was regardless of breast cancer molecular subtypes, we treated the HUVECs with the conditioned medium obtained from MDA-MB-231 cells with FRG1 overexpression. There we observed decreased activation of ERK and AKT in HUVECs (Fig. 4C.4.B). In both cases, no difference was found in the level of total ERK and total AKT.

This observation points out that reduced FRG1 levels might induce angiogenesis, irrespective of breast cancer molecular subtype, by the activation of the AKT/ERK signaling pathway.

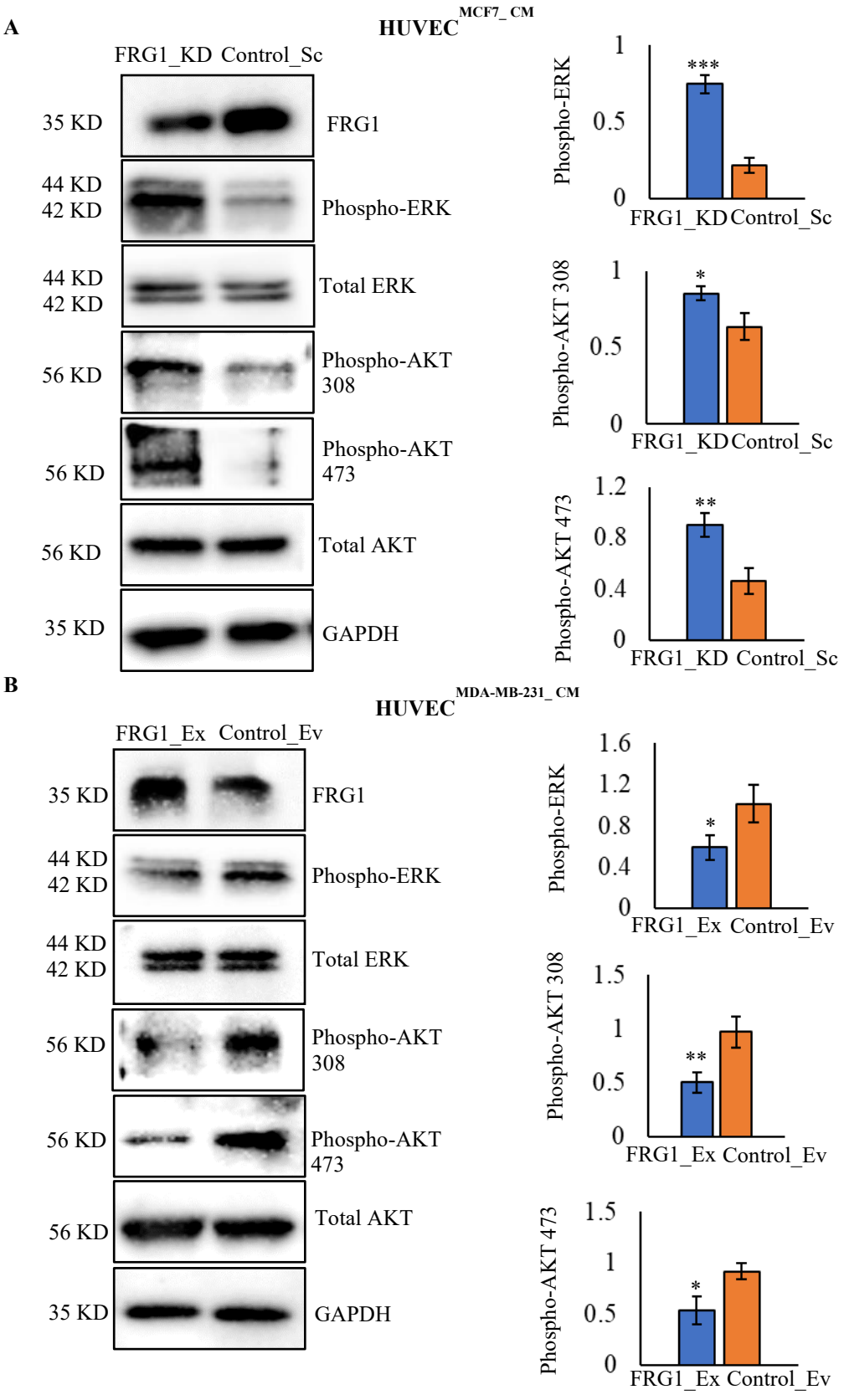
A
HUVEC MCF7_ CM
FRG1_KD Control_Sc
35 KD
FRG1
44 KD
42 KD
Phospho-ERK
44 KD
42 KD
Total ERK
56 KD
Phospho-AKT 308
56 KD
Phospho-AKT 473
56 KD
Total AKT
35 KD
GAPDH
Phospho-ERK
Phospho-AKT 308
Phospho-AKT 473
FRG1_KD Control_Sc
B
HUVEC MDA-MB-231_ CM
FRG1_Ex Control_Ev
35 KD
FRG1
44 KD
42 KD
Phospho-ERK
44 KD
42 KD
Total ERK
56 KD
Phospho-AKT 308
56 KD
Phospho-AKT 473
56 KD
Total AKT
35 KD
GAPDH
Phospho-ERK
Phospho-AKT 308
Phospho-AKT 473
FRG1_Ex Control_Ev

Figure 4C.4. Effect of FRG1 level alteration on the activation of ERK and AKT. **(A-B),** *HUVECs were treated for 24 hours with the conditioned medium (CM) obtained from MCF7 cells with reduced FRG1 levels and MDA-MB-231 cells with ectopic FRG1 levels. Thereafter, protein was harvested from the HUVECs, and Western blot was performed.* **(A),** *Representative Western blots and the corresponding densitometry-based bar graphs show the expression of phospho-ERK, phospho-AKT 308, and phospho-AKT 473 in HUVECs, co-cultured with the CM, collected from MCF7 cells with depleted FRG1 levels (FRG1_KD) and control (Control_Sc).*

(B), *Representative Western blots and the corresponding densitometry-based bar graphs depict the level of phospho-ERK, phospho-AKT 308, and phospho-AKT 473 in HUVECs that had been treated with CM from MDA-MB-231 cells with elevated FRG1 levels (FRG1_Ex) and its matching control (Control_Ev). GAPDH has been used as internal control. All the experiments were independently performed thrice. Two-tailed unpaired student's t-test was used to derive the statistical significance of differential protein expression between the two groups. The findings are shown as mean ± standard deviation (SD). *, $p \leq 0.05$; **, $p \leq 0.01$, ***, $p \leq 0.001$.*

4C.5. The *effect of FRG1 on angiogenesis is FGF2-mediated*

Next, we investigated if the activation of ERK and AKT in HUVECs was FGF2 mediated. As the HUVECs supplemented with FRG1-depleted conditioned medium led to increased activation of ERK and AKT, we sought if it was facilitated by elevated FGF2, present in the respective conditioned medium. Reports suggest that ERK and AKT are the two downstream target molecules of FGF signaling (267), (268). Inhibition of FGF receptor is associated with decreased activation of AKT and ERK (269). To evaluate this in our case, we carried out the Western blots and tubule formation assay.

4C.5.1. *Inhibition of the FGF receptor decreases the activation of ERK and AKT in FRG1-depleted MCF7 cells*

To delineate the impact of FGF2 on FRG1-mediated angiogenesis, we first performed the Western blot. We co-cultured the HUVECs with the EBM2 medium and the conditioned medium, obtained from FRG1-depleted MCF7 cells and control in a 1:1 ratio. After 24 hours of incubation, 100 nM of FGF receptor (FGFR) inhibitor Infigratinib or its solvent DMSO control was administrated to the HUVECs, and incubated for 6 hours. After six hours, we harvested the protein from the HUVECs and performed the Western blot. We observed that inhibition of FGFR in the aforementioned cells led to the abrogation of ERK and AKT activation, brought on by the impaired FGF2 signaling (Fig. 4C.5.1).

This observation leads to the conclusion that the knockdown of FRG1 in MCF7 cells secretes a higher level the FGF2 that, in turn, activate the ERK and AKT in endothelial cells.

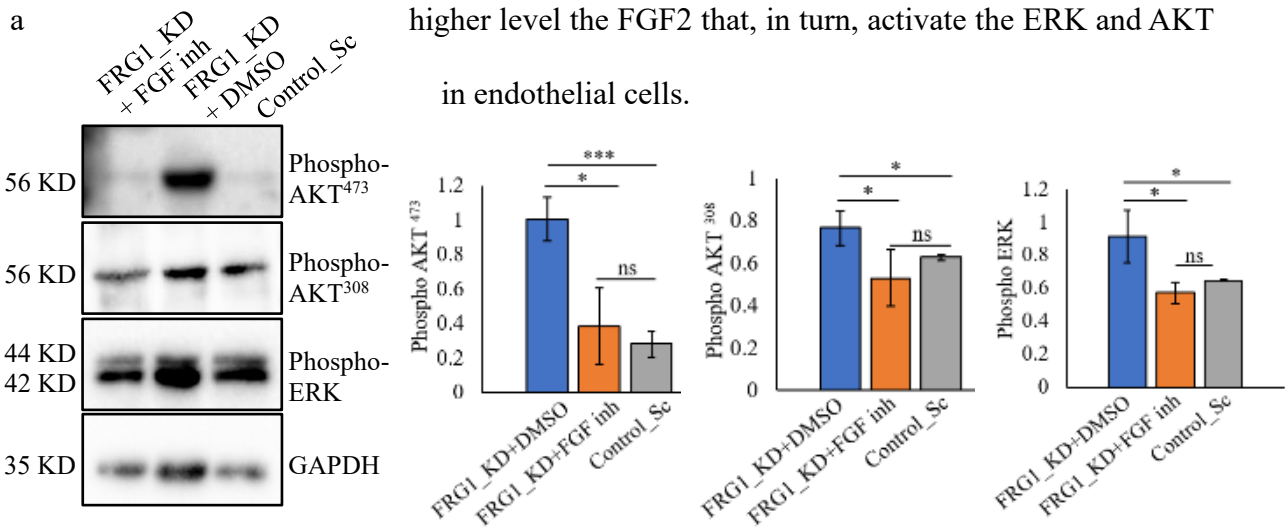

Figure. 4C.5.1. ERK and AKT activation via FRG1 is suppressed by inhibition of the FGF receptor. **(A-B)**, *HUVECs were grown in the conditioned medium (CM) obtained from MCF7*

*cells with FRG1 knockdown (FRG1_KD) and control (Control_Sc). 100 nM of FGFR inhibitor Infigratinib or its solvent DMSO was applied into the medium (FRG1_KD+FGF inh and FRG1_KD + DMSO respectively) for six hours. The Control_Sc group was left untreated. After six hours of incubation, protein lysate was collected, and the Western blot was carried out. The first and second lanes of the Western blot show the rescue in the activation of ERK, and AKT in 308 and 473 positions respectively. Corresponding bar graphs are showing the difference in the activation level of ERK and AKT in the same group. All the experiments were independently performed thrice. The statistical significance of differential protein expression among the sets was measured by using two-tailed unpaired student's t-test. The findings are shown as mean ± standard deviation (SD). ns, $p > 0.05$, *, $p \leq 0.05$; ***, $p \leq 0.001$.*

4C.5.2. Inhibition of the FGF receptor decreases tubulogenesis in FRG1-depleted MCF7 cells

Next, we investigated the phenotypic effect of FGF receptor inhibition on the tubulogenic properties of HUVECs. We supplemented the HUVECs with the EBM2 medium and the conditioned medium obtained from MCF7 cells with reduced FRG1 levels and corresponding control. After 24 hours, we administrated 100 nM FGF receptor inhibitor Infigratinib or its solvent control DMSO into the HUVECs and incubated for six hours. Inhibition of FGF2-mediated downstream signaling in HUVECs showed significantly lesser tubules in comparison to the HUVECs grown in the DMSO control (Fig. 4C.5.2.A). We further analyzed several tubulogenic parameters using the Angiogenesis Analyzer tool of ImageJ software. Analysis suggests a substantial decline in the tubulogenic properties of HUVECs, including number of nodes, junctions, master segments, master junction, segments, meshes, peaces, total segment length, branching interval, total master segment length, mesh index, mean mesh size, total

length, total branching length, total meshes area, total branches length, number of extremes, and number of branches due to FGFR inhibition (Fig. 4C.5.2.B).

Taken together, we propose that FRG1 reduction in breast cancer cells triggers the downstream AKT and ERK activation via FGF2. Inhibition of FGF2 resulted in decreased phosphorylation of AKT and ERK that, in turn, inhibits the tubulogenic properties of endothelial cells. This result further substantiates FGF2-mediated regulation of FRG1 in breast tumorigenesis.

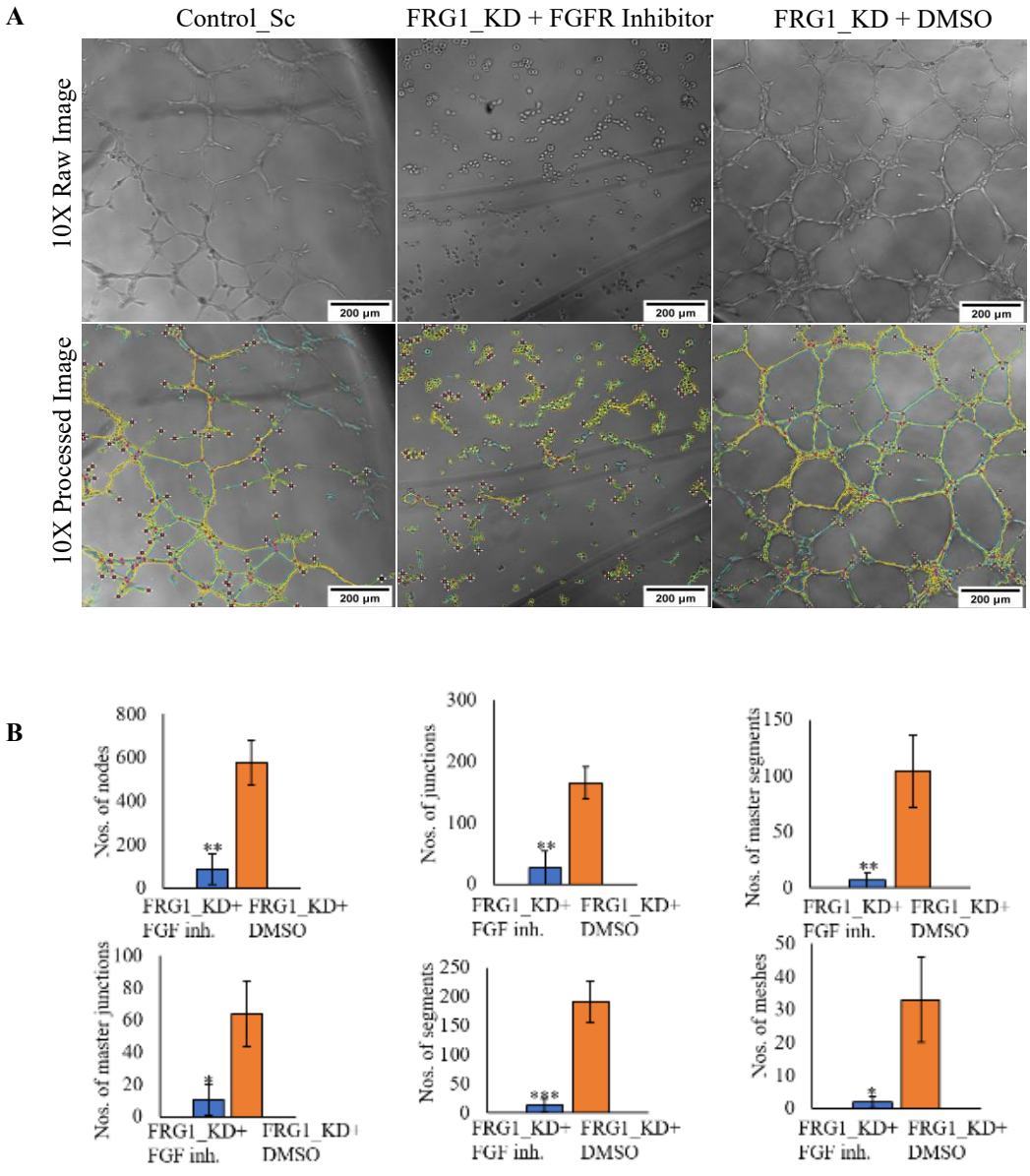

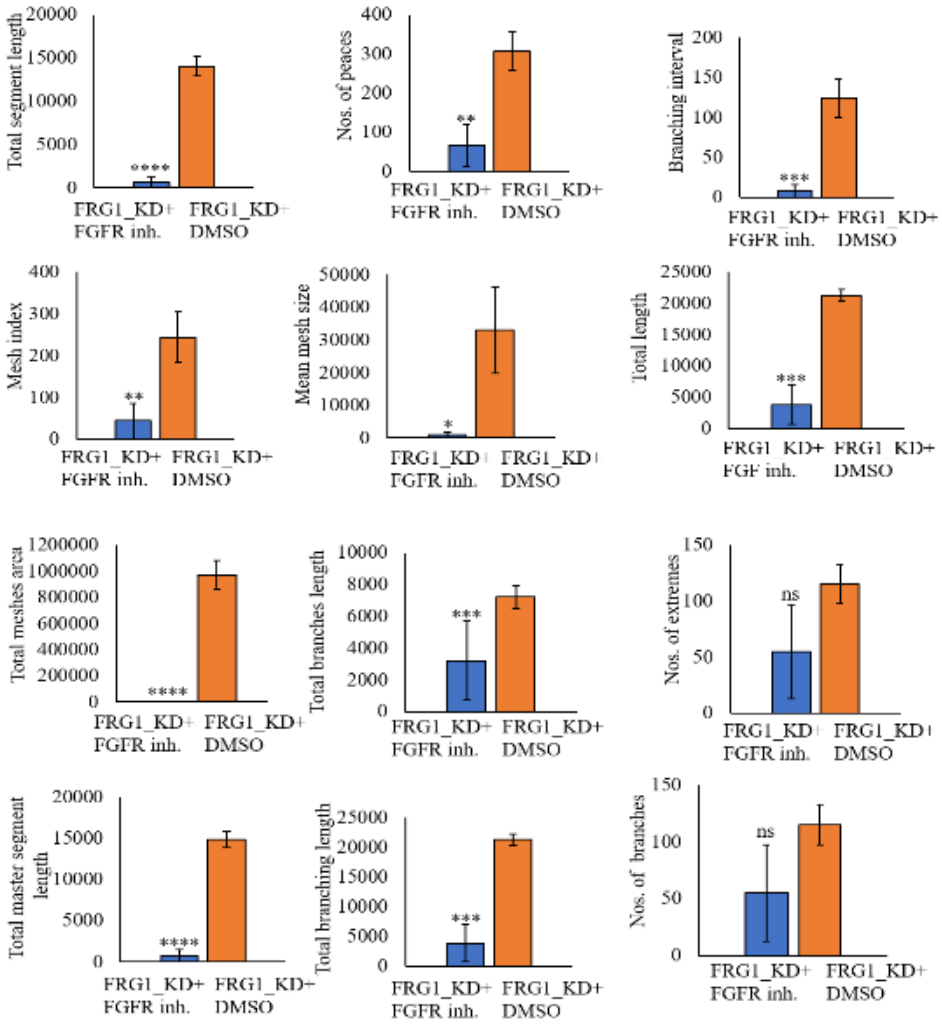

Figure. 4C.5.2. FGF receptor inhibition decreased the tubulogenesis **(A-B)**, *HUVECs were grown in the EBM-2 medium and conditioned medium (CM) from MCF7 cells with reduced FRG1 levels (FRG1_KD) along with the control (Control_Sc). After six hours, 100 nM of FGFR inhibitor Infigratinib or its solvent DMSO was applied into the medium (FRG1_KD + FGFR inhibitor and FRG1_KD + DMSO respectively) and incubated for six hours. The Control_Sc group was left untreated. Thereafter the images of the tubules that emerged from the aforementioned set were captured at 10X magnification.* **(A),** *Tubule formation assay depicts the effect of FGFR inhibition on the tubule formation properties of HUVECs, incubated with the CM from FRG1_KD + FGFR inhibitor, FRG1_KD + DMSO, and Control_Sc MCF7 cells.* **(B),** *The difference in the different tubulogenic parameters was analyzed and represented*

*by the bar graphs. The statistical significance of the difference among the sets was measured by using two-tailed unpaired student's t-test. The findings are shown as mean ± standard deviation (SD). ns, $p > 0.05$; *, $p \leq 0.05$; **, $p \leq 0.01$; ***, $p \leq 0.001$; ****, $p \leq 0.0001$.*

Chapter 5

Summary and Conclusion

Around 90% of the deaths associated with breast cancer are caused by metastatic spread (270). Hence, a significant focus has been paid by the researchers to unravel the mechanistic basis behind the metastatic process. Dysregulation in the function of tumor suppressor genes is frequently linked to enhanced metastasis that results in poor clinical outcomes. Distinct molecular subtypes in breast cancer correspond to different clinical consequences. Therefore, finding new targets that can function regardless of breast cancer molecular subtypes can aid in formulating a more potent therapeutic strategy.

The majority of the research has emphasized elucidating the role of FRG1 in the development of muscle, FSHD pathology, and angiogenesis since its discovery in 1996. Only a limited number of studies have found a direct connection between FRG1 and cancer. Previously our group showed a reduced level of FRG1 in gastric, colon, and oral cancer patients (26). The same study showed that reduced FRG1 levels in HEK 293T cells led to increased cell migration and invasion. In prostate cancer, FRG1 depletion triggered the activation of p38-MAPK signaling (27). The elevated transcript levels of many cancer-promoting cytokines and growth factors, including MMP1, PDGF A, CXCL1, and GM-CSF, were also discovered as a result of FRG1 depletion.

Our findings from the current study are the first to show an opposite correlation between FRG1 levels and breast cancer. Using several *in vitro* and *in vivo* experimental models, we have demonstrated the FRG1-mediated regulation of breast tumorigenesis. Enhanced ERK activation is associated with multiple tumorigenic events during malignant transformation, including EMT progression, proliferation, and angiogenesis (271), (272). The interplay of ERK and ER signaling in luminal cancer is reported to render the cells resistant to chemotherapy (273). We have found that MCF7 cells with partial and complete loss of FRG1 led to the activation of ERK. We have further shown that altered expression of EMT markers Snail, Slug, and Twist due to ERK activation in the cells with FRG1 level modulation is irrespective of

breast cancer molecular subtypes. Our findings may open up a plethora of possibilities for the development of potent therapeutic strategies in breast cancer that can target ERK's upstream regulators regardless of their subtypes. The interaction between ERK and AKT is a key factor in determining whether a cell will survive or undergo apoptosis (235). Unexpectedly in our case, reduced FRG1 levels abrogated the activation of AKT at the Thr^{308} position while leaving its Ser^{473} site unaffected. However, we found that the inhibition of ERK restored the AKT phosphorylation (Thr^{308}). This observation is supported by an earlier study which reports that hyperactivation of the ERK pathway can attenuate the AKT phosphorylation (274). This particular aspect of our discovery is also consistent with numerous preceding findings that point to several molecular mechanisms for the repression of AKT activation by the MEK-ERK signaling axis (275), (276), (277). To cite a few, ERK controls the coupling of Gab1 and PI3K negatively, which reduces the subsequent AKT-mediated signal transduction (275), (237). Additionally, ERK inhibition represses the activation of EGFR, that in turn elevates the phosphorylation of AKT (278). Apart from the p38-p53-induced apoptotic event, several investigations have revealed that ERK can directly affect apoptosis by regulating p53 (279). ERK inhibition facilitates apoptosis by promoting the nuclear translocation of the apoptosis-inducing factors (235). According to a different study, p53 is likely to be destroyed as ERK stimulates the expression of MDM2 (240). We observed decreased activation of p53 due to the knockdown of FRG1 in MCF7 cells, which was restored by ERK inhibition. This corresponds to the research suggesting that the MEK-ERK signaling axis can suppress p53 activation and increase cell viability (235). Therefore, we propose that the reduction of FRG1 stimulates the ERK signaling that, in turn, reduces the activation of AKT and p53, leading to the ERK-mediated suppression of apoptosis.

Despite numerous findings indicating elevated levels of GM-CSF in a number of non-haematopoietic malignancies, more research is needed to understand the underlying molecular

basis of GM-CSF-regulated metastasis. Previously it was reported that GM-CSF promotes breast cancer pathogenesis by recruiting CCL-18+ macrophages into the tumor microenvironment (31). Increased GM-CSF level in breast cancer is correlated with increased metastasis and poor patient survival (280). Higher expression of GM-CSF receptors on nonhematopoietic cells in multiple tumor types has suggested its potential role as a pro-tumorigenic factor, which is yet to be validated (281). Expression of GM-CSF in skin carcinoma cells enhanced the metastatic growth and proliferation of cancer cells (282). Also, in the head and neck (283), glioma (284), and osteosarcoma (285), autocrine stimulation of GM-CSF is reported to promote tumor growth. GM-CSF-mediated activation of the MAPK/ERK/ZEB1 signaling axis has been documented to promote colon cancer EMT (30); however, the mechanistic insight was unknown. For the first time, the current study has identified that FRG1 functions as a transcriptional repressor of GM-CSF and also uncovered the intricate involvement of GM-CSF in breast carcinoma. Lesser levels of cellular FRG1 cause higher GM-CSF secretion, leading to EMT induction by ERK. An earlier research which discovered that HER2+ breast cancer cells invading the cerebrospinal fluid, secreted GM-CSF that increased the expression of ERK1/2, AKT, and Stat5, lends support to this observation (286). Our finding of GM-CSF-mediated upregulation of Snail in EMT is further supported by a study that claims cancer associated mesenchymal stem cells secret GM-CSF, which is necessary for tumor cell proliferation, invasion, and trans-endothelial migration in pancreatic ductal adenocarcinoma (287). Numerous gaps among FRG1, GM-CSF, and ERK in controlling the EMT have been filled by our findings. Previously, a mathematical model by Szomolay et. al. predicted the effect of anti-GM-CSF treatment on reducing tumor growth in breast cancer (288). We have verified this model *in vivo*. We detected that anti-GM-CSF monoclonal antibody abrogated the growth of the tumors and the levels of EMT marker Snail in mice. Overall, our research emphasizes the clinical efficacy of anti-GM-CSF treatment in cancer

samples that have lower levels of FRG1. Although a clinical trial suggests that anti-GM-CSF therapy has no discernible effect on the invasive disease-free survival of breast cancer patients (289), checking the level of FRG1 to decide the efficacy of this treatment can pave the way for targeting GM-CSF in human clinical trials for breast cancer.

To corroborate our *in vitro* findings, we conducted a retrospective analysis of clinical specimens. The result revealed that levels of FRG1 were reduced in 71% of patients with breast carcinoma, with no differential expression pattern of FRG1 between ER+ and TNBC patients. In consistent to our *in vitro* observations, it further emphasizes that the effect of FRG1 is regardless of breast cancer subtypes. There has not been much work done identifying a single molecule that is effective regardless of the molecular subtypes of breast cancer. Our cell-based and patient data suggest the effect of FRG1 is independent of molecular subtypes. This observation opens up the possibility of treating breast cancer patients of different molecular subtypes using a similar treatment strategy.

Moreover, Kaplan-Meir and GEPIA-based survivance assessment indicates higher FRG1 expression levels in breast cancer patients are correlated with a greater disease-free survivorship. It suggests a protective function of FRG1 in determining the prognosis. This observation is supported in a multigene-based survival prediction study by Khan *et. al*., who reported that higher FRG1 levels in the cervix and gastric cancer patients were associated with better overall survival of the patients. The accuracy of this observation can be authenticated by testing it in a larger population.

To conclude the findings of the first two objectives of this thesis, we propose that decreased FRG1 levels turn on the enhanced transcription of GM-CSF in breast cancer cells that favors the activation of downstream ERK and induces EMT. The discovery of the underlying mechanism of GM-CSF-mediated ERK activation and the interaction between AKT and ERK may aid in the invention of a more beneficial treatment approach.

The process of tumorigenesis and metastasis is inevitably dependent on the formation of new blood vessels. Angiogenesis is facilitated by several growth factors and cytokines released by the cancerous cells (12). Inadequate circulatory support induces necrosis or even cell death (153), (154). Hence, the development of anti-angiogenic inhibitors has always received a lot of research interest (290). Members belonging to the VEGF and FGF families are reported as the most potent stimulators of angiogenesis (291). Other cytokines that are known to promote the angiogenic events in breast cancer include Interleukins- 1α/β, 6/8, TNF-α/β, TGF-β, and GM-CSF (7), (292). Regardless of the fact that VEGF-directed chemotherapy has a major impact on the survival benefits of the patients, they frequently stop functioning after a specific period of time due either to resistance development to VEGF inhibitors or the patient's evasive rejection (293). Hence, focusing on targeting alternative angiogenic regulators, such as the FGF family, has been a target of attention (294). There are compelling evidences to support the role of FGF signaling in tumor angiogenesis (295), (296). The FDA has authorized a number of medications that target FGF or its receptor (297), (298). Unfortunately, FGF suppression frequently triggers the other oncogenic signaling, such as EGFR, ERBB3, or MET, which eventually fails to improve patient life (298). Therefore, identifying further upstream angiogenic factors that have the ability to regulate tumorigenic functions can help with the thorough management of cancer treatment.

The observation that 75% of FSHD patients exhibit anomalies in their retinal vascularization led to the hypothesis that FRG1 levels and angiogenesis are interrelated (299). Despite being involved in suppressing metastatic growth, FRG1's contribution to tumor angiogenesis has largely gone unnoticed. The first conclusive evidence of FRG1's potential involvement in tumor angiogenesis was provided by a study by Tiwari *et al*. in 2017 (26). The current research has taken an important step towards identifying FRG1 as an angiogenic regulator with therapeutic benefits. We noticed that angiogenic factors present in the conditioned medium of

breast cancer cells with reduced and elevated FRG1 levels, influence higher proliferation, migration, and tubule formation of primary endothelial cells HUVECs.

From a mechanistic perspective, we investigated the role of the two most abled modulators of angiogenesis, VEGFA and FGF2. We previously found that the alteration of FRG1 expression levels in the HEK 293T cell line did not cause any change in the mRNA levels of VEGFA and FGF2 (26). Even though our study suggests an unaltered VEGFA expression in FRG1-depleted cells, the FGF2 transcript level was affected due to FRG1 level perturbation. Activation of signal transduction pathways through FGF receptors 1-4 enables the endothelial cells to survive, proliferate, migrate, and differentiate. Among the several FGF isoforms that control angiogenesis, FGF2 is the most effective one (266). A range of experimental systems, including CAM, rabbit/mouse cornea, and matrigel plug assay suggests FGF2 affects *in vivo* angiogenesis (300). Our results suggest that reduction in FRG1 levels in breast cancer cells secrete FGF2 that binds to the FGFR on HUVECs and triggers the FGF2-mediated signaling cascade, leading to enhanced angiogenesis. Activation of FGFR by FGF2 was alone enough to elicit the increased angiogenic properties in HUVECs. This finding is further corroborated by a prior report in which it was discovered that FGF2 was twice as effective as VEGF at infiltrating a collagen gel matrix and producing capillary-like structures (84).

Angiogenesis needs collaborative molecular communication, which is primarily made possible by the ERK-AKT pathway. Development of normal vasculature requires activated ERK signaling (301). AKT activation is important for the survival of endothelial cells (302). The PI3K-AKT signaling axis facilitates endothelial cell's capillary development and migration (303). Our findings that FGF2 stimulates the downstream ERK as well as AKT in HUVECs are consistent with earlier research (266). The binding of FGF2 on the FGF receptor and cell surface receptor heparan sulfate proteoglycans activates the signaling axis comprising of Ras, Raf, MAPK, and ERK (304).

To conclude our findings, we have identified a novel tumor suppressor, FRG1, which exerts its effect through the GM-CSF-ERK signaling cascade. Because of the enormous potential of FRG1 as a modulator of both tumorigenesis and angiogenesis, it can be beneficial to plan a therapeutic approach to target its downstream molecule, such as GM-CSF, in order to avoid resistance. Our findings have also deciphered that FRG1 has an impact on a number of pathways, including AKT and ERK and it works upstream of FGF2. FRG1 controls a number of tumorigenic features, encompassing from cancer cell proliferation, EMT to angiogenesis. Several tumorigenic or angiogenic inhibitors are currently being used as a part of the combination therapy (305). Only a small percentage of patients get benefited from single drug-based cancer treatments. Therefore, future research into exploring the potential effect of dual-purpose molecule such as FRG1 may lead to better clinical outcome.

References

1. Sørlie T, Perou CM, Tibshirani R, Aas T, Geisler S, Johnsen H, et al. Gene expression patterns of breast carcinomas distinguish tumor subclasses with clinical implications. Proc Natl Acad Sci USA. 2001 Sep 11;98(19):10869–74.

2. Higgins MJ, Baselga J. Targeted therapies for breast cancer. J Clin Invest. 2011 Oct 3;121(10):3797–803.

3. Sung H, Ferlay J, Siegel RL, Laversanne M, Soerjomataram I, Jemal A, et al. Global Cancer Statistics 2020: GLOBOCAN Estimates of Incidence and Mortality Worldwide for 36 Cancers in 185 Countries. CA A Cancer J Clin. 2021 May;71(3):209–49.

4. Rahman M, Mohammed S. Breast cancer metastasis and the lymphatic system. Oncology Letters. 2015 Sep;10(3):1233–9.

5. Addison JB, Voronkova MA, Fugett JH, Lin CC, Linville NC, Trinh B, et al. Functional Hierarchy and Cooperation of EMT Master Transcription Factors in Breast Cancer Metastasis. Molecular Cancer Research. 2021 May 1;19(5):784–98.

6. Geng Y, Chandrasekaran S, Hsu JW, Gidwani M, Hughes AD, King MR. Phenotypic Switch in Blood: Effects of Pro-Inflammatory Cytokines on Breast Cancer Cell Aggregation and Adhesion. Engler AJ, editor. PLoS ONE. 2013 Jan 23;8(1):e54959.

7. Esquivel-Velázquez M, Ostoa-Saloma P, Palacios-Arreola MI, Nava-Castro KE, Castro JI, Morales-Montor J. The Role of Cytokines in Breast Cancer Development and Progression. Journal of Interferon & Cytokine Research. 2015 Jan;35(1):1–16.

8. Morein D, Erlichman N, Ben-Baruch A. Beyond Cell Motility: The Expanding Roles of Chemokines and Their Receptors in Malignancy. Front Immunol. 2020 Jun 4;11:952.

9. Noë V. Proteolysis of E-cadherin by MMPs.

10. Ramos-DeSimone N, Hahn-Dantona E, Sipley J, Nagase H, French DL, Quigley JP. Activation of Matrix Metalloproteinase-9 (MMP-9) via a Converging Plasmin/Stromelysin-1 Cascade Enhances Tumor Cell Invasion. Journal of Biological Chemistry. 1999 May;274(19):13066–76.

11. Yu Q, Stamenkovic I. Cell surface-localized matrix metalloproteinase-9 proteolytically activates TGF-β and promotes tumor invasion and angiogenesis. Genes Dev. 2000 Jan 15;14(2):163–76.

12. Folkman J. Angiogenesis in cancer, vascular, rheumatoid and other disease. Nat Med. 1995 Jan;1(1):27–30.

13. Badodekar N, Sharma A, Patil V, Telang G, Sharma R, Patil S, et al. Angiogenesis induction in breast cancer: A paracrine paradigm. Cell Biochem Funct. 2021 Oct;39(7):860–73.

14. Rofstad EK, Halsør EF. Vascular endothelial growth factor, interleukin 8, platelet-derived endothelial cell growth factor, and basic fibroblast growth factor promote angiogenesis and metastasis in human melanoma xenografts. Cancer Res. 2000 Sep 1;60(17):4932–8.

15. Todorović-Raković N, Milovanović J. Interleukin-8 in Breast Cancer Progression. Journal of Interferon & Cytokine Research. 2013 Oct;33(10):563–70.

16. Moo TA, Sanford R, Dang C, Morrow M. Overview of Breast Cancer Therapy. PET Clinics. 2018 Jul;13(3):339–54.

17. Utku N. New approaches to treat cancer - what they can and cannot do. Biotechnol Healthc. 2011;8(4):25–7.

18. Davies E, Hiscox S. New therapeutic approaches in breast cancer. Maturitas. 2011 Feb;68(2):121–8.

19. GEMO Study Collaborators, EMBRACE Collaborators, KConFab Investigators, HEBON Investigators, ABCTB Investigators, Fachal L, et al. Fine-mapping of 150 breast cancer risk regions identifies 191 likely target genes. Nat Genet. 2020 Jan;52(1):56–73.

20. Hassan. Chemotherapy for breast cancer (Review). Oncol Rep [Internet]. 2010 Sep 27 [cited 2023 Feb 27];24(5). Available from: http://www.spandidos-publications.com/or/24/5/1121

21. Hussain SA, Palmer DH, Stevens A, Spooner D, Poole CJ, Rea DW. Role of chemotherapy in breast cancer. Expert Review of Anticancer Therapy. 2005 Dec;5(6):1095–110.

22. Haibe Y, Kreidieh M, El Hajj H, Khalifeh I, Mukherji D, Temraz S, et al. Resistance Mechanisms to Anti-angiogenic Therapies in Cancer. Front Oncol. 2020 Feb 27;10:221.

23. Yadav V, Zhang X, Liu J, Estrem S, Li S, Gong XQ, et al. Reactivation of Mitogen-activated Protein Kinase (MAPK) Pathway by FGF Receptor 3 (FGFR3)/Ras Mediates Resistance to Vemurafenib in Human B-RAF V600E Mutant Melanoma. Journal of Biological Chemistry. 2012 Aug;287(33):28087–98.

24. Manchado E, Weissmueller S, Morris JP, Chen CC, Wullenkord R, Lujambio A, et al. A combinatorial strategy for treating KRAS-mutant lung cancer. Nature. 2016 Jun 30;534(7609):647–51.

25. Lieu C, Heymach J, Overman M, Tran H, Kopetz S. Beyond VEGF: Inhibition of the Fibroblast Growth Factor Pathway and Antiangiogenesis. Clinical Cancer Research. 2011 Oct 1;17(19):6130–9.

26. Tiwari A, Pattnaik N, Mohanty Jaiswal A, Dixit M. Increased FSHD region gene1 expression reduces in vitro cell migration, invasion, and angiogenesis, ex vivo supported by reduced expression in tumors. Bioscience Reports. 2017 Oct 31;37(5):BSR20171062.

27. Tiwari A, Mukherjee B, Hassan MdK, Pattanaik N, Jaiswal AM, Dixit M. Reduced FRG1 expression promotes prostate cancer progression and affects prostate cancer cell migration and invasion. BMC Cancer. 2019 Dec;19(1):346.

28. Khan R, Palo A, Dixit M. Role of FRG1 in predicting the overall survivability in cancers using multivariate based optimal model. Sci Rep. 2021 Dec;11(1):22505.

29. Wuebbles RD, Hanel ML, Jones PL. FSHD region gene 1 (FRG1) is crucial for angiogenesis linking FRG1 to facioscapulohumeral muscular dystrophy-associated vasculopathy. Disease Models & Mechanisms. 2009 May 1;2(5–6):267–74.

30. Chen Y. An epithelial-to-mesenchymal transition-inducing potential of granulocyte macrophage colony-stimulating factor in colon cancer. Scientific Reports. 2017 Aug 15;7:8265.

31. Su S, Liu Q, Chen J, Chen J, Chen F, He C, et al. A Positive Feedback Loop between Mesenchymal-like Cancer Cells and Macrophages Is Essential to Breast Cancer Metastasis. Cancer Cell. 2014 May;25(5):605–20.

32. Bayne LJ, Beatty GL, Jhala N, Clark CE, Rhim AD, Stanger BZ, et al. Tumor-Derived Granulocyte-Macrophage Colony-Stimulating Factor Regulates Myeloid Inflammation and T Cell Immunity in Pancreatic Cancer. Cancer Cell. 2012 Jun;21(6):822–35.

33. Malvia S, Bagadi SA, Dubey US, Saxena S. Epidemiology of breast cancer in Indian women: Breast cancer epidemiology. Asia-Pac J Clin Oncol. 2017 Aug;13(4):289–95.

34. Dai X, Li T, Bai Z, Yang Y, Liu X, Zhan J, et al. Breast cancer intrinsic subtype classification, clinical. :15.

35. Makki J. Diversity of Breast Carcinoma: Histological Subtypes and Clinical Relevance. Clin Med Insights Pathol. 2015 Jan;8:CPath.S31563.

36. Shiovitz S, Korde LA. Genetics of breast cancer: a topic in evolution. Annals of Oncology. 2015 Jul;26(7):1291–9.

37. Turnbull C, Rahman N. Genetic Predisposition to Breast Cancer: Past, Present, and Future. Annu Rev Genom Hum Genet. 2008 Sep 1;9(1):321–45.

38. Frank TS. Hereditary Risk of Breast and Ovarian Cancer: BRCA1 and BRCA2. In: Bertino JR, editor. Encyclopedia of Cancer (Second Edition) [Internet]. Second Edition. New York: Academic Press; 2002. p. 381–5. Available from: https://www.sciencedirect.com/science/article/pii/B0122275551000903

39. Michailidou K, Beesley J, Lindstrom S, Canisius S, Dennis J, Lush MJ, et al. Genome-wide association analysis of more than 120,000 individuals identifies 15 new susceptibility loci for breast cancer. Nat Genet. 2015 Apr;47(4):373–80.

40. Hiatt RA, Brody JG. Environmental Determinants of Breast Cancer. Annu Rev Public Health. 2018 Apr 1;39(1):113–33.

41. DeSantis C, Howlader N, Cronin KA, Jemal A. Breast Cancer Incidence Rates in U.S. Women Are No Longer Declining. Cancer Epidemiology, Biomarkers & Prevention. 2011 May 1;20(5):733–9.

42. Glade MJ. Food, nutrition, and the prevention of cancer: a global perspective. American Institute for Cancer Research/World Cancer Research Fund, American Institute for Cancer Research, 1997. Nutrition. 1999 Jun;15(6):523–6.

43. Rumgay H, Shield K, Charvat H, Ferrari P, Sornpaisarn B, Obot I, et al. Global burden of cancer in 2020 attributable to alcohol consumption: a population-based study. The Lancet Oncology. 2021 Aug;22(8):1071–80.

44. Suzuki R, Orsini N, Mignone L, Saji S, Wolk A. Alcohol intake and risk of breast cancer defined by estrogen and progesterone receptor status-A meta-analysis of epidemiological studies. Int J Cancer. 2007 Dec 7;122(8):1832–41.

45. Oyesanmi O, Snyder D, Sullivan N, Reston J, Treadwell J, Schoelles KM. Alcohol consumption and cancer risk: understanding possible causal mechanisms for breast and colorectal cancers. Evid Rep Technol Assess (Full Rep). 2010 Nov;(197):1–151.

46. Cantor KP, Stewart PA, Brinton LA, Dosemeci M. Occupational Exposures and Female Breast Cancer Mortality in the United States: Journal of Occupational and Environmental Medicine. 1995 Mar;37(3):336–48.

47. McElroy JA, Shafer MM, Trentham-Dietz A, Hampton JM, Newcomb PA. Cadmium Exposure and Breast Cancer Risk. JNCI: Journal of the National Cancer Institute. 2006 Jun 21;98(12):869–73.

48. Cohn BA, Terry MB, Plumb M, Cirillo PM. Exposure to polychlorinated biphenyl (PCB) congeners measured shortly after giving birth and subsequent risk of maternal breast cancer before age 50. Breast Cancer Res Treat. 2012 Nov;136(1):267–75.

49. Carmichael A, Sami AS, Dixon JM. Breast cancer risk among the survivors of atomic bomb and patients exposed to therapeutic ionising radiation. European Journal of Surgical Oncology (EJSO). 2003 Jun;29(5):475–9.

50. Medicine I of. Breast Cancer and the Environment: A Life Course Approach [Internet]. Washington, DC: The National Academies Press; 2012. Available from: https://nap.nationalacademies.org/catalog/13263/breast-cancer-and-the-environment-a-life-course-approach

51. Kalluri R, Neilson EG. Epithelial-mesenchymal transition and its implications for fibrosis. J Clin Invest. 2003 Dec 15;112(12):1776–84.

52. Hay ED. An overview of epithelio-mesenchymal transformation. Acta Anat (Basel). 1995;154(1):8–20.

53. Carmichael A, Sami AS, Dixon JM. Breast cancer risk among the survivors of atomic bomb and patients exposed to therapeutic ionising radiation. European Journal of Surgical Oncology (EJSO). 2003 Jun 1;29(5):475–9.

54. Kalluri R, Weinberg RA. The basics of epithelial-mesenchymal transition. J Clin Invest. 2009 Jun 1;119(6):1420–8.

55. Thiery JP. Epithelial–mesenchymal transitions in tumour progression. Nat Rev Cancer. 2002 Jun 1;2(6):442–54.

56. Yang J, Weinberg RA. Epithelial-Mesenchymal Transition: At the Crossroads of Development and Tumor Metastasis. Developmental Cell. 2008 Jun;14(6):818–29.

57. Shi Y, Massagué J. Mechanisms of TGF-beta signaling from cell membrane to the nucleus. Cell. 2003 Jun 13;113(6):685–700.

58. Medici D, Hay ED, Olsen BR. Snail and Slug Promote Epithelial-Mesenchymal Transition through □-Catenin–T-Cell Factor-4-dependent Expression of Transforming Growth Factor-□3. Molecular Biology of the Cell. 2008;19:13.

59. Kokudo T, Suzuki Y, Yoshimatsu Y, Yamazaki T, Watabe T, Miyazono K. Snail is required for TGFβ-induced endothelial-mesenchymal transition of embryonic stem cell-derived endothelial cells. Journal of Cell Science. 2008 Oct 15;121(20):3317–24.

60. Wang Y, Zhou BP. Epithelial-mesenchymal transition in breast cancer progression and metastasis. Chin J Cancer. 2011 Sep 5;30(9):603–11.

61. Fedele M, Cerchia L, Chiappetta G. The Epithelial-to-Mesenchymal Transition in Breast Cancer: Focus on Basal-Like Carcinomas. Cancers. 2017 Sep 30;9(12):134.

62. Prat A, Parker JS, Karginova O, Fan C, Livasy C, Herschkowitz JI, et al. Phenotypic and molecular characterization of the claudin-low intrinsic subtype of breast cancer. Breast Cancer Res. 2010 Oct;12(5):R68.

63. Kast K, Link T, Friedrich K, Petzold A, Niedostatek A, Schoffer O, et al. Impact of breast cancer subtypes and patterns of metastasis on outcome. Breast Cancer Res Treat. 2015 Apr;150(3):621–9.

64. Mani SA, Guo W, Liao MJ, Eaton ENg, Ayyanan A, Zhou AY, et al. The Epithelial-Mesenchymal Transition Generates Cells with Properties of Stem Cells. Cell. 2008 May;133(4):704–15.

65. Morel AP, Lièvre M, Thomas C, Hinkal G, Ansieau S, Puisieux A. Generation of Breast Cancer Stem Cells through Epithelial-Mesenchymal Transition. Klefstrom J, editor. PLoS ONE. 2008 Aug 6;3(8):e2888.

66. Pattabiraman DR, Bierie B, Kober KI, Thiru P, Krall JA, Zill C, et al. Activation of PKA leads to mesenchymal-to-epithelial transition and loss of tumor-initiating ability. Science. 2016 Mar 4;351(6277):aad3680.

67. Li H, Huang J, Yang B, Xiang T, Yin X, Peng W, et al. Mangiferin exerts antitumor activity in breast cancer cells by regulating matrix metalloproteinases, epithelial to mesenchymal transition, and β-catenin signaling pathway. Toxicology and Applied Pharmacology. 2013 Oct 1;272(1):180–90.

68. Camorani S, Crescenzi E, Gramanzini M, Fedele M, Zannetti A, Cerchia L. Aptamer-mediated impairment of EGFR-integrin αvβ3 complex inhibits vasculogenic mimicry and growth of triple-negative breast cancers. Sci Rep. 2017 May;7(1):46659.

69. Moore KM, Thomas GJ, Duffy SW, Warwick J, Gabe R, Chou P, et al. Therapeutic Targeting of Integrin αvβ6 in Breast Cancer. JNCI: Journal of the National Cancer Institute [Internet]. 2014 Aug [cited 2022 Oct 5];106(8). Available from: https://academic.oup.com/jnci/article-lookup/doi/10.1093/jnci/dju169

70. Gilboa-Geffen A, Hamar P, Le MTN, Wheeler LA, Trifonova R, Petrocca F, et al. Gene Knockdown by EpCAM Aptamer–siRNA Chimeras Suppresses Epithelial Breast Cancers and Their Tumor-Initiating Cells. Molecular Cancer Therapeutics. 2015 Oct 1;14(10):2279–91.

71. Wang N, Wei L, Huang Y, Wu Y, Su M, Pang X, et al. miR520c blocks EMT progression of human breast cancer cells by repressing STAT3. Oncology Reports. 2017 Mar;37(3):1537–44.

72. Knezevic J, Pfefferle AD, Petrovic I, Greene SB, Perou CM, Rosen JM. Expression of miR-200c in claudin-low breast cancer alters stem cell functionality, enhances chemosensitivity and reduces metastatic potential. Oncogene. 2015 Dec 3;34(49):5997–6006.

73. Ma L, Reinhardt F, Pan E, Soutschek J, Bhat B, Marcusson EG, et al. Therapeutic silencing of miR-10b inhibits metastasis in a mouse mammary tumor model. Nat Biotechnol. 2010 Apr;28(4):341–7.

74. Risau W. Mechanisms of angiogenesis. :4.

75. Papetti M, Herman IM. Mechanisms of normal and tumor-derived angiogenesis. American Journal of Physiology-Cell Physiology. 2002 May 1;282(5):C947–70.

76. Denekamp J. Endothelial cell proliferation as a novel approach to targeting tumour therapy. Br J Cancer. 1982 Jan;45(1):136–9.

77. Yoo SY, Kwon SM. Angiogenesis and Its Therapeutic Opportunities. Mediators of Inflammation. 2013;2013:1–11.

78. Moses MA. The Regulation of Neovascularization by Matrix Metalloproteinases and Their Inhibitors. STEM CELLS. 1997 May;15(3):180–9.

79. Carmeliet P, Jain RK. Angiogenesis in cancer and other diseases. Nature. 2000 Sep;407(6801):249–57.

80. Folkman J, Watson K, Ingber D, Hanahan D. Induction of angiogenesis during the transition from hyperplasia to neoplasia. Nature. 1989 May 1;339(6219):58–61.

81. Chang YS, di Tomaso E, McDonald DM, Jones R, Jain RK, Munn LL. Mosaic blood vessels in tumors: Frequency of cancer cells in contact with flowing blood. Proc Natl Acad Sci USA. 2000 Dec 19;97(26):14608–13.

82. Siemann DW. The unique characteristics of tumor vasculature and preclinical evidence for its selective disruption by Tumor-Vascular Disrupting Agents. Cancer Treatment Reviews. 2011 Feb;37(1):63–74.

83. Rafii S. Circulating endothelial precursors: mystery, reality, and promise. J Clin Invest. 2000 Jan 1;105(1):17–9.

84. Pepper MS, Ferrara N, Orci L, Montesano R. Potent synergism between vascular endothelial growth factor and basic fibroblast growth factor in the induction of

angiogenesis in vitro. Biochemical and Biophysical Research Communications. 1992 Dec;189(2):824–31.

85. Yoshiji H, Gomez DE, Shibuya M, Thorgeirsson UP. Expression of vascular endothelial growth factor, its receptor, and other angiogenic factors in human breast cancer. Cancer Res. 1996 May 1;56(9):2013–6.

86. Tomisawa M, Tokunaga T, Oshika Y, Tsuchida T, Fukushima Y, Sato H, et al. Expression pattern of vascular endothelial growth factor isoform is closely correlated with tumour stage and vascularisation in renal cell carcinoma. European Journal of Cancer. 1999 Jan;35(1):133–7.

87. Sowter HM, Corps AN, Evans AL, Clark DE, Charnock-Jones DS, Smith SK. Expression and localization of the vascular endothelial growth factor family in ovarian epithelial tumors. Lab Invest. 1997 Dec;77(6):607–14.

88. Volm M, Koomägi R, Mattern J. Prognostic value of vascular endothelial growth factor and its receptor Flt-1 in squamous cell lung cancer. Int J Cancer. 1997 Feb 20;74(1):64–8.

89. Ferrara N, Carver-Moore K, Chen H, Dowd M, Lu L, O'Shea KS, et al. Heterozygous embryonic lethality induced by targeted inactivation of the VEGF gene. Nature. 1996 Apr 1;380(6573):439–42.

90. Koch S, Tugues S, Li X, Gualandi L, Claesson-Welsh L. Signal transduction by vascular endothelial growth factor receptors. Biochemical Journal. 2011 Jul 15;437(2):169–83.

91. Ferrara N, Adamis AP. Ten years of anti-vascular endothelial growth factor therapy. Nat Rev Drug Discov. 2016 Jun;15(6):385–403.

92. Ferrara N, Henzel WJ. Pituitary follicular cells secrete a novel heparin-binding growth factor specific for vascular endothelial cells. Biochemical and Biophysical Research Communications. 1989 Jun 15;161(2):851–8.

93. Regenfuss B, Cursiefen C. Concept of Angiogenic Privilege. In: Dartt DA, editor. Encyclopedia of the Eye [Internet]. Oxford: Academic Press; 2010. p. 334–8. Available from: https://www.sciencedirect.com/science/article/pii/B9780123742032001214

94. Silvestre JS, Tamarat R, Ebrahimian TG, Le-Roux A, Clergue M, Emmanuel F, et al. Vascular Endothelial Growth Factor-B Promotes In Vivo Angiogenesis. Circulation Research. 2003 Jul 25;93(2):114–23.

95. Mould AW, Greco SA, Cahill MM, Tonks ID, Bellomo D, Patterson C, et al. Transgenic Overexpression of Vascular Endothelial Growth Factor-B Isoforms by Endothelial Cells Potentiates Postnatal Vessel Growth In Vivo and In Vitro. Circulation Research [Internet]. 2005 Sep 16 [cited 2022 Oct 5];97(6). Available from: https://www.ahajournals.org/doi/10.1161/01.RES.0000182631.33638.77

96. Malik AK, Baldwin ME, Peale F, Fuh G, Liang WC, Lowman H, et al. Redundant roles of VEGF-B and PlGF during selective VEGF-A blockade in mice. Blood. 2006 Jan 15;107(2):550–7.

97. Reichelt M, Shi S, Hayes M, Kay G, Batch J, Gole GA, et al. Vascular endothelial growth factor-B and retinal vascular development in the mouse. Clin Exp Ophthalmol. 2003 Feb;31(1):61–5.

98. Zhang F, Tang Z, Hou X, Lennartsson J, Li Y, Koch AW, et al. VEGF-B is dispensable for blood vessel growth but critical for their survival, and VEGF-B targeting inhibits pathological angiogenesis. Proc Natl Acad Sci USA. 2009 Apr 14;106(15):6152–7.

99. Aase K, von Euler G, Li X, Pontén A, Thorén P, Cao R, et al. Vascular Endothelial Growth Factor-B–Deficient Mice Display an Atrial Conduction Defect. Circulation. 2001 Jul 17;104(3):358–64.

100. Veikkola T, Jussila L, Makinen T, Karpanen T, Jeltsch M, Petrova TV, et al. Signalling via vascular endothelial growth factor receptor-3 is sufficient for lymphangiogenesis in transgenic mice. EMBO J. 2001 Mar 15;20(6):1223–31.

101. Joukov V, Sorsa T, Kumar V, Jeltsch M, Claesson-Welsh L, Cao Y, et al. Proteolytic processing regulates receptor specificity and activity of VEGF-C. EMBO J. 1997 Jul 1;16(13):3898–911.

102. Rissanen TT, Markkanen JE, Gruchala M, Heikura T, Puranen A, Kettunen MI, et al. VEGF-D Is the Strongest Angiogenic and Lymphangiogenic Effector Among VEGFs Delivered Into Skeletal Muscle via Adenoviruses. Circulation Research. 2003 May 30;92(10):1098–106.

103. Olofsson B, Korpelainen E, Pepper MS, Mandriota SJ, Aase K, Kumar V, et al. Vascular endothelial growth factor B (VEGF-B) binds to VEGF receptor-1 and regulates plasminogen activator activity in endothelial cells. Proc Natl Acad Sci USA. 1998 Sep 29;95(20):11709–14.

104. Park JE, Chen HH, Winer J, Houck KA, Ferrara N. Placenta growth factor. Potentiation of vascular endothelial growth factor bioactivity, in vitro and in vivo, and high affinity binding to Flt-1 but not to Flk-1/KDR. Journal of Biological Chemistry. 1994 Oct;269(41):25646–54.

105. Kimura H, Weisz A, Ogura T, Hitomi Y, Kurashima Y, Hashimoto K, et al. Identification of hypoxia-inducible factor 1 ancillary sequence and its function in vascular endothelial growth factor gene induction by hypoxia and nitric oxide. J Biol Chem. 2001 Jan 19;276(3):2292–8.

106. Cai J, Ahmad S, Jiang WG, Huang J, Kontos CD, Boulton M, et al. Activation of Vascular Endothelial Growth Factor Receptor-1 Sustains Angiogenesis and Bcl-2 Expression Via the Phosphatidylinositol 3-Kinase Pathway in Endothelial Cells. Diabetes. 2003 Dec 1;52(12):2959–68.

107. Abu-Ghazaleh R, Kabir J, Jia H, Lobo M, Zachary I. Src mediates stimulation by vascular endothelial growth factor of the phosphorylation of focal adhesion kinase at tyrosine 861, and migration and anti-apoptosis in endothelial cells. 2001;10.

108. Gerber HP, McMurtrey A, Kowalski J, Yan M, Keyt BA, Dixit V, et al. Vascular Endothelial Growth Factor Regulates Endothelial Cell Survival through the

Phosphatidylinositol 3′-Kinase/Akt Signal Transduction Pathway. Journal of Biological Chemistry. 1998 Nov;273(46):30336–43.

109. Takahashi T, Yamaguchi S, Chida K, Shibuya M. A single autophosphorylation site on KDR/Flk-1 is essential for VEGF-A-dependent activation of PLC-gamma and DNA synthesis in vascular endothelial cells. EMBO J. 2001 Jun 1;20(11):2768–78.

110. Takahashi T, Ueno H, Shibuya M. VEGF activates protein kinase C-dependent, but Ras-independent Raf-MEK-MAP kinase pathway for DNA synthesis in primary endothelial cells. Oncogene. 1999 Apr 1;18(13):2221–30.

111. Chen XL, Nam JO, Jean C, Lawson C, Walsh CT, Goka E, et al. VEGF-induced vascular permeability is mediated by FAK. Dev Cell. 2012 Jan 17;22(1):146–57.

112. McMullen ME, Bryant PW, Glembotski CC, Vincent PA, Pumiglia KM. Activation of p38 has opposing effects on the proliferation and migration of endothelial cells. J Biol Chem. 2005 Jun 3;280(22):20995–1003.

113. Karkkainen MJ, Ferrell RE, Lawrence EC, Kimak MA, Levinson KL, McTigue MA, et al. Missense mutations interfere with VEGFR-3 signalling in primary lymphoedema. Nat Genet. 2000 Jun;25(2):153–9.

114. Kubo H, Fujiwara T, Jussila L, Hashi H, Ogawa M, Shimizu K, et al. Involvement of vascular endothelial growth factor receptor-3 in maintenance of integrity of endothelial cell lining during tumor angiogenesis. Blood. 2000 Jul 15;96(2):546–53.

115. Salameh A, Galvagni F, Bardelli M, Bussolino F, Oliviero S. Direct recruitment of CRK and GRB2 to VEGFR-3 induces proliferation, migration, and survival of endothelial cells through the activation of ERK, AKT, and JNK pathways. Blood. 2005 Nov 15;106(10):3423–31.

116. Mäkinen T, Veikkola T, Mustjoki S, Karpanen T, Catimel B, Nice EC, et al. Isolated lymphatic endothelial cells transduce growth, survival and migratory signals via the VEGF-C/D receptor VEGFR-3. EMBO J. 2001 Sep 3;20(17):4762–73.

117. Gadaleta RM, Moschetta A. Metabolic Messengers: fibroblast growth factor 15/19. Nat Metab. 2019 Jun;1(6):588–94.

118. Farooq M, Khan AW, Kim MS, Choi S. The Role of Fibroblast Growth Factor (FGF) Signaling in Tissue Repair and Regeneration. Cells. 2021 Nov 19;10(11).

119. Kin M, Sata M, Ueno T, Torimura T, Inuzuka S, Tsuji R, et al. Basic fibroblast growth factor regulates proliferation and motility of human hepatoma cells by an autocrine mechanism. J Hepatol. 1997 Oct;27(4):677–87.

120. Cronauer MV, Hittmair A, Eder IE, Hobisch A, Culig Z, Ramoner R, et al. Basic fibroblast growth factor levels in cancer cells and in sera of patients suffering from proliferative disorders of the prostate. The Prostate. 1997 Jun 1;31(4):223–33.

121. Giri D, Ropiquet F, Ittmann M. Alterations in expression of basic fibroblast growth factor (FGF) 2 and its receptor FGFR-1 in human prostate cancer. Clin Cancer Res. 1999 May;5(5):1063–71.

122. Hase T, Kawashiri S, Tanaka A, Nozaki S, Noguchi N, Kato K, et al. Correlation of basic fibroblast growth factor expression with the invasion and the prognosis of oral squamous cell carcinoma. J Oral Pathol Med. 2006 Mar;35(3):136–9.

123. Ruotsalainen T, Joensuu H, Mattson K, Salven P. High pretreatment serum concentration of basic fibroblast growth factor is a predictor of poor prognosis in small cell lung cancer. Cancer Epidemiol Biomarkers Prev. 2002 Nov;11(11):1492–5.

124. Korc M, Friesel R. The Role of Fibroblast Growth Factors in Tumor Growth. CCDT. 2009 Aug 1;9(5):639–51.

125. Presta M, Dell'Era P, Mitola S, Moroni E, Ronca R, Rusnati M. Fibroblast growth factor/fibroblast growth factor receptor system in angiogenesis. Cytokine & Growth Factor Reviews. 2005 Apr;16(2):159–78.

126. Ribatti D, Presta M. The role of fibroblast growth factor-2 in the vascularization of the chick embryo chorioallantoic membrane. J Cell Mol Med. 2002;6(3):439–46.

127. Herbert JM, Laplace MC, Maffrand JP. Effect of heparin on the angiogenic potency of basic and acidic fibroblast growth factors in the rabbit cornea assay. Int J Tissue React. 1988;10(3):133–9.

128. Seghezzi G, Patel S, Ren CJ, Gualandris A, Pintucci G, Robbins ES, et al. Fibroblast Growth Factor-2 (FGF-2) Induces Vascular Endothelial Growth Factor (VEGF) Expression in the Endothelial Cells of Forming Capillaries: An Autocrine Mechanism Contributing to Angiogenesis. Journal of Cell Biology. 1998 Jun 29;141(7):1659–73.

129. Ortega S, Ittmann M, Tsang SH, Ehrlich M, Basilico C. Neuronal defects and delayed wound healing in mice lacking fibroblast growth factor 2. Proc Natl Acad Sci USA. 1998 May 12;95(10):5672–7.

130. Fulgham DL, Widhalm SR, Martin S, Coffin JD. FGF-2 dependent angiogenesis is a latent phenotype in basic fibroblast growth factor transgenic mice. Endothelium. 1999;6(3):185–95.

131. Brüstle O, Aguzzi A, Talarico D, Basilico C, Kleihues P, Wiestler OD. Angiogenic activity of the K-fgf/hst oncogene in neural transplants. Oncogene. 1992 Jun;7(6):1177–83.

132. Gillis P, Savla U, Volpert OV, Jimenez B, Waters CM, Panos RJ, et al. Keratinocyte growth factor induces angiogenesis and protects endothelial barrier function. J Cell Sci. 1999 Jun;112 (Pt 12):2049–57.

133. Mattila MM, Ruohola JK, Valve EM, Tasanen MJ, Seppänen JA, Härkönen PL. FGF-8b increases angiogenic capacity and tumor growth of androgen-regulated S115 breast cancer cells. Oncogene. 2001 May 17;20(22):2791–804.

134. Costa M, Danesi R, Agen C, Paolo AD, Basolo F, Bianchi SD, et al. MCF-10A Cells Infected with the int-20ncogene Induce Angiogenesis in the Chick Chorioallantoic Membrane and in the Rat Mesentery. :3.

135. Larsson H, Klint P, Landgren E, Claesson-Welsh L. Fibroblast growth factor receptor-1-mediated endothelial cell proliferation is dependent on the Src homology (SH) 2/SH3 domain-containing adaptor protein Crk. J Biol Chem. 1999 Sep 3;274(36):25726–34.

136. Cross MJ, Claesson-Welsh L. FGF and VEGF function in angiogenesis: signalling pathways, biological responses and therapeutic inhibition. Trends Pharmacol Sci. 2001 Apr;22(4):201–7.

137. Mignatti P, Rifkin DB. Nonenzymatic Interactions between Proteinases and the Cell Surface: Novel Roles in Normal and Malignant Cell Physiology. In: Advances in Cancer Research [Internet]. Elsevier; 1999 [cited 2022 Oct 5]. p. 103–57. Available from: https://linkinghub.elsevier.com/retrieve/pii/S0065230X08610246

138. Katoh M. Fibroblast growth factor receptors as treatment targets in clinical oncology. Nat Rev Clin Oncol. 2019 Feb;16(2):105–22.

139. Ornitz DM, Itoh N. Fibroblast growth factors. Genome Biol. 2001;2(3):reviews3005.1.

140. Powers CJ, McLeskey SW, Wellstein A. Fibroblast growth factors, their receptors and signaling. Endocrine-related cancer. 2000 Sep;165–97.

141. Tassi E, Al-Attar A, Aigner A, Swift MR, McDonnell K, Karavanov A, et al. Enhancement of Fibroblast Growth Factor (FGF) Activity by an FGF-binding Protein. Journal of Biological Chemistry. 2001 Oct;276(43):40247–53.

142. Ardizzone A, Scuderi SA, Giuffrida D, Colarossi C, Puglisi C, Campolo M, et al. Role of Fibroblast Growth Factors Receptors (FGFRs) in Brain Tumors, Focus on Astrocytoma and Glioblastoma. Cancers. 2020 Dec 18;12(12):3825.

143. Farooq M, Khan AW, Kim MS, Choi S. The Role of Fibroblast Growth Factor (FGF) Signaling in Tissue Repair and Regeneration. Cells. 2021 Nov 19;10(11):3242.

144. Chae YK, Ranganath K, Hammerman PS, Vaklavas C, Mohindra N, Kalyan A, et al. Inhibition of the fibroblast growth factor receptor (FGFR) pathway: the current landscape and barriers to clinical application. Oncotarget. 2017 Feb 28;8(9):16052–74.

145. Mohammadi M, Honegger AM, Rotin D, Fischer R, Bellot F, Li W, et al. A tyrosine-phosphorylated carboxy-terminal peptide of the fibroblast growth factor receptor (Flg) is a binding site for the SH2 domain of phospholipase C-gamma 1. Mol Cell Biol. 1991 Oct;11(10):5068–78.

146. Hart KC, Robertson SC, Donoghue DJ. Identification of Tyrosine Residues in Constitutively Activated Fibroblast Growth Factor Receptor 3 Involved in Mitogenesis, Stat Activation, and Phosphatidylinositol 3-Kinase Activation. Guidotti G, editor. MBoC. 2001 Apr;12(4):931–42.

147. Javerzat S, Auguste P, Bikfalvi A. The role of fibroblast growth factors in vascular development. Trends in Molecular Medicine. 2002 Oct;8(10):483–9.

148. Bastaki M, Nelli EE, Dell'Era P, Rusnati M, Molinari-Tosatti MP, Parolini S, et al. Basic Fibroblast Growth Factor–Induced Angiogenic Phenotype in Mouse Endothelium: A

Study of Aortic and Microvascular Endothelial Cell Lines. ATVB. 1997 Mar;17(3):454–64.

149. Matsumoto T, Turesson I, Book M, Gerwins P, Claesson-Welsh L. p38 MAP kinase negatively regulates endothelial cell survival, proliferation, and differentiation in FGF-2–stimulated angiogenesis. Journal of Cell Biology. 2002 Jan 7;156(1):149–60.

150. Klein S, Giancotti FG, Presta M, Albelda SM, Buck CA, Rifkin DB. Basic fibroblast growth factor modulates integrin expression in microvascular endothelial cells. MBoC. 1993 Oct;4(10):973–82.

151. Bavisotto LM, Schwartz SM, Heimark RL. Modulation of Ca2+-dependent intercellular adhesion in bovine aortic and human umbilical vein endothelial cells by heparin-binding growth factors. J Cell Physiol. 1990 Apr;143(1):39–51.

152. Presta M, Dell'Era P, Mitola S, Moroni E, Ronca R, Rusnati M. Fibroblast growth factor/fibroblast growth factor receptor system in angiogenesis. Cytokine & Growth Factor Reviews. 2005 Apr;16(2):159–78.

153. Holmgren L, O'Reilly MS, Folkman J. Dormancy of micrometastases: Balanced proliferation and apoptosis in the presence of angiogenesis suppression. Nat Med. 1995 Feb;1(2):149–53.

154. Parangi S, O'Reilly M, Christofori G, Holmgren L, Grosfeld J, Folkman J, et al. Antiangiogenic therapy of transgenic mice impairs de novo tumor growth. Proc Natl Acad Sci USA. 1996 Mar 5;93(5):2002–7.

155. Turner N, Grose R. Fibroblast growth factor signalling: from development to cancer. Nat Rev Cancer. 2010 Feb;10(2):116–29.

156. Ayoub NM, Jaradat SK, Al-Shami KM, Alkhalifa AE. Targeting Angiogenesis in Breast Cancer: Current Evidence and Future Perspectives of Novel Anti-Angiogenic Approaches. Front Pharmacol. 2022 Feb 25;13:838133.

157. Bergers G, Hanahan D. Modes of resistance to anti-angiogenic therapy. Nat Rev Cancer. 2008 Aug;8(8):592–603.

158. Hui Q, Jin Z, Li X, Liu C, Wang X. FGF Family: From Drug Development to Clinical Application. IJMS. 2018 Jun 26;19(7):1875.

159. Zhou Y, Wu C, Lu G, Hu Z, Chen Q, Du X. FGF/FGFR signaling pathway involved resistance in various cancer types. J Cancer. 2020;11(8):2000–7.

160. Kazazi-Hyseni F, Beijnen JH, Schellens JHM. Bevacizumab. The Oncologist. 2010 Aug 1;15(8):819–25.

161. Miller KD, Chap LI, Holmes FA, Cobleigh MA, Marcom PK, Fehrenbacher L, et al. Randomized Phase III Trial of Capecitabine Compared With Bevacizumab Plus Capecitabine in Patients With Previously Treated Metastatic Breast Cancer. JCO. 2005 Feb 1;23(4):792–9.

162. Mackey JR, Kerbel RS, Gelmon KA, McLeod DM, Chia SK, Rayson D, et al. Controlling angiogenesis in breast cancer: A systematic review of anti-angiogenic trials. Cancer Treatment Reviews. 2012 Oct;38(6):673–88.

163. Singh AD, Parmar S. Ramucirumab (Cyramza): A Breakthrough Treatment for Gastric Cancer. P T. 2015 Jul;40(7):430–68.

164. Casak SJ, Fashoyin-Aje I, Lemery SJ, Zhang L, Jin R, Li H, et al. FDA Approval Summary: Ramucirumab for Gastric Cancer. Clinical Cancer Research. 2015 Aug 1;21(15):3372–6.

165. Vahdat LT, Layman R, Yardley DA, Gradishar W, Salkeni MA, Joy AA, et al. Randomized Phase II Study of Ramucirumab or Icrucumab in Combination with Capecitabine in Patients with Previously Treated Locally Advanced or Metastatic Breast Cancer. The Oncologist. 2017 Mar 1;22(3):245–54.

166. Yardley DA, Reeves J, Dees EC, Osborne C, Paul D, Ademuyiwa F, et al. Ramucirumab With Eribulin Versus Eribulin in Locally Recurrent or Metastatic Breast Cancer Previously Treated With Anthracycline and Taxane Therapy: A Multicenter, Randomized, Phase II Study. Clinical Breast Cancer. 2016 Dec;16(6):471-479.e1.

167. Fakhrejahani E, Toi M. Antiangiogenesis Therapy for Breast Cancer: An Update and Perspectives from Clinical Trials. Japanese Journal of Clinical Oncology. 2014 Mar;44(3):197–207.

168. Schwartzberg LS, Tauer KW, Hermann RC, Makari-Judson G, Isaacs C, Beck JT, et al. Sorafenib or Placebo with Either Gemcitabine or Capecitabine in Patients with HER-2–Negative Advanced Breast Cancer That Progressed during or after Bevacizumab. Clinical Cancer Research. 2013 May 15;19(10):2745–54.

169. Kane RC, Farrell AT, Saber H, Tang S, Williams G, Jee JM, et al. Sorafenib for the Treatment of Advanced Renal Cell Carcinoma. Clinical Cancer Research. 2006 Dec 15;12(24):7271–8.

170. Pitoia F, Jerkovich F. Selective use of sorafenib in the treatment of thyroid cancer. DDDT. 2016 Mar;1119.

171. Le Tourneau C, Raymond E, Faivre S. Sunitinib: a novel tyrosine kinase inhibitor. A brief review of its therapeutic potential in the treatment of renal carcinoma and gastrointestinal stromal tumors (GIST). Therapeutics and Clinical Risk Management. 2007 Apr;3(2):341–8.

172. Blumenthal GM, Cortazar P, Zhang JJ, Tang S, Sridhara R, Murgo A, et al. FDA approval summary: sunitinib for the treatment of progressive well-differentiated locally advanced or metastatic pancreatic neuroendocrine tumors. Oncologist. 2012;17(8):1108–13.

173. Barrios CH, Liu MC, Lee SC, Vanlemmens L, Ferrero JM, Tabei T, et al. Phase III randomized trial of sunitinib versus capecitabine in patients with previously treated HER2-negative advanced breast cancer. Breast Cancer Res Treat. 2010 May;121(1):121–31.

174. Bergh J, Bondarenko IM, Lichinitser MR, Liljegren A, Greil R, Voytko NL, et al. First-Line Treatment of Advanced Breast Cancer With Sunitinib in Combination With Docetaxel Versus Docetaxel Alone: Results of a Prospective, Randomized Phase III Study. JCO. 2012 Mar 20;30(9):921–9.

175. Taylor SK, Chia S, Dent S, Clemons M, Agulnik M, Grenci P, et al. A phase II study of pazopanib in patients with recurrent or metastatic invasive breast carcinoma: a trial of the Princess Margaret Hospital phase II consortium. Oncologist. 2010;15(8):810–8.

176. Vafopoulou P, Kourti M. Anti-angiogenic drugs in cancer therapeutics: a review of the latest preclinical and clinical studies of anti-angiogenic agents with anticancer potential. J Cancer Metastasis Treat. 2022;8:18.

177. Parton M. Studies of apoptosis in breast cancer. BMJ. 2001 Jun 23;322(7301):1528–32.

178. Elmore S. Apoptosis: A Review of Programmed Cell Death. Toxicol Pathol. 2007 Jun;35(4):495–516.

179. Saraste A. Morphologic and biochemical hallmarks of apoptosis. Cardiovascular Research. 2000 Feb;45(3):528–37.

180. Schneider P, Tschopp J. Apoptosis induced by death receptors. Pharmaceutica Acta Helvetiae. 2000;74(2):281–6.

181. H A Hahm NED. Apoptosis in the mammary gland and breast cancer. Endocrine-related cancer. 1988;5(3):199–211.

182. Kadam CY, Abhang SA. Apoptosis Markers in Breast Cancer Therapy. In: Advances in Clinical Chemistry [Internet]. Elsevier; 2016 [cited 2023 Mar 11]. p. 143–93. Available from: https://linkinghub.elsevier.com/retrieve/pii/S0065242315300032

183. Pietsch EC, Sykes SM, McMahon SB, Murphy ME. The p53 family and programmed cell death. Oncogene. 2008 Oct 27;27(50):6507–21.

184. Kucharczak J, Simmons MJ, Fan Y, Gélinas C. To be, or not to be: NF-κB is the answer – role of Rel/NF-κB in the regulation of apoptosis. Oncogene. 2003 Dec 8;22(56):8961–82.

185. Hardwick JM, Soane L. Multiple Functions of BCL-2 Family Proteins. Cold Spring Harbor Perspectives in Biology. 2013 Feb 1;5(2):a008722–a008722.

186. Brunelle JK, Letai A. Control of mitochondrial apoptosis by the Bcl-2 family. Journal of Cell Science. 2009 Feb 15;122(4):437–41.

187. Ghobrial IM, Witzig TE, Adjei AA. Targeting Apoptosis Pathways in Cancer Therapy. CA: A Cancer Journal for Clinicians. 2005 May 1;55(3):178–94.

188. Gee JMW, Robertson JFR, Ellis IO, Willsher P, McClelland RA, Hoyle HB, et al. Immunocytochemical localization of BCL-2 protein in human breast cancers and its relationship to a series of prognostic markers and response to endocrine therapy. Int J Cancer. 1994 Dec 1;59(5):619–28.

189. Zhang GJ, Kimijima I, Abe R, Watanabe T, Kanno M, Hara K, et al. Apoptotic index correlates to bcl-2 and p53 protein expression, histological grade and prognosis in invasive breast cancers. Anticancer Res. 1998;18(3B):1989–98.

190. Haldar S, Negrini M, Monne M, Sabbioni S, Croce CM. Down-regulation of bcl-2 by p53 in breast cancer cells. Cancer Res. 1994 Apr 15;54(8):2095–7.

191. Linjawi A, Kontogiannea M, Halwani F, Edwardes M, Meterissian S. Prognostic significance of p53, bcl-2, and Bax expression in early breast cancer. Journal of the American College of Surgeons. 2004 Jan;198(1):83–90.

192. Ostrakhovitch EA, Cherian MG. Inhibition of extracellular signal regulated kinase (ERK) leads to apoptosis inducing factor (AIF) mediated apoptosis in epithelial breast cancer cells: The lack of effect of ERK in p53 mediated copper induced apoptosis. J Cell Biochem. 2005 Aug 15;95(6):1120–34.

193. Balmanno K, Cook SJ. Tumour cell survival signalling by the ERK1/2 pathway. Cell Death Differ. 2009 Mar;16(3):368–77.

194. Lu Z, Xu S. ERK1/2 MAP kinases in cell survival and apoptosis. IUBMB Life (International Union of Biochemistry and Molecular Biology: Life). 2006 Nov 1;58(11):621–31.

195. Ries S, Biederer C, Woods D, Shifman O, Shirasawa S, Sasazuki T, et al. Opposing Effects of Ras on p53. Cell. 2000 Oct;103(2):321–30.

196. Tamm I, Schriever F, Dörken B. Apoptosis: implications of basic research for clinical oncology. The Lancet Oncology. 2001 Jan;2(1):33–42.

197. Reed JC. Dysregulation of Apoptosis in Cancer. JCO. 1999 Sep;17(9):2941–2941.

198. Moela P, Motadi LR. Apoptotic Molecular Advances in Breast Cancer Management. In: Ntuli TM, editor. Cell Death - Autophagy, Apoptosis and Necrosis [Internet]. InTech; 2015 [cited 2023 Mar 11]. Available from: http://www.intechopen.com/books/cell-death-autophagy-apoptosis-and-necrosis/apoptotic-molecular-advances-in-breast-cancer-management

199. Majno G, Joris I. Apoptosis, oncosis, and necrosis. An overview of cell death. Am J Pathol. 1995 Jan;146(1):3–15.

200. Oltersdorf T, Elmore SW, Shoemaker AR, Armstrong RC, Augeri DJ, Belli BA, et al. An inhibitor of Bcl-2 family proteins induces regression of solid tumours. Nature. 2005 Jun;435(7042):677–81.

201. Raffo AJ, Perlman H, Chen MW, Day ML, Streitman JS, Buttyan R. Overexpression of bcl-2 protects prostate cancer cells from apoptosis in vitro and confers resistance to androgen depletion in vivo. Cancer Res. 1995 Oct 1;55(19):4438–45.

202. Wong RS. Apoptosis in cancer: from pathogenesis to treatment. J Exp Clin Cancer Res. 2011 Dec;30(1):87.

203. Lain S, Hollick JJ, Campbell J, Staples OD, Higgins M, Aoubala M, et al. Discovery, In Vivo Activity, and Mechanism of Action of a Small-Molecule p53 Activator. Cancer Cell. 2008 May;13(5):454–63.

204. Shangary S, Qin D, McEachern D, Liu M, Miller RS, Qiu S, et al. Temporal activation of p53 by a specific MDM2 inhibitor is selectively toxic to tumors and leads to complete tumor growth inhibition. Proc Natl Acad Sci USA. 2008 Mar 11;105(10):3933–8.

205. Shangary S, Wang S. Small-Molecule Inhibitors of the MDM2-p53 Protein-Protein Interaction to Reactivate p53 Function: A Novel Approach for Cancer Therapy. Annu Rev Pharmacol Toxicol. 2009 Feb 1;49(1):223–41.

206. Simons A, Melamed-Bessudo C, Wolkowicz R, Sperling J, Sperling R, Eisenbach L, et al. PACT: cloning and characterization of a cellular p53 binding protein that interacts with Rb. Oncogene. 1997 Jan 16;14(2):145–55.

207. van Deutekom J. Identification of the first gene (FRG1) from the FSHD region on human chromosome 4q35. Human Molecular Genetics. 1996 May 1;5(5):581–90.

208. Gabellini D, D'Antona G, Moggio M, Prelle A, Zecca C, Adami R, et al. Facioscapulohumeral muscular dystrophy in mice overexpressing FRG1. Nature. 2006 Feb;439(7079):973–7.

209. van Koningsbruggen S, Dirks RW, Mommaas AM, Onderwater JJ, Deidda G, Padberg GW, et al. FRG1P is localised in the nucleolus, Cajal bodies, and speckles. :8.

210. Adams JC. Roles of fascin in cell adhesion and motility. Current Opinion in Cell Biology. 2004 Oct;16(5):590–6.

211. Peraud A, Mondal S, Hawkins C, Mastronardi M, Bailey K, Rutka JT. Expression of fascin, an actin-bundling protein, in astrocytomas of varying grades. Brain Tumor Pathol. 2003 Sep;20(2):53–8.

212. Hansda AK, Tiwari A, Dixit M. Current status and future prospect of FSHD region gene 1. J Biosci. 2017 Jun;42(2):345–53.

213. Liu Q, Jones TI, Tang VW, Brieher WM, Jones PL. Facioscapulohumeral muscular dystrophy region gene-1 (FRG-1) is an actin-bundling protein associated with muscle-attachment sites. Journal of Cell Science. 2010 Apr 1;123(7):1116–23.

214. Grewal PK, Carim Todd L, van der Maarel S, Frants RR, Hewitt JE. FRG1, a gene in the FSH muscular dystrophy region on human chromosome 4q35, is highly conserved in vertebrates and invertebrates. Gene. 1998 Aug;216(1):13–9.

215. Hanel ML, Wuebbles RD, Jones PL. Muscular dystrophy candidate gene FRG1 is critical for muscle development. Dev Dyn. 2009 Jun;238(6):1502–12.

216. Rappsilber J, Ryder U, Lamond AI, Mann M. Large-scale proteomic analysis of the human spliceosome. Genome Res. 2002 Aug;12(8):1231–45.

217. van Koningsbruggen S, Straasheijm KR, Sterrenburg E, de Graaf N, Dauwerse HG, Frants RR, et al. FRG1P-mediated aggregation of proteins involved in pre-mRNA processing. Chromosoma. 2007 Feb;116(1):53–64.

218. van Koningsbruggen S, Dirks RW, Mommaas AM, Onderwater JJ, Deidda G, Padberg GW, et al. FRG1P is localised in the nucleolus, Cajal bodies, and speckles. J Med Genet. 2004 Apr;41(4):e46–e46.

219. Hasegawa K, Wada H, Nagata K, Fujiwara H, Wada N, Someya H, et al. Facioscapulohumeral muscular dystrophy (FSHD) region gene 1 (FRG1) expression and possible function in mouse tooth germ development. J Mol Hist. 2016 Aug;47(4):375–87.

220. Hanel ML, Wuebbles RD, Jones PL. Muscular dystrophy candidate gene FRG1 is critical for muscle development. Dev Dyn. 2009 Jun;238(6):1502–12.

221. Hanel ML, Wuebbles RD, Jones PL. Muscular dystrophy candidate gene FRG1 is critical for muscle development. Dev Dyn. 2009 Jun;238(6):1502–12.

222. Chen SC, Frett E, Marx J, Bosnakovski D, Reed X, Kyba M, et al. Decreased Proliferation Kinetics of Mouse Myoblasts Overexpressing FRG1. Feany MB, editor. PLoS ONE. 2011 May 16;6(5):e19780.

223. Helin K, Harlow E, Fattaey A. Inhibition of E2F-1 transactivation by direct binding of the retinoblastoma protein. Mol Cell Biol. 1993 Oct;13(10):6501–8.

224. Padberg GW, Brouwer OF, de Keizer RJ, Dijkman G, Wijmenga C, Grote JJ, et al. On the significance of retinal vascular disease and hearing loss in facioscapulohumeral muscular dystrophy. Muscle Nerve Suppl. 1995;(2):S73-80.

225. Osborne RJ, Welle S, Venance SL, Thornton CA, Tawil R. Expression profile of FSHD supports a link between retinal vasculopathy and muscular dystrophy. Neurology. 2007 Feb 20;68(8):569–77.

226. Dmitriev P, Kairov U, Robert T, Barat A, Lazar V, Carnac G, et al. Cancer-related genes in the transcription signature of facioscapulohumeral dystrophy myoblasts and myotubes. J Cell Mol Med. 2014 Feb;18(2):208–17.

227. Kawamura-Saito M, Yamazaki Y, Kaneko K, Kawaguchi N, Kanda H, Mukai H, et al. Fusion between CIC and DUX4 up-regulates PEA3 family genes in Ewing-like sarcomas with t(4;19)(q35;q13) translocation. Hum Mol Genet. 2006 Jul 1;15(13):2125–37.

228. Lemmers RJLF, van der Vliet PJ, Klooster R, Sacconi S, Camaño P, Dauwerse JG, et al. A unifying genetic model for facioscapulohumeral muscular dystrophy. Science. 2010 Sep 24;329(5999):1650–3.

229. Patsialou A, Wang Y, Lin J, Whitney K, Goswami S, Kenny PA, et al. Selective gene-expression profiling of migratory tumor cells in vivo predicts clinical outcome in breast cancer patients. Breast Cancer Res. 2012 Oct;14(5):R139.

230. Liu M, Zhou X, Liu J, Lu C, Zhang G, Zhang J, et al. Predictive Biomarkers of Dicycloplatin Resistance or Susceptibility in Prostate Cancer. Front Genet. 2021 Jul 27;12:669605.

231. Xu Y, Mu T. A cohort study on the molecular mechanism of distinct therapeutic effects and prognosis in Chinese colorectal cancer patients who underwent neoadjuvant or surgical therapies. JCO. 2021 May 20;39(15_suppl):e15544–e15544.

232. Green MR, Sambrook J. The Inoue Method for Preparation and Transformation of Competent *Escherichia coli* : "Ultracompetent" Cells. Cold Spring Harb Protoc. 2020 Jun;2020(6):pdb.prot101196.

233. Froger A, Hall JE. Transformation of Plasmid DNA into E. coli Using the Heat Shock Method. JoVE. 2007 Aug 1;(6):253.

234. De Luca A, Maiello MR, D'Alessio A, Pergameno M, Normanno N. The RAS/RAF/MEK/ERK and the PI3K/AKT signalling pathways: role in cancer pathogenesis and implications for therapeutic approaches. Expert Opinion on Therapeutic Targets. 2012 Apr;16(sup2):S17–27.

235. Ostrakhovitch EA, Cherian MG. Inhibition of extracellular signal regulated kinase (ERK) leads to apoptosis inducing factor (AIF) mediated apoptosis in epithelial breast cancer cells: The lack of effect of ERK in p53 mediated copper induced apoptosis. J Cell Biochem. 2005 Aug 15;95(6):1120–34.

236. Chan CH, Jo U, Kohrman A, Rezaeian AH, Chou PC, Logothetis C, et al. Posttranslational regulation of Akt in human cancer. Cell Biosci. 2014 Dec;4(1):59.

237. Turke AB, Song Y, Costa C, Cook R, Arteaga CL, Asara JM, et al. MEK Inhibition Leads to PI3K/AKT Activation by Relieving a Negative Feedback on ERBB Receptors. Cancer Res. 2012 Jul 1;72(13):3228–37.

238. Hanahan D, Weinberg RA. Hallmarks of Cancer: The Next Generation. Cell. 2011 Mar;144(5):646–74.

239. Pfeffer C, Singh A. Apoptosis: A Target for Anticancer Therapy. IJMS. 2018 Feb 2;19(2):448.

240. Ries S, Biederer C, Woods D, Shifman O, Shirasawa S, Sasazuki T, et al. Opposing Effects of Ras on p53: Transcriptional Activation of mdm2 and Induction of p19ARF. :10.

241. Heerboth S, Housman G, Leary M, Longacre M, Byler S, Lapinska K, et al. EMT and tumor metastasis. Clinical and Translational Medicine [Internet]. 2015 Dec [cited 2022 Jan 12];4(1). Available from: https://onlinelibrary.wiley.com/doi/abs/10.1186/s40169-015-0048-3

242. Smith BN, Burton LJ, Henderson V, Randle DD, Morton DJ, Smith BA, et al. Snail Promotes Epithelial Mesenchymal Transition in Breast Cancer Cells in Part via Activation of Nuclear ERK2. Anto RJ, editor. PLoS ONE. 2014 Aug 14;9(8):e104987.

243. Chen H, Zhu G, Li Y, Padia RN, Dong Z, Pan ZK, et al. Extracellular Signal–Regulated Kinase Signaling Pathway Regulates Breast Cancer Cell Migration by Maintaining slug Expression. Cancer Res. 2009 Dec 15;69(24):9228–35.

244. Weiss MB, Abel EV, Mayberry MM, Basile KJ, Berger AC, Aplin AE. TWIST1 Is an ERK1/2 Effector That Promotes Invasion and Regulates MMP-1 Expression in Human Melanoma Cells. Cancer Res. 2012 Dec 15;72(24):6382–92.

245. Dranoff G. Cytokines in cancer pathogenesis and cancer therapy. Nat Rev Cancer. 2004 Jan;4(1):11–22.

246. Russo RC, Garcia CC, Teixeira MM, Amaral FA. The CXCL8/IL-8 chemokine family and its receptors in inflammatory diseases. Expert Review of Clinical Immunology. 2014 May;10(5):593–619.

247. Hassan MdK, Kumar D, Patel SA, Dixit M. EEF1A2 triggers stronger ERK mediated metastatic program in ER negative breast cancer cells than in ER positive cells. Life Sciences. 2020 Dec;262:118553.

248. Chen Y. An epithelial-to-mesenchymal transition-inducing potential of granulocyte macrophage colony-stimulating factor in colon cancer. Scientific Reports. :12.

249. Palo A, Patel SA, Sahoo B, Chowdary TK, Dixit M. FRG1 is a direct transcriptional regulator of nonsense-mediated mRNA decay genes. Genomics. 2023 Jan;115(1):110539.

250. Xue M, Zhang K, Mu K, Xu J, Yang H, Liu Y, et al. Regulation of estrogen signaling and breast cancer proliferation by an ubiquitin ligase TRIM56. Oncogenesis. 2019 Apr 18;8(5):30.

251. Forouzanfar MH, Foreman KJ, Delossantos AM, Lozano R, Lopez AD, Murray CJL, et al. Breast and cervical cancer in 187 countries between 1980 and 2010: a systematic analysis. The Lancet. 2011 Oct;378(9801):1461–84.

252. Saha Roy S, Vadlamudi RK. Role of Estrogen Receptor Signaling in Breast Cancer Metastasis. International Journal of Breast Cancer. 2012;2012:1–8.

253. Bratton MR, Antoon JW, Duong BN, Frigo DE, Tilghman S, Collins-Burow BM, et al. Gαo potentiates estrogen receptor α activity via the ERK signaling pathway. Journal of Endocrinology. 2012 Jul;214(1):45–54.

254. Kim SC, Boese AC, Moore MH, Cleland RM, Chang L, Delafontaine P, et al. Rapid estrogen receptor-α signaling mediated by ERK activation regulates vascular tone in male and ovary-intact female mice. American Journal of Physiology-Heart and Circulatory Physiology. 2018 Feb 1;314(2):H330–42.

255. Smith BN, Burton LJ, Henderson V, Randle DD, Morton DJ, Smith BA, et al. Snail Promotes Epithelial Mesenchymal Transition in Breast Cancer Cells in Part via Activation of Nuclear ERK2. Anto RJ, editor. PLoS ONE. 2014 Aug 14;9(8):e104987.

256. Norton KA, Popel AS. Effects of endothelial cell proliferation and migration rates in a computational model of sprouting angiogenesis. Sci Rep. 2016 Nov 14;6(1):36992.

257. Senger DR, Davis GE. Angiogenesis. Cold Spring Harbor Perspectives in Biology. 2011 Aug 1;3(8):a005090–a005090.

258. Passaniti A, Taylor RM, Pili R, Guo Y, Long PV, Haney JA, et al. A simple, quantitative method for assessing angiogenesis and antiangiogenic agents using reconstituted basement membrane, heparin, and fibroblast growth factor. Lab Invest. 1992 Oct;67(4):519–28.

259. Nowak-Sliwinska P, Alitalo K, Allen E, Anisimov A, Aplin AC, Auerbach R, et al. Consensus guidelines for the use and interpretation of angiogenesis assays. Angiogenesis. 2018 Aug;21(3):425–532.

260. Martin P. Wound Healing--Aiming for Perfect Skin Regeneration. Science. 1997 Apr 4;276(5309):75–81.

261. Witte MB, Barbul A. GENERAL PRINCIPLES OF WOUND HEALING. Surgical Clinics of North America. 1997 Jun;77(3):509–28.

262. Greaves NS, Ashcroft KJ, Baguneid M, Bayat A. Current understanding of molecular and cellular mechanisms in fibroplasia and angiogenesis during acute wound healing. Journal of Dermatological Science. 2013 Dec;72(3):206–17.

263. Abraham JA, Klagsbrun M. Modulation of Wound Repair by Members of the Fibroblast Growth Factor Family. In: Clark RAF, editor. The Molecular and Cellular Biology of Wound Repair [Internet]. Boston, MA: Springer US; 1988 [cited 2023 Mar 26]. p. 195–248. Available from: http://link.springer.com/10.1007/978-1-4899-0185-9_6

264. Eckes B, Aumailley M, Krieg T. Collagens and the Reestablishment of Dermal Integrity. In: Clark RAF, editor. The Molecular and Cellular Biology of Wound Repair [Internet]. Boston, MA: Springer US; 1988 [cited 2023 Mar 26]. p. 493–512. Available from: http://link.springer.com/10.1007/978-1-4899-0185-9_16

265. Chen PY, Simons M, Friesel R. FRS2 via Fibroblast Growth Factor Receptor 1 Is Required for Platelet-derived Growth Factor Receptor β-mediated Regulation of Vascular Smooth Muscle Marker Gene Expression. Journal of Biological Chemistry. 2009 Jun;284(23):15980–92.

266. Akl MR, Nagpal P, Ayoub NM, Tai B, Prabhu SA, Capac CM, et al. Molecular and clinical significance of fibroblast growth factor 2 (FGF2 /bFGF) in malignancies of solid and hematological cancers for personalized therapies. Oncotarget. 2016 Jul 12;7(28):44735–62.

267. Maehara O, Suda G, Natsuizaka M, Ohnishi S, Komatsu Y, Sato F, et al. Fibroblast growth factor-2–mediated FGFR/Erk signaling supports maintenance of cancer stem-like cells in esophageal squamous cell carcinoma. Carcinogenesis. 2017 Oct 26;38(11):1073–83.

268. Itoh N, Ornitz DM. Fibroblast growth factors: from molecular evolution to roles in development, metabolism and disease. Journal of Biochemistry. 2011 Feb 1;149(2):121–30.

269. Ma Y, Kakudo N, Morimoto N, Lai F, Taketani S, Kusumoto K. Fibroblast growth factor-2 stimulates proliferation of human adipose-derived stem cells via Src activation. Stem Cell Res Ther. 2019 Nov 27;10(1):350.

270. Seyfried TN, Huysentruyt LC. On the Origin of Cancer Metastasis. Crit Rev Oncog . 2013;18:43–73.

271. McCubrey JA, Steelman LS, Chappell WH, Abrams SL, Wong EWT, Chang F, et al. Roles of the Raf/MEK/ERK pathway in cell growth, malignant transformation and drug resistance. Biochimica et Biophysica Acta (BBA) - Molecular Cell Research. 2007 Aug;1773(8):1263–84.

272. Shin S, Buel GR, Nagiec MJ, Han MJ, Roux PP, Blenis J, et al. ERK2 regulates epithelial-to-mesenchymal plasticity through DOCK10-dependent Rac1/FoxO1 activation. Proc Natl Acad Sci USA. 2019 Feb 19;116(8):2967–76.

273. Mirzoeva OK, Das D, Heiser LM, Bhattacharya S, Siwak D, Gendelman R, et al. Basal Subtype and MAPK/ERK Kinase (MEK)-Phosphoinositide 3-Kinase Feedback Signaling Determine Susceptibility of Breast Cancer Cells to MEK Inhibition. Cancer Res. 2009 Jan 15;69(2):565–72.

274. Hayashi H, Tsuchiya Y, Nakayama K, Satoh T, Nishida E. Down-regulation of the PI3-kinase/Akt pathway by ERK MAP kinase in growth factor signaling. Genes to Cells. 2008 Sep;13(9):941–7.

275. Yu CF, Liu ZX, Cantley LG. ERK Negatively Regulates the Epidermal Growth Factor-mediated Interaction of Gab1 and the Phosphatidylinositol 3-Kinase. Journal of Biological Chemistry. 2002 May;277(22):19382–8.

276. Turke AB, Song Y, Costa C, Cook R, Arteaga CL, Asara JM, et al. MEK Inhibition Leads to PI3K/AKT Activation by Relieving a Negative Feedback on ERBB Receptors. Cancer Res. 2012 Jul 1;72(13):3228–37.

277. Berra E, Diaz-Meco MT, Moscat J. The Activation of p38 and Apoptosis by the Inhibition of Erk Is Antagonized by the Phosphoinositide 3-Kinase/Akt Pathway. Journal of Biological Chemistry. 1998 Apr;273(17):10792–7.

278. Gan Y, Shi C, Inge L, Hibner M, Balducci J, Huang Y. Differential roles of ERK and Akt pathways in regulation of EGFR-mediated signaling and motility in prostate cancer cells. Oncogene. 2010 Sep;29(35):4947–58.

279. Cagnol S, Chambard JC. ERK and cell death: Mechanisms of ERK-induced cell death - apoptosis, autophagy and senescence: ERK and cell death. FEBS Journal. 2010 Jan;277(1):2–21.

280. Su X, Xu Y, Fox GC, Xiang J, Kwakwa KA, Davis JL, et al. Breast cancer–derived GM-CSF regulates arginase 1 in myeloid cells to promote an immunosuppressive microenvironment. Journal of Clinical Investigation. 2021 Oct 15;131(20):e145296.

281. Mueller MM, Fusenig NE. Constitutive expression of G-CSF and GM-CSF in human skin carcinoma cells with functional consequence for tumor progression. Int J Cancer. 1999 Dec 10;83(6):780–9.

282. Obermueller E, Vosseler S, Fusenig NE, Mueller MM. Cooperative Autocrine and Paracrine Functions of Granulocyte Colony-Stimulating Factor and Granulocyte-Macrophage Colony-Stimulating Factor in the Progression of Skin Carcinoma Cells. Cancer Res. 2004 Nov 1;64(21):7801–12.

283. Gutschalk CM, Herold-Mende CC, Fusenig NE, Mueller MM. Granulocyte Colony-Stimulating Factor and Granulocyte-Macrophage Colony-Stimulating Factor Promote Malignant Growth of Cells from Head and Neck Squamous Cell Carcinomas *In vivo*. Cancer Res. 2006 Aug 15;66(16):8026–36.

284. Mueller MM, Herold-Mende CC, Riede D, Lange M, Steiner HH, Fusenig NE. Autocrine Growth Regulation by Granulocyte Colony-Stimulating Factor and Granulocyte Macrophage Colony-Stimulating Factor in Human Gliomas with Tumor Progression. The American Journal of Pathology. 1999 Nov;155(5):1557–67.

285. Thacker JD, Dedhar S, Hogge DE. The effect of GM-CSF and G-CSF on the growth of human osteosarcoma cellsin vitro andin vivo. Int J Cancer. 1994 Jan 15;56(2):236–43.

286. Ansari KI, Bhan A, Saotome M, Tyagi A, De Kumar B, Chen C, et al. Autocrine GMCSF Signaling Contributes to Growth of HER2+ Breast Leptomeningeal Carcinomatosis. Cancer Research. 2021 Sep 16;81(18):4723–35.

287. Waghray M, Yalamanchili M, Dziubinski M, Zeinali M, Erkkinen M, Yang H, et al. GM-CSF Mediates Mesenchymal–Epithelial Cross-talk in Pancreatic Cancer. Cancer Discovery. 2016 Aug 1;6(8):886–99.

288. Szomolay B, Eubank TD, Roberts RD, Marsh CB, Friedman A. Modeling the inhibition of breast cancer growth by GM-CSF. Journal of Theoretical Biology. 2012 Jun;303:141–51.

289. Tiwari A, Clifton G, Calfa C, Alatrash G, Holmes J, Bedrosian I, et al. Abstract P4-07-23: Results of a Phase 2 Trial of Combination Immunotherapy with Concurrent Nelipepimut-S + GM-CSF and Trastuzumab in High-risk HER2+ Breast Cancer Patients. Cancer Research. 2023 Mar 1;83(5_Supplement):P4-07-23-P4-07–23.

290. Turner N, Grose R. Fibroblast growth factor signalling: from development to cancer. Nat Rev Cancer. 2010 Feb;10(2):116–29.

291. Lewis CE, Leek R, Harris A, McGee JO. Cytokine regulation of angiogenesis in breast cancer: the role of tumor-associated macrophages. J Leukoc Biol. 1995 May;57(5):747–51.

292. Zheng Q, Li X, Cheng X, Cui T, Zhuo Y, Ma W, et al. Granulocyte-macrophage colony-stimulating factor increases tumor growth and angiogenesis directly by promoting endothelial cell function and indirectly by enhancing the mobilization and recruitment of proangiogenic granulocytes. Tumour Biol. 2017 Feb;39(2):101042831769223.

293. Bergers G, Hanahan D. Modes of resistance to anti-angiogenic therapy. Nat Rev Cancer. 2008 Aug;8(8):592–603.

294. Szymczyk J, Sluzalska KD, Materla I, Opalinski L, Otlewski J, Zakrzewska M. FGF/FGFR-Dependent Molecular Mechanisms Underlying Anti-Cancer Drug Resistance. Cancers. 2021 Nov 18;13(22):5796.

295. Winter SF, Acevedo VD, Gangula RD, Freeman KW, Spencer DM, Greenberg NM. Conditional activation of FGFR1 in the prostate epithelium induces angiogenesis with concomitant differential regulation of Ang-1 and Ang-2. Oncogene. 2007 Jul 26;26(34):4897–907.

296. Casanovas O, Hicklin DJ, Bergers G, Hanahan D. Drug resistance by evasion of antiangiogenic targeting of VEGF signaling in late-stage pancreatic islet tumors. Cancer Cell. 2005 Oct;8(4):299–309.

297. Hui Q, Jin Z, Li X, Liu C, Wang X. FGF Family: From Drug Development to Clinical Application. IJMS. 2018 Jun 26;19(7):1875.

298. Zhou Y, Wu C, Lu G, Hu Z, Chen Q, Du X. FGF/FGFR signaling pathway involved resistance in various cancer types. J Cancer. 2020;11(8):2000–7.

299. Fitzsimons RB, Gurwin EB, Bird AC. RETINAL VASCULAR ABNORMALITIES IN FACIOSCAPULOHUMERAL MUSCULAR DYSTROPHY: A GENERAL ASSOCIATION WITH GENETIC AND THERAPEUTIC IMPLICATIONS. Brain. 1987;110(3):631–48.

300. Jia T, Jacquet T, Dalonneau F, Coudert P, Vaganay E, Exbrayat-Héritier C, et al. FGF-2 promotes angiogenesis through a SRSF1/SRSF3/SRPK1-dependent axis that controls VEGFR1 splicing in endothelial cells. BMC Biol. 2021 Dec;19(1):173.

301. Shin M, Beane T, Quillien A, Male I, Zhu LJ, Lawson ND. Vegfa signals through ERK to promote angiogenesis, but not artery differentiation. Development. 2016 Jan 1;dev.137919.

302. Gerber HP, McMurtrey A, Kowalski J, Yan M, Keyt BA, Dixit V, et al. Vascular Endothelial Growth Factor Regulates Endothelial Cell Survival through the Phosphatidylinositol 3′-Kinase/Akt Signal Transduction Pathway. Journal of Biological Chemistry. 1998 Nov;273(46):30336–43.

303. Morales-Ruiz M, Fulton D, Sowa G, Languino LR, Fujio Y, Walsh K, et al. Vascular Endothelial Growth Factor–Stimulated Actin Reorganization and Migration of Endothelial Cells Is Regulated via the Serine/Threonine Kinase Akt. Circulation Research. 2000 Apr 28;86(8):892–6.

304. Ibrahimi OA, Zhang F, Lang Hrstka SC, Mohammadi M, Linhardt RJ. Kinetic Model for FGF, FGFR, and Proteoglycan Signal Transduction Complex Assembly. Biochemistry. 2004 Apr 1;43(16):4724–30.

305. Ansari MJ, Bokov D, Markov A, Jalil AT, Shalaby MN, Suksatan W, et al. Cancer combination therapies by angiogenesis inhibitors; a comprehensive review. Cell Commun Signal. 2022 Dec;20(1):49.

Appendices

Appendix I: List of the antibodies used

Sr. No.	Antibody	Brand	Catalog No.	Dilution	Source
1.	Recombinant Anti-FRG1 (EPR13098)	Abcam, MA, USA	ab181083	1:10,000	Rabbit
2.	Phospho-p44/42 MAPK (Erk1/2) (Thr202/Tyr204) (D13.14.4E) XP®	CST, MA, USA	4370S	1:1000	Rabbit
3.	p44/42 MAPK (Erk1/2)	CST, MA, USA	9102S	1:1000	Rabbit
4.	Phospho-MEK1/2 (Ser217/221) (41G9)	CST, MA, USA	9154S	1:1000	Rabbit
5.	MEK1/2	CST, MA, USA	9122S	1:1000	Rabbit
6.	Snail (C15D3)	CST, MA, USA	3879S	1:1000	Rabbit
7.	Slug (C19G7)	CST, MA, USA	9585S	1:1000	Rabbit
8.	Anti-Twist1	CST, MA, USA	46702S	1:1000	Rabbit
9.	Phospho-Akt (Thr308) (D25E6) XP®	CST, MA, USA	13038S	1:1000	Rabbit
10.	Phospho-Akt (Ser473) (D9E) XP®	CST, MA, USA	4060S	1:1000	Rabbit
11.	Akt (pan) (C67E7)	CST, MA, USA	4691S	1:1000	Rabbit
12.	Phospho-p53 (Ser46) Antibody	CST, MA, USA	2521S	1:1000	Rabbit
13.	Phospho-Estrogen Receptor α (Ser118)	CST, MA, USA	2511S	1:1000	Mouse
14.	Phospho-p38 MAPK (Thr180/Tyr182)	CST, MA, USA	9211S	1:1000	Rabbit
15.	GAPDH (Clone: ABM22C5)	Abgenex, India	1-10011	1:10000	Mouse
16.	Anti-Rabbit IgG (whole molecule)–Peroxidase antibody produced in goat	Sigma-Aldrich, MO, USA	A9169	1:50,000	Goat
17.	Rabbit anti-Mouse IgG (H+L) Cross-Adsorbed Secondary Antibody, HRP	Invitrogen, USA	31452	1:10,000	Rabbit

Appendix II: List of the primers used for q-RT PCR

Sr. No.	Primer Name	Primer Sequence (5'-3')
1.	FRG1 F	TGATATTGTTGGAATCTGGTGGACA
2.	FRG1 R	CCATTGTCGAGTGCATGTATATAGG
3.	GAPDH F	ACCCAGAAGACTGTGGATGG
4	GAPDH R	TCTAGACGGCAGGTCAGGTC
5.	CSF2 F	GCCCTGGGAGCATGTGAATG
6.	CSF2 R	CTGTTTCATTCATCTCAGCAGCA
7.	PDGFα F	GCCAACCAGATGTGAGGTGA
8.	PDGFα R	GGAGGAGAACAAAGACCGCA
9.	PDGFβ F	ACCTGCGTCTGGTCAGC
10.	PDGFβ R	ATCTTCCTCTCCGGGGTCTC
11.	CXCL1 F	AACCGAAGTCATAGCCACAC
12.	CXCL1 R	GTTGGATTTGTCACTGTTCAGC
13.	CXCL8 F	ACCGGAAGGAACCATCTCAC
14.	CXCL8 R	GGCAAAACTGCACCTTCACAC
15.	CSF2 (ChIP)F	GAGGGGCACAGTTTGGACTT
16.	CSF2 (ChIP)R	CAAAGGCCCCTGGGATTACA
17.	VEGFA F	AGGAGGAGGGCAGAATCATCA
18.	VEGFA R	CTCGATTGGATGGCAGTAGCT
19.	VEGFB F	GATCCGGTACCCGAGCAGTCAG
20.	VEGFB R	CACCTGCAGGTGTCTGGGTTGA
21.	VEGFD F	ATCTGTATGAACACCAGCACCTC
22.	VEGFD R	TGGCAACTTTAACAGGCACTAAT
23.	FGF2 F	GCTGTACTGCAAAAACGGGG
24.	FGF2 R	TAGCTTGATGTGAGGGTCGC

Appendix III: List of the probes used for EMSA

Sr. No.	Name of the probe	Sequence (5'-3')
1.	CSF2 Biotinylated Labelled	CCAAAGGCCCCTGGGATTACAGGCA
2.	CSF2 Biotinylated Labelled Complementary	TGCCTGTAATCCCAGGGGCCTTTGG
3.	CSF2 Unlabelled	CCAAAGGCCCCTGGGATTACAGGCA
4.	CSF2 Unlabelled Complementary	TGCCTGTAATCCCAGGGGCCTTTGG
5.	CSF2 Mutated Unlabelled	CCAAAGGCCCCACGGATTACAGGCA
6.	CSF2 Mutated Unlabelled Complementary	TGCCTGTAATCCGTGGGGCCTTTGG

Appendix IV: Assay Procedures

IV.1. Extraction of RNA from the cell lines using the RNeasy Mini Kit

1. Cells were grown in a 60 mm dish to harvest the RNA.
2. Cells were washed with 1 ml of DPBS
3. 10 µL of β-mercaptoethanol was added to 1 ml of lysis buffer RLT. 350 µL of this lysis buffer was directly added to the cells and evenly distributed with a scraper.
4. 350 µL of 70% ethanol was added to the cells, and a homogenized mixture was made.
5. 700 µL of the cell suspension was transferred to an RNeasy Mini spin column and placed in a 2 ml collection tube.
6. The column was centrifuged at 10000 RCF for 30 seconds, and the flow through was discarded.
7. Next, 700 µL of buffer RW1 was added to the RNeasy Mini spin column, followed by 30 seconds of centrifugation at 10,000 RCF. The flow-through was discarded.
8. 500 µL of wash buffer RPE was added to the column and centrifuged for 2 minutes at 10,000 RCF. This step was performed twice, followed by an empty centrifugation of the column at the same speed and time to dry the membrane completely.
9. The RNeasy Mini spin column was placed in a new 1.5 ml nuclease-free centrifuge tube. 30 µL of RNase-free water was added to the spin column and incubated at room temperature for 3 minutes.
10. In the last step, the column was centrifuged at 10,000 RCF for 2 minutes to elute the RNA into the centrifuge tube.

IV.2. Extraction of plasmid using the QIAprep Spin Miniprep Kit

1. The bacterial culture was grown overnight, and the cells were harvested by centrifuging at 15000 RCF for 15 minutes at 4ºC.
2. The bacterial cell pellet was resuspended into 250 µL buffer P1 and transferred to a 1.5 ml centrifuge tube. The sample was gently mixed by pipetting.
3. 250 µL of buffer P2 was added to the mixture and evenly homogenized by inverting the centrifuge tube 4-6 times. Because of the presence of lyse blue in the buffer P1, the solution turned blue after adding the P2. Harsh mixing should be avoided to eliminate the chance of DNA shearing.
4. The transparent and viscous appearance of the sample indicated complete cell lysis.
5. 350 µL of neutralizing buffer N3 was immediately added to the sample and thoroughly mixed by inverting the tube 4 - 6 times.
6. The tube was centrifuged at 13,000 RPM (17,900 RCF) for 10 minutes.
7. 800 µL of the supernatant was gently taken in a QIAprep 2.0 Spin Column and centrifuged for a minute at 13,000 RPM (17,000 RCF).
8. The flow-through was discarded, and the column was washed with 750 µL of wash buffer PE by centrifuging at 13,000 RPM (17,900 RCF) for 2 minutes. The step was performed twice, followed by an empty spin at the same speed and time.
9. Next, the QIAprep 2.0 Spin Column was placed in a fresh 1.5 ml centrifuge tube, and 30 µL of elution buffer was added to the tube. The sample was incubated at room temperature for 10 minutes.
10. At the last step, the DNA was eluted by centrifuging at 15,000 RPM (17,900 RCF) for 2 minutes.

IV.3. Extraction of DNA from the agarose gel using the QIAquick Gel Extraction Kit

1. The PCR product was kept under a UV transilluminator and excised from the gel using a new scalpel. The cut DNA fragment was kept in a 1.5 ml centrifuge tube.
2. Three volumes of QG buffer were added to one volume of gel (100 mg gel = 100 µL QG buffer).
3. To dissolve the gel slice, the gel was incubated for 10 minutes at 50ºC. Once the gel had entirely dissolved, the mixture turned yellowish.
4. 200 µL of isopropanol was added to the sample and mixed thoroughly.
5. A QIAquick column was placed in a 2 ml collection tube, and the sample was dispensed into the column.
6. The column was centrifuged for 1.5 minutes at 10,000 RCF, and the flow through was discarded.
7. 500 µL of buffer QG was added to the column and centrifuged at 10,000 RCF for 1.5 minutes.
8. Next, 750 µL of wash buffer PE was added to the column and centrifuged at 2 minutes to wash the bound DNA. The step was repeated twice, followed by an empty spin at the same speed and time.
9. The QIAquick column was placed in a fresh nuclease-free 1.5 ml centrifuge tube.
10. 30 µL elution buffer was added to the column and incubated at room temperature for 10 minutes.
11. Lastly, the column was centrifuged at 10,000 RCF for 2 minutes to elute the DNA.

IV.4. Quantification of GM-CSF and VEGFA using the Quantikine ELISA Kit

1. All the reagents of the kit and the conditioned medium were brought to room temperature.
2. Assay diluent RD1-6 was mixed well, and 100 µL of the diluent was added to each well of the ELISA plate.
3. 100 µL of standards and samples were dispensed into the same well containing RD1-6. The plate was covered with an adhesive strip and incubated for 2 hours at room temperature.
4. Each well was thoroughly washed by adding 400 µL of wash buffer after being aspirated using a multichannel pipette with 200 µL tips. The washing procedure was repeated four times.
5. 200 µL human GM-CSF conjugate and VEGF-A conjugate were added to their respective plates. The plate was covered with an adhesive strip and incubated for an hour at room temperature. The samples turned blue once the incubation was done.
6. Washing was done as described in step 4.
7. 200 µL of substrate solution (Color Reagent A + Color Reagent B) was added to each well and incubated for 20 minutes. The plate was covered with aluminum foil to protect it from the light.
8. At the end, 50 µL stop solution was added to each well. Following the dispersion of the stop solution, the color of the samples became blue to yellow.
9. The optical density of the samples was measured using a microplate reader at 450 nm and 540 nm. In the final O.D. values, the reading at 540 nm was subtracted from the reading at 450 nm to correct the optical imperfection of the plate.

IV.5. Extraction of DNA from cell lines

1. From a T-75 flask, cells were trypsinized, collected in a 1.5 ml microcentrifuge tube, and suspended in DPBS.
2. Cells were centrifuged at 12,000 RPM (17,000 RCF) for 5 minutes, and the supernatant was discarded.
3. The cell pellet was re-suspended into 200 µL of proteinase K and 10 µL 10% SDS.
4. The cell suspension was gently mixed with a 1 ml blunt cut pipette tip.
5. 100 µL of pre-chilled NaCl (5M) was added to the sample and mixed well.
6. 200 µL autoclaved Milli-Q water was added to the sample and gently mixed to form a homogenized solution.
7. 400 µL of phenol-chloroform isoamyl alcohol (PCI) was added to the microcentrifuge tube and gently swirled up and down.
8. The tube was incubated for 5 minutes at room temperature, followed by centrifugation at 12,000 RPM (17,000 RCF) for 10 minutes.
9. After the centrifugation, the sample was divided into three parts. The phenol is less-polar and denser than the chloroform-containing water. Hence the protein part, along with the cellular debris, dissolved into the phenol and remained at the bottom of the tube. Due to the negative charge, the genomic DNA dissolved into the water and remained at the top of the water-soluble part of the tube.
10. The DNA was carefully collected from the upper aqueous layer without disturbing the lower layers and transferred to a new 1.5 ml microcentrifuge tube.
11. Pre-chilled molecular grade absolute ethanol (100%) was added, and the tube was gently whirled up and down.
12. The tube was kept at -80ºC for 30 minutes.

13. Next, the tube was centrifuged at 15,000 RPM (17,000 RCF) for 10 minutes at 4ºC.
14. After removing the entire supernatant, 300 µL of 70% alcohol was added to the tube. Right away, centrifugation was carried out at 15,000 RPM (17,000 RCF) for 10 minutes.
15. The supernatant was discarded. The invisible DNA pellet was left overnight to air-dry at room temperature.
16. Next day, the DNA was eluted in 30 µL TAE buffer.
17. The concentration of the DNA was measured using a NanoDrop, and the quality of the DNA was checked by running it into 0.8% agarose gel.

IV.6. Luciferase Assay using the Dual-Luciferase® Reporter Assay System

1. The media was discarded, and the cells were washed with DPBS.
2. 50 µL of Passive Lysis Buffer was added to each well (24 well plate) to lyse the cells. The cells were scraped off and taken in a 1.5 ml microcentrifuge tube.
3. The tube was incubated into the ice for 15 minutes with occasional gentle vortexing.
4. 10 µL of this cell lysate was taken in a white-colored Nunclon^{TM} Delta Surface plate.
5. 50 µL of Luciferase Assay Reagent II (LAR II) was added to each sample.
6. The firefly luciferase luminescent signal was immediately measured in a luminometer.
7. 50 µL of Stop and glo® buffer was added to each sample, followed by measuring the Renilla luciferase signal in a luminometer.

IV.7. Annealing of the EMSA probes

1. First, 10 µM of the working probe sample was prepared from the 100 µM probe stock.
2. 30 µL of each oligo (10 µM) and its complementary oligo (10 µM) were mixed well, followed by incubation for 5 minutes at 95ºC in a pre-warmed water bath.
3. The oligo-pairs were left overnight in the water bath for slow cooling.

4. Next day, when the water came to room temperature, the probe sets were taken out and run in the 12% native get at 100V for an hour.
5. Annealing of the probes was visualized in a ChemiDoc system.

Appendix V: Buffer Composition

V.1. SDS-PAGE and Western Blot

Sr. No.	Buffer Name	Components	Weight/Volume
1.	**30% Acrylamide (100 mL)**	Acrylamide	29 gm
		N, N'-Methylene-bis-Acrylamide	1 gm
		Autoclaved Milli-Q water	Upto 100 mL
2.	**Tris 1.5M (pH: 8.8) (500 mL)**	Tris base	90.75 gm
		Autoclaved Milli-Q water	400 mL
		Concentrated HCl	Till the pH reaches 8.8
		Autoclaved Milli-Q water	Upto 500 mL
3.	**Tris 1M (pH: 6.8) (500 mL)**	Tris base	30 gm
		Autoclaved Milli-Q water	400 mL
		Concentrated HCl	Till the pH reaches 6.8
		Autoclaved Milli-Q water	Upto 500 mL
4.	**10% SDS (w/v) (100 mL)**	SDS	10 gm
		Autoclaved Milli-Q water	Upto 100 mL
5.	**10% APS (w/v) (100 mL)**	Ammonium Persulfate	10 gm
		Autoclaved Milli-Q water	Upto 100 mL
6.	**Water-saturated n-Butanol (55 mL)**	n-Butanol	50 mL
		Autoclaved Milli-Q water	5 mL
7.	**4X Laemmli Buffer (gel loading dye) (5 mL)**	Tris 1M(pH: 6.8)	1.2 mL
		100% Glycerol	2 mL
		Bromophenol Blue	2 mg
		2-Mercaptoethanol	0.25 mL
		SDS	0.4 gm
		Autoclaved Milli-Q water	1.55 mL
8.	**10X TGS Running Buffer (1 litre)**	Tris base	30 gm
		Glycine	144 gm
		SDS	10 gm
		Autoclaved Milli-Q water	Upto 1 litre
9.	**10X Transfer Buffer for Western Blot (1 litre)**	Tris base	23.3 gm
		Glycine	14.4 gm
		Methanol	200 mL
		Autoclaved Milli-Q water	Upto 1 litre
10.	**10X TBS Buffer (1 litre)**	Tris base	6.05 gm
		NaCl	8.76 gm

		Autoclaved Milli-Q water	800 mL
		Concentrated HCl	Till the pH reaches 7.5
		Autoclaved Milli-Q water	Upto 1 litre
11.	**0.1% TBST Buffer (1 litre)**	1X TBS Buffer Tween 20	1 litre 1 mL

V.2. Agarose Gel Electrophoresis

Sr. No.	Buffer Name	Components	Weight/Volume
1.	**50X TAE Buffer (1 litre)**	Tris base	242 gm
		Glacial acetic acid	57.1 mL
		0.5M EDTA (pH: 8)	100 mL
		Autoclaved Milli-Q water	Upto 1 litre

V.3 Other Buffers

Sr. No.	Buffer Name	Components	Weight/Volume
1.	**10X PBS**	$Na_2HPO_4 \cdot 7H_2O$	25.6 gm
		NaCl	80 gm
		KCl	2 gm
		KH_2PO_4	2 gm
		Autoclaved Milli-Q water	Upto 1 litre
2.	**Giemsa's Stain (50 mL)**	Giemsa Powder	0.76 gm
		Methanol	50 mL
		Heat at 60ºC till it dissolves	
		100% Glycerol	Upto 100 mL

Appendix VI:

The quadrant gate was put according to the double negative population of the unstained cells. The same gating was followed in the control and FRG1_KD cells.

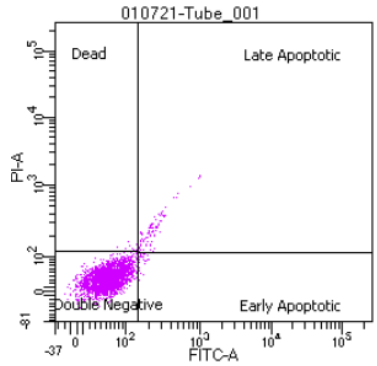

Flowcytometric data of unstained cells: All the control cells were present in the quadrant named as double negative and showed negative expression for FITC and PI. Very nominal percentage of cells were seen in the quadrants marked as early apoptotic, late apoptotic and dead.